Refining techniques for radiocarbon dating small archaeological bone samples

Fewlass, H.K.

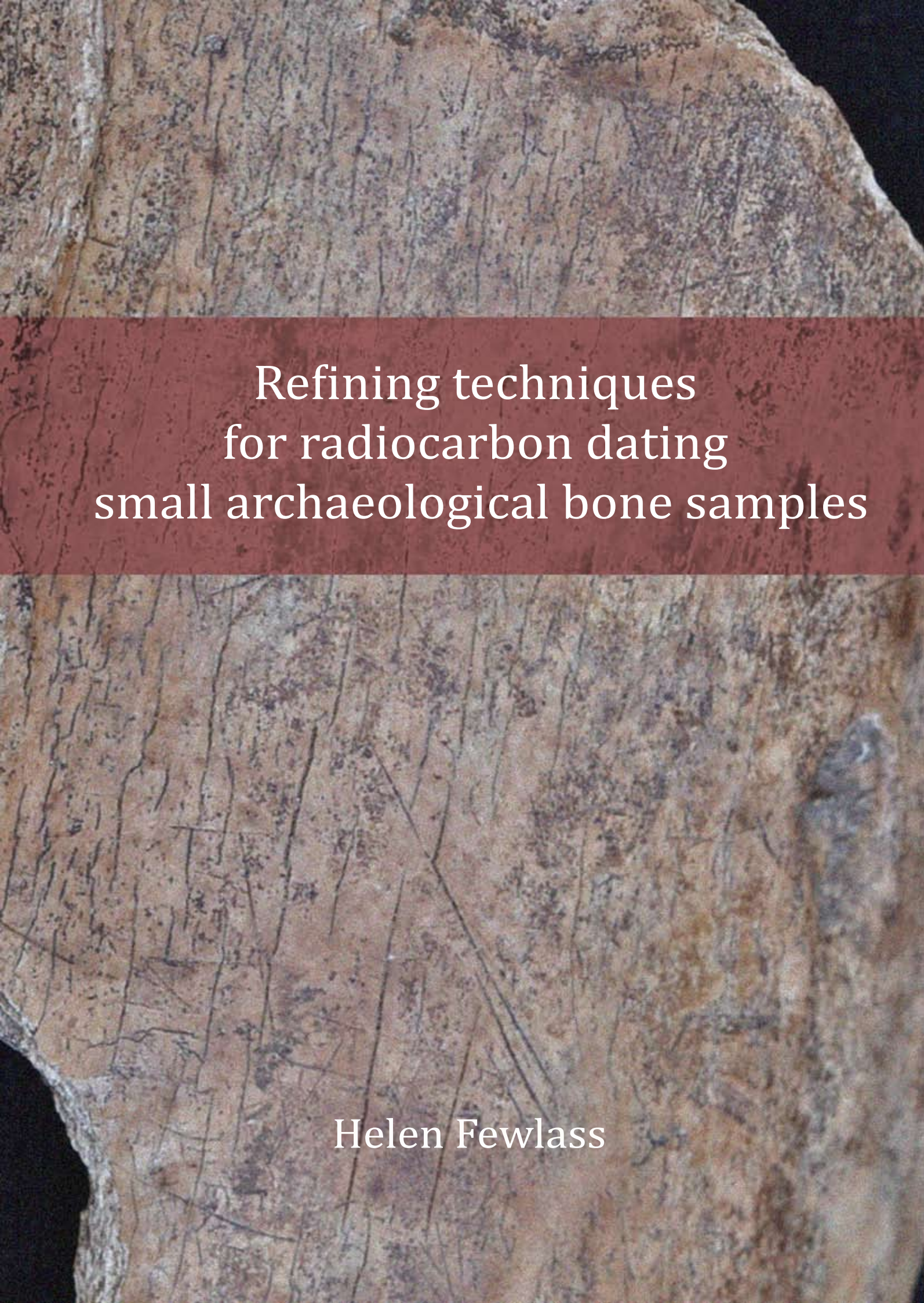

Refining techniques for radiocarbon dating small archaeological bone samples

Helen Fewlass

Refining techniques for radiocarbon dating small archaeological bone samples

Proefschrift

ter verkrijging van
de graad van Doctor aan de Universiteit Leiden,
op gezag van Rector Magnificus Prof. mr. C.J.J.M. Stolker,
volgens besluit van het College voor Promoties
te verdedigen op dinsdag 24 maart 2020
klokke 15:00 uur

door

Helen Fewlass
geboren te London, UK
in 1991

Promotor: Prof. dr. J.-J. Hublin (Universiteit Leiden)

Co-promotor: Prof. dr. S. Talamo (University of Bologna)

Co-promotor: Dr. B. Kromer (University of Heidelberg)

Promotiecommissie:

Chair: Prof.dr. J.C.A. Kolen (Universiteit Leiden)

Secretary: Prof. dr. J.W.M Roebroeks (Universiteit Leiden)

Prof. dr. M.A. Soressi (Universiteit Leiden)

Prof. dr. J. van der Plicht (Universiteit Leiden)

Prof. S. Benazzi (University of Bologna)

Dr. M. Mannino (Aarhus University)

This research was funded by the Max Planck Society.

“I'm made up of the memories of my parents and my grandparents, all my ancestors. They're in the way I look, in the colour of my hair. And I'm made up of everyone I've ever met who's changed the way I think.”

— Terry Pratchett, 2004, ‘A Hat Full of Sky’

Contents

Chapter One
Introduction

1. Radiocarbon and archaeology

2019 marks the 70th anniversary of Libby et al. (1949) publishing the first paper on radiocarbon dating. In these 70 years, radiocarbon dating has become inextricably intertwined with the field of archaeology, providing a fundamental chronological basis on which our interpretations of the past 50,000 years are built.

The study of archaeology gives us invaluable insights into the lives of people who lived thousands of years ago: how they exploited their environments, what they ate, the diseases that ravaged their bodies and the migrations they undertook. Chronology underpins how we track changes in these processes. Only by understanding when these things occurred and when they changed can we understand their implications for human history. Prior to the development of the ^{14}C dating method, archaeological sites and artefacts could be dated relatively in comparison to geological, palaeontological and environmental landmarks or by looking at changes in form through time and cross-referencing to known historical dates, but these relative chronologies could not be linked to calendar ages. Radiocarbon dating made the study of world prehistory possible by providing the first chronometric scale that could transcend regional boundaries (Clark, 1970). As the late African archaeologist Desmond Clark said, without the ^{14}C time scale, pre-historians would still be foundering *'… in a sea of imprecisions sometimes bred of inspired guesswork but more often of imaginative speculation*' (Clark, 1979).

Since the introduction of the radiocarbon method, the field has continually advanced through developments in laboratory techniques, instrumentation and understanding. Numerous 'Radiocarbon Revolutions' have occurred, from the first application of radiocarbon dating to archaeology to the construction of a calibration curve, the development of accelerator mass spectrometers (AMS) to measure ^{14}C and the wide-spread use of Bayesian statistics to analyse and interpret radiocarbon data (Renfrew, 1973; Bronk Ramsey, 2008; Bayliss, 2009; Wood, 2015).

This chapter will briefly introduce the basic concepts of radiocarbon dating and outline the aims of this dissertation.

2. Introduction to Radiocarbon

2.1 Radiocarbon production and distribution

Carbon is the basis for all life on our planet. It has three naturally occurring isotopes. Carbon-12 (^{12}C), containing six neutrons and six protons in its nucleus, constitutes 99% of carbon on earth. Carbon-13 (^{13}C) contains six protons and seven neutrons in its nucleus and makes up only 1% of global carbon. Both ^{12}C and ^{13}C are stable isotopes. Carbon-14 (denoted variously as ^{14}C, C^{14}, C_{14}, radiocarbon) is present only in trace amounts on earth (10^{-10}% of global carbon) and has an imbalanced nucleus containing six protons and eight neutrons which make it unstable (radioactive).

^{14}C is produced naturally in the upper atmosphere as a secondary product of in-coming cosmic radiation interacting with atmospheric gases (N, O, Ar) (Fig. 1; Taylor, 2001; Taylor and Bar-Yosef, 2014). This process produces free neutrons that react with the nuclei of nitrogen-14 (^{14}N; which constitutes 78% of our atmosphere) to form ^{14}C:

$$n + {}^{14}_{7}N \rightarrow {}^{14}_{6}C + p \qquad [1]$$

The ^{14}C is rapidly oxidised to carbon monoxide (^{14}CO) and then more slowly to carbon dioxide ($^{14}CO_2$). In this form, it enters the global carbon cycle and is distributed throughout the atmosphere, becoming fairly evenly mixed by the time it reaches the surface of the earth within a few weeks of its production. Most ^{14}C (>90%) ends up in the world's oceans as dissolved CO_2 (dissolved organic carbon; DOC) and dissolved inorganic carbon (DIC) in the form of carbonates and bicarbonates. 1-2% becomes part of the terrestrial biosphere (in the tissues of plants and animals) by means of CO_2 fixation during photosynthesis (Fig. 1).

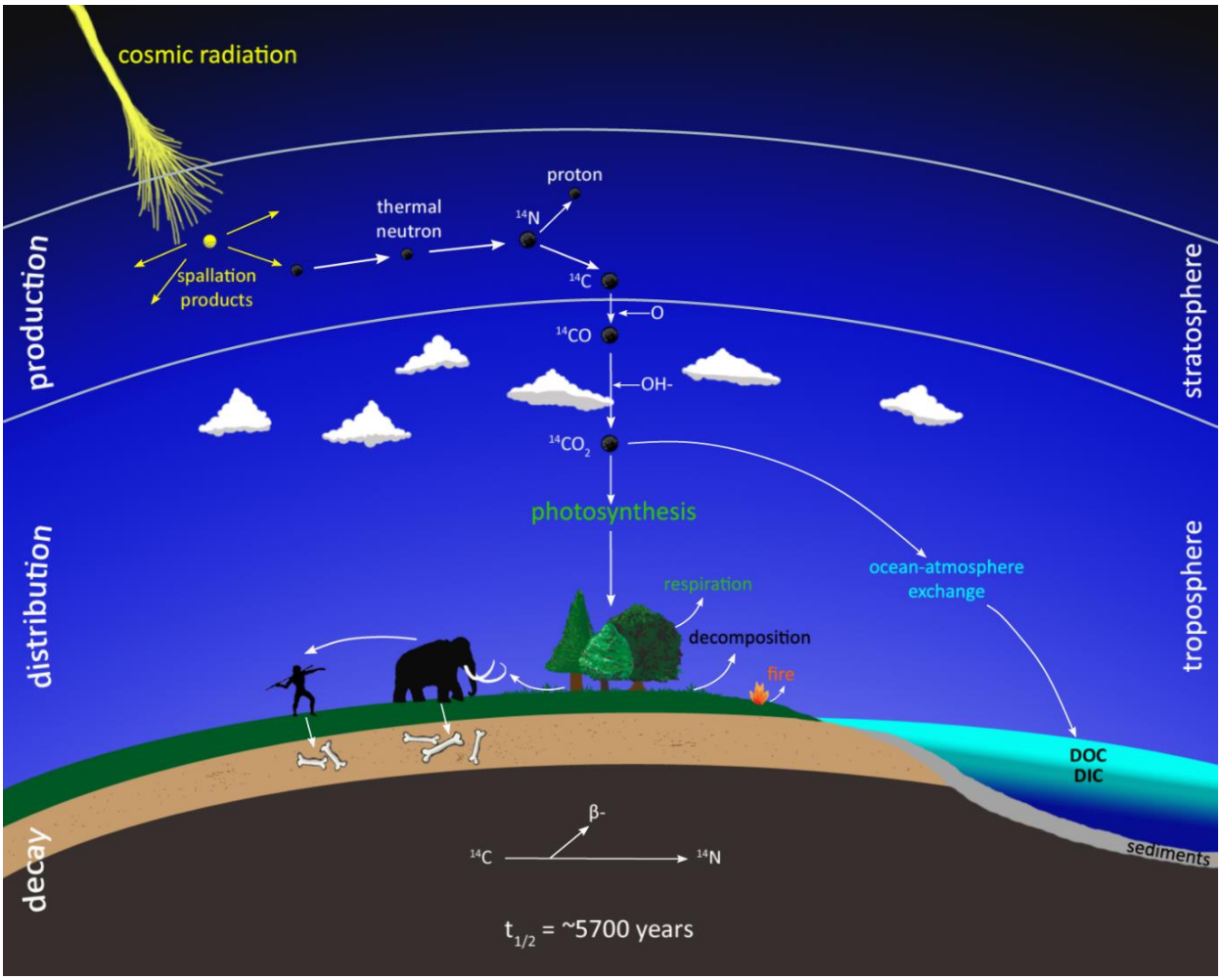

Figure 1. *Production, distribution and decay of radiocarbon in the global carbon cycle. Based on Taylor (2001); Taylor and Bar-Yosef (2014).*

2.2 Radiocarbon decay

The unstable nucleus of ^{14}C makes it undergo negative beta decay (β^-) into the stable isotope ^{14}N (containing seven protons and seven neutrons):

$$^{14}_{6}C \rightarrow {}^{14}_{7}N + e^- + \overline{\nu}_e \quad [2]$$

During life, plants and animals continually replenish their ^{14}C content through metabolic processes and ingestion so their tissues remain in equilibrium with the atmosphere. However, once an animal or plant dies it stops replenishing its ^{14}C content, which starts to decay with respect to the global atmospheric concentration. This decay occurs at a steady rate with a half-life of approximately 5,700 years (the amount of time it takes for the amount of ^{14}C in the tissues of a dead plant or animal to halve) (Fig. 2). This exponential decay mechanism is the basis of the

'radiocarbon clock'. The method is used to date carbonaceous material from around 250 ^{14}C years old to roughly 50,000 ^{14}C years old, at which point the amount of residual ^{14}C in the plant or animal tissue is so small it can no longer be routinely detected.

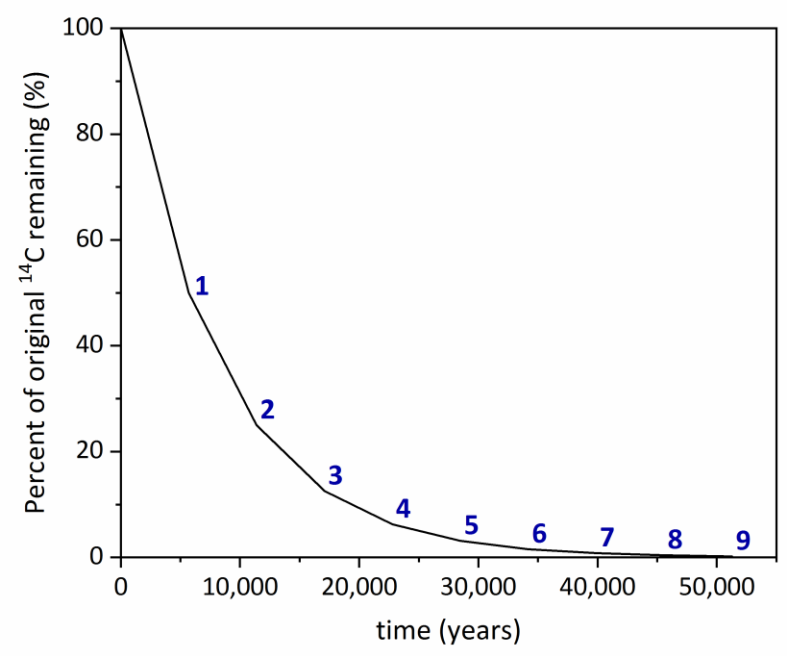

Figure 2. *Exponential decay of radiocarbon based on its half-life of ~5,700 years. The blue numbers to the right of the curve show the number of half-lives that have elapsed.*

2.3 The radiocarbon clock: considerations

When radiocarbon dating was first applied, it was assumed that the level of ^{14}C in the atmosphere had remained constant over time and that ^{14}C is distributed equally within each hemisphere rapidly after its production (Libby et al., 1949). These assumptions implied that conventional radiocarbon (^{14}C) years are equal to calendar (or 'solar') years across the radiocarbon timescale. However, it was realised fairly soon after the initial applications of radiocarbon dating that ^{14}C ages did not match historical dates or tree-ring records (de Vries, 1958; Willis et al., 1960; Stuiver and Suess, 1966). It is now well understood that although the decay rate of ^{14}C is stable, the level of ^{14}C in the atmosphere is not constant because the production rate and distribution of ^{14}C varies over time (Stuiver and Quay, 1980a; b). Variation in production rates stems from changes in cosmic ray influx and changes in the magnetic fields of the sun and the earth that affect the interaction of cosmic radiation with our upper atmosphere. The global distribution of ^{14}C also varies as carbon exchange rates between different carbon reservoirs (e.g. the atmosphere and oceans) fluctuate due to climatic or environmental factors. This means that ^{14}C years are not equivalent to calendar years for most of the ^{14}C timescale (Fig. 3). The offset is much larger during

the late Pleistocene than in the Holocene, reaching an offset of ~4000 years during the period 25,000 - 40,000 years.

Due to the variation in ^{14}C atmospheric levels over time, it was realised that radiocarbon dates must be calibrated to calendar years with temporal proxies (de Vries, 1958; Willis et al., 1960; Stuiver and Suess, 1966). This has been achieved with dendrochronology for the Holocene. The annual growth of long-lived tree species means that tree rings can be counted in calendar years and radiocarbon dated (initially on a decadal scale and now annually) to provide a continuous calibration curve stretching back thousands of years. Tree ring records from a variety of species from different locations have been combined to provide calibration curves which can be applied to ^{14}C samples across the northern (IntCal13; Reimer et al., 2013) and southern hemispheres (SHCal13; Hogg et al., 2013). Beyond 14,000 years a variety of other terrestrial and marine records have been combined to extend the curve over the full range of the ^{14}C timescale back to 50,000 years ago, although at a lower level of precision than the dendrochronological dataset (Fig. 3; Hogg et al., 2013; Reimer et al., 2013). This composite curve includes radiocarbon determinations on organics extracted from varved lake sediment cores (e.g. Lake Suigetsu; Bronk Ramsey et al., 2012) and marine sediment cores (corrected for reservoir offsets) (e.g. Cariaco Basin; Hughen et al., 2004; Hughen et al., 2006), which can be linked to climatic signals in the Greenland ice cores, and paired ^{14}C/uranium-thorium (U/Th) dating of speleothems (e.g. Hulu Cave; Southon et al., 2012; Cheng et al., 2018) and marine corals (e.g. Tahiti corals; Durand et al., 2013). The construction of an accurate and increasingly precise calibration curve has been an on-going international effort by the radiocarbon community for decades (Stuiver and Suess, 1966; Damon et al., 1974), and has been updated multiple times as datasets are added and revised - see IntCal98 (Stuiver et al., 1998), IntCal04 (McCormac et al., 2004; Reimer et al., 2004), IntCal09 (Reimer et al., 2009), IntCal13 (Hogg et al., 2013; Reimer et al., 2013) and the forthcoming IntCal19 (see Cheng et al., 2018; Reimer et al., 2018).

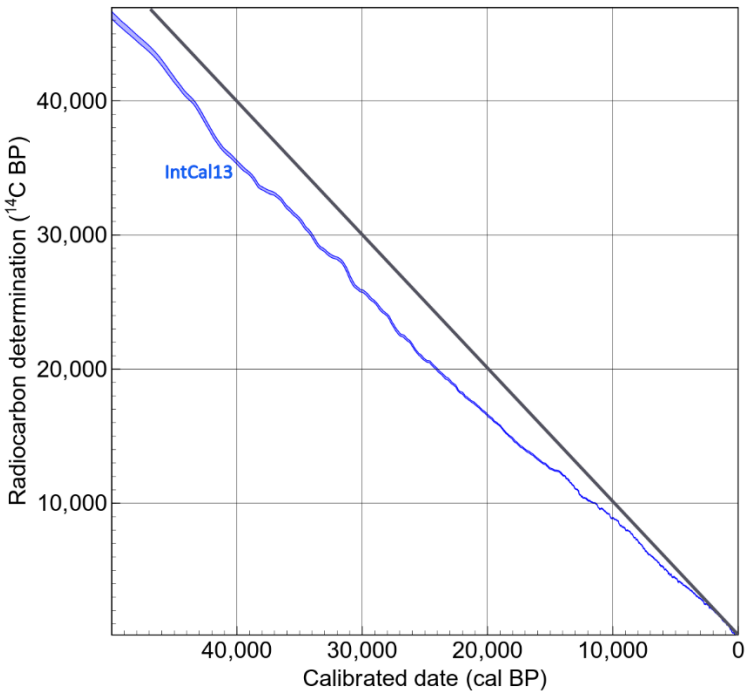

Figure 3. *The IntCal13 calibration curve (blue) (Reimer et al., 2013) plotted in OxCal (Bronk Ramsey, 2009). The grey line represents a hypothetical constant atmospheric ^{14}C concentration over time. For the majority of the ^{14}C timescale, radiocarbon determinations deviate from 'true' calendar ages by hundreds or thousands of years.*

In addition to natural variation in atmospheric ^{14}C concentrations, the level of ^{14}C in the atmosphere has been significantly altered by anthropogenic inputs over the last three centuries. The burning of fossil fuels on an industrial scale since the 18th century has introduced a huge amount of ^{14}C-free (radiocarbon dead) CO_2 into the atmosphere (the Suess Effect). In contrast, the detonation of nuclear weapons (hydrogen bombs) in the 1950s and 1960s released enormous amounts of artificial ^{14}C into the atmosphere, doubling the concentration. The high level of ^{14}C decreased rapidly (at a rate of ~1% per year), and the atmospheric concentration is almost back to the pre-bomb level. Although the bomb pulse has in fact proved useful in many biological and forensics radiocarbon dating applications back to 1963, the strong fluctuations in atmospheric ^{14}C since the 18th century mean that any radiocarbon ages falling in this period will intersect the calibration curve at multiple points, introducing ambiguity into their interpretation. Essentially, AD 1750 is therefore the lower limit of routine radiocarbon dating, although samples where an ordered set of dates is possible, such as wooden artefacts with >50 rings, can be wiggle matched to achieve a narrow calibrated age range. Any sample exhibiting an age of less than 200 ^{14}C years is generally referred to as 'modern' and any exhibiting an age of greater than the contemporary standard as 'greater than modern' (Stuiver and Polach, 1977).

Although ^{14}C is distributed fairly evenly within the atmosphere within a matter of weeks following production (although small regional offsets exist, see Kromer et al., 2001; Manning et al., 2001), the exchange rate between the atmosphere and other carbon reservoirs varies considerably both geographically and temporally. This leads to offsets in ^{14}C determinations between contemporary samples incorporating carbon from different reservoirs, called 'reservoir effects'. This occurs in the case of marine shells or animals eating a high proportion of marine foods when upwelling from the deep ocean (which exchanges very slowly with the atmosphere) causes 'old' carbon to be incorporated into the tissues of modern organisms. Ocean surface waters generally have a reasonably stable reservoir effect of around -400 years but offsets may reach over 1000 years in different locations. A marine calibration curve (Marine13) has been constructed from the IntCal13 curve incorporating regional marine reservoir variations to account for these offsets (Reimer et al., 2013). Reservoir corrections are increasingly complicated in fresh-water scenarios as the reservoir effect is difficult to model in dynamic systems with multiple carbon reservoirs (e.g. dissolved carbonates from geological limestone, 'old' ground water). The bones of humans who consumed large amounts of freshwater fish can exhibit a wide range of reservoir ages extending beyond -1000 years, which can have large implications for samples of Neolithic age and younger where the standard deviation associated with radiocarbon dates is in the order of decades (e.g. Cook et al., 2002; Nadeau et al., 2012).

3. Sample preparation for radiocarbon dating

The efficacy of the radiocarbon dating method depends on the context and geochemical history of the sample, pretreatment method, accuracy and precision of measurement and finally, interpretation of the date. The process for obtaining a radiocarbon date is shown in Fig. 4.

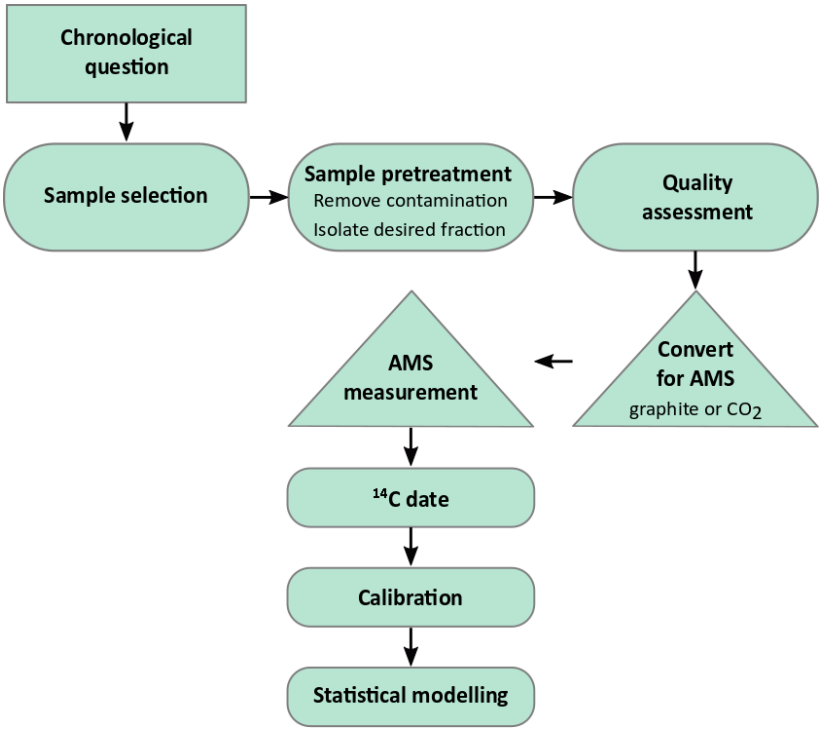

Figure 4. *Flow chart of the radiocarbon dating process.*

3.1 Sample selection and pretreatment

Careful sample selection is of utmost importance in obtaining reliable and useful radiocarbon data. The chronological question must be determined, and the physical relationship between the ^{14}C sample and the archaeological event of interest must be explicitly defined before pretreatment and measurement. The most commonly dated materials are wood, charcoal, shell and bone. Prior to ^{14}C measurement, samples are pretreated to extract the endogenous carbon whilst removing any contaminating molecules introduced during death and burial and simultaneously ensuring that no modern carbon is introduced during the laboratory procedure. Rather than dating a bulk sample, the pretreatment procedure often involves isolating a certain fraction of the sample material more resistant to diagenesis or contamination, such as collagen from bone or cellulose from wood. Each additional stage of pretreatment increases the risk of introducing lab-based contaminants, so much work has gone into establishing rigorous protocols for different sample pretreatments (Bird et al., 1999; Bronk Ramsey et al., 2004a; Talamo and Richards, 2011; Wood et al., 2012).

The preservation of organic material is highly dependent on the burial environment. The loss of organic material is accelerated by elevated temperatures, extreme pH and fluctuating moisture contents. In general, archaeological sites in temperate European contexts experience much

higher levels of organic preservation than sites in the tropics (van Klinken, 1999). However, even in temperate or cold climates, over time the organic fraction degrades and is lost, in general leaving relatively little organic material preserved in Pleistocene contexts in comparison to Holocene ones. As samples are increasingly degraded with age, more sample material is generally needed to extract sufficient carbon for dating from older samples.

Carbon contaminants (e.g. organic molecules from the soil or preservatives applied by museums) with a different level of ^{14}C activity to the original sample will lead to erroneous ^{14}C dating results. The effect on the ^{14}C age depends on the activity level (age) of the contamination. Adding 1% 'radiocarbon-dead' carbon will make a radiocarbon result around 80 years older, which will have a large impact on a recent sample with a precision of *ca.* ±20 years but a negligible effect on a sample older than 20,000 years. In contrast, 1% modern carbon will make ages appear younger than their 'real' ^{14}C age with the effect increasingly catastrophic for older samples (Fig. 5; Bronk Ramsey, 2008). Contamination of samples by exogenous carbon may also alter the stable carbon isotopic ratio of a sample. Due to the serious errors introduced, modern carbon contaminants have to be kept <0.1%, which is increasingly challenging as sample size is decreased (Hedges and van Klinken, 1992; Bronk Ramsey, 2008).

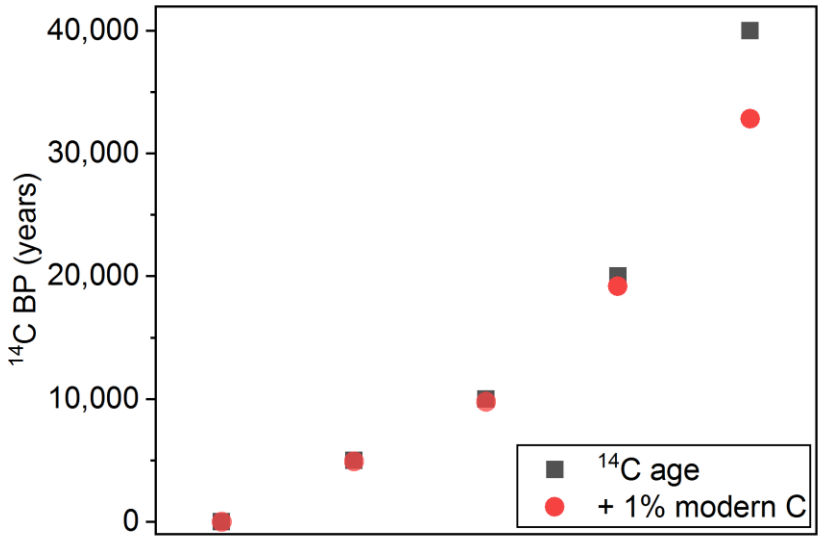

Figure 5. *The effect of 1% modern carbon contamination on ^{14}C ages across the ^{14}C timescale.*

It should be noted that there is a differentiation between the sample size needed from the original material (bone, wood, charcoal, in the order of milligrams to grams) and the sample size needed for AMS measurement (5 – 1000 micrograms of carbon (µg C)). The relationship between

the two depends on the proportion of carbon in the original material, the level of preservation of the material and the pretreatment method employed (Taylor and Bar-Yosef, 2014).

3.2 Archaeological bone

Bone is abundant at many archaeological sites and can often be directly related to the presence of humans. It is commonly the subject of genetic and palaeoproteomic investigations, faunal analysis and stable isotopic analysis for studying palaeodiet, mobility and palaeoenvironment. These considerations make bone highly attractive for radiocarbon dating, but the complex composition of bone means that purifying endogenous carbon is a complex process (Hedges and van Klinken, 1992).

Bone is composed of protein (predominantly collagen which makes up *ca.* 22% weight of modern bone) in a bioapatite (mineral) matrix (Collins et al., 2002). The most common method for dating bone is to isolate the collagen fraction, which is somewhat protected from the surrounding burial environment by the mineral matrix (Hedges and van Klinken, 1992; Collins et al., 2002). Collagen content declines with time since deposition at a rate dependent on the moisture, temperature and pH of the burial environment (van Klinken, 1999).

Since the 1970s, collagen has generally been extracted from bulk bone using an acid-base-acid method followed by gelatinisation, based on Longin (1971). The application of ultrafiltration, first proposed by Brown et al. (1988), led to vast improvements in purifying gelatin extracts by removing degraded collagen fragments and small molecular weight (<30 kDa) contaminants (Fig. 6). The necessity of collagen purification depends on the individual history of the sample, which cannot always be fully determined prior to pretreatment. In some cases standard collagen extraction protocols are sufficient to isolate endogenous carbon and yield identical ^{14}C results to more stringently purified extracts. This has led some to question the necessity of ultrafiltration methods (Fulop et al., 2013; Kuzmin, 2019) whilst other criticisms include the loss of endogenous collagen and the risk of contamination from the humectant coated filter (Jørkov et al., 2007; Hüls et al., 2009). However, in numerous cases the re-dating of bones with ultrafiltration methods has led to much older ages than previous dates from non-ultrafiltered extracts and has been shown to be particularly effective for Palaeolithic bones (Higham et al., 2006; Higham, 2011; Wood et al., 2013).

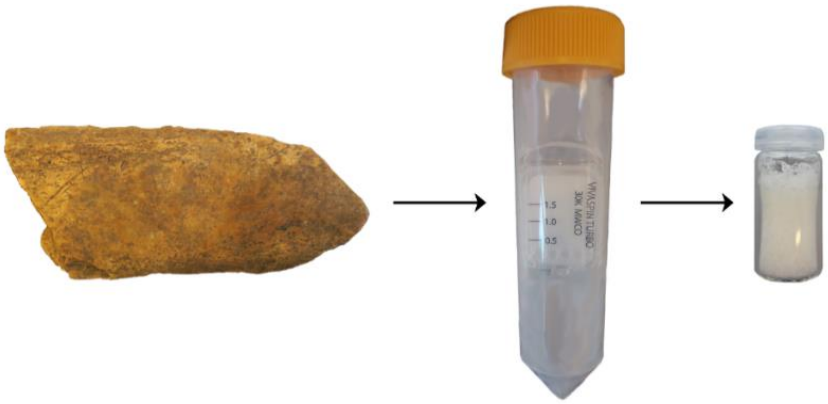

Figure 6. *Fragment of archaeological bone before pretreatment (left), an ultrafilter (centre) used to purify the gelatin extract and an ultra-filtered bone collagen extract (right) after pretreatment and freeze-drying.*

Efforts have been made to further eliminate the risk of contamination by purifying individual amino acids from bone collagen for compound specific dating (Stafford et al., 1982; Gillespie et al., 1984; van Klinken and Mook, 1990; Hedges and van Klinken, 1992). Hydroxyproline (HYP) is the preferred choice as it constitutes ~10% of the carbon in collagen and is rare in other mammalian proteins. The isolation of HYP has the advantage of removing large molecular weight contaminants (from conservatives or the soil) which are not removed by ultrafiltration methods. Recent improvements in the efficiency of applying the method have led to age revisions of important samples in several cases and indicate that the method is useful for cases where glues have been applied to bone (Marom et al., 2012; Nalawade-Chavan et al., 2014; Devièse et al., 2017b), although the reliability of the technique is not unanimously accepted (Kuzmin, 2019). As HYP only constitutes a small amount of the total carbon in bone, large amounts of bone need to be pretreated to gain enough C for dating. The method is therefore less suitable for bone samples with low levels of preservation and impractical for small samples such as individual teeth.

4. Measurement of radiocarbon

In order to obtain a radiocarbon date, once the carbon in the sample has been isolated the ratios of $^{14}C/^{12}C$ and $^{13}C/^{12}C$ ($\delta^{13}C$) in the organic material must be measured and compared to isotopic ratios in a standard. The isotopic ratio is converted to an age using the formula (Stafford et al., 1991):

$$t = -T \ln\left(\frac{A}{A_0}\right) \quad [3]$$

Where:
t is the age in radiocarbon years
T = 8033 years (the mean life of ^{14}C based on the Libby half-life of 5568 years)
A_0 is the initial ^{14}C activity at 0 BP (AD 1950), corrected to $\delta^{13}C$ = -25‰
A is the present ^{14}C activity, corrected to $\delta^{13}C$ = -25‰

The radiocarbon result depends on both the accuracy (obtaining the correct age of a sample) and the precision (the degree of uncertainty associated with the measurement) of the ^{14}C measurement. During the 1950s - 1970s, decay counters (gas proportional counters and liquid scintillation counters) were routinely used to determine the level of ^{14}C in a sample (Kromer and Münnich, 1992). These instruments detected and measured ^{14}C beta decay events which could be used to determine the age of a sample. The measurement of a single sample could take several weeks and required many grams of carbon (up to 20 g) to make an accurate, precise determination. Although conventional gas counters are still in use today for a number of applications, in the 1970s the development of accelerator mass spectrometers (AMS) revolutionised the field of radiocarbon dating (for a comprehensive review, see Gove, 1992). Rather than counting decay events, AMS instruments directly count the ^{12}C, ^{13}C and ^{14}C ions in a sample. As there are so many more of these to detect than individual ^{14}C decay events, routine measurements by AMS are made on much smaller samples sizes in a matter of hours, rather than days or weeks (Gove, 1992). This reduction in sample size was crucial for widespread archaeological applications as it allowed increasingly rigorous sample pretreatment of much smaller sample sizes (Bronk Ramsey, 2008; Taylor and Bar-Yosef, 2014). The caveat is that as sample size decreases, the proportional effect of exogenous carbon contamination on the result increases.

Most AMS systems are tandem electrostatic accelerators with negative ion sources, meaning that the particles are accelerated in a two-step process (Fig. 7; Taylor and Bar-Yosef, 2014). Carbon can be introduced into the ion source of an AMS in the form of solid graphitised carbon or CO_2 gas. In the ion source, the carbon atoms of the sample are bombarded with caesium ions. This ionizes the sample carbon with a negative charge (C^-) and the carbon ions are accelerated in a beam. As ^{14}N (which is present in the atmosphere at much greater magnitudes than ^{14}C) does not form negative ions, they are eliminated from the acceleration process. The ion beam passes through an electromagnetic field in a low-energy mass spectrometer that changes the trajectory of the ions according to mass, as 'heavier' ^{14}C isotopes will be deflected less than 'lighter' ^{12}C or ^{13}C isotopes. The negatively charged ions are pulled towards the positively charged high-voltage tandem accelerator, which contains a solid or gas 'stripper'. The stripper removes the outer

electrons of the ions, changing them from negatively to positively charged ions, which are then repelled away from the positive charge of the accelerator. The stripping process breaks apart any non-^{14}C particles of mass 14 ($^{12}CH_2$, ^{13}CH) which would otherwise interfere with the accurate measurement of ^{14}C. The positive ion beam is accelerated through a second magnetic field in the high-energy mass spectrometer. This separates out the ^{12}C and ^{13}C ions, which are measured in faraday cups, and the ^{14}C ions that are measured by a much more sensitive ion detector. As the precision of ^{14}C measurement is a function of how many ^{14}C ions are detected, older samples have lower levels of precision as they contain less residual ^{14}C.

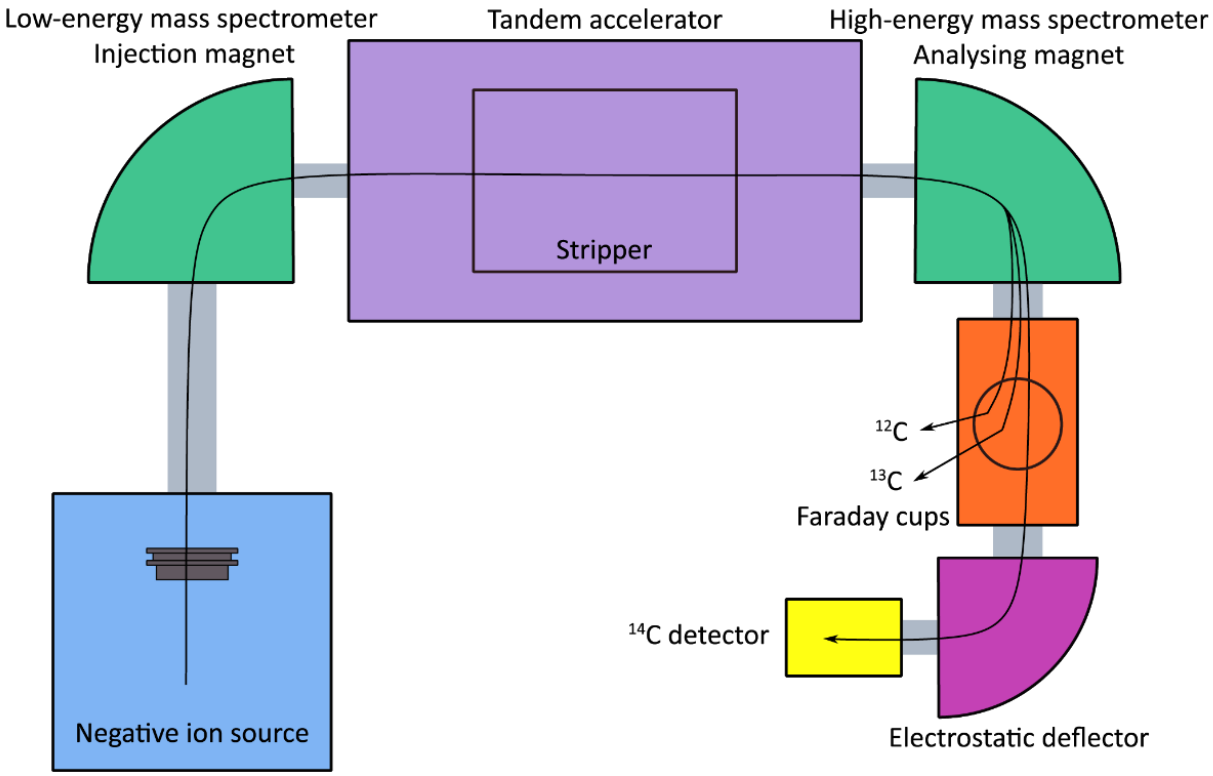

Figure 7. *Simplified schematic of a tandem accelerator AMS system measuring ^{14}C.*

All AMS labs convert pretreated samples into CO_2 through combustion. Most labs then convert the CO_2 into a solid form, typically by catalytically reducing it to filamentous graphite which is pressed into a target (routinely requiring 500 - 1000 µg C), to be introduced into the AMS. Solid forms are preferred as they produce higher ion beam currents (a higher amount of ions are

produced per unit time), which provide a higher level of precision, and less memory effect in the ion source between samples than directly introduced CO_2. Many labs have worked on various methods to reduce the amount of carbon necessary for dating with graphite targets to <500 µg C (e.g. Pearson et al., 1998; Hua et al., 2004; Ertun et al., 2005; Santos et al., 2007a; Santos et al., 2007b; Smith et al., 2007; Genberg et al., 2010; Delqué-Količ et al., 2013; Liebl et al., 2013; Walter et al., 2015; Freeman et al., 2016; Steier et al., 2016). However, these have often proved to be complex and subject to large contamination effects (see Ertun et al., 2005; Ruff et al., 2010a) which has limited the ability to reduce the sample sizes needed for dating samples such as archaeological bone. The direct measurement of CO_2 gas has the benefit of requiring much smaller sample sizes (in the order of 5 - 100 µg C) and cutting out the time-consuming graphitisation step (Middleton, 1984; Bronk Ramsey and Hedges, 1997), but the lower ion beam currents mean that in the past the method was only suitable for small sample sizes where high precision was unnecessary (Bronk Ramsey et al., 2004b).

In 2007, the Laboratory of Ion Beam Physics at ETH Zurich announced the development of the **MI**ni **CA**rbon **DA**ting **S**ystem (MICADAS), a compact AMS equipped with an ion source capable of accepting both solid and gas samples (Fig. 8; Ruff et al., 2007; Synal et al., 2007). Modifications to the gas ion source over the last decade mean that higher ion beam currents can be produced, thus increasing the level of precision possible for CO_2 samples in the range of 5 – 100 µg C (Ruff et al., 2007; Ruff et al., 2010b; Ruff et al., 2010a; Wacker et al., 2010; Fahrni et al., 2013; Wacker et al., 2013b). Initial reports indicated the system was highly reliable and contamination issues were reported to be much lower for small gaseous samples compared to small graphite samples (Ruff et al., 2010a). The system has been successfully utilised for the ^{14}C measurement of ice (Hoffmann, 2016), aerosols (Zhang et al., 2015; Bonvalot et al., 2016), carbonates (Wacker et al., 2013a; Bard et al., 2015; Fagault et al., 2017) and modern paintings (Hendriks et al., 2016).

The technological improvements in direct CO_2 measurement presents an attractive prospect for dating small archaeological bone samples in order to limit sample destruction. However, given the increasing sensitivity of bone collagen to contamination as sample size is reduced rigourous testing at both the pretreatment and measurement stages are necessary before the system is utilised for unknown samples.

Figure 8. *The AixMICADAS (Bard et al., 2015) AMS system at CEREGE in Aix-en-Provence in France.*

4.1 Reporting of radiocarbon data

A number of conventions have been established so that radiocarbon ages can be internationally compared and assessed (Stuiver and Polach, 1977).

When ^{14}C dates are correlated with independent dating methods such as U/Th or Argon/Argon the accuracy of the ^{14}C half-life is critical, and several revisions have been made to this value since Libby first published the method. Since 1962 the generally accepted value for the ^{14}C half-life is the Cambridge half-life of 5730 (±40) years (Godwin, 1962; Stuiver and Polach, 1977) but more recently it has been suggested that the real value may be closer to 6000 years (Chiu et al., 2007). Although the Libby half-life is accepted as incorrect, conventional radiocarbon ages are calculated using the Libby half-life of 5568 (±30) years, as many dates were already published using the value and during calibration, as long as the same half-life value is used for the sample ^{14}C age and the calibration dataset, the effect of any error in the half-life calculation is rendered insignificant (Stuiver and Suess, 1966).

Carbon isotopic ratios in a sample may be affected by fractionation (discrimination against heavier ^{13}C and ^{14}C isotopes during a phase transition) depending on the carbon reservoir from which the samples derive. As ^{13}C is discriminated against half as much as ^{14}C, the $\delta^{13}C$ value of a sample is measured with an isotope ratio mass spectrometer (IRMS) so that fractionation in ^{14}C

can be corrected. To account for different $\delta^{13}C$ values between samples, such as in marine shells ($\delta^{13}C$ = ~0‰) and terrestrial C_3 plants ($\delta^{13}C$ = ~-25‰), conventional ^{14}C ages are normalised to $\delta^{13}C$ = -25‰ with reference to an international standard (Peedee belemnite $\delta^{13}C$ = 0‰ or associated material) (Stuiver and Polach, 1977).

AD 1950 is defined as the zero point from which ^{14}C time is counted (Godwin, 1962). All ^{14}C measurements are made against an internationally recognised modern reference standard (Oxalic Acid (OX) I or II) with a defined ^{14}C age of zero (AD 1950) or a secondary modern standard with a known relationship to OXI/OXII (Stuiver and Polach, 1977). The background level of each AMS instrument is determined by the measurement of samples understood to contain no appreciable ^{14}C (radiocarbon dead) and will vary between instruments. It is crucial that measurements of fossil samples are made to monitor lab-based contamination and to calculate appropriate background subtractions for Pleistocene samples of unknown age. Beyond approximately 50,000 years the level of ^{14}C in the sample cannot be distinguished from the background level in the machine, making this the practical upper limit of radiocarbon dating. In such cases, only infinite ^{14}C ages can be expressed (denoted by a '>' prefix), meaning that the sample could be any age older than the value quoted.

All ^{14}C age determinations should be reported with the AMS lab number and an estimate of the precision (Stuiver and Polach, 1977). This is dominated by the counting statistics associated with ^{14}C measurement so is often referred to as the statistical uncertainty and is typically expressed as ±1 standard deviation. Conventional ^{14}C ages are reported with the suffix 'BP', which is internationally understood to mean '^{14}C years before AD 1950'. This is in contrast to the suffix 'cal BP' which specifically indicates that the value is an interpreted calibrated range (the calibration dataset and software should always be indicated).

For decades, many radiocarbon labs have voluntarily undertaken international inter-comparisons to monitor reproducibility and identify systematic problems (e.g. FIRI, VIRI, SIRI; Scott et al., 2018). The published results provide a level of quality assurance to submitters of radiocarbon samples.

5. The Bayesian revolution

The application of Bayesian statistics to chronological data represented a revolution in the interpretation of radiocarbon dates (Bayliss, 2009). Bayesian chronological modelling combines radiocarbon dates (or other chronometric information) with prior information on the relative order of the dates, usually meaning stratigraphic information from the archaeological context, to increase the precision of age determinations and to detect unreliable dates (Bronk Ramsey,

2009). This type of formal analysis allows individual radiocarbon dates to be modelled statistically within site-wide or regional chronologies, greatly increasing their power and precision (e.g. Hublin et al., 2012; Douka et al., 2014; Higham et al., 2014).

By assigning boundaries to archaeological phases, Bayesian modelling enables the timing and tempo of social changes to be investigated. The accuracy is highly dependent on the data input, with sample selection, sufficient sample pretreatment and prior assumptions (stratigraphic interpretations by archaeologists) playing critical roles (Bayliss, 2015; Bayliss and Marshall, 2019). The effect of sampling criteria on the output of chronological models is demonstrated by the case of Grotte du Renne (Arcy-sur-Cure) in south-western France. The site has a statigraphic sequence spanning the Middle to Upper Palaeolithic transition, including several 'transitional' Châtelperronian layers. These layers are notable for the association of Neanderthal remains with personal body ornaments, which were traditionally associated with Upper Palaeolithic assemblages made by *Homo sapiens*. An initial attempt at establishing a chronological framework for the transition period was based on ^{14}C dates of worked bone artefacts, many of which had been consolidated and/or yielded low collagen percentages (Higham et al., 2010). After modelling the results, the authors inferred a significant degree of mixing between layers which led them to question the biological identify of the makers of the Châtelperronian artefacts. A second attempt to determine a reliable chronology based on modelling of ^{14}C dates from bone samples with high levels of collagen preservation produced stratigraphically consistent results which supported the Neanderthal association with the ornaments (Hublin et al., 2012), a finding which has been further supported through proteomic analysis (Welker et al., 2016).

Where direct dating is not possible or suitable, Bayesian statistical analysis provides the opportunity to calculate probability distributions for the likely age of artefacts or fossils based on their relative stratigraphic position within a formal chronological framework. Such methods have been applied to fossils representing the early appearance of *Homo sapiens* in Europe, such as hominin teeth from the Uluzzian levels of the Grotta del Cavallo, Italy (Benazzi et al., 2011) and the KC4 human maxilla from Kent's Cavern in the UK (Higham et al., 2011a). However, the validity of these methods are open to debate over the reliability of the underlying stratigraphic associations (for example, in the case of Kent's Cavern and Cavallo, see White and Pettitt, 2012; Zilhão, 2013). The technique can only yield reliable estimations when the relationship with the associated artefacts is clear.

Bayesian modelling of absolute chronological data from multiple sites enables us to move beyond individual site chronologies to explore broader regional narratives. Higham and colleagues (2014) used Bayesian techniques to analyse radiocarbon data from 40 Mousterian sites to investigate the spatio-temporal patterning of the disappearance of Neanderthals and their potential overlap with *Homo sapiens* following their arrival in Eurasia. The model suggested that Neanderthals

disappeared from different regions at different times with the last appearance of the Mousterian at ~39,000 cal BP. The modelled overlap of 2,600-5,400 years with *Homo sapiens* supports the cultural, technological and biological interactions witnessed through archaeological and genetics analyses (e.g. Green et al., 2010; Ahern et al., 2013; Soressi et al., 2013; Fu et al., 2015; Hublin, 2015; Fu et al., 2016). Although such models can provide useful information on broad patterns of human behaviour, the output is sensitive to the quality of data included.

6. Problems in the Palaeolithic

The majority of the radiocarbon timescale covers the prehistoric period. This includes many of the most fascinating events in human history including the expansion of Upper Palaeolithic *Homo sapiens* from Africa to the rest of the world and the worldwide origins and spread of agriculture (Bar-Yosef, 2000). Unfortunately, relatively few archaeological sites and fossils from the late Middle and early Upper Palaeolithic exist and where they do, they are typically plagued by poor preservation due to their extreme age. During the 19th and 20th centuries it was common practice for museum curators to consolidate important archaeological bone artefacts or fossils (for example, fragmented bones glued together or entire bones dipped in glue) but detailed records of conservatives are often lost or non-existent, leading to complications for subsequent attempts at radiocarbon dating.

In a recent analysis of replicability, Bayliss and Marshall (2019) analysed replicate ^{14}C dates from 1089 archaeological samples commissioned by Historic England and found that one in 10 dates (on all sample types) measured before 1993 were outside 2σ of their true value, although this increased to one in five for bone/antler. The analysis was almost exclusively based on well-preserved material dating to less than 6000 years old but for the late Middle and Upper Palaeolithic the low level of preservation and the higher number of ^{14}C half-lives elapsed makes the process much more technically challenging. Higham has estimated that up to 70% of dates from the European Middle to Upper Palaeolithic made prior to the establishment of robust pretreatment methods are unreliable due to inappropriate sample selection and inadequate sample de-contamination (Higham et al., 2009; Higham, 2011). A commentary on radiocarbon dates from the Upper Palaeolithic site Sunghir in Russia found that more than two thirds of the 60 ^{14}C dates made since the 1970s should be considered unreliable due to laboratory inconsistencies, a lack of provenience data, and a lack of correlation between the dated material and the archaeological features (Soldatova, 2019).

Unfortunately, many primary publications fail to report information on sample context, pretreatment methods, quality criteria or measurement conditions, meaning that the reliability of many published radiocarbon dates is impossible to judge. In the past, AMS labs published

'datelists' of measured samples along with contextual information and comments on pretreatment and results (e.g. Hedges et al., 1989; Hedges et al., 1994; Higham et al., 2007). This practice became increasingly unfeasible due to the vast quantity of samples measured with AMS. Databases of ^{14}C dates published in the literature exist, such as the Radiocarbon Palaeolithic Europe Database, the latest version of which includes over 12,000 ^{14}C determinations (Vermeersch, 2019). Unfortunately, in many cases basic sample information is lacking as are references to publications, or even lab codes, which would enable further information to be obtained. Several recent inititives have taken these short-comings into consideration and aim to facilitate easier dissemination of data. Resources such as IntChron and the Southern African Radiocarbon Database (SARD) provide user-friendly interfaces and, crucially, these resources require references to publications so that further sample information can be easily obtained and sample quality assessed (Bronk Ramsey et al., 2019; Loftus et al., 2019). This increased transparency and accessibility of open-access data represents a great improvement for those undertaking large-scale analysis of chronological data.

Huge efforts have been made in recent decades to address the issue of accuracy by establishing stringent methods of sample pretreatment for bone collagen (Stafford et al., 1982; Brown et al., 1988; van Klinken and Mook, 1990; Brock et al., 2010a; Talamo and Richards, 2011; Devièse et al., 2017b), charcoal (Bird et al., 1999; Bird et al., 2014) and shell carbonates (Douka et al., 2010). Numerous pre-screening techniques for bone, including infra-red spectroscopy and elemental analysis, are employed to assess collagen preservation prior to sampling in order to limit needless sample destruction (e.g. D'Elia et al., 2007; Brock et al., 2010b; Brock et al., 2012; Pestle et al., 2015; Lebon et al., 2016). Various protocols have also been explored for the removal of different conservatives from bone prior to collagen extraction (Brock et al., 2017).

The reduction in sample size facilitated by AMS, the application of Bayesian statistics over the past two decades and the vast improvements in sample pretreatment have permitted key archaeological questions to be addressed at increasingly high resolution (Mellars, 2006; Higham, 2011). Chronologically positioned at the limit of the ^{14}C dating method, the Middle to Upper Palaeolithic transition has always presented a great technical challenge for the radiocarbon community and has therefore particularly benefited from methodological advances. With the application of these advanced techniques, a more robust chronological framework has begun to emerge for this period in Europe (e.g. Higham et al., 2011b; Hublin et al., 2012; Talamo et al., 2012; Douka, 2013; Wood et al., 2013; Higham et al., 2014; Dinnis et al., 2019).

Yet even with these developments, many precious archaeological bone artefacts are too small, rare or precious for the destructive sampling that comes with direct dating. Many of the more stringent pretreatment methods decrease the yield of carbon for dating, meaning that larger starting sample sizes are routinely required. Important bone artefacts or human remains are

therefore often dated indirectly through associated faunal remains or charcoal (e.g. Benazzi et al., 2011; Hublin et al., 2012; Benazzi et al., 2015; Bosch et al., 2015). Yet lamentably, many sites and artefacts excavated before and during the 20th century lack robust contextual information, and even with modern excavation techniques, the stratigraphy at archaeological sites can be complicated through the movement of objects between layers. These issues can lead to debates over the reliability of associated radiocarbon dates (White and Pettitt, 2012; Douka et al., 2015). In numerous cases where direct dating has been undertaken, supposed Palaeolithic remains have turned out to be Holocene intrusions (e.g. Trinkaus and Pettitt, 2000; Svoboda et al., 2002; Svoboda et al., 2004; Tillier et al., 2009; Hoffmann et al., 2011; Benazzi et al., 2014; Talamo et al., 2016a; Douka et al., 2017; Di Maida et al., 2019), leading to dramatic revisions of the catalogue of Upper Palaeolithic human remains in Eurasia in recent decades (Ahern et al., 2013). Such instances demonstrate how crucial direct radiocarbon dating can be for accurate interpretation, not only for individual objects but particularly because key specimens are often drawn into broader interpretations of large scale movements or cultural developments in human history (e.g. Svoboda et al., 1996; Hublin, 2015; Bae et al., 2017).

In some cases, direct radiocarbon dating has produced age estimations inconsistent with the stratigraphic context of the artefact, and the reliability of the ^{14}C data is questioned or rejected (e.g. Trinkaus et al., 1999; Toussaint and Pirson, 2006; Higham et al., 2011a). Several re-dating programs have been undertaken to establish accurate ages for key fossils using more rigourous pretreatment methods but this is largely dependent on the amount of sample material available (e.g. Jacobi and Higham, 2008; Devièse et al., 2017a). Although in some situations it is suspected that ultrafiltration or compound specific methods may provide results with increased accuracy, it is often difficult to justify further destruction of important fossils until reliable results can be obtained from smaller amounts of bone.

Recent developments in palaeoproteomics are having transformative effects on analyses of archaeological sites. Zooarchaeology by Mass Spectrometry, known as ZooMS, is being increasingly applied to large collections of undiagnostic bone fragments to identify hominin remains (Brown et al., 2016; Charlton et al., 2016; Welker et al., 2016). Small fragments of bone, which would have been overlooked in past decades, are fast becoming one of the most important resources at archaeological sites since they can represent the only available hominin remains. The lack of morphological features makes these fragments more suitable for destructive sampling and they are unlikely to have been conserved by curators. However, the application of different molecular analyses (^{14}C dating, ancient DNA, palaeoproteomics, stable isotopes) means that the amount of bone available is generally highly limited.

Figure 9. *Typical undiagnostic bone fragment (R-EVA 2664; chapter 5) analysed by ZooMS where limited material is available for analysis.*

The reduction in sample size for radiocarbon dating Palaeolithic bone is therefore a vital area of on-going research. Bearing in mind the archaeological questions and requirements, this dissertation aims to build apon the recent methodological advances in pretreatment and AMS measurement to test the effects of sample size reduction for the radiocarbon dating of archaeological bone.

7. Project aims

The overall objective of this project is to determine ways to obtain accurate and precise radiocarbon dates directly from precious archaeological bones with minimal sample destruction. Chapters 2 and 3 of this thesis focus on methodological questions concerning the pretreatment and measurement of <100 mg bone samples of known age. Chapters 3 and 4 demonstrate the application of these methods to important European Palaeolithic bones of unknown age.

Chapter 2 - Project 1

Testing the suitability of the MICADAS gas ion source for dating Palaeolithic collagen

It has been demonstrated that the recently updated gas ion source of the MICADAS AMS is suitable for measuring ^{14}C from <100 µg C in environmental applications. The first aim of this dissertation is to test the accuracy and precision of the gas ion source for dating small samples of collagen to determine whether the method is suitable for measuring ^{14}C of Palaeolithic bones when sample size is limited.

Project 1 is a pilot study testing the instrumental capabilities of the gas ion source for dating bone collagen and is published in *Radiocarbon*: **H. Fewlass**, S. Talamo, T. Tuna, Y. Fagault, B. Kromer, H. Hoffmann, C. Pangrazzi, J.J. Hublin, E. Bard (2017) Size matters: radiocarbon dates of <200 µg ancient collagen samples with AixMICADAS and its gas ion source. *Radiocarbon* 60, 425-439.

Chapter 3 - Project 2

Pretreatment of <100 mg bone samples

A successful protocol for bone collagen extraction and ultrafiltration was previously established in the Human Evolution department of the Max Planck Institute for Evolutionary Anthropology, Leipzig (Talamo and Richards, 2011). This protocol has been demonstrated to produce high yields of high quality collagen from ~500 mg of Palaeolithic bone and has been applied at range of archaeological sites across Europe (e.g. Hublin et al., 2012; Talamo et al., 2012; Talamo et al., 2016b). The second aim of this dissertation is to refine this protocol for <100 mg bone material whilst maintaining high yields of high quality collagen for radiocarbon dating. The quality of the extracts will be assessed through elemental, stable isotopic and ^{14}C dating with the AixMICADAS gas ion source.

The results of this project are published in *Scientific Reports*: **H. Fewlass**, T. Tuna, Y. Fagault, J.J. Hublin, B. Kromer, E. Bard, S. Talamo (2019) Pretreatment and gaseous radiocarbon dating of 40–100 mg archaeological bone. *Scientific Reports* 9(1):5342.

Chapter 4 - Project 3

Pretreatment and dating of human remains from Dolní Věstonice II and Pavlov I, Czech Republic

The sites of Dolní Věstonice II and Pavlov I in the Czech Republic offer fascinating insights into human behaviour in the Gravettian period in Europe. The sites are famed for their spectacular examples of ritual ochre burials and the large human skeletal collection has been the focus of intense analysis (Trinkaus and Svoboda, 2006). Radiocarbon dates of charcoal and animal bone placed the main period of occupation between 31,000 and 29,000 cal BP (Svoboda, 2016) but none of the human remains have previously been directly dated. In 2013, human bones from the two sites were sampled for aDNA analysis and the results played a large role in the discussion of the genetic history of *Homo sapiens* in Europe (Fu et al., 2016; Mittnik and Krause, 2016). Very small amounts of bone material were left over from the aDNA sampling of seven individuals, providing the first opportunity to date the human remains directly.

The aim of this project is to extract collagen from small aliquots of the Dolní Věstonice and Pavlov human bones for ^{14}C dating and stable isotope analysis. Depending on the pretreatment outcome, the samples will be measured with the Aix-MICADAS (graphite targets or the gas ion source) to obtain robust radiocarbon dates at the highest level of precision possible.

This project is published in the *Journal of Archaeological Science: Reports*: **H. Fewlass**, S. Talamo, B. Kromer, E. Bard, T. Tuna, Y. Fagault, M. Sponheimer, C. Ryder, J.J. Hublin, A. Perri, S. Sazelova, J. Svoboda. (2019) Direct radiocarbon dates of mid Upper Palaeolithic human remains from Dolní Věstonice II and Pavlov I, Czech Republic. *Journal of Archaeological Science: Reports* 27, 102000

Chapter 5 - Project 4

Pretreatment and dating of small human bone fragments from Bacho Kiro Cave, Bulgaria

The stratigraphic sequence at Bacho Kiro Cave, Bulgaria, contains an Initial Upper Palaeolithic (IUP) assemblage which is considered by some to represent one of the earliest occupations of Europe by Upper Palaeolithic *Homo sapiens* (Kozłowski, 1982; Hublin, 2015). Radiocarbon dates from excavations in the 1970s produced results that were inconsistent with the stratigraphic

sequence. New excavations (2015-2019) have been established at the site to provide new material for analysis (^{14}C dating, ZooMS, aDNA, zooarch and lithic analysis). During ZooMS screening of the faunal collection, four fragments of human bone from the IUP layer were identified, in addition to two fragments of human bone from the overlying Upper Palaeolithic layers. The small IUP human bone fragments present the first opportunity to directly radiocarbon date *Homo sapiens* remains securely associated with an IUP assemblage but sample material is very limited.

Small fragments (<100 mg) of the six human bones from Bacho Kiro Cave will be pretreated to obtain collagen for radiocarbon dating and isotopic analysis (chapter 4). In order to cross-check the ^{14}C results, the Upper Palaeolithic human bone fragments will be dated with both graphite targets and the CO_2 dating method.

Furthermore, rigourous methods of sample selection, pretreatment and ^{14}C measurement will be applied to a large sample of faunal bone spanning the site stratigraphy in order to establish a robust, high precision radiocarbon chronology for the eponym site.

This project is under review at *Nature Ecology and Evolution*: **H. Fewlass**, S. Talamo, L. Wacker, B. Kromer, T. Tuna, Y. Fagault, E. Bard, S. McPherron, V. Aldeias, R. Maria, N.L. Martisius, L. Paskulin, Z. Rezek, V. Sinet-Mathiot, S. Sirakova, G. Smith, R. Spasov, F. Welker, T. Tsanova, N. Sirakov, J.J. Hublin. New ^{14}C chronology for Middle–to–Upper Palaeolithic transition at Bacho Kiro cave, Bulgaria. *Nature Ecology & Evolution*.

Chapter 6 – Conclusion

The final section of this dissertation will provide a brief conclusion of the outcomes of this study and discuss the implications for future applications.

References

Ahern J.C.M., Janković I., Voisin J.-L., Smith F.H. 2013. Modern human origins in Central Europe. In: Smith FH, Ahern JCM, editors. The Origins of Modern Humans: Biology Reconsidered. 2 ed. Hoboken, NJ: John Wiley & Sons, Inc. p 151-221.

Bae C.J., Douka K., Petraglia M.D. 2017. On the origin of modern humans: Asian perspectives. Science 358(6368).

Bar-Yosef O. 2000. The impact of radiocarbon dating on Old World archaeology: past achievements and future expectations. Radiocarbon 42(1):23-39.

Bard E., Tuna T., Fagault Y., Bonvalot L., Wacker L., Fahrni S., Synal H.-A. 2015. AixMICADAS, the accelerator mass spectrometer dedicated to ^{14}C recently installed in Aix-en-Provence, France. Nuclear Instruments and Methods in Physics Research Section B: Beam Interactions with Materials and Atoms 361:80-86.

Bayliss A. 2009. Rolling out revolution: using radiocarbon dating in archaeology. Radiocarbon 51(1):123-147.

Bayliss A. 2015. Quality in Bayesian chronological models in archaeology. World Archaeology 47(4):677-700.

Bayliss A., Marshall P. 2019. Confessions of a serial polygamist: the reality of radiocarbon reproducibility in archaeological samples. Radiocarbon:1-16.

Benazzi S., Douka K., Fornai C., Bauer C.C., Kullmer O., Svoboda J., Pap I., Mallegni F., Bayle P., Coquerelle M., Condemi S., Ronchitelli A., Harvati K., Weber G.W. 2011. Early dispersal of modern humans in Europe and implications for Neanderthal behaviour. Nature 479(7374):525-528.

Benazzi S., Peresani M., Talamo S., Fu Q.M., Mannino M.A., Richards M.P., Hublin J.-J. 2014. A reassessment of the presumed Neandertal remains from San Bernardino Cave, Italy. Journal of Human Evolution 66:89-94.

Benazzi S., Slon V., Talamo S., Negrino F., Peresani M., Bailey S.E., Sawyer S., Panetta D., Vicino G., Starnini E., Mannino M.A., Salvadori P.A., Meyer M., Pääbo S., Hublin J.-J. 2015. The makers of the Protoaurignacian and implications for Neandertal extinction. Science 348(6236):793-796.

Bird M.I., Ayliffe L.K., Fifield L.K., Turney C.M., Cresswell R.G., Barrows T.T., David B. 1999. Radiocarbon dating of "old" charcoal using a wet oxidation, stepped-combustion procedure. Radiocarbon 41(2):127-140.

Bird M.I., Levchenko V., Ascough P.L., Meredith W., Wurster C.M., Williams A., Tilston E.L., Snape C.E., Apperley D.C. 2014. The efficiency of charcoal decontamination for radiocarbon dating by three pre-treatments- ABOX, ABA and hypy. Quaternary Geochronology 22:25-32.

Bonvalot L., Tuna T., Fagault Y., Jaffrezo J.L., Jacob V., Chevrier F., Bard E. 2016. Estimating contributions from biomass burning and fossil fuel combustion by means of radiocarbon analysis of carbonaceous aerosols: application to the Valley of Chamonix. Atmospheric Chemistry and Physics 16:13753-13772.

Bosch M.D., Mannino M.A., Prendergast A.L., O'Connell T.C., Demarchi B., Taylor S.M., Niven L., van der Plicht J., Hublin J.-J. 2015. New chronology for Ksâr 'Akil (Lebanon) supports Levantine route of modern human dispersal into Europe. Proceedings of the National Academy of Sciences 112(25):7683-7688.

Brock F., Higham T., Ditchfield P., Bronk Ramsey C. 2010a. Current pretreatment methods for AMS radiocarbon dating at the oxford radiocarbon accelerator unit (ORAU). Radiocarbon 52:103-112.

Brock F., Higham T., Bronk Ramsey C. 2010b. Pre-screening techniques for identification of samples suitable for radiocarbon dating of poorly preserved bones. Journal of Archaeological Science 37(4):855-865.

Brock F., Wood R., Higham T.F.G., Ditchfield P., Bayliss A., Bronk Ramsey C. 2012. Reliability of nitrogen content (%N) and carbon:nitrogen atomic ratios (C:N) as indicators of collagen preservation suitable for radiocarbon dating. Radiocarbon 54(3-4):879-886.

Brock F., Dee M., Hughes A., Snoeck C., Staff R., Bronk Ramsey C. 2017. Testing the effectiveness of protocols for removal of common conservation treatments for radiocarbon dating. Radiocarbon 60(1):35-50.

Bronk Ramsey C., Hedges R.E.M. 1997. Hybrid ion sources: radiocarbon measurements from microgram to milligram. Nuclear Instruments and Methods in Physics Research Section B: Beam Interactions with Materials and Atoms 123(1):539-545.

Bronk Ramsey C., Higham T., Bowles A., Hedges R. 2004a. Improvements to the pretreatment of bone at Oxford. Radiocarbon 46(1):155-164.

Bronk Ramsey C., Ditchfield P., Humm M. 2004b. Using a gas ion source for radiocarbon AMS and GC-AMS. Radiocarbon 46(1):25-32.

Bronk Ramsey C. 2008. Radiocarbon dating: revolutions in understanding. Archaeometry 50(2):249-275.

Bronk Ramsey C. 2009. Bayesian analysis of radiocarbon dates. Radiocarbon 51(1):337-360.

Bronk Ramsey C., Staff R.A., Bryant C.L., Brock F., Kitagawa H., van der Plicht J., Schlolaut G., Marshall M.H., Brauer A., Lamb H.F., Payne R.L., Tarasov P.E., Haraguchi T., Gotanda K., Yonenobu H., Yokoyama Y., Tada R., Nakagawa T. 2012. A complete terrestrial radiocarbon record for 11.2 to 52.8 kyr B.P. Science 338(6105):370-374.

Bronk Ramsey C., Blaauw M., Kearney R., Staff R.A. 2019. The importance of open access to chronological data: the IntChron initiative. Radiocarbon:1-11.

Brown S., Higham T., Slon V., Pääbo S., Meyer M., Douka K., Brock F., Comeskey D., Procopio N., Shunkov M., Derevianko A., Buckley M. 2016. Identification of a new hominin bone from Denisova Cave, Siberia using collagen fingerprinting and mitochondrial DNA analysis. Scientific Reports 6:23559.

Brown T.A., Nelson D.E., Vogel J.S., Southon J.R. 1988. Improved collagen extraction by modified Longin method. Radiocarbon 30(2):171-177.

Charlton S., Alexander M., Collins M., Milner N., Mellars P., O'Connell T.C., Stevens R.E., Craig O.E. 2016. Finding Britain's last hunter-gatherers: a new biomolecular approach to 'unidentifiable' bone fragments utilising bone collagen. Journal of Archaeological Science 73:55-61.

Cheng H., Edwards R.L., Southon J., Matsumoto K., Feinberg J.M., Sinha A., Zhou W., Li H., Li X., Xu Y., Chen S., Tan M., Wang Q., Wang Y., Ning Y. 2018. Atmospheric $^{14}C/^{12}C$ changes during the last glacial period from Hulu Cave. Science 362(6420):1293-1297.

Chiu T.-C., Fairbanks R.G., Cao L., Mortlock R.A. 2007. Analysis of the atmospheric ^{14}C record spanning the past 50,000 years derived from high-precision $^{230}Th/^{234}U/^{238}U$, $^{231}Pa/^{235}U$ and ^{14}C dates on fossil corals. Quaternary Science Reviews 26(1):18-36.

Clark G. 1970. Aspects of prehistory. Berkeley and Los Angeles: University of California Press.

Clark J.D. 1979. Radiocarbon dating and African archaeology. In: Berger R, Suess HE, editors. Radiocarbon Dating. Berkeley: University of California Press. p 7-31.

Collins M.J., Nielsen-Marsh C.M., Hiller J., Smith C.I., Roberts J.P., Prigodich R.V., Wess T.J., Csapo J., Millard A.R., Turner-Walker G. 2002. The survival of organic matter in bone: A review. Archaeometry 44:383-394.

Cook G.T., Bonsall C., Hedges R.E.M., McSweeney K., Boroneant V., Bartosiewicz L., Pettitt P.B. 2002. Problems of dating human bones from the Iron Gates. Antiquity 76(291):77-85.

D'Elia M., Gianfrate G., Quarta G., Giotta L., Giancane G., Calcagnile L. 2007. Evaluation of possible contamination sources in the ^{14}C analysis of bone samples by FTIR spectroscopy. Radiocarbon 49(2):201-210.

Damon P.E., Ferguson C.W., Long A., Wallick E.I. 1974. Dendrochronologic calibration of the radiocarbon time scale. American Antiquity 39(2):350-366.

de Vries H. 1958. Variation in concentration of radiocarbon with time and location on earth. Proc. Koninkl. Nederl. Akad. Wetenschappen, B 61:1-9.

Delqué-Količ E., Caffy I., Comby-Zerbino C., Dumoulin J.-P., Hain S., Massault M., Moreau C., Quiles A., Setti V., Souprayen C., Tannau J.-F., Thellier B., Vincent J. 2013. Advances in handling small radiocarbon samples at the Laboratoire de Mesure du Carbone 14 in Saclay, France. Radiocarbon 55(2):648-656.

Devièse T., Karavanić I., Comeskey D., Kubiak C., Korlević P., Hajdinjak M., Radović S., Procopio N., Buckley M., Pääbo S., Higham T. 2017a. Direct dating of Neanderthal remains from the site of Vindija Cave and implications for the Middle to Upper Paleolithic transition. Proceedings of the National Academy of Sciences 114(40):10606-10611.

Devièse T., Comeskey D., McCullagh J., Bronk Ramsey C., Higham T. 2017b. New protocol for compound-specific radiocarbon analysis of archaeological bones. Rapid Communications in Mass Spectrometry 32(5):373-379.

Di Maida G., Mannino M., Krause-Kyora B., Zetner T., Talamo S. 2019. Radiocarbon dating and isotope analysis on the purported Aurignacian skeletal remains from Fontana Nuova (Ragusa, Italy). PLoS ONE 14:e0213173.

Dinnis R., Bessudnov A., Reynolds N., Devièse T., Pate A., Sablin M., Sinitsyn A., Higham T. 2019. New data for the Early Upper Paleolithic of Kostenki (Russia). Journal of Human Evolution 127:21-40.

Douka K., Hedges R.E.M., Higham T.F.G. 2010. Improved AMS ^{14}C dating of shell carbonates using high-precision X-Ray diffraction and a novel density separation protocol (CarDS). Radiocarbon 52(2):735-751.

Douka K. 2013. Exploring “the great wilderness of prehistory”: the chronology of the Middle to the Upper Paleolithic transition in the Northern Levant. Mitteilungen der Gesellschaft für Urgeschichte 22:11-40.

Douka K., Higham T.F.G., Wood R., Boscato P., Gambassini P., Karkanas P., Peresani M., Ronchitelli A.M. 2014. On the chronology of the Uluzzian. Journal of Human Evolution 68:1-13.

Douka K., Higham T.F.G., Bergman C.A. 2015. Statistical and archaeological errors invalidate the proposed chronology for the site of Ksar Akil. Proceedings of the National Academy of Sciences 112(51):E7034.

Douka K., Slon V., Stringer C., Potts R., Hübner A., Meyer M., Spoor F., Pääbo S., Higham T. 2017. Direct radiocarbon dating and DNA analysis of the Darra-i-Kur (Afghanistan) human temporal bone. Journal of Human Evolution 107:86-93.

Durand N., Deschamps P., Bard E., Hamelin B., Camoin G., Thomas A.L., Henderson G.M., Yokoyama Y., Matsuzaki H. 2013. Comparison of ^{14}C and U-Th Ages in Corals from IODP #310 Cores Offshore Tahiti. Radiocarbon 55(4):1947-1974.

Ertun T., Xu S., Bryant C.L., Maden C., Murray C., Currie M., Freeman S.T. 2005. Progress in AMS target production of sub-milligram samples at the NERC radiocarbon laboratory. Radiocarbon 47(3):453–464.

Fagault Y., Tuna T., Rostek F., Bard E. 2017. Radiocarbon dating of small foraminifera samples with a gas ion source. 14th International AMS Conference, Ottawa.

Fahrni S.M., Wacker L., Synal H.-A., Szidat S. 2013. Improving a gas ion source for ^{14}C AMS. Nuclear Instruments and Methods in Physics Research Section B: Beam Interactions with Materials and Atoms 294:320-327.

Freeman E., Skinner L.C., Reimer R., Scrivner A., Fallon S. 2016. Graphitization of small carbonate samples for paleoceanographic research at the Godwin Radiocarbon Laboratory, University of Cambridge. Radiocarbon 58:89-97.

Fu Q., Hajdinjak M., Moldovan O.T., Constantin S., Mallick S., Skoglund P., Patterson N., Rohland N., Lazaridis I., Nickel B., Viola B., Prufer K., Meyer M., Kelso J., Reich D., Pääbo S. 2015. An early modern human from Romania with a recent Neanderthal ancestor. Nature 524(7564):216-219.

Fu Q., Posth C., Hajdinjak M., Petr M., Mallick S., Fernandes D., Furtwängler A., Haak W., Meyer M., Mittnik A., Nickel B., Peltzer A., Rohland N., Slon V., Talamo S., Lazaridis I., Lipson M., Mathieson I., Schiffels S., Skoglund P., Derevianko A.P., Drozdov N., Slavinsky V., Tsybankov A., Cremonesi R.G., Mallegni F., Gély B., Vacca E., Morales M.R.G., Straus L.G., Neugebauer-Maresch C., Teschler-Nicola M., Constantin S., Moldovan O.T., Benazzi S., Peresani M., Coppola D., Lari M., Ricci S., Ronchitelli A., Valentin F., Thevenet C., Wehrberger K., Grigorescu D., Rougier H., Crevecoeur I., Flas D., Semal P., Mannino M.A., Cupillard C., Bocherens H., Conard N.J., Harvati K., Moiseyev V., Drucker D.G., Svoboda J., Richards M.P., Caramelli D., Pinhasi R., Kelso J., Patterson N., Krause J., Pääbo S., Reich D. 2016. The genetic history of Ice Age Europe. Nature 534(7606):200-205.

Fulop R.-H., Heinze S., John S., Rethemeyer J. 2013. Ultrafiltration of bone samples is neither the problem nor the solution. Radiocarbon 55(2):491-500.

Genberg J., Stenstrom K., Elfman M., Olsson M. 2010. Development of graphitization of µg-sized samples at Lund University. Radiocarbon 52(3):1270-1276.

Gillespie R., Hedges R.E.M., Wand J.O. 1984. Radiocarbon dating of bone using accelerator mass spectometry. Journal of Archaeological Science 11:165-170.

Godwin H. 1962. Half-life of radiocarbon. Nature 195(4845):984-984.

Gove H.E. 1992. The history of AMS, its advantages over decay counting: applications and prospects. In: Taylor RE, Long A, Kra RS, editors. Radiocarbon After Four Decades. New York, NY: Springer New York. p 214-229.

Green R.E., Krause J., Briggs A.W., Maricic T., Stenzel U., Kircher M., Patterson N., Li H., Zhai W., Fritz M.H.-Y., Hansen N.F., Durand E.Y., Malaspinas A.-S., Jensen J.D., Marques-Bonet T., Alkan C., Prüfer K., Meyer M., Burbano H.A., Good J.M., Schultz R., Aximu-Petri A., Butthof A., Höber B., Höffner B., Siegemund M., Weihmann A., Nusbaum C., Lander E.S., Russ C., Novod N., Affourtit J., Egholm M., Verna C., Rudan P., Brajkovic D., Kucan Ž., Gušic I., Doronichev V.B., Golovanova L.V., Lalueza-Fox C., de la Rasilla M., Fortea J., Rosas A., Schmitz R.W., Johnson P.L.F., Eichler E.E., Falush D., Birney E., Mullikin J.C., Slatkin M., Nielsen R., Kelso J., Lachmann M., Reich D., Pääbo S. 2010. A draft sequence of the Neandertal genome. Science 328(5979):710-722.

Hedges R.E.M., Housley R.A., Law I.A., Bronk Ramsey C. 1989. Radiocarbon dates from the Oxford AMS system: Archaeometry datelist 9. Archaeometry 31(2):207-234.

Hedges R.E.M., van Klinken G.J. 1992. A review of current approaches in the pretreatment of bone for radiocarbon dating by AMS. Radiocarbon 34(3):279-291.

Hedges R.E.M., Housley R.A., Bronk Ramsey C., van Klinken G.J. 1994. Radiocarbon dates from the Oxford AMS system: Archaeometry datelist 18. Archaeometry 36(2):337-374.

Hendriks L., Hajdas I., McIntyre C., Küffner M., Scherrer N.C., Ferreira E.S.B. 2016. Microscale radiocarbon dating of paintings. Applied Physics A 122(3):1-10.

Higham T., Jacobi R.M., Bronk Ramsey C. 2006. AMS radiocarbon dating of ancient bone using ultrafiltration. Radiocarbon 48(2):179-195.

Higham T., Brock F., Peresani M., Broglio A., Wood R., Douka K. 2009. Problems with radiocarbon dating the Middle to Upper Palaeolithic transition in Italy. Quaternary Science Reviews 28(13–14):1257-1267.

Higham T., Jacobi R., Julien M., David F., Basell L., Wood R., Davies W., Bronk Ramsey C. 2010. Chronology of the Grotte du Renne (France) and implications for the context of ornaments and human remains within the Châtelperronian. Proceedings of the National Academy of Sciences 107(47):20234-20239.

Higham T., Compton T., Stringer C., Jacobi R., Shapiro B., Trinkaus E., Chandler B., Groening F., Collins C., Hillson S., O'Higgins P., FitzGerald C., Fagan M. 2011a. The earliest evidence for anatomically modern humans in northwestern Europe. Nature 479(7374):521-524.

Higham T. 2011. European Middle and Upper Palaeolithic radiocarbon dates are often older than they look: problems with previous dates and some remedies. Antiquity 85(327):235-249.

Higham T., Jacobi R., Basell L., Bronk Ramsey C., Chiotti L., Nespoulet R. 2011b. Precision dating of the Palaeolithic: A new radiocarbon chronology for the Abri Pataud (France), a key Aurignacian sequence. Journal of Human Evolution 61(5):549-563.

Higham T., Douka K., Wood R., Bronk Ramsey C., Brock F., Basell L., Camps M., Arrizabalaga A., Baena J., Barroso-Ruiz C., Bergman C., Boitard C., Boscato P., Caparros M., Conard N.J., Draily C., Froment A., Galvan B., Gambassini P., Garcia-Moreno A., Grimaldi S., Haesaerts P., Holt B., Iriarte-Chiapusso M.-J., Jelinek A., Jorda Pardo J.F., Maillo-Fernandez J.-M., Marom A., Maroto J., Menendez M., Metz L., Morin E., Moroni A., Negrino F., Panagopoulou E., Peresani M., Pirson S., de la Rasilla M., Riel-Salvatore J., Ronchitelli A., Santamaria D., Semal P., Slimak L., Soler J., Soler N., Villaluenga A., Pinhasi R., Jacobi R. 2014. The timing and spatiotemporal patterning of Neanderthal disappearance. Nature 512(7514):306-309.

Higham T.F.G., Bronk Ramsey C., Brock F., Baker D., Ditchfield P. 2007. Radiocarbon dates from the Oxford AMS system: Archaeometry datelist 32. Archaeometry 49(s1):S1-S60.

Hoffmann A., Hublin J.-J., Hüls M., Terberger T. 2011. The *Homo aurignaciensis hauseri* from Combe-Capelle – A Mesolithic burial. Journal of Human Evolution 61(2):211-214.

Hoffmann H.M. 2016. Micro radiocarbon dating of the particulate organic carbon fraction in Alpine glacier ice: method refinement, critical evaluation and dating applications: Universität Heidelberg.

Hogg A.G., Hua Q., Blackwell P.G., Niu M., Buck C.E., Guilderson T.P., Heaton T.J., Palmer J.G., Reimer P.J., Reimer R.W., Turney C.S.M., Zimmerman S.R.H. 2013. SHCal13 Southern Hemisphere calibration, 0–50,000 years cal BP. Radiocarbon 55(4):1889-1903.

Hua Q., Zoppi U., Williams A.A., Smith A.M. 2004. Small-mass AMS radiocarbon analysis at ANTARES. Nuclear Instruments and Methods in Physics Research Section B: Beam Interactions with Materials and Atoms 223:284-292.

Hublin J.-J., Talamo S., Julien M., David F., Connet N., Bodu P., Vandermeersch B., Richards M.P. 2012. Radiocarbon dates from the Grotte du Renne and Saint-Césaire support a Neandertal origin for the Châtelperronian. Proceedings of the National Academy of Sciences 109(46):18743-18748.

Hublin J.-J. 2015. The modern human colonization of western Eurasia: when and where? Quaternary Science Reviews 118:194-210.

Hughen K., Lehman S., Southon J., Overpeck J., Marchal O., Herring C., Turnbull J. 2004. ^{14}C activity and global carbon cycle changes over the past 50,000 Years. Science 303(5655):202-207.

Hughen K., Southon J., Lehman S., Bertrand C., Turnbull J. 2006. Marine-derived ^{14}C calibration and activity record for the past 50,000 years updated from the Cariaco Basin. Quaternary Science Reviews 25(23):3216-3227.

Hüls C.M., Grootes P.M., Nadeau M.J. 2009. Ultrafiltration: boon or bane? Radiocarbon 51(2):613-625.

Jacobi R.M., Higham T. 2008. The “Red Lady” ages gracefully: new ultrafiltration AMS determinations from Paviland. Journal of Human Evolution 55(5):898-907.

Jørkov M.L.S., Heinemeier J., Lynnerup N. 2007. Evaluating bone collagen extraction methods for stable isotope analysis in dietary studies. Journal of Archaeological Science 34(11):1824-1829.

Kozłowski J.K. 1982. Excavation in the Bacho Kiro Cave (Bulgaria): Final Report. Warszawa: Państwowe Wydawnictwo Naukowe. 172 p.

Kromer B., Münnich K.O. 1992. CO_2 gas proportional counting in radiocarbon dating—review and perspective. In: Taylor RE, Long A, Kra RS, editors. Radiocarbon after four decades. New York: Springer. p 184-197.

Kromer B., Manning S.W., Kuniholm P.I., Newton M.W., Spurk M., Levin I. 2001. Regional $^{14}CO_2$ offsets in the troposphere: magnitude, mechanisms, and consequences. Science 294(5551):2529-2532.

Kuzmin Y.V. 2019. The older, the better? On the radiocarbon dating of Upper Palaeolithic burials in Northern Eurasia and beyond. Antiquity 93(370):1061-1071.

Lebon M., Reiche I., Gallet X., Bellot-Gurlet L., Zazzo A. 2016. Rapid quantification of bone collagen content by ATR-FTIR spectroscopy. Radiocarbon 58(01):131-145.

Libby W.F., Anderson E.C., Arnold J.R. 1949. Age determination by radiocarbon content: world-wide assay of natural radiocarbon. Science 109(2827):227-228.

Liebl J., Steier P., Golser R., Kutschera W., Mair K., Priller A., Vonderhaid I., Wild E.M. 2013. Carbon background and ionization yield of an AMS system during ^{14}C measurements of microgram-size graphite samples. Nuclear Instruments and Methods in Physics Research Section B: Beam Interactions with Materials and Atoms 294:335-339.

Loftus E., Mitchell P.J., Bronk Ramsey C. 2019. An archaeological radiocarbon database for southern Africa. Antiquity 93(370):870-885.

Longin R. 1971. New method of collagen extraction for radiocarbon dating. Nature 231:241-242.

Manning S.W., Kromer B., Kuniholm P.I., Newton M.W. 2001. Anatolian tree rings and a new chronology for the East Mediterranean Bronze-Iron Ages. Science 294(5551):2532-2535.

Marom A., McCullagh J.S.O., Higham T.F.G., Sinitsyn A.A., Hedges R.E.M. 2012. Single amino acid radiocarbon dating of Upper Paleolithic modern humans. Proceedings of the National Academy of Sciences 109(18):6878-6881.

McCormac F.G., Hogg A.G., Blackwell P.G., Buck C.E., Higham T.F.G., Reimer P.J. 2004. Shcal04 Southern Hemisphere Calibration, 0–11.0 Cal Kyr BP. Radiocarbon 46(3):1087-1092.

Mellars P. 2006. A new radiocarbon revolution and the dispersal of modern humans in Eurasia. Nature 439(7079):931-935.

Middleton R. 1984. A review of ion sources for accelerator mass spectrometry. Nuclear Instruments and Methods in Physics Research Section B: Beam Interactions with Materials and Atoms 5(2):193-199.

Mittnik A., Krause J. 2016. Genetic analysis of the Dolní Věstonice human remains. In: Svoboda J, editor. Dolní Věstonice II: Chronostratigraphy, Paleoethnology, Palaeoanthropology. Brno: Academy of Sciences of the Czech Republic, Institute of Archaeology. p 377-384.

Nadeau M.-J., Huels M., Grootes P., Fernandes R., Kromer B., Lindauer S. 2012. Dating the finds contained in the cenotaph of Queen Editha. In: Meller H, Schenkluhn W, Schmuhl BEH, editors. Königin Editha und ihre Grablegen in Magdeburg. Halle: Landesamt für Denkmalpflege und Archäologie Sachsen-Anhalt - Landesmuseum für Vorgeschichte. p 157-168.

Nalawade-Chavan S., McCullagh J., Hedges R. 2014. New hydroxyproline radiocarbon dates from Sungir, Russia, confirm early Mid Upper Palaeolithic burials in Eurasia. PLoS ONE 9(1):e76896.

Pearson A., McNichol A.P., Schneider R.J., Von Reden K.F., Zheng Y. 1998. Microscale AMS ^{14}C measurement at NOSAMS. Radiocarbon 40(1):61-75.

Pestle W.J., Brennan V., Sierra R.L., Smith E.K., Vesper B.J., Cordell G.A., Colvard M.D. 2015. Hand-held Raman spectroscopy as a pre-screening tool for archaeological bone. Journal of Archaeological Science 58:113-120.

Reimer P.J., Baillie M.G.L., Bard E., Bayliss A., Beck J.W., Bertrand C.J.H., Blackwell P.G., Buck C.E., Burr G.S., Cutler K.B., Damon P.E., Edwards R.L., Fairbanks R.G., Friedrich M., Guilderson T.P., Hogg

A.G., Hughen K.A., Kromer B., McCormac F.G., Manning S.W., Bronk Ramsey C., Reimer R.W., Remmele S., Southon J.R., Stuiver M., Talamo S., Taylor F.W., van der Plicht J., Weyhenmeyer C.E. 2004. IntCal04 terrestrial radiocarbon age calibration, 0-26 cal kyr BP. Radiocarbon 46(3):1029-1058.

Reimer P.J., Baillie M.G.L., Bard E., Bayliss A., Beck J.W., Blackwell P.G., Bronk Ramsey C., Buck C.E., Burr G.S., Edwards R.L., Friedrich M., Grootes P.M., Guilderson T.P., Hajdas I., Heaton T.J., Hogg A.G., Hughen K.A., Kaiser K.F., Kromer B., McCormac F.G., Manning S.W., Reimer R.W., Richards D.A., Southon J.R., Talamo S., Turney C.S.M., van der Plicht J., Weyhenmeyer C.E. 2009. IntCal09 and Marine09 radiocarbon age calibration curves, 0-50,000 years cal BP. Radiocarbon 51(4):1111-1150.

Reimer P.J., Bard E., Bayliss A., Beck J.W., Blackwell P.G., Bronk Ramsey C., Buck C.E., Cheng H., Edwards R.L., Friedrich M., Grootes P.M., Guilderson T.P., Haflidason H., Hajdas I., Hatté C., Heaton T.J., Hoffmann D.L., Hogg A.G., Hughen K.A., Kaiser K.F., Kromer B., Manning S.W., Niu M., Reimer R.W., Richards D.A., Scott E.M., Southon J.R., Staff R.A., Turney C.S.M., van der Plicht J. 2013. IntCal13 and Marine13 radiocarbon age calibration curves 0–50,000 years cal BP. Radiocarbon 55(4):1869–1887.

Reimer P.J., Austin W.E.N., Bard E., Bayliss A., Bronk Ramsey C., Cheng H., Edwards L., Friedrich M., Grootes P.M., Guilderson T.P., Hajdas I., Heaton T.J., Hogg A.G., Hughen K.A., Kromer B., Manning S.W., Muscheler R., Palmer J.G., Pearson C.L., Reimer R.W., Richards D.A., Scott M., Southon J.R., Turney C.S.M., van der Plicht J., Wacker L. 2018. A preview of the IntCal19 radiocarbon calibration curves. 23rd International Radiocarbon conference. Trondheim, Norway.

Renfrew C. 1973. Before civilization: the radiocarbon revolution and prehistoric Europe. New York A.A. Knopf.

Ruff M., Wacker L., Gäggeler H.W., Suter M., Synal H.-A., Szidat S. 2007. A gas ion source for radiocarbon measurements at 200 kV. Radiocarbon 49(2):307-314.

Ruff M., Szidat S., Gäggeler H.W., Suter M., Synal H.-A., Wacker L. 2010a. Gaseous radiocarbon measurements of small samples. Nuclear Instruments and Methods in Physics Research Section B: Beam Interactions with Materials and Atoms 268(7–8):790-794.

Ruff M., Fahrni S., Gäggeler H.W., Hajdas I., Suter M., Synal H.-A., Szidat S., Wacker L. 2010b. On-line radiocarbon measurements of small samples using elemental analyzer and MICADAS gas ion source. Radiocarbon 52(4):1645-1656.

Santos G.M., Moore R.B., Southon J.R., Griffin S., Hinger E., Zhang D. 2007a. AMS ^{14}C sample preparation at the KCCAMS/UCI facility: status report and performance of small samples. Radiocarbon 49(2):255-269.

Santos G.M., Southon J.R., Griffin S., Beaupre S.R., Druffel E.R.M. 2007b. Ultra small-mass AMS C-14 sample preparation and analyses at KCCAMS/UCI Facility. Nuclear Instruments & Methods in Physics Research Section B-Beam Interactions with Materials and Atoms 259(1):293-302.

Scott E.M., Naysmith P., Cook G.T. 2018. Why do we need ^{14}C inter-comparisons?: The Glasgow ^{14}C inter-comparison series, a reflection over 30 years. Quaternary Geochronology 43:72-82.

Smith A.M., Petrenko V.V., Hua Q., Southon J., Brailsford G. 2007. The effect of N_2O, catalyst, and means of water vapor removal on the graphitization of small CO_2 samples. Radiocarbon 49(2):245–254.

Soldatova T. 2019. Spatial distribution and problems in the interpretation of radiocarbon dates of the Sungir site, Russia. Radiocarbon 61(4):e1-e15.

Soressi M., McPherron S.P., Lenoir M., Dogandzic T., Goldberg P., Jacobs Z., Maigrot Y., Martisius N.L., Miller C.E., Rendu W., Richards M., Skinner M.M., Steele T.E., Talamo S., Texier J.P. 2013. Neandertals made the first specialized bone tools in Europe. Proceedings of the National Academy of Sciences 110(35):14186-14190.

Southon J., Noronha A.L., Cheng H., Edwards R.L., Wang Y. 2012. A high-resolution record of atmospheric ^{14}C based on Hulu Cave speleothem H82. Quaternary Science Reviews 33:32-41.
Stafford T.W., Duhamel R.C., Vance Haynes C., Brendel K. 1982. Isolation of proline and hydroxyproline from fossil bone. Life Sciences 31(9):931-938.
Stafford T.W., Hare P.E., Currie L., Jull A.J.T., Donahue D.J. 1991. Accelerator radiocarbon dating at the molecular-level. Journal of Archaeological Science 18(1):35-72.
Steier P., Liebl J., Kutschera W., Wild E.M., Golser R. 2016. Preparation methods of µg carbon samples for ^{14}C measurements. Radiocarbon 59(03):1-12.
Stuiver M., Suess H.E. 1966. On the relationship between radiocarbon dates and true sample ages. Radiocarbon 8:534-540.
Stuiver M., Polach H.A. 1977. Reporting of ^{14}C data. Radiocarbon 19(3):355-363.
Stuiver M., Quay P.D. 1980a. Changes in atmospheric carbon-14 attributed to a variable sun. Science 207(4426):11-19.
Stuiver M., Quay P.D. 1980b. Patterns of atmospheric ^{14}C changes. Radiocarbon 22(2):166-176.
Stuiver M., Reimer P.J., Bard E., Beck J.W., Burr G.S., Hughen K.A., Kromer B., McCormac G., van der Plicht J., Spurk M. 1998. INTCAL98 radiocarbon age calibration, 24,000-0 cal BP. Radiocarbon 40(3):1041-1083.
Svoboda J., Lozek V., Vlcek E. 1996. Hunters between East and West: The Paleolithic of Moravia. New York: Plenum Press.
Svoboda J., van der Plicht J., Kuželka V. 2002. Upper Palaeolithic and Mesolithic human fossils from Moravia and Bohemia (Czech Republic): some new ^{14}C dates. Antiquity 76(294):957-962.
Svoboda J., van der Plicht J., Vlček E., Kuželka V. 2004. New radiocarbon datings of human fossils from caves and rockshelters in Bohemia (Czech Republic). Anthropologie 42(2):161-166.
Svoboda J., editor. 2016. Dolní Věstonice II: Chronostratigraphy, Paleoethnology, Palaeoanthropology. Brno: Academy of Sciences of the Czech Republic, Institute of Archaeology.
Synal H.-A., Stocker M., Suter M. 2007. MICADAS: A new compact radiocarbon AMS system. Nuclear Instruments and Methods in Physics Research Section B: Beam Interactions with Materials and Atoms 259(1):7-13.
Talamo S., Richards M. 2011. A comparison of bone pretreatment methods for AMS dating of samples >30,000 BP. Radiocarbon 53(3):443-449.
Talamo S., Soressi M., Roussel M., Richards M., Hublin J.-J. 2012. A radiocarbon chronology for the complete Middle to Upper Palaeolithic transitional sequence of Les Cottes (France). Journal of Archaeological Science 39(1):175-183.
Talamo S., Hajdinjak M., Mannino M.A., Fasani L., Welker F., Martini F., Romagnoli F., Zorzin R., Meyer M., Hublin J.-J. 2016a. Direct radiocarbon dating and genetic analyses on the purported Neanderthal mandible from the Monti Lessini (Italy). Scientific Reports 6:29144.
Talamo S., Blasco R., Rivals F., Picin A., Gema Chacón M., Iriarte E., Manuel López-García J., Blain H.-A., Arilla M., Rufà A., Sánchez-Hernández C., Andrés M., Camarós E., Ballesteros A., Cebrià A., Rosell J., Hublin J.-J. 2016b. The radiocarbon approach to Neanderthals in a carnivore den site: a well-defined chronology for Teixoneres Cave (Moià, Barcelona, Spain). Radiocarbon 58(02):247-265.
Taylor R.E. 2001. Radiocarbon Dating. In: Brothwell DR, Pollard AM, editors. Handbook of Archaeological Sciences. London: John Wiley & Sons, Ltd. p 23-34.
Taylor R.E., Bar-Yosef O. 2014. Radiocarbon Dating: An Archaeological Perspective. Walnut Creek, CA: Left Coast Press.
Tillier A.M., Mester Z., Bocherens H., Henry-Gambier D., Pap I. 2009. Direct dating of the "Gravettian" Balla child's skeleton from Bukk Mountains (Hungary): unexpected results. Journal of Human Evolution 56(2):209-212.

Toussaint M., Pirson S. 2006. Neandertal studies in Belgium: 2000-2005. Periodicum Biologorum 108:373-387.

Trinkaus E., Jelinek J., Pettitt P.B. 1999. Human remains from the Moravian Gravettian: the Dolní Věstonice 35 femoral diaphysis. Anthropologie 37(2):167-175.

Trinkaus E., Pettitt P. 2000. The Krems-Hundssteig "Gravettian" human remains are Holocene. HOMO 51(2):258-260.

Trinkaus E., Svoboda J., editors. 2006. Early Modern Human Evolution in Central Europe: the People of Dolní Věstonice and Pavlov. New York: Oxford University Press.

van Klinken G.J., Mook W.G. 1990. Preparative high-performance liquid chromatographic separation of individual amino acids derived from fossil bone collagen. Radiocarbon 32(2):155-164.

van Klinken G.J. 1999. Bone collagen quality indicators for palaeodietary and radiocarbon measurements. Journal of Archaeological Science 26:687–695.

Vermeersch P.M. 2019. Radiocarbon Palaeolithic Europe Database, Version 25. http://ees.kuleuven.be/geography/projects/14c-palaeolithic/index.html.

Wacker L., Bonani G., Friedrich M., Hajdas I., Kromer B., Nemec N., Ruff M., Suter M., Synal H.-A., Vockenhuber C. 2010. MICADAS: routine and high-precision radiocarbon dating. Radiocarbon 52(2-3):252–262.

Wacker L., Lippold J., Molnár M., Schulz H. 2013a. Towards radiocarbon dating of single foraminifera with a gas ion source. Nuclear Instruments and Methods in Physics Research Section B: Beam Interactions with Materials and Atoms 294:307-310.

Wacker L., Fahrni S.M., Hajdas I., Molnar M., Synal H.-A., Szidat S., Zhang Y.L. 2013b. A versatile gas interface for routine radiocarbon analysis with a gas ion source. Nuclear Instruments and Methods in Physics Research Section B: Beam Interactions with Materials and Atoms 294:315-319.

Walter S.R.S., Gagnon A.R., Roberts M.L., McNichol A.P., Gaylord M.C.L., Klein E. 2015. Ultra-small graphitization reactors for ultra-microscale ^{14}C analysis at the National Ocean Sciences accelerator mass spectrometry (NOSAMS) facility. Radiocarbon 57(1):109-122.

Welker F., Hajdinjak M., Talamo S., Jaouen K., Dannemann M., David F., Julien M., Meyer M., Kelso J., Barnes I., Brace S., Kamminga P., Fischer R., Kessler B.M., Stewart J.R., Pääbo S., Collins M.J., Hublin J.-J. 2016. Palaeoproteomic evidence identifies archaic hominins associated with the Châtelperronian at the Grotte du Renne. Proceedings of the National Academy of Sciences 113(40):11162–11167.

White M., Pettitt P. 2012. Ancient Digs and Modern Myths: The Age and Context of the Kent's Cavern 4 Maxilla and the Earliest *Homo sapiens* Specimens in Europe. European Journal of Archaeology 15(3):392-420.

Willis E.H., Tauber H., Münnich K.O. 1960. Variations in the atmospheric radiocarbon concentration over the past 1300 years. Radiocarbon 2:1-4.

Wood R. 2015. From revolution to convention: the past, present and future of radiocarbon dating. Journal of Archaeological Science 56:61-72.

Wood R.E., Douka K., Boscato P., Haesaerts P., Sinitsyn A., Higham T.F.G. 2012. Testing the ABOx-SC method: dating known-age charcoals associated with the Campanian Ignimbrite. Quaternary Geochronology 9:16-26.

Wood R.E., Barroso-Ruíz C., Caparrós M., Jordá Pardo J.F., Galván Santos B., Higham T.F.G. 2013. Radiocarbon dating casts doubt on the late chronology of the Middle to Upper Palaeolithic transition in southern Iberia. Proceedings of the National Academy of Sciences 110(8):2781.

Zhang Y.L., Huang R.J., El Haddad I., Ho K.F., Cao J.J., Han Y., Zotter P., Bozzetti C., Daellenbach K.R., Canonaco F., Slowik J.G., Salazar G., Schwikowski M., Schnelle-Kreis J., Abbaszade G., Zimmermann R., Baltensperger U., Prévôt A.S.H., Szidat S. 2015. Fossil vs. non-fossil sources of

fine carbonaceous aerosols in four Chinese cities during the extreme winter haze episode of 2013. Atmospheric Chemistry and Physics 15(3):1299-1312.
Zilhão J. 2013. Neandertal-Modern Human Contact in Western Eurasia: Issues of Dating, Taxonomy, and Cultural Associations. In: Akazawa T, Nishiaki Y, Aoki K, editors. Dynamics of Learning in Neanderthals and Modern Humans Volume 1: Cultural Perspectives. Tokyo: Springer. p 21-57.

Chapter Two

Size matters: radiocarbon dates of <200 µg ancient collagen samples with AixMICADAS and its gas ion source

H. Fewlass, S. Talamo, T. Tuna, Y. Fagault, B. Kromer, H. Hoffmann, C. Pangrazzi, J.-J. Hublin, E. Bard

Published in *Radiocarbon*, 2018, volume 60, issue 02, pages 425-439
DOI:10.1017/RDC.2017.98

Radiocarbon, Vol 60, Nr 2, 2018, p 425–439
DOI:10.1017/RDC.2017.98

SIZE MATTERS: RADIOCARBON DATES OF <200 µg ANCIENT COLLAGEN SAMPLES WITH AIXMICADAS AND ITS GAS ION SOURCE

Helen Fewlass[1*] · Sahra Talamo[1] · Thibaut Tuna[2] · Yoann Fagault[2] · Bernd Kromer[1,3] · Helene Hoffmann[3] · Caterina Pangrazzi[4] · Jean-Jacques Hublin[1] · Edouard Bard[2]

[1]Department of Human Evolution, Max-Planck Institute for Evolutionary Anthropology, Leipzig, Germany.
[2]CEREGE, Aix-Marseille University, CNRS, IRD, Collège de France, Aix-en-Provence, France.
[3]Institut für Umweltphysik, University of Heidelberg, Heidelberg, Germany.
[4]Dipartimento di Lettere e Filosofia, Università degli studi di Trento, Trento, Italy.

ABSTRACT. For many of archaeology's rarest and most enigmatic bone artifacts (e.g. human remains, bone ornaments, worked bone), the destruction of the 500 mg material necessary for direct accelerator mass spectrometry (AMS) dating on graphite targets would cause irreparable damage; therefore many have not been directly dated. The recently improved gas ion source of the MICADAS (MIni CArbon DAting System) offers a solution to this problem by measuring gaseous samples of 5–100 µg carbon at a level of precision not previously achieved with an AMS gas ion source. We present the results of the first comparison between "routine" graphite dates of ca. 1000 µg C (2–3 mg bone collagen) and dates from aliquots of gaseous samples of <100 µg C (<0.2 mg bone collagen), undertaken with the highest possible precision in mind. The experiment demonstrates the performance of the AixMICADAS in achieving reliable radiocarbon measurements from <0.2 mg collagen samples back to 40,000 ^{14}C BP. The technique has great implications for resolving chronological questions for key archaeological artifacts.

KEYWORDS: accelerator mass spectrometry, archaeology, collagen, gas ion source, radiocarbon.

INTRODUCTION

The development of accelerator mass spectrometry (AMS) revolutionized the field of radiocarbon (^{14}C) dating by reducing required sample sizes from grams to milligrams. This was an especially crucial improvement for the field of archaeology, and for decades the technique has been central for establishing reliable chronologies back to 50,000 cal BP (calibrated years before 1950). In order to produce enough high-quality collagen for AMS dating on solid targets, current pretreatment protocols for archaeological bone samples require ca. 500 mg material for collagen extraction, ultrafiltration, and graphitization (Longin 1971; Brown et al. 1988; Ramsey et al. 2004a; Higham et al. 2006; Talamo and Richards 2011). However, rare and precious bone samples of such antiquity (including Middle-Upper Paleolithic human remains, bone tools, worked bones and ornaments) are often small or fragmented and the destruction of even 500 mg would result in irreparable damage.

Several AMS labs have worked on developing techniques for measuring samples <0.5 mg carbon on graphite targets (Pearson 1998; Hua et al. 2004; Santos et al. 2007a; Santos et al. 2007b; Smith et al. 2007; Ertun et al. 2005; de Rooij et al. 2010; Genberg et al. 2010; Smith et al. 2010; Delqué-Količ et al. 2013; Liebl et al. 2013; Walter et al. 2015). However, the latest developments in AMS technology now offer an alternative solution for the high-precision measurement of samples of 100 µg carbon or less. AMS instruments with a gas ion source have offered a practical way to measure ^{14}C since the 1980s (Middleton 1984; Bronk and Hedges 1987; Ramsey and Hedges 1997). The direct measurement of sample CO_2 in a gas ion source cuts out the graphitization step, reducing the required sample size and risk of contamination while speeding up the dating procedure, making it a highly attractive prospect. Although successful in measuring ^{14}C of small samples in environmental applications, the low ion currents obtained during initial use (<5 µA compared to currents of >40 µA using graphite) meant that the precision required for archaeological questions was not possible (Ramsey et al. 2004b; Uhl et al. 2005). However, AMS has considerably improved over the past decade.

*Corresponding author. Email: helen_fewlass@eva.mpg.de.

The MICADAS (MIni CArbon DAting System), the first compact AMS with a hybrid ion source, was developed at ETH Zurich (Ruff et al. 2007; Synal et al. 2007). Initial use demonstrated the extraordinary reproducibility and stability of the instrument, and thus its suitability for high-precision measurement (Wacker et al. 2010b). Measurements over a 2-yr period in Zurich indicated that contamination issues were much smaller for gaseous samples compared to small graphite samples, as well as more constant (Ruff et al. 2010a). Following several years of operation, the gas ion source was updated for increased precision (Fahrni et al. 2013). The MICADAS offers a way to measure gaseous samples of 5–100 µg carbon (Wacker et al. 2013b), and the newest improvements resulted in a more than threefold increase of the ion current (15–20 µA) compared to the previous versions, essential for precision (Fahrni et al. 2013; Hendriks et al. 2016).

These gas ion sources have thus far been utilized for the measurement of small (<100 µg carbon) and ultra-small (<10 µg carbon) samples of gaseous carbon from ice samples (Hoffmann 2016), aerosols (Zhang et al. 2015; Bonvalot et al. 2016) and carbonates (Wacker et al. 2013a; Bard et al. 2015) where samples sizes were small (generally <30 µg C) but precision was not of highest concern. On the contrary, the gas ion source of the MICADAS has neither been tested for samples towards the limit of the method e.g. Middle-Upper Paleolithic transition, nor for collagen samples.

Our primary goal for this present study was therefore to test the instrument capabilities using this updated measurement technique specifically for collagen samples toward the ^{14}C limit. In order to test the precision and accuracy achievable across the range of the ^{14}C method, we converted collagen from medieval human bone and Pleistocene faunal bone samples to CO_2 using three different preparatory techniques and dated them using the gas interface system (GIS) coupled to the gas ion source of AixMICADAS (Bard et al. 2015). We present here a comparison of "routine" 2–3 mg collagen dates (≥1000 µg carbon on graphite targets) with dates from small gaseous samples of <100 µg carbon, demonstrating the reliable measurement of precise ^{14}C dates across the breadth of the method with a greater than tenfold decrease in sample size.

METHODS

Archaeological Samples

We selected a human bone and a human tooth sample from two early medieval burial contexts in San Martino and Palazzo Fulcis, Northern Italy. In order to test the method on samples of Pleistocene age we selected mammoth and bison bones from Brown Bank on the North Sea plains. These samples were previously described and dated by Talamo and Richards (2011).

Pretreatment

Many preparation issues concerning collagen yield, contamination, reproducibility, and blanks are associated with the extraction of small bone samples (<100 mg). However, as this paper focuses on the AMS measurement techniques, initially a large quantity of collagen was prepared as outlined below, and from these batches microgram-size samples were selected for MICADAS analysis. This strategy was adopted to allow us to differentiate between the instrumental limitations and those associated with the pretreatment of small bone samples. Pretreatment of <100 mg bone samples will be discussed elsewhere (Fewlass et al. in prep.).

Bones (500–700 mg material) were pretreated in the Department of Human Evolution at the Max Planck Institute for Evolutionary Anthropology in Leipzig, Germany (lab code: R-EVA),

following our standard collagen pretreatment protocol: acid-base-acid followed by ultrafiltration (Talamo and Richards 2011). In order to monitor contamination introduced during the pretreatment stage, a background cave bear bone (R-EVA 800) kindly provided by D. Döppes (Mannheim, Germany) was extracted with each batch of samples (throughout we refer to measurements of this bone as "background," in contrast to "blank," which refers to blank instrumental levels). Elemental and stable isotopic data (C% and N% content, C:N, $\delta^{13}C$, and $\delta^{15}N$) of extracted collagen from all samples was measured in-house at the MPI-EVA. Collagen yields were sufficiently high from all samples to allow the collagen to be split into multiple aliquots and submitted for dating using a range of techniques (Table 1).

Graphitization

Our initial step was to date the collagen via our regular dating routine. In order to obtain independent dates, collagen was sent to two AMS laboratories. Ca. 5 mg collagen from each sample was weighed into pre-cleaned tin cups at the MPI-EVA and sent to the Klaus-Tschira-AMS facility in Mannheim, Germany (lab code: MAMS). The samples were combusted in an elemental analyzer (EA) and CO_2 was converted catalytically to graphite. The samples were dated using the MICADAS-AMS (Kromer et al. 2013). The error calculation was performed using BATS software (Wacker et al. 2010a), with background collagen samples and standards used for the age calculation of the unknown samples, plus an added external error of 1‰, as per their standard practice (R. Friedrich, personal communication).

Collagen was also measured at the Centre de Recherche et d'Enseignement de Geosciences de l'Environnement (CEREGE) in Aix-en-Provence, France (lab code: AIX), where two samples of ca. 2 mg collagen from each bone were weighed into tin cups and graphitized using the AGE III (Automated Graphitization Equipment, IonPlus AG, Switzerland) (Wacker et al. 2010c) and dated using the AixMICADAS (Bard et al. 2015). Oxalic acid standards and background collagen samples run in the same batch were used in the age calculation of the unknown samples. An additional external error of 1‰ was also propagated in the uncertainty calculation.

Conversion to CO_2

We employed three methods of extracting and purifying CO_2 from collagen in order to monitor sources of contamination and identify the optimum route.

Method 1. CEREGE in Aix-en-Provence: EA directly coupled to the gas ion source via zeolite trap

Four collagen aliquots (each 170 µg) from each bone sample were weighed into cleaned (800°C, 2 hr) silver cups. These were placed into the auto-sampler of an Elementar Vario MICRO cube EA (Elementar Analysensysteme GmbH, Germany) directly coupled to the gas ion source of the AixMICADAS via a gas interface system (GIS). Following combustion, sample CO_2 was adsorbed on a zeolite trap. After heating of the trap, the CO_2 was released and expanded to the syringe of the GIS (Ruff et al. 2010b; Wacker et al. 2013b).

Method 2. MPI-EVA in Leipzig: EA coupled to cryogenic gas collection system

For the second method of CO_2 preparation, collagen was converted to CO_2 at the MPI-EVA using a SerCon ANCA SL EA coupled to an Oxford gas collection system. From each sample four aliquots of 170 µg collagen were weighed out on a microbalance into cleaned (800°C, 2 hr) silver cups and placed in the auto-sampler of the EA. Samples were combusted and CO_2 and N_2 were separated. A small proportion of CO_2 and N_2 gas was diverted for isotopic measurement

in a SERCON 20-20 mass spectrometer. The rest of the CO_2 was diverted to the gas collection system where it was cryogenically purified and trapped into borosilicate glass ampoules (80 mm length, 4 mm diameter) which were flame-sealed. These ampoules were then measured by means of the cracker of the AixMICADAS in Aix-en-Provence (Wacker et al. 2013b). Phthalic acid (≥99.5%) blank samples were run prior to and following sample runs. Blanks (cleaned silver cups) were run between aliquots to monitor instrumental contamination and purge the system.

Method 3. University of Heidelberg: sealed tube combustion and vacuum line

The extraction and purification of CO_2 from bone collagen was also achieved manually using a vacuum line at the Institute of Environmental Physics, University of Heidelberg, adapted from the CARMEN (Carbon AeRosol Muffel Extraction liNe), designed by Hammer (2003) for aerosol filters. This method was carried out for background and medieval samples only due to time constraints. Silver wool was inserted to the bottom of cleaned quartz tubes (150 mm length, 6.5 mm internal diameter; 850°C, 2 hr) to catch sulfur and halides during combustion. Collagen was weighed out using a microbalance and inserted to the bottom of the quartz tubes. Individual sample tubes were inserted into the vacuum line. The line was evacuated while the sample tube was heated to 70°C. The quartz tube was flooded with oxygen (450–550 mbar) and flame-sealed, as wire-form copper oxide was previously found to introduce tiny amounts of carbon to the sample (Hoffmann, personal communication). Samples were combusted for 6 hr at 800°C. Quartz tubes were then broken in the vacuum line and sample CO_2 was isolated from the other combustion products using liquid nitrogen (77 K) and acetone dry ice (195 K) cold traps. The CO_2 was trapped in a region of known volume and quantified through temperature and pressure readings. The sample was then cryogenically captured in the final sample ampoule (80 mm length, 4 mm diameter) which was flame-sealed, and measured via the cracker of the AixMICADAS.

AMS Measurement with the Gas Ion Source of AixMICADAS

Oxalic acid II NIST standards (gas canister) were measured to normalize and correct samples for fractionation and blank CO_2 (gas canister) was measured to purge the system and check the blank level of AixMICADAS in gas configuration prior to measurement of samples (0.4 pMC threshold) (not used in sample age calculation). Samples containing carbonate reference material (blank IAEA-C1) were run prior to samples of method 1 to begin the measurement of old samples under optimal conditions. The different samples were measured in order of increasing activity (i.e. from oldest to youngest), as per standard procedure (Wacker et al. 2013a). Sample CO_2 released from the ampoules or zeolite trap was expanded to the syringe where it was mixed with He (5% CO_2). The mixture was introduced to the gas ion source at a flow rate of ca. 2 µg C/min. The system was flushed with helium between samples. The target magazine can hold up to 39 new titanium (Ti) gas targets which can be changed during measurement. Targets were pre-sputtered for ca. 2 minutes in the ion source to remove any remaining surface contamination before the sample CO_2 injection. All steps of the process were fully controlled via the gas-interface handling software. In the software BATS (Wacker et al. 2010a) the uncorrected background collagen samples (cave bear bone R-EVA 800) were used in the age calculation of the four unknown archaeological samples (shown in Tables 3–6).

The gas ion source of the MICADAS has been predominantly used for measuring samples limited by C amount (<30 µg C), whereas for collagen samples a reduction in sample size to 50–100 µg C still represents a sizeable decrease compared to standard dating on graphite targets (>500 µg C). Therefore, for this exploratory test relatively large samples were combusted in order to reach

maximum precision. However, as any C above the limit of 100 µg C in the syringe after combustion/cracking leads to a flushing of excess sample, only around 170 µg collagen (ca. 70–80 µg C) was measured out. During measurement only 30–40 µg C was consumed for the AMS due to a typical degradation of the Ti target performance (Fahrni et al. 2013) and the rest was lost. In future we would measure out a suitable sample size (30–40 µg C in 70–80 µg collagen) for one target. The measurement of a large sample (>40 µg C) over a second or even a third Ti target has been performed on carbonate samples using the AixMICADAS with positive outcomes (Fagault et al. 2017; Tuna et al. 2017). Although this was not carried out for collagen samples during this preliminary study, such a strategy is an interesting avenue for further exploration.

RESULTS AND DISCUSSION

Preservation

For all samples the elemental and stable isotopic data indicate well-preserved collagen, and are well within the acceptable range (C:N = 2.9–3.6) (van Klinken 1999) (Table 1). All samples produced a collagen yield of >10%, confirming a high level of preservation, hence their suitability for dating (Ambrose 1990; van Klinken 1999) (Table 1).

Dating on Graphite Targets

The results of samples measured on solid targets in the two labs, MAMS and AIX, are in agreement (Table 2; Figure 1). The Italian samples date to the early medieval period as expected from the archaeological context. The dates of the mammoth bone fall perfectly within the range found previously (Talamo and Richards 2011). The ages of the bison bone reported here are the oldest yet for this specimen. The oldest dates obtained by Talamo and Richards (2011) were >44,800 BP (conventional ^{14}C yr before AD 1950) from collagen extracted, ultra-filtered, graphitized and dated at the Oxford Radiocarbon Accelerator Unit (ORAU) and from collagen extracts pretreated at the MPI-EVA and subsequently graphitized and dated at ORAU (47,300 +910/–820 BP) and MAMS (47,000 +1190/–1040 BP). All measurements in the previous study were also corrected for collagen extraction backgrounds and standards measured in the same batch. The older ages of the bison bone obtained on graphite targets in this study may be a reflection of the updated pretreatment method now employed at the MPI-EVA, as well as stringent contamination criteria observed at MAMS and AIX during the graphitization

Table 1 Elemental and stable isotopic data (C%, N%, C:N, δ^{13}C and δ^{15}N), and collagen yields of the collagen extracts measured in-house at the MPI-EVA on a ThermoFinnigan Delta V Advantage isotope ratio mass spectrometer coupled to a Flash 2000 EA. Stable carbon isotope ratios were expressed relative to VPDB (Vienna PeeDee Belemnite) and stable nitrogen isotope ratios were measured relative to AIR (atmospheric N_2), using the delta notation (δ) in parts per thousand (‰). Repeated analysis of both internal and international standards indicates an analytical error of 0.2 ‰ (1σ) for δ^{13}C and δ^{15}N.

Material	MPI-EVA lab code	Site	δ^{13}C ‰)	δ^{15}N (‰)	C%	N%	C:N	Collagen (%)
Background	R-EVA 800.30	Austria	−21.1	0.0	46.7	17.1	3.2	14.1
Cave bear bone	R-EVA 800.33	Austria	−21.3	−0.2	46.4	17.5	3.1	7.6
Bison bone	R-EVA 124.43	North Sea Plains	−20.0	3.3	45.9	17.2	3.1	11.7
Mammoth bone	R-EVA 123.53	North Sea Plains	−21.1	7.1	45.6	16.9	3.2	11.2
Human tooth	R-EVA 1516.1	Belluno Palazzo Fulcis	−16.5	9.7	44.8	16.4	3.2	17.7
Human bone	R-EVA 1489.1	San Martino Lundo Lomaso	−16.4	8.8	45.4	16.7	3.2	17.9

Table 2 Results from collagen samples measured on graphite targets at MAMS and AIX. Both labs used ^{12}C currents on graphite targets in the order of 40 µA (low energy side). In Aix, the collagen background measurements (R-EVA 800) had a standard deviation of 0.01 pMC (5%). Rather than propagating this variation in the error calculation of the unknown samples, a conservative value of 0.04 pMC (20%) was used based on observed long-term reproducibility of Phthalic acid standards. An additional 0.1 pMC relative variability was included in the error propagation to take into account the long-term variation on OXA2 standards. In MAMS, samples were corrected for collagen back-ground measurements (cave bear R-EVA 800) and standards run in the same batch using BATS software, with an added external error of 0.1 pMC as per their standard practice. Asymmetrical age uncertainties are shown where pMC ≤ error × 10. All ages >15,000 BP are rounded to nearest 10 yr.

		MAMS					AixMICADAS				
Material	MPI-EVA lab code	Lab code	pMC	±	^{14}C age BP (yr)	± (yr)	Lab code	pMC	±	^{14}C age BP (yr)	± (yr)
Background cave bear bone* (used in correction of unknown samples)	R-EVA 800.30	MAMS-26330	0.27	0.02	47430	480	Aix-12001.1.2	0.21	0.01	49630	410
		MAMS-26331	0.27	0.02	47590	470	Aix-12001.1.3	0.22	0.01	49310	400
		MAMS-26332	0.33	0.02	45920	470					
			weighted mean		**47020**	**270**					
	R-EVA 800.33	MAMS-26878	0.20	0.01	50120	600	Aix-12000.1.2	0.20	0.01	49990	360
							Aix-12000.1.3	0.19	0.01	50280	370
								weighted mean		**49850**	**190**
Bison bone	R-EVA 124.43	MAMS-26877	0.19	0.04	50150	+2080/−1650	Aix-12002.1.2	0.22	0.04	49300	+1610/−1340
							Aix-12002.1.3	0.23	0.04	48800	+1530/−1290
								weighted mean		**49040**	**+1040/−920**
Mammoth bone	R-EVA 123.53	MAMS-26876	1.4	0.05	34360	300	Aix-12003.1.1	1.38	0.04	34390	240
							Aix-12003.1.2	1.40	0.04	34320	240
								weighted mean		**34350**	**170**
Human tooth	R-EVA 1516.1	MAMS-26328	83.6	0.2	1436	23	Aix-12005.1.1	82.99	0.18	1498	18
							Aix-12005.1.2	83.38	0.18	1460	18
								weighted mean		**1479**	**13**
Human bone	R-EVA 1489.1	MAMS-26317	83.2	0.2	1481	23	Aix-12004.1.1	83.07	0.18	1490	17
							Aix-12004.1.2	83.28	0.18	1470	17
								weighted mean		**1480**	**12**

*R-EVA 800.30 and R-EVA 800.33 represent two separate collagen extractions from one bone (R-EVA 800). R-EVA 800.30 was extracted alongside the medieval samples, and R-EVA 800.33 was extracted alongside the Paleolithic samples.

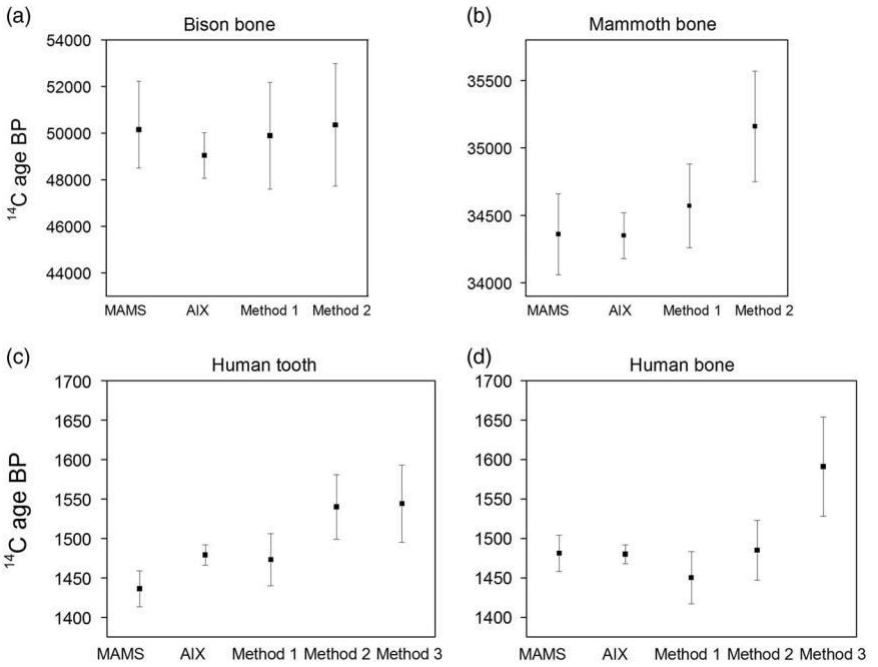

Figure 1 Comparison of graphite dates from MAMS and AixMICADAS against the CO_2 weighted mean dates and weighted errors (error 2 in Tables 3–5) of replicates for the four bone samples: (a) R-EVA 124.43, (b) R-EVA 123.53, (c) R-EVA 1516.1, and (d) R-EVA 1489.1. MAMS graphite dates are the results of a single run, whereas AixMICADAS graphite dates are the weighted mean of two replicates, shown in Table 2. Errors are shown to 1σ. In part (d) the mean value for method 3 is somewhat older and less precise than all other values. This mean for method 3 is only based on two replicates, which are not overlapping at 1σ: 1521 ± 80 and 1708 ± 100 BP. The first replicate agrees with those of other methods, while the second and older value is clearly an outlier. More data and work are needed to decipher the cause of this.

process, and further instrumental improvements. We conclude that the agreement between results of large samples measured on solid targets at MAMS and with the AixMICADAS provide a suitable reference dataset for comparison to small gaseous samples measured with the gas ion source of AixMICADAS.

CO_2 Dating

Tables 3–5 show the results of measurements of collagen CO_2 samples, prepared via three different techniques (methods 1–3). Results are shown in both ^{14}C years and percent modern carbon (pMC = $F^{14}C \times 100$). The first error column (error 1) in the tables shows the error calculated in BATS (Wacker et al. 2010a) propagating only the variance of the standards and collagen backgrounds included in the same batch as the samples. A second error (error 2 column in Tables 3–5) has also been calculated based on observed data. This added external error has been calculated from the long term variabilities observed on CO_2 blanks (0.1 pMC long-term standard deviation of blanks is used as the absolute blank error) and oxalic acid standards (3.5‰ relative error added). While the minimal error propagation of the first error column is optimistic, the second column may represent an overestimation of error as these measurements were made over a short period of time. A comparison of dates from each method is shown in Figure 1, using the weighted means and weighted errors (error 2) of the data in Tables 3–5.

Table 3 Results of AMS measurements using the gas ion source of AixMICADAS for collagen CO_2 samples prepared via method 1. The background cave bear concentrations have been subtracted from all four unknown samples, including the bison bone. The measured mass shows the amount of carbon (µg) trapped in the syringe after expansion; in reality only 20–40 µg C was used for each measurement. All errors are shown to 1σ: the error 1 column shows the minimal error, corrected for standards and backgrounds measured in the same batch. The error 2 column includes an external error taking into account long-term variability on standards (3.5‰ relative error added) and blanks (the 0.1 pMC long term standard deviation of blanks is used as the absolute blank error). The results with lab codes including asterisks (*) were measured as preliminary runs of limited duration which explains their lower precision and higher scatter (hence, error 2 is equal to error 1). Asymmetrical age uncertainties are shown where pMC ≤ error × 10. "Older than" ages have been calculated at 2σ, according to convention in van der Plicht and Hogg (2006). All ages >15,000 BP are rounded to nearest 10 yr.

Method 1: EA directly coupled to the gas ion source via zeolite trap

Material	MPI-EVA lab code	AIX lab code	Measured mass (C µg)	Run time (s)	pMC	Error 1 pMC ±	Error 2 pMC ±	^{14}C age BP (yr)	Error 1 (yr) (1σ)	Error 2 (yr) (1σ)
Background cave bear bone	R-EVA 800.33	Aix-12000.2.1*	88	374	0.72	0.11		39580	+1320/−1140	
(used in correction of	R-EVA 800.33	Aix-12000.2.2*	92	446	0.74	0.10		39450	+1170/−1020	
unknown samples)	R-EVA 800.33	Aix-12000.2.3*	96	446	0.53	0.07		42120	+1140/−1000	
	R-EVA 800.33	Aix-12000.5.4	87	576	0.61	0.05		40950	660	
	R-EVA 800.30	Aix-12001.5.1	84	403	0.66	0.06		40290	760	
	R-EVA 800.30	Aix-12001.5.2	86	748	0.68	0.05		40130	570	
			weighted mean		**0.64**	**0.03**		**40550**	**330**	
Bison bone	R-EVA 124.43	Aix-12002.4.1	84	331	0.11	0.10	0.12		>46400	>45430
		Aix-12002.4.2	89	561	0.21	0.08	0.11	49530	+3850/−2590	>43770
		Aix-12002.4.3	80	547	0.24	0.09	0.11	48610	+3780/−2560	+4930/-3030
		Aix-12002.4.4	74	547	0.22	0.08	0.11	48980	+3630/−2490	>43590
			weighted mean		**0.20**	**0.04**	**0.06**	**49890**	**+1790/−1460**	**+2690/-2010**
Mammoth bone	R-EVA 123.53	Aix-12003.2.1*	89	418	1.32	0.18	0.18	34750	+1180/−1030	+1180/-1030
		Aix-12003.2.2*	96	475	1.25	0.17	0.17	35210	+1170/−1020	+1170/-1020
		Aix-12003.2.3*	96	575	1.41	0.15	0.15	34250	+900/−810	+900/-810
		Aix-12003.5.1	89	490	1.41	0.11	0.13	34260	620	750
		Aix-12003.5.2	78	590	1.31	0.10	0.13	34820	620	770
		Aix-12003.5.3	75	993	1.33	0.08	0.11	34710	510	675
		Aix-12003.5.4	98	633	1.41	0.11	0.13	34260	630	760
			weighted mean		**1.35**	**0.04**	**0.05**	**34570**	**260**	**310**
Human tooth	R-EVA 1516.1	Aix-12005.3.1	71	619	83.25	0.61	0.69	1473	59	67
		Aix-12005.3.2	72	590	83.07	0.68	0.75	1490	65	73
		Aix-12005.3.3	69	978	82.88	0.51	0.60	1508	49	59
		Aix-12005.3.4	69	431	84.11	0.69	0.77	1390	66	73
			weighted mean		**83.25**	**0.30**	**0.35**	**1473**	**29**	**33**
Human bone	R-EVA 1489.1	Aix-12004.3.1	84	561	84.00	0.72	0.79	1401	68	75
		Aix-12004.3.2	74	561	82.65	0.67	0.74	1530	65	72
		Aix-12004.3.3	77	921	83.03	0.53	0.62	1494	51	60
		Aix-12004.3.4	74	633	84.34	0.59	0.68	1368	56	65
			weighted mean		**83.50**	**0.31**	**0.35**	**1450**	**30**	**33**

Table 4 Results of AMS measurement using the gas ion source of AixMICADAS for collagen CO_2 samples prepared via method 2. Columns: see Table 3.

Method 2: EA coupled to cryogenic gas collection system										
Material	MPI-EVA lab code	AIX lab code	Measured mass (C µg)	Run time (s)	pMC	Error 1 pMC ±	Error 2 pMC ±	^{14}C age BP (yr)	Error 1 (yr) (1σ)	Error 2 (yr) (1σ)
Background cave bear bone (used in correction of unknown samples)	R-EVA 800.33	Aix-12000.3.1	75	475	0.64	0.06		40560	700	
	R-EVA 800.33	Aix-12000.3.2	74	489	0.73	0.07		39550	770	
	R-EVA 800.30	Aix-12001.2.1	61	504	0.69	0.06		39980	740	
	R-EVA 800.30	Aix-12001.2.2	76	417	0.54	0.07		41910	+1120/−980	
	R-EVA 800.30	Aix-12001.2.4	81	403	0.59	0.07		41280	+1010/−900	
			weighted mean		**0.64**	**0.03**		**40590**	**360**	
Bison bone	R-EVA 124.43	Aix-12002.2.2	69	561	0.29	0.09	0.11	47080	+2980/−2170	+3830/−2580
		Aix-12002.2.3	77	633	0.08	0.09	0.11		>47810	>46660
		Aix-12002.2.4	77	576	0.21	0.09	0.11	49420	+4500/−2870	>43770
			weighted mean		**0.19**	**0.05**	**0.06**	**50350**	**+2450/−1880**	**+3050/−2200**
Mammoth bone	R-EVA 123.53	Aix-12003.3.1	67	576	1.16	0.11	0.13	36120	800	+950/−850
		Aix-12003.3.2	79	504	1.25	0.11	0.13	35180	720	+880/−790
		Aix-12003.3.3	81	547	1.26	0.12	0.13	35140	760	+870/−790
		Aix-12003.3.4	69	561	1.42	0.12	0.13	34160	670	750
			weighted mean		**1.26**	**0.06**	**0.06**	**35160**	**370**	**410**
Human tooth	R-EVA 1516.1	Aix-12005.2.1	69	489	82.45	0.88	0.92	1561	86	90
		Aix-12005.2.2	74	403	82.29	0.95	0.99	1577	93	96
		Aix-12005.2.3	67	532	83.60	0.70	0.75	1449	68	72
		Aix-12005.2.4	71	533	82.07	0.70	0.79	1599	73	77
			weighted mean		**82.57**	**0.40**	**0.42**	**1540**	**39**	**41**
Human bone	R-EVA 1489.1	Aix-12004.4.1	71	547	82.43	0.75	0.79	1563	73	77
		Aix-12004.4.2	79	576	83.00	0.76	0.80	1507	73	78
		Aix-12004.4.3	74	590	83.60	0.73	0.77	1449	70	74
		Aix-12004.4.4	72	561	83.87	0.74	0.77	1424	71	75
			weighted mean		**83.12**	**0.37**	**0.39**	**1485**	**36**	**38**

Table 5 Results of AMS measurement using the gas ion source of AixMICADAS for collagen CO_2 samples prepared via method 3. Columns: see Table 3. A limited samples set was prepared using this method due to time constraints.

Method 3: sealed tube combustion and vacuum line										
Material	MPI-EVA lab code	AIX lab code	Measured mass (C µg)	Run time (s)	pMC	Error 1 pMC ±	Error 2 pMC ±	^{14}C age BP (yr)	Error 1 (yr) (1σ)	Error 2 (yr) (1σ)
Background cave bear bone (used in correction of unknown samples)	R-EVA 800.30	Aix-12001.4.1	101	835	0.42	0.04		43950	750	
	R-EVA 800.30	Aix-12001.4.2	61	533	0.50	0.04		42620	710	
			weighted mean		**0.45**	**0.03**		**43340**	**520**	
Human tooth	R-EVA 1516.1	Aix-12005.4.1	99	461	81.72	0.97	1.03	1623	96	102
		Aix-12005.4.2	51	878	82.40	0.67	0.75	1557	65	73
		Aix-12005.4.4	51	345	83.30	0.83	0.90	1469	80	87
			weighted mean		**82.51**	**0.46**	**0.50**	**1544**	**45**	**49**
Human bone	R-EVA 1489.1	Aix-12004.5.1	48	504	82.76	0.75	0.82	1521	73	80
		Aix-12004.5.2	101	461	80.86	0.96	1.02	1708	95	101
			weighted mean		**82.03**	**0.59**	**0.64**	**1591**	**58**	**63**

Comparison between AMS Measurements

The results agree between measurements on graphite targets and gaseous collagen samples for all four samples, as seen in Figure 1. The dates between replicates are internally consistent for all samples prepared via methods 1 and 2 (Tables 3 and 4) (chi^2 test, $p > 0.05$ in all cases; Ward and Wilson 1978) and the weighted mean ages for each of the gas methods are statistically identical for all four samples (Mann-Whitney U test, $p > 0.05$ in all cases).

The background collagen samples (R-EVA 800) averaged 0.65 pMC for method 1 and 0.6 pMC for method 2 (see Table 6), both with a standard deviation (1σ) of 0.07 pMC, well within the long-term variability (0.1 pMC) observed on standards measured with the gas ion source. The same background collagen measured on graphite targets in Aix averaged 0.2 pMC with a standard deviation of 0.01 pMC.

Table 6 Comparison of AMS measurements obtained from the background cave bear bone R-EVA 800 for each method. R-EVA 800.30 and 800.33 denote two collagen extractions from the same bone; R-EVA 800.30 was extracted alongside the medieval samples, and R-EVA 800.33 was extracted alongside the Paleolithic samples. At MAMS, R-EVA 800.30 was used for background correction of the graphite measurements of the medieval samples and R-EVA 800.33 was used for background correction of the bison and mammoth samples as these batches were run on separate occasions. In Aix, measurements performed with AixMICADAS on samples R-EVA 800.30 and 800.33 were both used for background correction of the bison, mammoth and medieval human samples, measured on graphite or CO_2 gas, as all samples were measured in the same batch. Asymmetrical age uncertainties are shown where pMC ≤ error × 10. All ages >15,000 BP are rounded to nearest 10 yr.

Method	MPI-EVA lab code	AMS lab code	pMC	±	^{14}C age BP (yr)	Error (yr) (1σ)
Graphite	R-EVA 800.30	Aix-12001.1.2	0.21	0.01	49630	410
	R-EVA 800.30	Aix-12001.1.3	0.22	0.01	49310	400
	R-EVA 800.33	Aix-12000.1.2	0.20	0.01	49990	360
	R-EVA 800.33	Aix-12000.1.3	0.19	0.01	50280	370
		weighted mean	**0.20**	**0.005**	**49850**	**190**
	R-EVA 800.30	MAMS-26330	0.27	0.02	47480	480
	R-EVA 800.30	MAMS-26331	0.27	0.02	47630	470
	R-EVA 800.30	MAMS-26332	0.33	0.02	45970	470
	R-EVA 800.33	MAMS-26878	0.20	0.01	50120	600
		weighted mean	**0.28**	**0.01**	**47200**	**250**
Gas Method 1	R-EVA 800.30	Aix-12001.5.1	0.66	0.06	40290	760
	R-EVA 800.30	Aix-12001.5.2	0.68	0.05	40130	570
	R-EVA 800.33	Aix-12000.5.4	0.61	0.05	40950	660
		weighted mean	**0.64**	**0.03**	**40460**	**330**
Gas Method 2	R-EVA 800.30	Aix-12001.2.1	0.69	0.06	39980	740
	R-EVA 800.30	Aix-12001.2.2	0.54	0.07	41910	+1120/−980
	R-EVA 800.30	Aix-12001.2.4	0.59	0.07	41280	+1010/−900
	R-EVA 800.33	Aix-12000.3.1	0.64	0.06	40570	700
	R-EVA 800.33	Aix-12000.3.2	0.73	0.07	39550	770
		weighted mean	**0.65**	**0.03**	**40590**	**360**
Gas Method 3	R-EVA 800.30	Aix-12001.4.1	0.42	0.04	43950	750
	R-EVA 800.30	Aix-12001.4.2	0.50	0.04	42620	710
		weighted mean	**0.45**	**0.03**	**43340**	**520**

Although the results for the collagen background (R-EVA 800) are statistically the same between methods 1 and 2, those from method 3 are not, being older by ca. 3000 ^{14}C yr (0.2 pMC lower). This may relate to the absence of C contribution from the silver cups used for sample combustion in methods 1 and 2. It is clear that one of the two aliquots of the medieval human bone (R-EVA 1489.1) prepared using method 3 is an outlier (Aix-12004.5.2: 1708 ± 101 BP) compared to all other measurements for this bone, with the two replicates not overlapping at 1σ (Table 5). Due to this outlier the weighted mean for method 3 is older than the weighted means of methods 1 and 2 (Figure 1d). This aliquot was prepared in the Heidelberg vacuum line following the first preparation of the same bone (Aix-12004.5.1), interspersed with overnight evacuation of the system. Likewise, the outlier was measured with the GIS following Aix-12004.5.1. It is therefore unlikely that the older age is a result of a memory effect from an older sample. As the method 3 data set is limited, further analysis of small samples prepared via method 3 will be undertaken to expand the data set and explore the phenomenon observed in the "cleaner" collagen backgrounds. The results agree within statistics between the graphite and CO_2 techniques (methods 1 and 2) for the medieval samples and for the mammoth bone at ca. 34,500 BP (calibrated age ca. 39,000 cal BP), with low error ranges.

As shown by the graphite measurements in Table 2, the bison bone is very close to the cave bear background value (ca. 0.2 pMC). In Tables 3–4, the bison gas analyses are corrected for a more sizable background value (ca. 0.65 pMC). Consequently, the CO_2 results vary widely between replicates although this variation is still within the quoted 1σ errors (see Tables 3 and 4). Nevertheless, after propagation of the blank scatter in the error calculation (error 2 discussed above), the gas measurements (weighted mean and error of 50120 +2950/–2150 BP for the 7 replicates in Tables 3 and 4) are compatible with those performed on solid graphite (49,040 +1040/–920 BP based on duplicates in Table 2) at the limit of the ^{14}C timescale. In any case, this sample suggests that the realistic limits of the gas source for relatively precise measurements is ca. 0.6 pMC, equivalent to an age of 41,000 BP (and a calibrated age of ca. 44,000 cal BP). Beyond that limit, the ^{14}C can still be detected and quantified, but the uncertainty of the background correction dominates accuracy and precision.

Precision

Although ion currents remain higher for measurements of large samples on graphite targets (around 40 µA for these samples on the Low energy side), various modifications to the gas ion source (Fahrni et al. 2013), such as the addition and adjustment of the immersion lens, mean that currents from the MICADAS gas ion source are now achievable which were impossible eight years ago (in the range of 15 µA for this study), and the use of helium as a stripper gas has further increased transmission (48% for AixMICADAS in gas configuration).

While ca. 80 µg C (170 µg collagen) was weighed into each aliquot for these tests, only approximately 30 µg C was consumed during measurement. For future samples, an appropriate amount of collagen (ca. 70–80 µg) would be weighed out or measurements could be extended for the duration of a second or third titanium target to exhaust the whole sample. With such a reduction in sample size (e.g. half the amount combusted in this study), any external carbon in the EA-GIS system will make an increased contribution for samples prepared via methods 1 and 2. This will be explored in future tests using such sample sizes.

Although a single gaseous measurement of <100 µg C is not yet directly competitive with a 1000 µg C graphite measurement in terms of error, the level of precision we achieved with one

aliquot is still highly applicable for answering many archaeological questions. This is especially important for Paleolithic fossils and bone artifacts where 500 mg material is not available for sampling. This is demonstrated by the mammoth bone at ca. 34,500 BP, where a single gaseous measurement of <0.2 mg collagen has a precision of approximately ±800 yr (error 2).

For this test, four aliquots per sample were measured to test the consistency of the measurements. Although we are principally interested in the precision and accuracy we can reliably achieve with one run (<100 µg C), when we take the weighted mean and error of the four gaseous replicates for method one, the measurement error of the gas technique is more or less comparable with a graphite date (see Figure 1). For example, for the mammoth bone, the weighted mean of the four ca. 80 µg C (total 320 µg C combusted, ca. 120 µg C consumed) gas samples (method 1) was 34530 ± 300 BP, while the graphite date from MAMS was 34360 ± 300 BP and from Aix was 34350 ± 170 BP (each ca. 1000 µg C). This is especially apparent when con-sidering the calibrated ranges. For the medieval tooth, the calibrated range of the weighted mean age and error (1473 ± 33 BP) of the method 1 gas samples is 1389–1320 cal BP (1σ) and the weighted mean of the graphite measurements (1479 ± 13 BP) from Aix is 1380–1346 cal BP (1σ) (OxCal, v4.2). The strategy for dating gaseous samples could therefore be adjusted depending on the level of precision required for each individual sample and the amount of material available.

Choice of Optimal CO_2 Preparation

The preparation of samples using method 3 is very labor-intensive (overnight combustion is followed by around 3 hr of elaborate lab work for the preparation of one sample). However the collagen background suggests this may be the "cleaner" route of CO_2 preparation and further preparations using this method are planned for future tests. The larger data sets from methods 1 and 2 produced results in good agreement for the background cave bear bone and all four samples. The direct coupling of the EA to the gas ion source in method 1 reduces the time for combustion and isolation of collagen CO_2 to around 10 min per sample, reducing both time investment and minimizing handling steps (fully automated process with no sealing step). Considering the practicalities alongside the agreement of results between techniques in this study, method 1 is the preferable route of sample CO_2 isolation, allowing us to go from collagen to a high precision date in around an hour per sample (including a series of replicates and flushing).

CONCLUSION

We can now date gaseous samples of bone collagen of <100 µg C due to the improved design of the MICADAS hybrid ion source. Consistent agreement between replicate measurements in this preliminary study demonstrates the level of accuracy and precision that can be achieved using the gas ion source. The results here demonstrate the applicability of the method, particularly for Paleolithic bone samples, at least back to 40,000 BP. The directly coupled EA and gas ion source offer a fast, efficient method of sample preparation. This study opens the way for the direct dating of extremely precious and small archaeological bone objects.

ACKNOWLEDGMENTS

Research in Leipzig, as well as all measurements made in MAMS, was funded by the Max Planck Society. AixMICADAS was acquired and is operated in the framework of the EQUIPEX project ASTER-CEREGE (PI E. Bard) with additional matching funds from the Collège de France, which also supports the salaries of the authors from CEREGE. Many thanks extended to Lysann Klausnitzer for training in sample preparation, Sven Steinbrenner

for isotopic measurements and to Lise Bonvalot for advice on blanks with the EA-GIS. We would like to thank the three anonymous reviewers whose comments greatly improved the manuscript.

REFERENCES

Bard E, Tuna T, Fagault Y, Bonvalot L, Wacker L, Fahrni S, Synal H-A. 2015. AixMICADAS, the accelerator mass spectrometer dedicated to ^{14}C recently installed in Aix-en-Provence, France. Nuclear Instruments and Methods in Physics Research B 361:80–6.

Bonvalot L, Tuna T, Fagault Y, Jaffrezo JL, Jacob V, Chevrier F, Bard E. 2016. Estimating contributions from biomass burning and fossil fuel combustion by means of radiocarbon analysis of carbonaceous aerosols: application to the Valley of Chamonix. Atmosperic Chemistry Physics 16:13753–72.

Bronk Ramsey C, Hedges REM. 1987. A gas ion source for radiocarbon dating. Nuclear Instru-ments and Methods in Physics Research B 29(1–2): 45–9.

Bronk Ramsey C, Hedges R. 1997. Hybrid ion sour-ces: radiocarbon measurements from microgram to milligram. Nuclear Instruments and Methods in Physics Research B 123(1):539–45.

Bronk Ramsey C, Higham T, Bowles A, Hedges R. 2004a. Improvements to the pretreatment of bone at Oxford. Radiocarbon 46(1):155–64.

Bronk Ramsey C, Ditchfield P, Humm M. 2004b. Using a gas ion source for radiocarbon AMS and GC-AMS. Radiocarbon 46(1):25–32.

Brown TA, Nelson DE, Vogel JS, Southon JR. 1988. Improved collagen extraction by modified longin method. Radiocarbon 30(2):171–7.

de Rooij M, van der Plicht J, Meijer HAJ. 2010. Porous iron pellets for AMS ^{14}C analysis of small samples down to ultra-microscale size (10–25 μgC). Nuclear Instruments and Methods in Physics Research B 268(7–8):947–51.

Delqué-Količ E, Caffy I, Comby-Zerbino C, Dumoulin J-P, Hain S, Massault M, Moreau C, Quiles A, Setti V, Souprayen C, Tannau J-F, Thellier B, Vincent J. 2013. Advances in Handling Small Radiocarbon Samples at the Laboratoire de Mesure du Carbone 14 in Saclay, France. Radio-carbon 55(2-3):648–56.

Ertun T, Xu S, Bryant CL, Maden C, Murray C, Currie M, Freeman ST. 2005. Progress in AMS target production of sub-milligram samples at the NERC radiocarbon laboratory. Radiocarbon 47(3):453–64

Fagault Y, Tuna T, Rostek F, Bard E. 2017. Radio-carbon dating of small foraminifera samples with a gas ion source. 14th International AMS Conference, Ottawa.

Fahrni SM, Wacker L, Synal H-A, Szidat S. 2013. Improving a gas ion source for ^{14}C AMS. Nuclear Instruments and Methods in Physics Research B 294:320–7.

Genberg J, Stenstrom K, Elfman M, Olsson M. 2010. Development of graphitization of μg-sized samples at Lund University. Radiocarbon 52(3):1270–6.

Hammer S. 2003. Einsatz von Radioisotopen zur Interpretation der raum - zeitlichen Variabilität von organischem Aerosol. Ruprecht-Karls-Universität Heidelberg.

Hendriks L, Hajdas I, McIntyre C, Küffner M, Scherrer NC, Ferreira ESB. 2016. Microscale radiocarbon dating of paintings. Applied Physics A 122(3):1–10.

Higham TFG, Jacobi RM, Bronk Ramsey C. 2006. AMS radiocarbon dating of ancient bone using ultrafiltration. Radiocarbon 48(2):179–95.

Hoffmann HM. 2016. Micro radiocarbon dating of the particulate organic carbon fraction in Alpine glacier ice: method refinement, critical evaluation and dating applications. Universität Heidelberg.

Hua Q, Zoppi U, Williams AA, Smith AM. 2004. Small-mass AMS radiocarbon analysis at ANTARES. Nuclear Instruments and Methods in Physics Research B 223:284–92.

Kromer B, Lindauer S, Synal H-A, Wacker L. 2013. MAMS - A new AMS facility at the Curt-Engelhorn-Centre for Achaeometry, Mannheim, Germany. Nuclear Instruments and Methods in Physics Research B 294:11–3.

Liebl J, Steier P, Golser R, Kutschera W, Mair K, Priller A, Vonderhaid I, Wild EM. 2013. Carbon background and ionization yield of an AMS system during C-14 measurements of microgram-size graphite samples. Nuclear Instruments and Methods in Physics Research B 294:335–9.

Longin R. 1971. New method of collagen extraction for radiocarbon dating. Nature 231:241–2.

Middleton R. 1984. A review of ion sources for accel-erator mass spectrometry. Nuclear Instruments and Methods in Physics Research B 5(2):193–9.

Pearson A. 1998. Microscale AMS ^{14}C measurement at NOSAMS. Radiocarbon 40(1):61–75.

Ruff M, Wacker L, Gaggeler HW, Suter M, Synal H-A, Szidat S. 2007. A gas ion source for radiocarbon measurements at 200 kV. Radiocarbon 49(2): 307–14.

Ruff M, Szidat S, Gäggeler HW, Suter M, Synal H-A, Wacker L. 2010a. Gaseous radiocarbon measure-ments of small samples. Nuclear Instruments and Methods in Physics Research B 268(7–8):790–4.

Ruff M, Fahrni S, Gäggeler HW, Hajdas I, Suter M, Synal H-A, Szidat S, Wacker L. 2010b. On-line radiocarbon measurements of small samples using elemental analyzer and MICADAS gas ion source. Radiocarbon 52(4):1645–56.

Santos GM, Moore RB, Southon JR, Griffin S, Hinger E, Zhang D. 2007a. AMS ^{14}C sample

preparation at the KCCAMS/UCI facility: Status report and performance of small samples. Radiocarbon 49(2):255–69.

Santos GM, Southon JR, Griffin S, Beaupre SR, Druffel ERM. 2007b. Ultra small-mass AMS ^{14}C sample preparation and analyses at KCCAMS/ UCI Facility. Nuclear Instruments and Methods in Physics Research B 259(1):293–302.

Smith AM, Petrenko VV, Hua Q, Southon J, Brailsford G. 2007. The Effect of N_2O, Catalyst, and Means of Water Vapor Removal on the Graphitization of Small CO_2 Samples. Radiocarbon 49(2):245–54

Smith AM, Hua Q, Williams A, Levchenko V, Yang B. 2010. Developments in micro-sample ^{14}C AMS at the ANTARES AMS facility. Nuclear Instruments and Methods in Physics Research B 268(7–8):919–23.

Synal H-A, Stocker M, Suter M. 2007. MICADAS: A new compact radiocarbon AMS system. Nuclear Instruments and Methods in Physics Research B 259(1):7–13.

Talamo S, Richards M. 2011. A Comparison of Bone Pretreatment Methods for AMS Dating of Samples >30,000 BP. Radiocarbon 53(3):443–9.

Tuna T, Fagault Y, Bonvalot L, Capano M, Bard E. 2017. Status report of AixMICADAS performances with solid and gas samples. 14th Inter-national AMS Conference, Ottawa.

Uhl T, Kretschmer W, Luppold W, Scharf A. 2005. AMS measurements from microgram to milligram. Nuclear Instruments and Methods in Physics Research B 240(1-2):474–7.

van der Plicht J, Hogg A. 2006. A note on reporting radiocarbon. Quaternary Geochronology 1(4): 237–40.

van Klinken GJ. 1999. Bone collagen quality indicators for palaeodietary and radiocarbon. Journal of Archaeological Science 26:687–95.

Wacker L, Christl M, Synal HA. 2010a. Bats: a new tool for AMS data reduction. Nuclear Instruments and Methods in Physics Research B 268(7–8):976–9.

Wacker L, Bonani G, Friedrich M, Hajdas I, Kromer B, Nemec N, Ruff M, Suter M, Synal H-A, Vockenhuber C. 2010b. MICADAS: routine and high-precision radiocarbon dating. Radiocarbon 52(2–3):252–62

Wacker L, Němec M, Bourquin J. 2010c. A revolutionary graphitisation system: Fully automated, compact and simple. Nuclear Instruments and Methods in Physics Research B 268(7–8):931–4.

Wacker L, Lippold J, Molnár M, Schulz H. 2013a. Towards radiocarbon dating of single foraminifera with a gas ion source. Nuclear Instruments and Methods in Physics Research B 294:307–10.

Wacker L, Fahrni SM, Hajdas I, Molnar M, Synal HA, Szidat S, Zhang YL. 2013b. A versatile gas interface for routine radiocarbon analysis with a gas ion source. Nuclear Instruments and Methods in Physics Research B 294:315–9.

Walter SRS, Gagnon AR, Roberts ML, McNichol AP, Gaylord MCL, Klein E. 2015. Ultra-small graphitization reactors for ultra-microscale ^{14}C Analysis at the National Ocean Sciences Accelerator Mass Spectrometry (NOSAMS) facility. Radiocarbon 57(1):109–22.

Ward GK, Wilson SR. 1978. Procedures for com-paring and combining radiocarbon age determinations: a critique. Archaeometry 20(1):19–31.

Zhang YL, Huang RJ, El Haddad I, Ho KF, Cao JJ, Han Y, Zotter P, Bozzetti C, Daellenbach KR, Canonaco F, Slowik JG, Salazar G, Schwikowski M, Schnelle-Kreis J, Abbaszade G, Zimmermann R, Baltensperger U, Prévôt ASH, Szidat S. 2015. Fossil vs. non-fossil sources of fine carbonaceous aerosols in four Chinese cities during the extreme winter haze episode of 2013. Atmospheric Chemistry Physics 15(3):1299–312.

Chapter Three

Pretreatment and gaseous radiocarbon dating of 40–100 mg archaeological bone

H. Fewlass, T. Tuna, Y. Fagault, J.-J. Hublin, B. Kromer, E. Bard, S. Talamo

Published in *Scientific Reports,* 2019, volume 9, article number: 5342
DOI: 10.1038/s41598-019-41557-8

SCIENTIFIC REPORTS

OPEN

Pretreatment and gaseous radiocarbon dating of 40–100 mg archaeological bone

Received: 8 October 2018
Accepted: 11 March 2019
Published online: 29 March 2019

H. Fewlass[1], T. Tuna[2], Y. Fagault[2], J.-J. Hublin[1], B. Kromer[1,3], E. Bard[2] & S. Talamo[1]

Radiocarbon dating archaeological bone typically requires 300–1000 mg material using standard protocols. We report the results of reducing sample size at both the pretreatment and ^{14}C measurement stages for eight archaeological bones spanning the radiocarbon timescale at different levels of preservation. We adapted our standard collagen extraction protocol specifically for <100 mg bone material. Collagen was extracted at least twice (from 37–100 mg material) from each bone. Collagen aliquots containing <100 µg carbon were measured in replicate using the gas ion source of the AixMICADAS. The effect of sample size reduction in the EA-GIS-AMS system was explored by measuring ^{14}C of collagen containing either *ca*. 30 µg carbon or *ca*. 90 µg carbon. The gas dates were compared to standard-sized graphite dates extracted from large amounts (500–700 mg) of bone material pretreated with our standard protocol. The results reported here demonstrate that we are able to reproduce accurate radiocarbon dates from <100 mg archaeological bone material back to 40,000 BP.

Bone is one of the most frequently radiocarbon-dated materials recovered from archaeological sites. However, many precious archaeological bones, such as human remains or Palaeolithic bone tools, are too small or valuable for extensive destructive sampling. The reduction of sample size to enable direct dating of precious bone is therefore a key concern for the archaeological community.

In the 1960s and 1970s, gas proportional counters required many grams of bone to produce a radiocarbon date[1,2]. The development and utilisation of Accelerator Mass Spectrometers (AMS) in the 1980s represented a revolutionary step in the reduction of sample size and time required for dating[3]. Routine measurements today typically require 500–1000 micrograms of carbon (µg C) to produce a high precision date. In recent years, several AMS labs have worked on modifications to the graphitisation and AMS measurement process for smaller samples containing <500 µg C[4–13]. However, the graphitisation of small sample sizes is often time consuming and can be prone to large contamination effects[14,15]. A recent study by Cersoy, *et al*.[16] demonstrated that graphite targets containing *ca*. 200 µg C from archaeological bones can be successfully produced and measured using the IonPlus Automated Graphitisation Equipment III (AGE 3)[17] and MIni CArbon DAting System (MICADAS)[18,19] developed at ETH Zurich. However, the hybrid nature of the MICADAS system offers an alternative solution to the complex process of graphitising small samples. Organic samples containing <100 µg C can be placed into an elemental analyser (EA) directly coupled to the gas ion source of the MICADAS via the gas interface system (GIS)[15,18,20–24]. The automated system reduces both sample preparation time and the risk of contamination through handling, and has been successfully utilised in environmental and climatic applications[23,25–28]. In our preliminary study[29] we demonstrated that the gas ion source of the AixMICADAS[30] is suitable for dating bone collagen CO_2 samples of <100 µg C back to 35,000 BP (uncalibrated radiocarbon years before AD 1950).

However, as sample size is reduced the effect of contamination during pretreatment and measurement increases greatly. Sample pretreatment involves the extraction and purification of carbon endogenous to the original bone. Any contamination remaining in the sample at the time of dating can lead to erroneous results. The effects become increasingly catastrophic with the increasing age of the sample due to the minute concentrations of residual ^{14}C. For example, in a bone extract *ca*. 40,000 BP, 1% modern carbon contamination would skew the resulting ^{14}C age by over 7,000 years.

[1]Department of Human Evolution, Max Planck Institute for Evolutionary Anthropology, Deutscher platz 6, D-04103, Leipzig, Germany. [2]CEREGE, Aix Marseille Univ, CNRS, IRD, INRA, Collège de France, Technopôle de l'Arbois, BP 80, 13545, Aix-en-Provence, France. [3]Institute of Environmental Physics, University of Heidelberg, INF 229, D-69120, Heidelberg, Germany. Correspondence and requests for materials should be addressed to H.F. (email: helen_fewlass@eva.mpg.de)

It is standard practice to extract the proteinaceous portion of bone for ^{14}C measurement, generally referred to as 'collagen'[31]. Although collagen forms around 22% weight of modern bone, degradation following death and burial makes collagen extraction increasingly challenging with advancing age[32]. Whilst the minimum threshold for reliable ^{14}C dating is generally considered to be 1%[32], it is common for the collagen portion of Palaeolithic bone to constitute <10% weight. The lower the level of collagen preservation, the more bone must be pretreated to obtain sufficient material to assess the quality of the extract (i.e. isotopic and elemental analysis) and for ^{14}C dating. Therefore, 300–1000 mg material is commonly sampled for dating Palaeolithic bones.

The majority of ^{14}C labs follow collagen extraction protocols based on Longin[33]. This involves demineralisation of either powdered bone or bone chunks using hydrochloric acid (HCl) followed by gelatinisation of the collagen in weakly acidic water and freeze-drying of the final extract. Different labs vary in the strength of reagents used, the duration of treatments and the inclusion of further decontamination steps. Many studies have been published comparing the collagen yields and isotopic values of the various extraction protocols published in the literature[34–38] as variations in pretreatment conditions can lead to differences in the quantity and quality of the final extracts. The addition of an ultrafiltration step, first proposed by Brown, *et al.*[39] has in particular improved the accuracy of ^{14}C dating of Palaeolithic bones[40]; gelatinised samples are filtered to concentrate large (>30 kDa) molecules to produce a 'cleaner' collagen extract. The technique is not unanimously agreed upon due to the risk of contamination from the humectant-coated filter[41], the effectiveness of the application[37] and the loss of collagen during filtration[34]. However, stringent cleaning steps have been established[42–44] and in many cases the re-dating of ancient bones with ultrafiltration methods has produced much older dates than previous measurements from non-ultrafiltered extracts[40,45,46]. The collagen pretreatment protocol routinely applied to Palaeolithic bone at the Max Planck Institute for Evolutionary Anthropology (MPI-EVA, Leipzig, Germany) is based on a modified Longin plus ultrafiltration protocol[36] and has a strong track record of obtaining high yields of high quality collagen from *ca*. 500 mg samples of Palaeolithic bone[47].

The aim of this study was to determine a suitable method to pretreat <100 mg bone material and further investigate if the gas ion source of the AixMICADAS[29,30] at CEREGE (Centre de Recherche et d'Enseignement de Geosciences de l'Environnement, Aix-en-Provence, France) is suitable for measuring small archaeological bone samples with sufficient accuracy and precision. We investigated the effect of sample size reduction at both the pretreatment and gas measurement stages. Tests were performed on a set of eight archaeological bones ranging from 1% to >10% collagen preservation known to date from >50,000–1,400 BP. Each bone was pretreated multiple times from starting weights of 37–100 mg bone material. Each collagen extract was split and dated multiple times with the gas ion source of the AixMICADAS to test replicability. The gas dates were compared with graphite dates from collagen extracted from >500 mg material of the same bones. We further compared gas dates of *ca*. 30 µg C and *ca*. 90 µg C to explore the effect of sample size on the blank level of the EA-GIS-AMS system. The results demonstrate our ability to obtain accurate and moderately precise radiocarbon dates from <100 µg C extracted from 37–100 mg bone material back to 40,000 BP. The methods described will be used to extract and ^{14}C date collagen from precious archaeological bone artefacts with minimal sample destruction.

Results

Bone pretreatment. Prior to this study, 500 to 700 mg of each bone had been pretreated using our standard collagen extraction protocol[36]. The extracts were analysed by EA-IRMS at the MPI-EVA to assess their suitability for dating (C%, N%, C:N, $\delta^{13}C$, $\delta^{15}N$) and were measured at the Klaus-Tschira-AMS lab in Mannheim, Germany (lab code: MAMS). The same collagen extracts from R-EVA 1489, R-EVA 123 and R-EVA 124 were also dated at the AixMICADAS facility to cross-check the ages[29]. The results were used as a reference for the preparation of small (<100 mg) aliquots of bone.

Modifications to our standard pretreatment protocol were carried out for five bones (Fig. 1): three relatively 'well-preserved' (>10% collagen preservation) archaeological bones (Fig. 1a,b,e) and two 'poorly-preserved' bones (<5% collagen preservation) (Fig. 1c,d). Once we had determined the optimum pretreatment protocol for <100 mg material, we applied this to three more archaeological samples: R-EVA 1489, R-EVA 1905 and R-EVA 1860 (two extracts per bone) (pretreatment information shown in Supplementary Dataset S1).

The standard practice in our lab is to extract large bone aliquots (*ca*. 500 mg material) as a solid piece. Although this method requires a large time investment (demineralisation can take up to four weeks with the HCl 0.5 M changed twice per week), we observe much higher collagen yields using this technique compared to powdered extracts of equal starting weight. Small aliquots (<100 mg) of the test bones were initially pretreated as both fine powder and as solid chunks. For solid pieces of bone, in most cases the collagen yield from small extracts (<100 mg) equalled or exceeded the collagen yields of large extracts (500–700 mg material) and no difference was observed between aliquots of 50 mg bone compared to 70 mg or 100 mg bone material (Fig. 1). In contrast, the powdered aliquots of well-preserved bones generally yielded around half the amount of collagen compared to solid pieces, in line with our observation for large starting weights of bone. Powdered aliquots from the poorly preserved bones either yielded nothing or small amounts (<1 mg) of crumbly yellow material. Due to the poor results from the pretreatment of powdered samples, our protocol for small amounts of bone is based on the extraction of solid pieces as per our standard protocol for larger aliquots. The pretreatment information for powdered extracts is included in the supplementary information.

We initially applied our standard collagen extraction protocol to <100 mg bone material of the well-preserved bones. Three steps of the pretreatment protocol were then modified to see what effect this had on the collagen yield and quality of extracts from small bone aliquots (Fig. 1): step (1) the duration of the demineralisation stage; step (2) the strength of HCl during the demineralisation stage; step (3) the temperature and duration of the gelatinisation stage. Bone collagen yields along with elemental (C%, N% and C:N) and stable isotopic data ($\delta^{13}C$ and $\delta^{15}N$) were used to evaluate the extracts from the different methods. In addition, Fourier Transform Infrared Spectroscopy (FTIR) was used to double check the preservation of the extracted collagen, and to detect

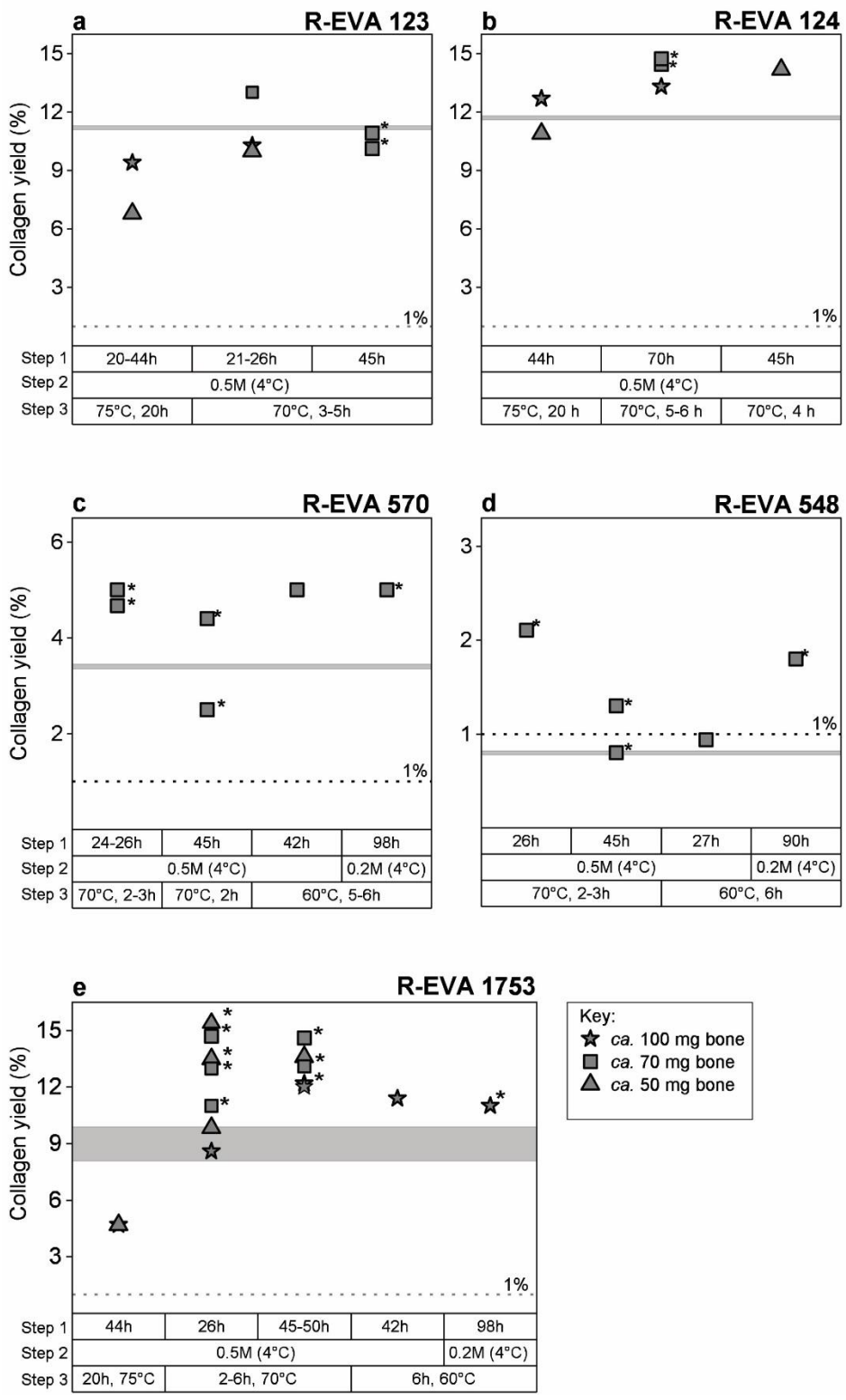

Figure 1. Graphs showing the collagen yields from small aliquots of bone according to variations in pretreatment conditions: (**a**) R-EVA 123, (**b**) R-EVA 124 (**c**) R-EVA 570, (**d**) R-EVA 548 and (**e**) R-EVA 1753. Step 1: duration of the demineralisation stage. Step 2: strength of HCl during demineralisation. Step 3: duration and temperature of the gelatinisation stage (HCl pH3). In (**a**–**d**) the horizontal grey line shows the collagen yield from a large aliquot (>500 mg material) of the same bone. A higher number of data points are present for R-EVA 1753 (**e**) as an aliquot of this bone was extracted alongside each batch of samples. The horizontal grey band in e shows the range in collagen yield of repeated large extractions from the background bone. The dashed lines at 1% show the guideline minimum requirement for reliable ^{14}C dating. Asterisks mark extracts which were dated using the gas ion source (see Fig. 3).

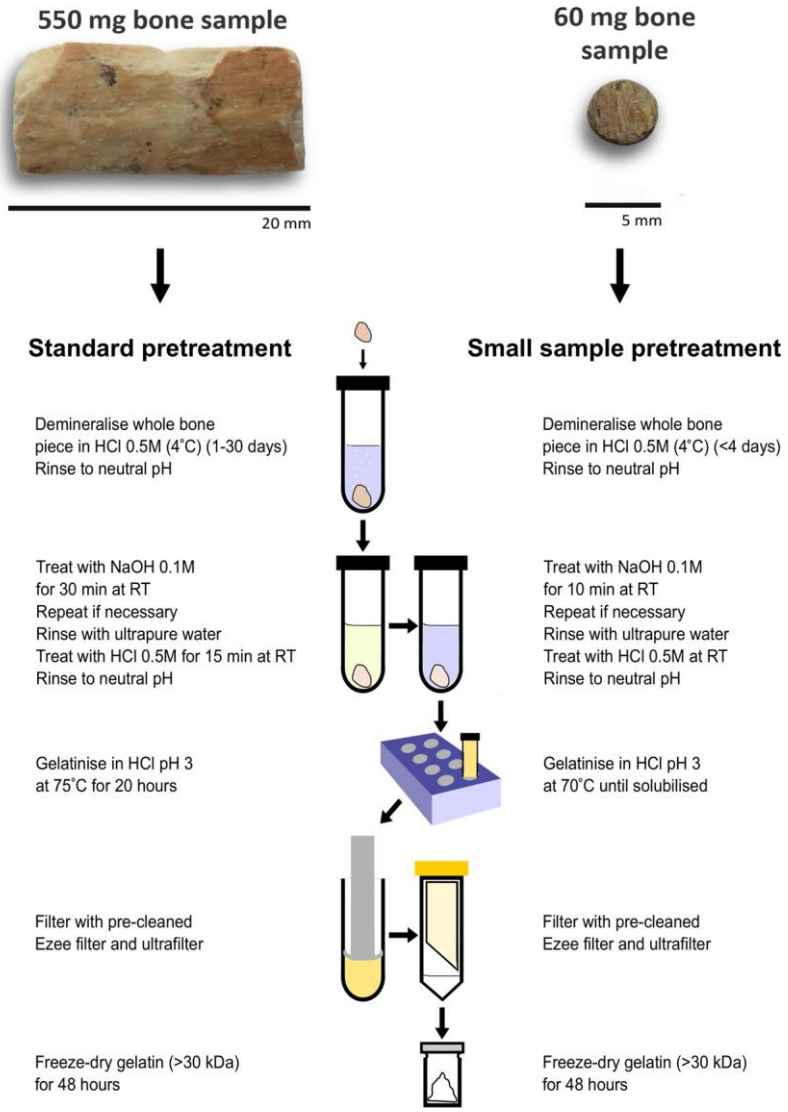

Figure 2. Summary of bone pretreatment protocols used at the MPI-EVA for large (left) and small (right) bone samples.

the presence of possible carbon contaminants[31,48,49]. Detailed pretreatment information for all extracts can be seen in Supplementary Dataset S1.

For the poorly preserved bones (Fig. 1c: R-EVA 570 and Fig. 1d: R-EVA 548) the pretreatment was softened in order to minimise collagen loss during the extraction. The weaker HCl (0.2 M) (step 2) and lower gelatinisation temperature (60 °C) (step 3) required a greater time investment and did not necessarily increase the yield of collagen compared to using stronger acid (HCl 0.5 M) during demineralisation and higher temperatures (70 °C) during gelatinisation. For the poorly preserved samples, demineralisation in HCl 0.5 M generally occurred after one day (4 °C). As Schoeninger, *et al*.[50] observed that one disadvantage of extracting collagen from solid chunks was the tendency for incomplete demineralisation, several extracts were demineralised in HCl 0.5 M for two days. This resulted in lower collagen yields for the poorly preserved bones and in the case of R-EVA 548, the yield of these extracts was so low that the extracts were affected by C contamination to a large extent.

During the gelatinisation stage (step 3), the collagen yield was higher from aliquots which were removed from the heater block as soon as solubilisation had occurred compared to those left on the heater block for 20 h as per our standard protocol for >500 mg. For all bone samples >30,000 BP, solubilisation occurred in <6 h (Fig. 1), whereas R-EVA 1489 and R-EVA 1905 required up to 27 h for full solubilisation (Supplementary Dataset S1).

Of the extracts dated, two (R-EVA 548.13 and R-EVA 548.14) fell close to or under the minimum threshold (1%) for reliable ^{14}C dating (Supplementary Dataset S1). There were small variations in elemental values between pretreatments of the same bone but all values (Supplementary Dataset S1) fell within the accepted ranges of 'well-preserved' collagen[32]. The stable isotopic values were in keeping with the palaeodietary expectations for each animal and were consistent between extracts. Analysis with FTIR was performed for all collagen extracts; each extract dated had a spectra characteristic of well-preserved collagen when compared to library spectra (see

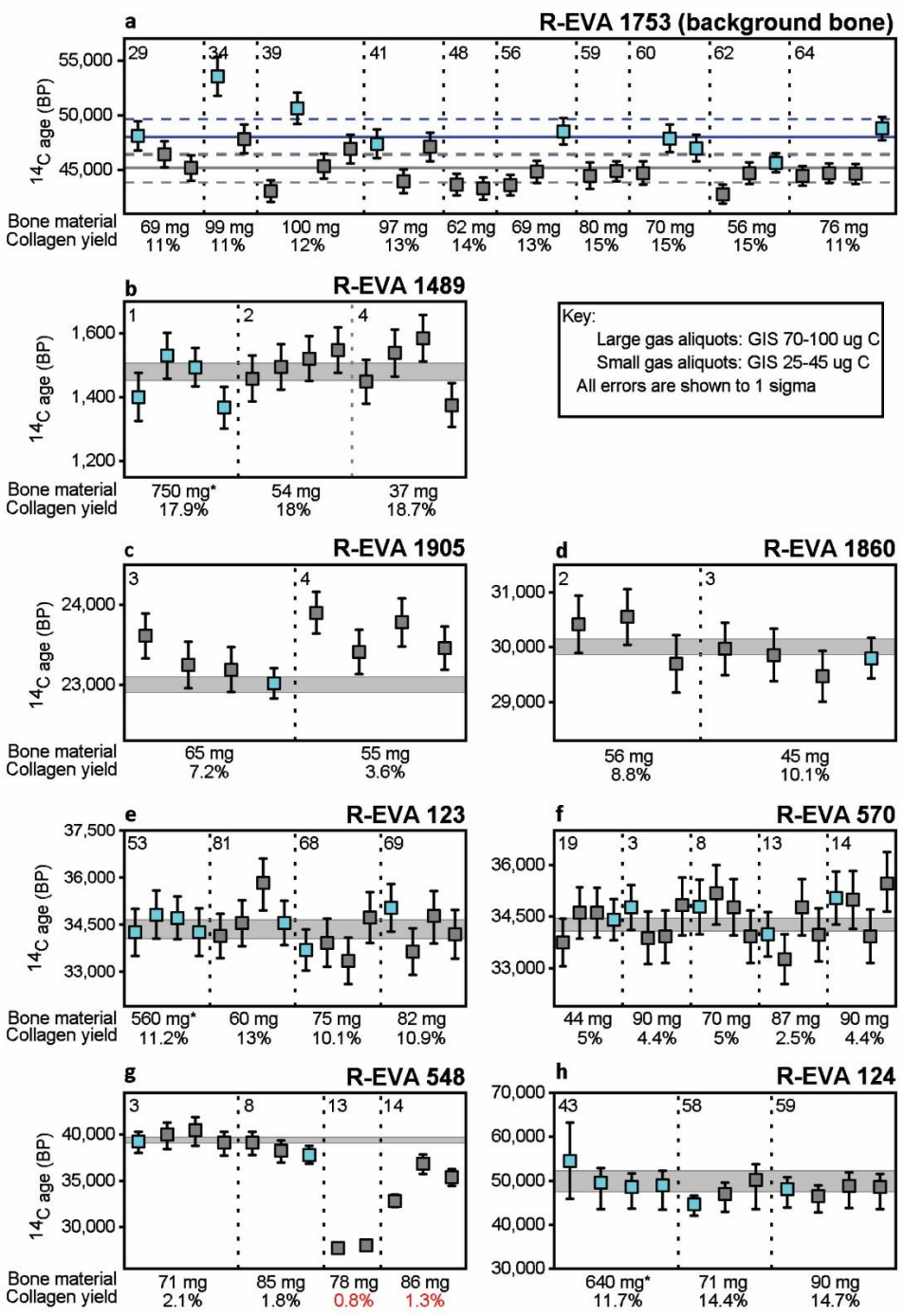

Figure 3. ^{14}C gas measurements of small (25–40 μgC) and large (70–100 μgC) aliquots of collagen extracted from eight bones (**a**–**h**) spanning the ^{14}C time range. Each data point shows the ^{14}C age (BP) and 1σ error (years) of a single EA-GIS-AMS measurement. a) Shows the uncorrected measurements of background bone R-EVA 1753 (>50,000 BP). An aliquot of this bone was prepared alongside every batch of samples from sampling to measurement to monitor contamination introduced during sample preparation. These measurements were used in the age calculation of the other archaeological samples (**b**–**h**), according to session, size (small or large) and type (solid bone extract). The arithmetic mean and associated SD of system blank (IAEA-C1/phthalic anhydrite) measurements are shown as a solid horizontal blue line and dashed blue lines respectively for large 80–100 μgC measurements and as a solid horizontal grey line and dashed grey line for small 25–40 μgC measurements. For all gas measurements in graphs b-h: the absolute error of the blank has been set to 0.001 and an external error of 3.5‰ has been added to all measurements based on the long term standard deviation of standards. Dates >15,000 BP have been rounded to the nearest 10 years. Asymmetrical errors are shown where $F14C \leq 1\sigma*10$. Grey shaded bands show the 1σ range of graphite dates measured from large extracts of the same bone. In a-h, the vertical dotted lines separate different collagen extracts of the same bone with the bone starting weight and collagen yield shown below. The number in the top left of each section is the preparation number of the bone, corresponding to Supplementary Dataset S1. Asterisks mark collagen extracts dated with the gas ion source reported in Fewlass, *et al.*[29].

Supplementary Fig. S3). Considering the collagen yields and ^{14}C measurements, the optimum pretreatment protocol for small aliquots of bone (<100 mg) is shown in Fig. 2.

^{14}C dating. For each of the bones, several collagen extracts (bone weight ranging from 37–100 mg, marked with asterisks in Fig. 1) were dated using the EA-GIS-AixMICADAS (Fig. 3). Each collagen extract was split and measured multiple times. Between two and four replicates were measured containing *ca*. 30–40 µg C, run for the duration of one titanium (Ti) target (*ca*. 12 minutes) and for each bone >20,000 BP, a single aliquot containing *ca*. 80–90 µg C was measured over the duration of three targets to increase precision (see Supplementary Dataset S2). The gas ages obtained were compared to one or more graphite dates measured from collagen extracted from 500–700 mg bone material (Supplementary Dataset S2). Discussed here are measurements made from collagen extracted from solid pieces of bone. Details of measurements made from powdered aliquots (lower collagen yields) are included in the supplementary information.

Figure 3 shows the ages obtained for each bone. The accuracy of the dates generated by the gas ion source is clearly seen in comparison with the graphite dates. Of the 74 new measurements made with the EA-GIS-AMS system shown in Fig. 3b–h, 69 measurements agree within the 95% confidence limit (2σ) of the corresponding graphite dates and 57 agree within 1σ. There are five measurements outside 2σ: four are measurements of the two collagen extracts (R-EVA 548.13; R-EVA 548.14) which fell at or below the minimum threshold of preservation suitable for ^{14}C dating (Fig. 3g), and the last (R-EVA 1905.4.1; Aix-12023.2.1) is slightly older than the other replicates of the same extract (Fig. 3c).

Chi-squared tests (χ^2)[51] were performed using the R_Combine feature in OxCal 4.2[52] using the F^{14}C and associated error for gas replicates of each collagen extract individually and for all replicates per bone. The replicate measurements are statistically indistinguishable for R-EVA 1489, R-EVA 1905, R-EVA 1860, R-EVA 123, R-EVA 570 and R-EVA 124 (output of all statistical tests are included in Supplementary Dataset S2), demonstrating the reproducibility of the measurements and consistency between different pretreatment batches across the range of the ^{14}C timescale. In addition, all of the measurements of R-EVA 1489, R-EVA 123 and R-EVA 124 from this study agree with the EA-GIS-AMS measurements made in 2016 reported in Fewlass, *et al*.[29] (Supplementary Dataset S2).

The exception is the roughly 40,000 year old bone R-EVA 548, which at *ca*. 1% collagen preservation represents the limits of C^{14} dating. The gas dates obtained from the two low yield extracts (R-EVA 548.13 and R-EVA 548.14) were much younger than the other extracts of this bone (Fig. 3g), showing they had been affected by contamination from modern carbon. Due to the low yield, under normal circumstances R-EVA 548.13 would not have been passed for dating following pretreatment. Excluding these two extracts, the replicates from R-EVA 548.3 and R-EVA 548.8 are consistent with the graphite date for this bone.

For background bone R-EVA 1753 (>50,000 BP), the dates from the collagen extracts (Supplementary Dataset S3) were on par with the blank standards (IAEA-C1/phthalic anhydride) of equal size (Supplementary Dataset S4). As expected, the blank level in the EA-GIS system was affected by the reduction in sample size from 90 µg C to 30 µg C (Fig. 3a). The ages of the seven <50,000 BP samples were corrected with background collagen measurements of the same size (*ca*. 30 µg C or *ca*. 90 µg C) and type (solid/powder) measured during the same session.

Discussion

Using a slightly modified version of our standard pretreatment protocol the collagen yield from <100 mg bone material was of equally high quality as extracts from 'large' (>500 mg) bone samples. Decreasing sample size from *ca*. 100 mg to <50 mg bone material also had no detrimental effect on collagen yield. The agreement in age between multiple collagen extracts from different starting weights of bone (Fig. 3) indicates firstly that we obtain reproducible results with the pretreatment protocol and secondly, that the reduction in material during pretreatment did not detrimentally affect the results of ^{14}C dating. In particular, the results indicate that the cleaning steps used for the ultrafilters are sufficient as any C remaining in the filters after cleaning would have a more pronounced effect on reduced sample sizes.

The main alteration to our standard protocol involved reduction in the duration of the gelatinisation stage, with samples removed from the heater block as soon as they had gelatinised (see Fig. 2). Different gelatinisation conditions have been well documented to affect the final extract quality and yield[38,39,53,54]. The higher collagen yields from these extracts supports observations that gelatinised collagen is degraded by prolonged exposure to higher temperatures and acidity[39,53].

R-EVA 548 represents a very challenging prospect for collagen extraction and radiocarbon dating due to the exceptionally low levels of preservation (<1% weight collagen) and old age (*ca*. 39,400 BP), even working with larger sample sizes. The harshest demineralisation (HCl 0.5 M, 2 days, 4 °C) applied to small aliquots of this bone (R-EVA 548.13; R-EVA 548.14) resulted in very low yields of ≤1 mg collagen, likely due to the solubilisation of collagen during the longer demineralisation stage. The resultant underestimated dates clearly show that these aliquots were massively affected by modern carbon contamination. Prior to dating, the consideration of the quality of the extract is crucial in order to obtain reliable dates. Given the low yield of collagen (≤1%) following pretreatment, under normal circumstances these extracts would not been dated or would have been treated with caution. This bone demonstrates the difficulty of pretreatment of poorly preserved bones at the limit of the ^{14}C method.

At such small sample sizes, the consideration of the background correction is crucial. The gas measurements of R-EVA 1489, R-EVA 1905, R-EVA 1860, R-EVA 123, R-EVA 570, R-EVA 548 and R-EVA 124 were all corrected with gas measurements of background bone collagen (R-EVA 1753) of equal size (*ca*. 30 µg C or *ca*. 90 µg C) prepared alongside every batch of samples and measured during the same measurement session to account for any C added during sample preparation and measurement. Figure 3a shows the ages obtained for the

background bone containing *ca*. 25–40 μg C (small) and *ca*. 80–100 μg C (large). The large measurements (mean $F^{14}C = 0.0024$, SD = 0.0006, n = 9, equivalent to 48,600 BP) are on par with the system blank (either IAEA-C1 or phthalic anhydride) measurements of equal size (mean $F^{14}C = 0.0026$, SD = 0.0006, n = 7, equivalent to 48,000 BP) (Supplementary Datasets S3 and S4), indicating that no carbon contamination was introduced during sample preparation. An increased sensitivity to modern ^{14}C is to be expected at lower levels of carbon and it is clear that the smaller background collagen measurements are generally younger. The 25–40 μg C background collagen samples (mean $F^{14}C = 0.0039$, SD = 0.0007, n = 22, equivalent to 44,530 BP) are likewise equal to the system blank measurements of equal size (mean $F^{14}C = 0.0036$, SD = 0.0006, n = 5, equivalent to 45,180 BP) (Supplementary Datasets S3 and S4). These values are lower than previously published values for blank IAEA-C1 samples measured at CEREGE reported in Bard, *et al*.[30] ($F^{14}C = 0.02$ for sample sizes around 30 μg C and $F^{14}C = 0.005$ for samples of 80–100 μg C) and to phthalic anhydride blanks measured at ETH Zurich reported in McIntyre, *et al*.[24] (mean $F^{14}C = 0.0046 \pm 0.0012$, n = 6, size range 84–100 μg C). The results indicate the lower limit of ^{14}C detection with the gas ion source to be around $F^{14}C = 0.004$. As demonstrated by R-EVA 124, beyond this limit the minute levels of ^{14}C can be measured but the uncertainty of the background correction dominates accuracy and precision.

The system blank of the EA-GIS-AMS is affected by the carbon content of the silver cups, cross-talk of the zeolite trap and the cleanliness of the ion source at the time of the measurement[24]. The mass (M_c) and $F^{14}C$ ($F^{14}C_c$) of the constant contamination of the EA + GIS system was deduced by least square regression of modern carbonate and blanks (IAEA-C1) with sample weights ranging between 3 and 100 μg C to be $M_c = 0.55 \pm 0.05$ μg C and $F^{14}C_c = 0.12 \pm 0.03$[55]. The silver cups (5 × 3 mm from Elementar; cleaned at 800 °C, 2 h) had a consistent carbon contribution of 0.049 ± 0.02 μg C. The zeolite trap was heated (450 °C) and the system was flushed with helium between samples to minimize cross-contamination. However, small amounts of C may reside in the zeolite trap after flushing which has been demonstrated to have a large influence on samples <20 μg carbon[23,55]. With this in mind, even our 'small' samples were kept >20 μg carbon. To further alleviate problems of cross-talk, samples were run in order of increasing activity (oldest to youngest) according to the standard practice[55]. Background corrections of samples were applied according to sample size and an external error was added during the age calculation of all samples based on the long term standard deviation of standards and blanks (error 2 described in Fewlass, *et al*.[29]).

In a real life situation, if a small bone sample yielded a high amount of collagen (for example, the mammoth bone R-EVA 123 or the Medieval human bone R-EVA 1489 included in this study), dating with graphite targets would be preferentially undertaken as the precision achieved is much higher and measurements can be made routinely. However, the results of this study demonstrate that the gas ion source can produce an accurate radiocarbon date at low precision from as little as 30 μg C. The precision of the date can be improved when larger sample sizes (up to 100 μg C) are available for measurement over several targets (as demonstrated in Fig. 3). In order to assess variability in handling and blank contribution, in this study we compared multiple measurements of *ca*. 30 μg C with larger aliquots containing *ca*. 90 μg C. When taking the weighted mean and error of the three small aliquots the precision achieved is higher compared to the single large measurement of a roughly equal amount of carbon. However, as the likelihood of contamination being introduced via handling, the EA-GIS or the silver cup is increased for the smaller sample sizes, the preferred method for measuring larger samples would be to measure several targets from a single syringe, rather than splitting a sample into smaller aliquots. Although the measurement of gas samples requires more supervision than graphite targets, the direct coupling of the EA with the GIS significantly reduces sample preparation time by cutting out the graphitisation step which poses a large risk of contamination at such small sample sizes. Therefore in situations where sample size is limited the gas ion source offers an attractive solution for archaeological, as well as environmental, applications.

Even working with the assumption of 1% collagen preservation, in theory sufficient collagen could be extracted from less than 10 mg bone material to obtain a ^{14}C date using the EA-GIS-AMS. However in order to assess the quality of the extract prior to dating and obtain high-resolution stable isotopic data for palaeodietary reconstruction, collagen should also be analysed with an EA-IRMS. At 1%, around 40 mg bone material would supply enough collagen for dating and isotopic analysis. For any sample >1% preservation, excess collagen would be available for further analyses and/or multiple aliquots could be measured with the gas ion source to achieve better counting statistics and thus increase precision. Bearing this in mind, when dating highly precious bone it would be useful to assess the preservation of the artefact prior to sampling or have an understanding of collagen preservation at the archaeological site (for example if other fauna has been sampled for isotopic or ^{14}C dating purposes). Bones of high patrimonial value could be sampled strategically – i.e. for older samples expected to have less than 10% collagen preservation 40 mg bone material could be sampled, whereas for well-preserved Holocene bone much smaller samples could be taken. The case of R-EVA 548 demonstrates that for very old samples (>35,000 BP) with very poor levels of preservation (1–2%), yields falling below 1 mg collagen can be subject to severe contamination issues.

The results presented here provide further confirmation that ^{14}C measurements using the gas ion source of the MICADAS are stable, reproducible and accurate, reaching a level of precision suitable for dating archaeological samples particularly for Palaeolithic samples back to 40,000 BP. In this respect this technique will be highly useful for directly dating precious archaeological bone where limited material is available.

Methods

Sample selection. Eight bones were selected to span the ^{14}C timescale (back to 50,000 BP) at a range of preservation typical for archaeological bones. Collagen extracts from bones R-EVA 124, R-EVA 123 and R-EVA 1489 were previously dated using both graphite targets and the gas ion source in Fewlass, *et al*.[29]. R-EVA 124 was previously labelled as a bison bone but recent aDNA analysis has identified it as belonging to a woolly rhinoceros[56]. R-EVA 548 and R-EVA 570 are two faunal long bones from Teixoneres, Spain. R-EVA 1860 is a faunal long bone excavated from the site of Ranis, Germany and R-EVA 1905 is a predominantly trabecular fragment of horse bone

excavated from Pietraszyn, Poland. R-EVA 1753 is a well-preserved cave bear rib known to date beyond the ^{14}C timescale based on repeated measurements. As standard practice, an aliquot of this bone is extracted and dated alongside every batch of samples to monitor contamination introduced during sample preparation and is used in the age correction of the unknown samples. This is the referred to in the text as the 'background bone'.

Collagen extraction. For each bone, large aliquots (500–700 mg material) were pretreated using our standard acid-base-acid + gelatinisation + ultrafiltration protocol (see Fig. 2) based on Talamo and Richards[36] to produce collagen for dating with graphite targets.

In order to optimise our standard protocol for sample sizes <100 mg, small aliquots of each bone were pretreated multiple times to compare collagen yields and sample quality. Firstly, the outer surface of bone was removed using a sandblaster and aliquots were taken using a rotary drill. Fine diamond grit disc drill pieces were used to remove solid pieces of bone. Fine powder was drilled using round tungsten carbide burs (2.3 mm diameter). Aliquots were weighed via a microbalance into cleaned glass tubes. Solid samples were demineralised in HCl at 4°C with regular visual and mechanical checks and monitoring of CO_2 effervescence. For powdered samples, HCl was added and samples were monitored at room temperature (RT) until CO_2 effervescence had stopped. Following demineralisation, samples were rinsed with ultra-pure Milli-Q water to a neutral pH. Samples were treated with NaOH (0.1 M) at RT for 10 min to remove humic acid contamination and re-acidified with HCl (0.5 M). If a considerable colour change was observed, NaOH was changed and left for another 10 min. Samples were then gelatinised in weak HCl (pH 3) on a heater block set to 60 °C, 70 °C or 75 °C. Samples were either left for 20 h (as per our standard pretreatment), or regularly monitored and removed from the heater block when the sample had fully solubilised. The resultant gelatin was filtered to remove large particles >80 μm (Ezee filters, Elkay labs, UK) and ultrafiltered with Sartorius VivaSpin Turbo 15 (30 kDa MWCO) ultrafilters precleaned according to Brock, *et al*.[43] to separate the high molecular weight fraction (>30kD) for freeze drying (48 h). For details of acid strength, duration of treatment and temperature during pretreatment of samples <100 mg, see Fig. 1 and Supplementary Dataset S1.

Collagen quality assessment. To assess the quality of the collagen, all extracts were analysed via EA-IRMS to obtain elemental (C%, N%, C:N) and stable isotopic data ($\delta^{13}C$ and $\delta^{15}N$). Collagen (*ca*. 400 μg) was weighed into tin cups using a microbalance and measured on a ThermoFinnigan Flash EA coupled to a Thermo Delta plus XP isotope ratio mass spectrometer (IRMS). Stable carbon isotope ratios were expressed relative to VPDB (Vienna PeeDee Belemnite) and stable nitrogen isotope ratios were measured relative to AIR (atmospheric N_2), using the delta notation (δ) in parts per thousand (‰). Repeated analysis of both internal and international standards indicates an analytical error of 0.2‰ (1σ) for $\delta^{13}C$ and $\delta^{15}N$. Where sufficient material was available, collagen (*ca*. 300 μg) was homogenized and mixed with ~40 mg of IR grade KBr powder in an agate mortar and pestle, pressed into a pellet using a manual hydraulic press (Wasserman) and analysed with an Agilent Technologies Cary FTIR Spectrometer with a DTGS detector. Spectra were recorded in transmission mode at 4 cm^{-1} resolution with averaging of 34 scans between 4000 and 400 cm^{-1} using Resolution Pro software (Agilent Technologies). The spectra were evaluated and compared to library spectra of well-preserved collagen and bone to look for evidence of incomplete demineralisation, degraded collagen or the presence of any exogenous material in the extracts.

AMS graphite measurements. Each bone was pretreated as per our standard protocol from approximately 500 mg material. From theses extracts, approximately 3–5 mg collagen was weighed into pre-cleaned tin cups at the MPI-EVA and sent to the Curt-Engelhorn-Centre for Archaeometry Klaus-Tschira-AMS facility in Mannheim, Germany (lab code: MAMS) for graphite dating. The samples were combusted in an EA and the sample CO_2 was converted catalytically to graphite. The samples were dated using the MICADAS-AMS[57]. Age and error calculation of unknown samples was performed using BATS software[58], using background collagen samples and standards measured in the same batch, with an added external error of 1‰ as per their standard practice. Collagen samples measured at CEREGE were weighed into tin cups (*ca*. 2 mg), combusted in a vario MICRO cube EA (Elementar Analysensysteme GmbH, Germany), graphitized using the AGE 3 and dated using the AixMICADAS. Oxalic acid standards and background collagen samples measured in the same session were used to calculate the age of the samples. An external error of 1‰ was also propagated in the error calculation.

AMS gas ion source measurements. Small aliquots (<100 mg) of the same bones were pretreated to purify the collagen. Three or four aliquots of each collagen extract (containing *ca*. 25–40 μg C and a single aliquot per bone containing *ca*. 80–100 μg C) were measured via a microbalance into pre-cleaned silver cups (800 °C, 2 h). These were placed into the auto-sampler of a vario MICRO cube EA which was directly coupled to the gas ion source of the AixMICADAS via the GIS[20,22]. Following combustion, sample CO_2 was adsorbed on a zeolite trap and subsequently expanded to the syringe of the GIS where it was mixed with He (5% CO_2) and introduced to the gas ion source at a flow rate of *ca*. 2 μg C/min. The EA-GIS system was flushed with helium between samples. Pre-cleaned titanium (Ti) gas targets were pre-sputtered for approximately two minutes in the ion source to remove any remaining surface contamination before the sample CO_2 injection. Around 30–40 μg C was consumed by the AMS over the duration of one Ti target[21,55]. For the large aliquots containing *ca*. 80–90 μg C measurements were performed over multiple targets (which can be changed during measurement). Each step was fully controlled via the gas-interface handling software.

The gas measurements in this study were made over two measurement sessions six months apart, both carried out shortly after the ion source had been cleaned. Each measurement session commenced with two oxalic acid II NIST standards (from a gas canister) to normalize and correct samples for fractionation. Blank (^{14}C-free) CO_2 samples (also from a gas canister) were then measured to purge the system and reach a stable operational level ($F^{14}C$ < 0.004) (these measurements were not used in age calculation). In the first session, carbonate reference

material (IAEA-C1) were run prior to the collagen samples to check the background level of the instrument and begin the measurement of old samples under optimal conditions. In the second measurement session, phthalic anhydride was run for the same purpose. In order to alleviate problems of memory effect, the GIS system was flushed with helium between samples and samples were measured in order of increasing activity as per standard procedure (for further discussion, see Tuna, *et al.*[55]). Low energy ion currents for the gas analyses were in the range of 10–15 μA. BATS[58] was used for data reduction. The uncorrected collagen background (R-EVA 1753) measurements of the corresponding type (piece/powder) and equal size were used to correct the archaeological samples measured in the same session (i.e. 'small' sample aliquots were corrected only with 'small' background collagen samples). For all samples, the long term standard deviation of blanks ($F^{14}C = 0.001$) was used as the absolute blank error and an external error of 3.5‰ was added to take into account the long-term variability of standards ('error 2' described in Fewlass, *et al.*[29]).

Data Availability

All data generated or analysed during this study are included in this article and the accompanying supplementary information files.

References

1. Oakley, K. P. Dating Skeletal Material. *Science* **140**, 488, https://doi.org/10.1126/science.140.3566.488 (1963).
2. Berger, R., Horney, A. G. & Libby, W. F. Radiocarbon Dating of Bone and Shell from Their Organic Components. *Science* **144**, 995–1001, https://doi.org/10.1126/science.144.3621.995 (1964).
3. Wood, R. From revolution to convention: the past, present and future of radiocarbon dating. *Journal of Archaeological Science* **56**, 61–72, https://doi.org/10.1016/j.jas.2015.02.019 (2015).
4. Pearson, A. Microscale AMS 14C Measurement at NOSAMS. *Radiocarbon* **40**, 61–75 (1998).
5. Hua, Q., Zoppi, U., Williams, A. A. & Smith, A. M. Small-mass AMS radiocarbon analysis at ANTARES. *Nuclear Instruments and Methods in Physics Research Section B: Beam Interactions with Materials and Atoms* **223**, 284–292, https://doi.org/10.1016/j.nimb.2004.04.057 (2004).
6. Santos, G. M., Southon, J. R., Griffin, S., Beaupre, S. R. & Druffel, E. R. M. Ultra small-mass AMS 14C sample preparation and analyses at KCCAMS/UCI Facility. *Nuclear Instruments and Methods in Physics Research Section B: Beam Interactions with Materials and Atoms* **259**, 293–302, https://doi.org/10.1016/j.nimb.2007.01.172 (2007).
7. Smith, A. M., Petrenko, V. V., Hua, Q., Southon, J. & Brailsford, G. The Effect of N2O, Catalyst, and Means of Water Vapor Removal on the Graphitization of Small CO2 Samples. *Radiocarbon* **49**, 245–254 (2007).
8. Genberg, J., Stenstrom, K., Elfman, M. & Olsson, M. Development of graphitization of μg-sized samples at Lund University. *Radiocarbon* **52**, 1270–1276 (2010).
9. Delqué-Količ, E. *et al*. Advances in Handling Small Radiocarbon Samples at the Laboratoire de Mesure du Carbone 14 in Saclay, France. *Radiocarbon* **55**, 648–656, https://doi.org/10.1017/S0033822200057805 (2013).
10. Liebl, J. *et al*. Carbon background and ionization yield of an AMS system during C-14 measurements of microgram-size graphite samples. *Nuclear Instruments and Methods in Physics Research Section B: Beam Interactions with Materials and Atoms* **294**, 335–339, https://doi.org/10.1016/j.nimb.2012.06.015 (2013).
11. Walter, S. R. S. *et al*. Ultra-Small Graphitization Reactors for Ultra-Microscale C-14 Analysis at the National Ocean Sciences Accelerator Mass Spectrometry (NOSAMS) Facility. *Radiocarbon* **57**, 109–122, https://doi.org/10.2458/azu_rc.57.18118 (2015).
12. Freeman, E., Skinner, L. C., Reimer, R., Scrivner, A. & Fallon, S. Graphitization of Small Carbonate Samples for Paleoceanographic Research at the Godwin Radiocarbon Laboratory, University of Cambridge. *Radiocarbon* **58**, 89–97, https://doi.org/10.1017/RDC.2015.8 (2016).
13. Steier, P., Liebl, J., Kutschera, W., Wild, E. M. & Golser, R. Preparation Methods of μg Carbon Samples for 14C Measurements. *Radiocarbon* **59**, 803–814, https://doi.org/10.1017/RDC.2016.94 (2016).
14. Ertun, T. *et al*. Progress in AMS target production of sub-milligram samples at the NERC radiocarbon laboratory. *Radiocarbon* **47**, 453–464 (2005).
15. Ruff, M. *et al*. Gaseous radiocarbon measurements of small samples. *Nuclear Instruments and Methods in Physics Research Section B: Beam Interactions with Materials and Atoms* **268**, 790–794, https://doi.org/10.1016/j.nimb.2009.10.032 (2010).
16. Cersoy, S. *et al*. Radiocarbon dating minute amounts of bone (3–60 mg) with ECHoMICADAS. *Scientific Reports* **7**, 7141, https://doi.org/10.1038/s41598-017-07645-3 (2017).
17. Wacker, L., Němec, M. & Bourquin, J. A revolutionary graphitisation system: Fully automated, compact and simple. *Nuclear Instruments and Methods in Physics Research Section B: Beam Interactions with Materials and Atoms* **268**, 931–934, https://doi.org/10.1016/j.nimb.2009.10.067 (2010).
18. Ruff, M. *et al*. A gas ion source for radiocarbon measurements at 200 kV. *Radiocarbon* **49**, 307–314 (2007).
19. Wacker, L. *et al*. MICADAS: Routine and High-Precision Radiocarbon Dating. *Radiocarbon* **52**, 252–262 (2010).
20. Ruff, M. *et al*. On-line radiocarbon measurements of small samples using elemental analyzer and MICADAS gas ion source. *Radiocarbon* **52**, 1645–1656 (2010).
21. Fahrni, S. M., Wacker, L., Synal, H.-A. & Szidat, S. Improving a gas ion source for 14C AMS. *Nuclear Instruments and Methods in Physics Research Section B: Beam Interactions with Materials and Atoms* **294**, 320–327, https://doi.org/10.1016/j.nimb.2012.03.037 (2013).
22. Wacker, L. *et al*. A versatile gas interface for routine radiocarbon analysis with a gas ion source. *Nuclear Instruments and Methods in Physics Research Section B: Beam Interactions with Materials and Atoms* **294**, 315–319, https://doi.org/10.1016/j.nimb.2012.02.009 (2013).
23. Wacker, L., Lippold, J., Molnár, M. & Schulz, H. Towards radiocarbon dating of single foraminifera with a gas ion source. *Nuclear Instruments and Methods in Physics Research Section B: Beam Interactions with Materials and Atoms* **294**, 307–310, https://doi.org/10.1016/j.nimb.2012.08.038 (2013).
24. McIntyre, C. P. *et al*. Online 13C and 14C Gas Measurements by EA-IRMS–AMS at ETH Zürich. *Radiocarbon* **59**, 893–903, https://doi.org/10.1017/RDC.2016.68 (2016).
25. Bonvalot, L. *et al*. Estimating contributions from biomass burning and fossil fuel combustion by means of radiocarbon analysis of carbonaceous aerosols: application to the Valley of Chamonix. *Atmos. Chem. Phys.* **16**, 13753–13772, https://doi.org/10.5194/acp-2016-351 (2016).
26. Hoffmann, H. M. *Micro radiocarbon dating of the particulate organic carbon fraction in Alpine glacier ice: method refinement, critical evaluation and dating applications*, Universität Heidelberg (2016).
27. Gottschalk, J. *et al*. Radiocarbon Measurements of Small-Size Foraminiferal Samples with the Mini Carbon Dating System (Micadas) at the University of Bern: Implications for Paleoclimate Reconstructions. *Radiocarbon* **60**, 469–491, https://doi.org/10.1017/Rdc.2018.3 (2018).

28. Haghipour, N. *et al*. Compound-Specific Radiocarbon Analysis by Elemental Analyzer–Accelerator Mass Spectrometry: Precision and Limitations. *Analytical Chemistry* **91**, 2042–2049, https://doi.org/10.1021/acs.analchem.8b04491 (2019).
29. Fewlass, H. *et al*. Size Matters: Radiocarbon Dates of <200 µg Ancient Collagen Samples with AixMICADAS and Its Gas Ion Source. *Radiocarbon* **60**, 425–439, https://doi.org/10.1017/rdc.2017.98 (2017).
30. Bard, E. *et al*. AixMICADAS, the accelerator mass spectrometer dedicated to 14C recently installed in Aix-en-Provence, France. *Nuclear Instruments and Methods in Physics Research Section B: Beam Interactions with Materials and Atoms* **361**, 80–86, https://doi.org/10.1016/j.nimb.2015.01.075 (2015).
31. DeNiro, M. J. & Weiner, S. Chemical, enzymatic and spectroscopic characterization of "collagen" and other organic fractions from prehistoric bones. *Geochimica et Cosmochimica Acta* **52**, 2197–2206, https://doi.org/10.1016/0016-7037(88)90122-6 (1988).
32. van Klinken, G. J. Bone Collagen Quality Indicators for Palaeodietary and Radiocarbon Measurements. *Journal of Archaeological Science* **26**, 687–695 (1999).
33. Longin, R. New Method of Collagen Extraction for radiocarbon Dating. *Nature* **231**, 241–242 (1971).
34. Jørkov, M. L. S., Heinemeier, J. & Lynnerup, N. Evaluating bone collagen extraction methods for stable isotope analysis in dietary studies. *Journal of Archaeological Science* **34**, 1824–1829, https://doi.org/10.1016/j.jas.2006.12.020 (2007).
35. Pestle, W. J. Chemical, elemental, and isotopic effects of acid concentration and treatment duration on ancient bone collagen: an exploratory study. *Journal of Archaeological Science* **37**, 3124–3128, https://doi.org/10.1016/j.jas.2010.07.013 (2010).
36. Talamo, S. & Richards, M. A comparison of bone pretreatment methods for AMS dating of samples >30,000 BP. *Radiocarbon* **53**, 443–449 (2011).
37. Fulop, R.-H., Heinze, S., John, S. & Rethemeyer, J. Ultrafiltration of bone samples is neither the problem nor the solution. *Radiocarbon* **55**, 491–500 (2013).
38. Cersoy, S., Zazzo, A., Lebon, M., Rofes, J. & Zirah, S. Collagen Extraction and Stable Isotope Analysis of Small Vertebrate Bones: A Comparative Approach. *Radiocarbon* **59**, 679–694, https://doi.org/10.1017/rdc.2016.82 (2016).
39. Brown, T. A., Nelson, D. E., Vogel, J. S. & Southon, J. R. Improved collagen extraction by modified longin method. *Radiocarbon* **30**, 171–177 (1988).
40. Higham, T. European Middle and Upper Palaeolithic radiocarbon dates are often older than they look: problems with previous dates and some remedies. *Antiquity* **85**, 235–249 (2011).
41. Hüls, C. M., Grootes, P. M. & Nadeau, M. J. Ultrafiltration: Boon or Bane? *Radiocarbon* **51**, 613–625, https://doi.org/10.1017/S003382220005596X (2009).
42. Bronk Ramsey, C., Higham, T., Bowles, A. & Hedges, R. Improvements to the pretreatment of bone at Oxford. *Radiocarbon* **46**, 155–164 (2004).
43. Brock, F., Bronk Ramsey, C. & Higham, T. Quality assurance of ultrafiltered bone dating. *Radiocarbon* **49**, 187–192 (2007).
44. Brock, F., Higham, T., Ditchfield, P. & Bronk Ramsey, C. Current pretreatment methods for AMS radiocarbon dating at the Oxford Radiocarbon Accelerator Unit (ORAU). *Radiocarbon* **52**, 103–112 (2010).
45. Higham, T. F. G., Jacobi, R. M. & Ramsey, C. B. AMS radiocarbon dating of ancient bone using ultrafiltration. *Radiocarbon* **48**, 179–195 (2006).
46. Wood, R. E. *et al*. Radiocarbon dating casts doubt on the late chronology of the Middle to Upper Palaeolithic transition in southern Iberia. *Proceedings of the National Academy of Sciences* **110**, 2781–2786 (2013).
47. Hublin, J.-J. *et al*. Radiocarbon dates from the Grotte du Renne and Saint-Cesaire support a Neandertal origin for the Chatelperronian. *Proceedings of the National Academy of Sciences* **109**, 18743–18748, https://doi.org/10.1073/pnas.1212924109 (2012).
48. Yizhaq, M. *et al*. Quality Controlled Radiocarbon Dating of Bones and Charcoal from the Early Pre-Pottery Neolithic B (PPNB) of Motza (Israel). *Radiocarbon* **47**, 193–206, https://doi.org/10.1017/S003382220001969X (2005).
49. D'Elia, M. *et al*. Evaluation of possible contamination sources in the 14C analysis of bone samples by FTIR spectroscopy. *Radiocarbon* **49**, 201–210 (2007).
50. Schoeninger, M. J., Moore, K. M., Murray, M. L. & Kingston, J. D. Detection of bone preservation in archaeological and fossil samples. *Applied Geochemistry* **4**, 281–292, https://doi.org/10.1016/0883-2927(89)90030-9 (1989).
51. Ward, G. K. & Wilson, S. R. Procedures for Comparing and Combining Radiocarbon Age Determinations: A Critique. *Archaeometry* **20**, 19–31, https://doi.org/10.1111/j.1475-4754.1978.tb00208.x (1978).
52. Bronk Ramsey, C. Bayesian Analysis of Radiocarbon Dates. *Radiocarbon* **51**, 337–360 (2009).
53. Semal, P. & Orban, R. Collagen Extraction from Recent and Fossil Bones: Quantitative and Qualitative Aspects. *Journal of Archaeological Science* **22**, 463–467, https://doi.org/10.1006/jasc.1995.0045 (1995).
54. Brock, F., Geoghegan, V., Thomas, B., Jurkschat, K. & Higham, T. F. G. Analysis of Bone "Collagen" Extraction Products for Radiocarbon Dating. *Radiocarbon* **55**, 445–463, https://doi.org/10.1017/S0033822200057581 (2013).
55. Tuna, T., Fagault, Y., Bonvalot, L., Capano, M. & Bard, E. Development of small CO2 gas measurements with AixMICADAS. *Nuclear Instruments and Methods in Physics Research Section B: Beam Interactions with Materials and Atoms* **437**, 93–97, https://doi.org/10.1016/j.nimb.2018.09.012 (2018).
56. Korlević, P., Talamo, S. & Meyer, M. A combined method for DNA analysis and radiocarbon dating from a single sample. *Scientific Reports* **8**, 4127, https://doi.org/10.1038/s41598-018-22472-w (2018).
57. Kromer, B., Lindauer, S., Synal, H.-A. & Wacker, L. MAMS - A new AMS facility at the Curt-Engelhorn-Centre for Achaeometry, Mannheim, Germany. *Nuclear Instruments and Methods in Physics Research Section B: Beam Interactions with Materials and Atoms* **294**, 11–13, https://doi.org/10.1016/j.nimb.2012.01.015 (2013).
58. Wacker, L., Christl, M. & Synal, H.-A. Bats: A new tool for AMS data reduction. *Nuclear Instruments and Methods in Physics Research Section B: Beam Interactions with Materials and Atoms* **268**, 976–979, https://doi.org/10.1016/j.nimb.2009.10.078 (2010).

Acknowledgements

We would like to thank the Max Planck Society for funding this research. The AixMICADAS was acquired and is operated in the framework of the EQUIPEX project ASTER-CEREGE (PI E. Bard) with additional matching funds from the Collège de France, which also supports the salaries of the authors from CEREGE. We are indebted to Dr. Raquel Silva Maria and Sven Steinbrenner of the Department of Human Evolution at the MPI-EVA for technical assistance. We give kind thanks to Caterina Pangrazzi, Jordi Rosell, Ruth Blasco, Marcel Weiss and Andrzej Wisniewski for access to samples during the course of the study.

Author Contributions

H.F., S.T., B.K., J.-J.H. and E.B. devised the study; H.F. carried out sample pretreatment, FTIR and EA-IRMS analyses under the supervision of S.T.; T.T. and Y.F. performed EA-GIS-AMS measurements; T.T., B.K. and H.F. performed data reduction; H.F. wrote the paper with input from all authors.

Additional Information

Supplementary information accompanies this paper at https://doi.org/10.1038/s41598-019-41557-8.

Competing Interests: The authors declare no competing interests.

Publisher's note: Springer Nature remains neutral with regard to jurisdictional claims in published maps and institutional affiliations.

Pretreatment and gaseous radiocarbon dating of 40-100 mg archaeological bone

Fewlass, H., Tuna, T., Fagault, Y., Hublin, J-J., Kromer, B., Bard, E., Talamo, S.

Supplementary information:

- Dataset S1 – Pretreatment information for all collagen extracts in the study
- Dataset S2 – Radiocarbon dates for all samples in the study dated with graphite targets and the gas ion source
- Dataset S3 – EA-GIS-AMS data from background bone R-EVA 1753
- Dataset S4 – EA-GIS-AMS data from system blanks
- Figure S1 – Gas dates from background bone R-EVA 1753 according to the amount of C in the EA-GIS
- Figure S2 – Gas measurements of R-EVA 123 and R-EVA 124 from both solid and powdered extracts
- Figure S3 - Example FTIR spectra of collagen extracted in the study

Supplementary Text

Pretreatment and ^{14}C dating of powdered bone samples

Bone aliquots were extracted in two forms: fine powder and solid pieces (as per our standard protocol for *ca.* 500mg bone). We attempted to extract collagen from finely powdered bone to increase our sampling options for precious bones (i.e. a key hole drilling technique). However, the collagen yield of powdered bone was much lower than solid pieces for all samples in the study (Supplementary Fig. S2; Supplementary Dataset S1). Where collagen was recovered often the extracted material appeared poorly preserved with a crumbly texture and was often dark grey or yellow in colour. Where enough material was available for analysis, these extracts were still identified as collagen when analysed with FTIR (Supplementary Fig. S3), although several extracts from the poorly preserved bones showed evidence of incomplete demineralisation. Anecdotally, the striking difference between the two forms was observed at the demineralisation stage; for the older, poorly preserved bones much of the powdered material was lost as soon as HCl was added to the tube. Although the powdered method has the benefit of being faster, increased solubilisation of collagen during demineralisation in powdered bones compared to solid bone sherds was also observed by Schoeninger, et al. [1] and Collins and Galley [2]. As the length of demineralisation is based on visual inspection, a suitable duration is much easier to judge for solid pieces (transparency, softness, buoyancy, CO_2 effervescence).

As a consequence of the low yield of collagen for the poorly preserved bones (R-EVA 570 and R-EVA 548) no powdered extracts from these bones were dated. Despite the lower collagen yield, sufficient collagen was available for gas dating from powdered aliquots of the well-preserved bones, R-EVA 123, R-EVA 124 and R-EVA 1753. The age of the background collagen extracts were slightly younger than their solid counterparts (Supplementary Fig. S1) but it is unknown whether this reflected the limited number of measurements made, the lower collagen yield from these pretreatments and/or the small size of the aliquots measured in the EA-GIS-AMS (*ca*. 25 µg C).The ages of the <50,000 BP samples were corrected with background collagen measurements of the same size (*ca*. 30 µg C or *ca.* 90 µg C) and type (solid/powder) measured during the same session. The exception to this are the large (*ca.* 90 µg C) powder samples from R-EVA 123 and R-EVA 124 (Aix-12002.7.1; 12002.8.1; 12003.8.5; 12003.9.5) which are marked with an asterisk in Supplementary Figure S2. No background measurement of corresponding size/type was made so these were corrected with small (*ca.* 30 µg C) powder backgrounds meaning they are slightly over-corrected. Even with this over-correction, the age of Aix-12002.8.1 is younger than other measurements for this bone. We do not have an explanation for this measurement.

Despite this, there is no difference between the gas measurements obtained from powdered versus solid extracts for R-EVA 123 or R-EVA 124, which all agree within X^2 despite the over-corrected samples (Supplementary Fig. S2; Supplementary Dataset S2). Further, the gas dates from the powdered extracts of R-EVA 123 and R-EVA 124 all agree with the graphite dates

within 2σ. However, due to the reduced collagen yield we will continue our standard practice of extracting collagen from solid chunks of bone (also documented in Tuross [3]).

References

1 Schoeninger, M. J., Moore, K. M., Murray, M. L. & Kingston, J. D. Detection of bone preservation in archaeological and fossil samples. *Applied Geochemistry* **4**, 281-292, doi:10.1016/0883-2927(89)90030-9 (1989).

2 Collins, M. J. & Galley, P. Towards an optimal method of archaeological collagen extraction: The influence of pH and grinding. *Ancient Biomolecules* **2**, 209 (1998).

3 Tuross, N. Comparative Decalcification Methods, Radiocarbon Dates, and Stable Isotopes of the Viri Bones. *Radiocarbon* **54**, 837-844 (2012).

4 Fewlass, H. *et al.* Size Matters: Radiocarbon Dates of <200 µg Ancient Collagen Samples with AixMICADAS and Its Gas Ion Source. *Radiocarbon* **60**, 425-439, doi:10.1017/rdc.2017.98 (2017).

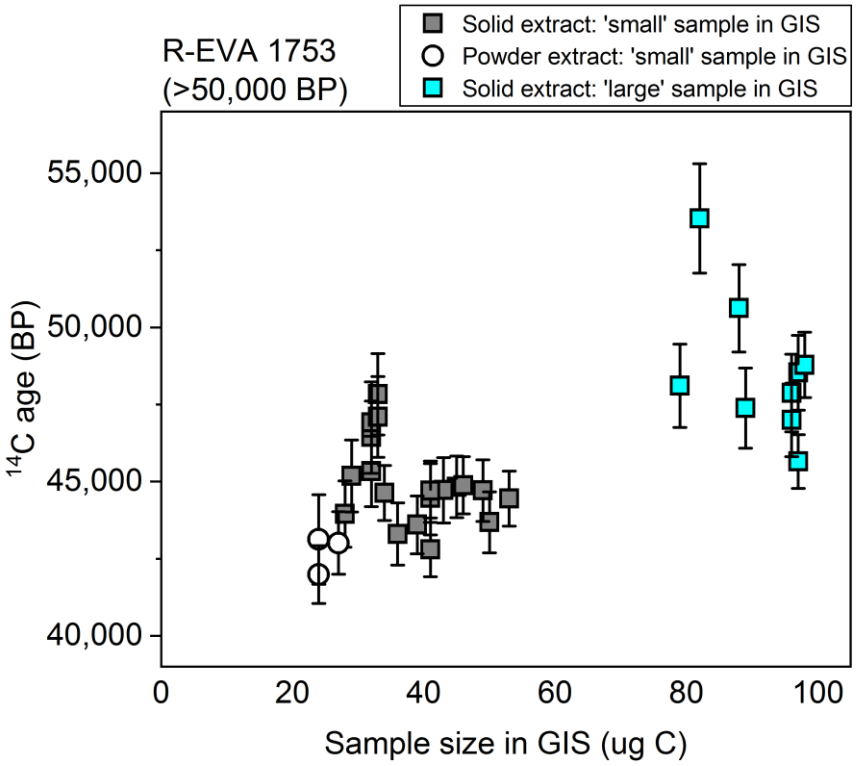

Supplementary figure S1 Gas measurements of collagen from background bone R-EVA 1753 according to the amount of carbon in the EA-GIS system. Error bars are shown to 1σ.

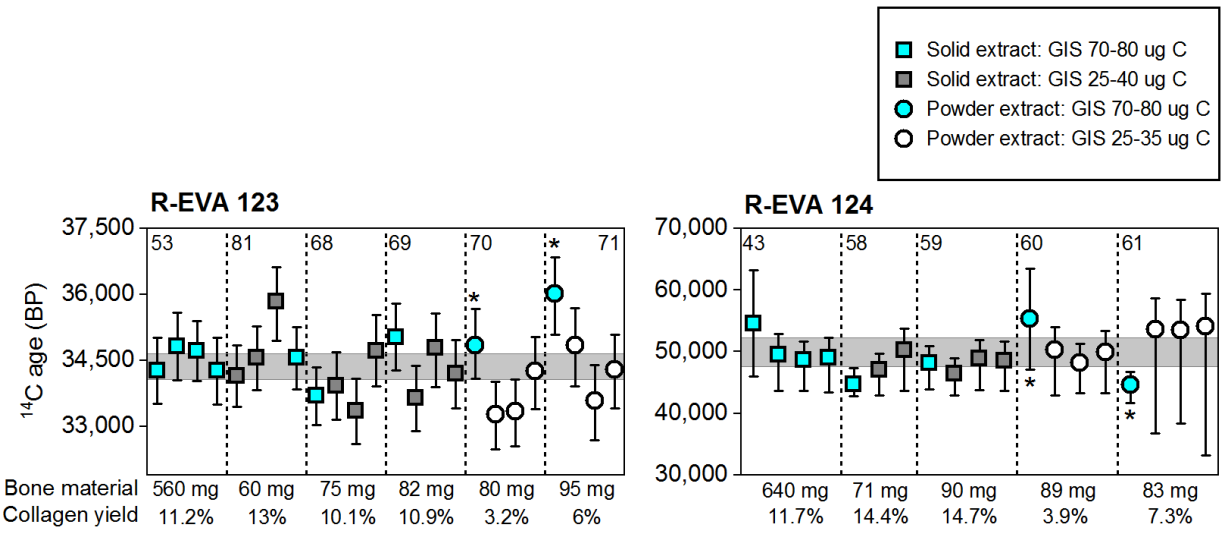

Supplementary figure S2 Gas measurements of collagen from R-EVA 123 and R-EVA 124. Figure amended from Figure 3 in the main text to include gas measurements of collagen extracted from powdered bone.

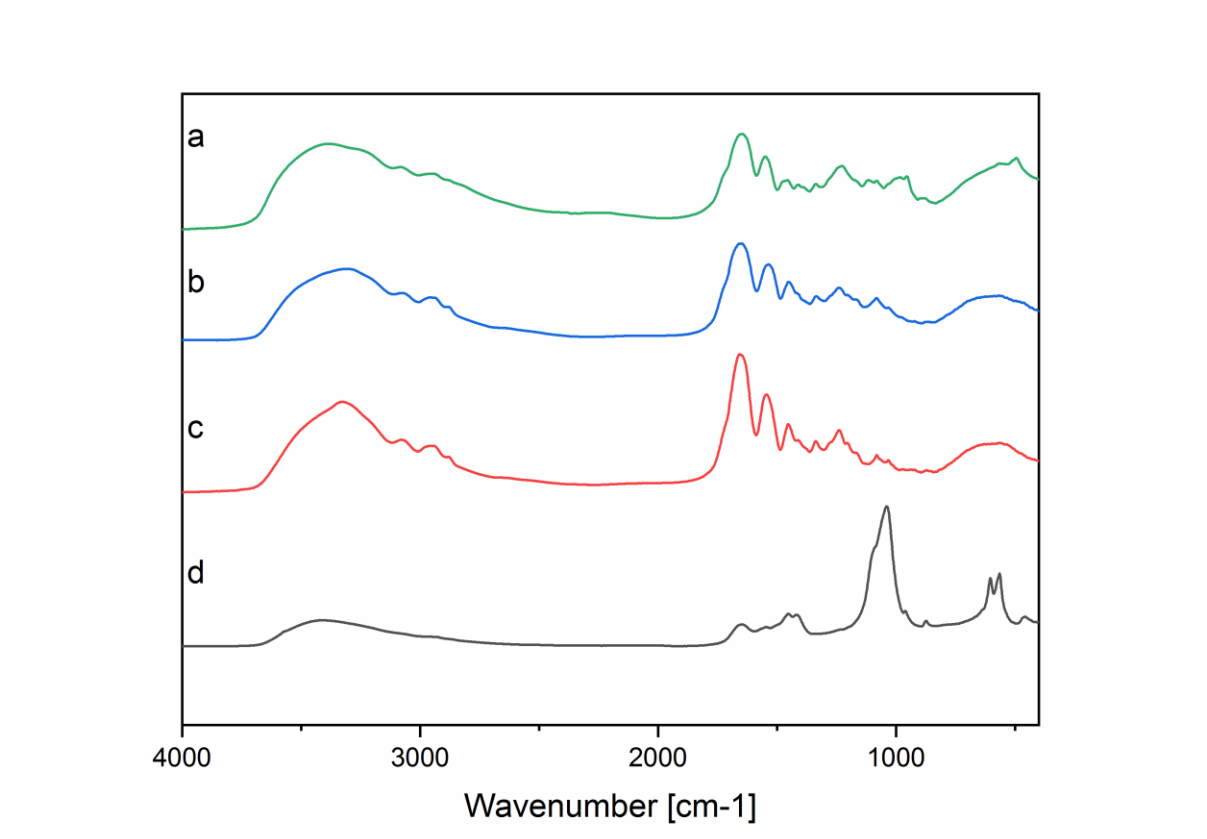

Supplementary figure S3 FTIR spectra of collagen extracted from a) R-EVA 570.15 (powder) and b) R-EVA 1489.2 (solid) in comparison to characteristic FTIR spectra of c) well-preserved collagen and d) bone.

Pretreatment and gaseous radiocarbon dating of 40-100 mg archaeological bone
Supplementary Dataset S1 – Pretreatment information for all collagen extracts in the study

R-EVA	AMS lab code	prep no	batch	form	bone wt (mg)	Demineralisation			Gelatinisation		Quality control									^{14}C dated
						HCl strength	Temp	Duration	Temp	Duration	Coll yld (mg)	Coll yld (%)	$\delta^{13}C$	$\delta^{15}N$	C%	N%	C:N	FTIR	Collagen appearance	
1753	Aix-12018	2	A	piece	97.1	0.5M	4°C	44h	75°C	20h	4.6	4.7	-22.55	1.45	40.8	14.8	3.2	collagen	white and fluffy	
		3	A	piece	55.4	0.5M	4°C	20h	75°C	20h	2.6	4.7	-22.76	1.26	40.5	14.7	3.2	collagen	white and fluffy	
		4	B	piece	102.5	0.5M	4°C	26h	70°C	4h	8.8	8.6	-22.67	1.44	39.7	14.8	3.1	collagen	white and fluffy	
		5	B	piece	55.9	0.5M	4°C	26h	70°C	2h	5.5	9.8	-22.65	1.59	49.5	18.3	3.2	collagen	white and fluffy	
		29	H	piece	69.2	0.5M	4°C	26h	70°C	6h	7.6	11.0	-22.88	1.64	41.1	15.3	3.1	collagen	white and fluffy	gas
		48	L	piece	62.0	0.5M	4°C	27h	70°C	5h	8.4	13.5	-22.72	1.37	43.9	16.1	3.2	collagen	white and fluffy	gas
		56	P	piece	68.7	0.5M	4°C	29h	70°C	3h	8.9	13.0	-23.24	1.70	45.0	15.6	3.4	collagen	white and fluffy	gas
		60	S	piece	69.3	0.5M	4°C	29h	70°C	3h	10.2	14.7	-22.85	1.44	44.6	16.0	3.3	collagen	white and fluffy	gas
		61	T	piece	40.8	0.5M	4°C	24h	70°C	20h	5.5	13.5	-22.86	1.94	44.8	16.2	3.2	collagen	white and fluffy	gas
		62	U	piece	55.9	0.5M	4°C	32h	70°C	3h	8.6	15.4	-23.21	1.52	45.4	15.6	3.4	collagen	white and fluffy	gas
		39	A1	piece	99.7	0.5M	4°C	50h	70°C	3h	12.2	12.2	-22.94	1.53	43.0	15.9	3.2	collagen	white and fluffy	gas
		40	A1	piece	74.5	0.5M	4°C	45h	70°C	3h	10.1	13.6	-23.16	1.91	43.4	15.9	3.2	collagen	white and fluffy	
		41	A2	piece	97.6	0.5M	4°C	50h	70°C	3h	12.8	13.1	-22.99	1.81	43.7	16.1	3.2	collagen	white and fluffy	gas
		42	A2	piece	92.8	0.5M	4°C	50h	70°C	3h	11.1	12.0	-23.06	2.16	42.3	15.8	3.1	collagen	white and fluffy	
		59	R	piece	79.9	0.5M	4°C	50h	70°C	3h	11.7	14.6	-22.85	1.28	45.0	16.1	3.2	collagen	white and fluffy	gas
		33	J	piece	90.3	0.5M	4°C	42h	60°C	6h	10.3	11.4	-22.31	1.36	43.7	15.8	3.2	collagen	white and fluffy	
		34	J	piece	99.4	0.2M	4°C	98h	60°C	6h	10.9	11.0	-22.28	1.25	44.2	15.7	3.3	collagen	white and fluffy	gas
		6	C	powder	97.4	0.5M	RT	40min	75°C	20h	2.9	3.0	-22.65	1.90	34.5	12.9	3.1	collagen	white and fluffy	
		7	C	powder	51.6	0.5M	RT	40min	75°C	20h	1.7	3.3	-22.63	1.52	38.4	14.2	3.2	collagen	white and fluffy	
		8	D	powder	97.3	0.5M	4°C	2h	70°C	3h	6.2	6.4	-22.35	1.25	37.0	13.5	3.2	collagen	white and fluffy	
		9	D	powder	51.3	0.5M	4°C	2h	70°C	3h	3.4	6.6	-22.57	1.30	42.2	15.4	3.2	collagen	white and fluffy	
		30	H2	powder	68.0	0.5M	RT	10min	70°C	4h	4.2	6.2	-23.04	1.90	41.5	15.4	3.2	collagen	white and fluffy	
		43	A3	powder	80.9	0.2M	RT	10min	70°C	4h	1.9	2.3	-23.20	1.99	35.2	12.9	3.2	collagen	white and fluffy	gas
		44	A3	powder	76.4	0.2M	RT	30min	70°C	3h	1.0	1.3	-23.08	2.73	41.7	15.3	3.2	collagen	white and fluffy	
		45	A4	powder	87.8	0.2M	RT	20min	70°C	6h	5.1	5.8	-22.90	1.85	34.9	12.9	3.2	collagen	white and fluffy	gas
		46	A4	powder	83.3	0.2M	RT	20min	70°C	6h	4.5	5.4	-23.00	1.75	35.8	13.1	3.2	collagen	white and fluffy	

Pretreatment and gaseous radiocarbon dating of 40-100 mg archaeological bone
Supplementary Dataset S1 – Pretreatment information for all collagen extracts in the study

R-EVA	AMS lab code	prep no	batch	form	bone wt (mg)	Demineralisation HCl strength	Demineralisation Temp	Demineralisation Duration	Gelatinisation Temp	Gelatinisation Duration	Quality control Coll yld (mg)	Coll yld (%)	$\delta^{13}C$	$\delta^{15}N$	C%	N%	C:N	FTIR	Collagen appearance	^{14}C dated
124	Aix-12002	43	2016	piece	639.5	0.5M	4°C	16days	75°C	20h	74.6	11.7	-20.00	3.30	45.9	17.2	3.1	-	white and fluffy	graphite + gas
		46	A	piece	106	0.5M	4°C	44h	75°C	20h	13.5	12.7	-20.30	2.90	42.2	15.3	3.2	collagen	white and fluffy	
		47	A	piece	58.8	0.5M	4°C	44h	75°C	20h	6.4	10.9	-20.28	2.93	42.8	15.6	3.2	collagen	white and fluffy	
		48	B	piece	95.5	0.5M	4°C	69h	70°C	5h	12.7	13.3	-20.41	3.05	42.1	15.8	3.1	collagen	white and fluffy	
		49	B	piece	55	0.5M	4°C	44h	70°C	4h	7.8	14.2	-20.34	3.08	46.9	17.6	3.1	collagen	white and fluffy	
		58	A1	piece	70.6	0.5M	4°C	71h	70°C	6h	10.2	14.4	-20.38	4.12	42.6	15.7	3.2	collagen	white and fluffy	gas
		59	A2	piece	90.2	0.5M	4°C	71h	70°C	6h	13.3	14.7	-20.32	3.16	44.6	16.1	3.2	collagen	white and fluffy	gas
		51	C	powder	51.5	0.5M	RT	45min	75°C	20h	1.6	3.1	-20.38	3.14	38.8	14.3	3.2	collagen	black and crumbly	
		52	D	powder	99.6	0.5M	4°C	2h	70°C	3h	5.0	5.0	-20.34	3.08	32.9	11.9	3.2	collagen	dark grey	
		53	D	powder	52	0.5M	4°C	2h	70°C	3h	1.5	2.9	-20.43	3.09	37.6	13.7	3.2	collagen	dark grey	
		60	A3	powder	88.8	0.2M	RT	35min	70°C	4h	3.5	3.9	-20.13	3.26	40.3	14.7	3.2	collagen	grey and fluffy	gas
		61	A4	powder	83.1	0.2M	RT	30min	70°C	6h	6.1	7.3	-20.29	3.08	41.7	15.3	3.2	collagen	white and fluffy	gas
548	Aix-12017	17	2017	piece	597.5	0.5M	4°C	15days	75°C	20h	5.0	0.8	-20.27	4.74	40.4	13.9	3.4	collagen	white and fluffy	graphite
		3	H	piece	71.2	0.5M	4°C	26h	70°C	3h	1.5	2.1	-20.43	4.70	38.5	13.8	3.2	collagen	white and fluffy	gas
		13	A1	piece	78.1	0.5M	4°C	45h	70°C	2h	0.6	0.8	-20.73	4.20	42.9	14.8	3.4	-	white and fluffy	gas
		14	A2	piece	86.4	0.5M	4°C	45h	70°C	2h	1.1	1.3	-20.33	4.33	41.5	14.6	3.3	-	white and fluffy	gas
		7	J	piece	74.7	0.5M	4°C	27h	60°C	6h	0.7	0.9	-	-	-	-	-	collagen	white and fluffy	
		8	J	piece	84.7	0.2M	4°C	90h	60°C	6h	1.5	1.8	-20.29	5.40	41.5	15.1	3.2	collagen	white and fluffy	gas
		4	H	powder	80.6	0.5M	RT	5min	70°C	2h	0.2	0.2	-	-	-	-	-	-	white marks	
		15	A3	powder	82.4	0.2M	RT	10min	70°C	3h	0.5	0.6	-	-	-	-	-	-	white marks	
		16	A4	powder	80.7	0.2M	RT	20min	70°C	4h	0.9	1.1	-	-	-	-	-		white marks	
		9	J	powder	86.7	0.5M	RT	5min	60°C	4h	0.5	0.6	-	-	-	-	-	-	white marks	
		10	J	powder	86.5	0.2M	RT	50min	60°C	4h	0.3	0.3	-	-	-	-	-	-	white marks	

Pretreatment and gaseous radiocarbon dating of 40-100 mg archaeological bone
Supplementary Dataset S1 – Pretreatment information for all collagen extracts in the study

						Demineralisation			Gelatinisation		Quality control									
R-EVA	AMS lab code	prep no	batch	form	bone wt (mg)	HCl strength	Temp	Duration	Temp	Duration	Coll yld (mg)	Coll yld (%)	$\delta^{13}C$	$\delta^{15}N$	C%	N%	C:N	FTIR	Collagen appearance	^{14}C dated
570	Aix-12015	17	2017	piece	451.9	0.5M	4°C	13days	75°C	20h	15.2	3.4	-18.41	7.34	44.5	15.4	3.4	collagen	white and fluffy	graphite
		3	H	piece	62.1	0.5M	4°C	26h	70°C	2h	2.9	4.7	-19.13	7.63	43.3	15.4	3.3	collagen	white and fluffy	gas
		19	U	piece	43.8	0.5M	4°C	24h	70°C	2h	2.2	5.0	-18.43	7.89	44.0	15.1	3.4	collagen	white and fluffy	gas
		13	A1	piece	87	0.5M	4°C	45h	70°C	2h	2.2	2.5	-19.47	7.28	43.9	15.3	3.3	collagen	white and fluffy	gas
		14	A2	piece	90.1	0.5M	4°C	45h	70°C	2h	4.0	4.4	-18.87	7.21	43.1	15.2	3.3	collagen	white and fluffy	gas
		7	J	piece	77.9	0.5M	4°C	42h	60°C	5.5h	3.9	5.0	-18.83	7.67	41.5	14.7	3.3	collagen	white and fluffy	
		8	J	piece	69.8	0.2M	4°C	98h	60°C	5h	3.5	5.0	-18.72	7.86	43.5	15.2	3.3	collagen	white and fluffy	gas
		18	P	piece	53.2	0.5M	4°C	24h	70°C	3h	2.1	3.9	-19.45	7.39	42.6	15.2	3.3	collagen	white and fluffy	
		4	H	powder	62.6	0.5M	RT	5min	70°C	3h	0.4	0.6	-	-	-	-	-	-	tiny white fluff	
		9	J	powder	83	0.5M	RT	5min	60°C	4h	0.9	1.1	-	-	-	-	-	collagen	white and crumbly	
		10	J	powder	72	0.2M	RT	50min	60°C	4h	0.8	1.1	-	-	-	-	-	collagen	white and fluffy	
		15	A3	powder	85.9	0.2M	RT	10min	70°C	3h	0.8	0.9	-	-	-	-	-	collagen + other peaks	yellow and crumbly	
		16	A4	powder	88.1	0.2M	RT	20min	70°C	4h	1.5	1.7	-	-	-	-	-	-	tiny yellow fluff	
123	Aix-12003	53	2016	piece	559.4	0.5M	4°C	12days	75°C	20h	62.6	11.2	-21.10	7.10	45.6	17.2	3.2	-	white and fluffy	graphite + gas
		60	A	piece	100.2	0.5M	4°C	44h	75°C	20h	9.4	9.4	-21.19	6.81	37.9	13.7	3.2	collagen	white and fluffy	
		61	A	piece	51.7	0.5M	4°C	20h	75°C	20h	3.5	6.8	-21.44	6.79	38.8	14.2	3.2	collagen	white and fluffy	
		62	B	piece	101.1	0.5M	4°C	26h	70°C	3.5h	10.4	10.3	-21.37	6.84	42.2	15.6	3.2	collagen	white and fluffy	
		63	B	piece	50	0.5M	4°C	21h	70°C	3h	5.0	10.0	-21.41	6.84	43.2	16.0	3.2	collagen	white and fluffy	
		81	P	piece	60.7	0.5M	4°C	24h	70°C	5h	7.9	13.0	-21.23	6.79	41.8	15.0	3.2	collagen	white and fluffy	gas
		68	A1	piece	75	0.5M	4°C	45h	70°C	4h	7.6	10.1	-21.24	6.86	43.4	15.6	3.2	collagen	white and fluffy	gas
		69	A2	piece	82.4	0.5M	4°C	45h	70°C	4h	9.0	10.9	-21.00	6.92	44.2	15.9	3.2	collagen	white and fluffy	gas
		64	C	powder	100.5	0.5M	RT	50min	75°C	20h	9.4	9.4	-21.33	6.90	37.3	13.8	3.2	collagen	white and fluffy	
		65	C	powder	50.5	0.5M	RT	50min	75°C	20h	2.8	5.5	-21.24	6.88	41.0	15.4	3.1	collagen	white and fluffy	
		66	D	powder	103.3	0.5M	4°C	2h	70°C	3h	7.5	7.3	-21.27	6.80	35.9	13.2	3.2	collagen	white and fluffy	
		67	D	powder	50.3	0.5M	4°C	2h	70°C	3h	4.0	8.0	-21.10	6.84	36.7	13.6	3.2	collagen	white and fluffy	
		70	A3	powder	79.9	0.2M	RT	35min	70°C	4h	2.4	3.0	-21.24	6.82	36.0	13.1	3.2	collagen	grey and fluffy	gas
		71	A4	powder	94.5	0.2M	RT	30min	70°C	6h	5.7	6.0	-21.14	6.98	31.8	11.8	3.1	collagen	grey and fluffy	gas

Pretreatment and gaseous radiocarbon dating of 40-100 mg archaeological bone

Supplementary Dataset S1 – Pretreatment information for all collagen extracts in the study

						Demineralisation			Gelatinisation		Quality control									
R-EVA	AMS lab code	prep no	batch	form	bone wt (mg)	HCl strength	Temp	Duration	Temp	Duration	Coll yld (mg)	Coll yld (%)	$\delta^{13}C$	$\delta^{15}N$	C%	N%	C:N	FTIR	Collagen appearance	^{14}C dated
1860	Aix-12022	1	2017	piece	454.4	0.5M	4°C	10days	75°C	20h	41.1	9.0	-18.04	4.64	42.6	15.4	3.2	-	white and fluffy	graphite
		2	R	piece	55.7	0.5M	4°C	72h	70°C	4h	4.9	8.8	-18.34	4.54	45.2	15.8	3.3	collagen	white and fluffy	gas
		3	S	piece	44.6	0.5M	4°C	24h	70°C	6h	4.5	10.1	-18.11	4.66	43.2	15.3	3.3	collagen	white and fluffy	gas
1905	Aix-12023	1	2017	piece	582.9	0.5M	4°C	26days	75°C	20h + 20h	31.9	5.5	-20.70	5.62	41.4	15.0	3.2	-	white and fluffy	graphite
		3	S	piece	65.0	0.5M	4°C	24h	70°C	27h	4.7	7.2	-20.71	5.53	43.6	15.4	3.3	collagen	white and fluffy	gas
		4	T	piece	54.9	0.5M	4°C	9h	70°C	25h	2.0	3.6	-20.53	5.44	41.1	15.3	3.1	collagen	white and fluffy	gas
1489	Aix-12004	1	2016	piece	753.2	0.5M	4°C	18days	75°C	20h	134.5	17.9	-16.40	8.80	45.4	16.7	3.2	-	white and fluffy	graphite + gas
		2	L	piece	53.9	0.5M	4°C	21h	70°C	11h	9.7	18.0	-16.35	8.79	45.0	16.4	3.2	collagen	white and fluffy	gas
		4	T	piece	37.4	0.5M	4°C	24h	70°C	20h	7.0	18.7	-16.27	8.74	45.1	16.3	3.2	collagen	white and fluffy	gas

Pretreatment and gaseous radiocarbon dating of 40-100 mg archaeological bone

Supplementary Dataset S2 – Radiocarbon dates for all samples in the study dated with graphite targets and the gas ion source

		~500mg extraction, solid graphite target dates							~500mg bone extraction, EA-GIS-AMS dates (Fewlass et al., 2018)					<100mg bone extraction							
R-EVA	Site	R-EVA	Bone wt (mg)	Coll yld (%)	C:N	AMS lab code	^{14}C age	±	R-EVA	AMS lab code	GIS C (µg)	^{14}C age	± (err 2)	Session	R-EVA	Batch	Form	Bone wt (mg)	Coll yld (mg)	Coll yld (%)	C:N
1489	San Martino Lundo Lomaso, Italy	1489.1	753.2	17.9	3.2	Aix-12004.1.1	1490	17	1489.1	Aix-12004.3.1	84	1401	75	Dec-17	1489.2	L	piece	53.9	9.7	18.0	3.2
	Human, long bone					Aix-12004.1.2	1470	17	1489.1	Aix-12004.3.2	74	1530	72								
						MAMS-26317	1481	23	1489.1	Aix-12004.3.3	77	1494	60								
									1489.1	Aix-12004.3.4	74	1368	65	Dec-17	1489.4	T	piece	37.4	7.0	18.7	3.2
1905	Pietraszyn, Poland	1905.1	582.9	2.3/5.5	3.2	MAMS-31228	23000	100						Dec-17	1905.3	S	piece	65.0	4.7	7.2	3.3
	Horse, trabecular													Dec-17	1905.4	T	piece	54.9	2.0	3.6	3.1
1860	Ranis, Germany Unknown fauna, long bone	1860.1	454.4	9	3.2	MAMS-30401	30010	140						Dec-17	1860.2	R	piece	55.7	4.9	8.8	3.3
														Dec-17	1860.3	S	piece	44.6	4.5	10.1	3.3

Pretreatment and gaseous radiocarbon dating of 40-100 mg archaeological bone

Supplementary Dataset S2 – Radiocarbon dates for all samples in the study dated with graphite targets and the gas ion source

R-EVA	<100mg bone extraction, EA-GIS-AMS dates							Adjusted age		Statistical agreement of replicate measurements	Notes
	AMS lab code	Coll wgt (µg)	GIS C (µg)	$F^{14}C$	±	^{14}C age	±	^{14}C age	±	*T is the calculated χ2 value and should be lower than the value given in brackets to be considered contamporaneous at 95% confidence. The degrees of freedom are given by 'df'.*	
1489	Aix-12004.6.1	107	42	0.8339	0.0074	1,459	72	1,459	72		χ2 test including the Fewlass et al 2017 gas measurements:
	Aix-12004.6.2	96	42	0.8302	0.0073	1,495	71	1,495	71	χ^2 test: (df = 3, N = 4) T=0.8 (5% 7.8)	(df = 11, N = 12) T = 11.2 (5% 19.7)
	Aix-12004.6.3	96	42	0.8275	0.0072	1,521	70	1,521	70	weighted mean: 1506 +/- 36	weighted mean: 1480 +/- 20
	Aix-12004.6.4	93	40	0.8248	0.0073	1,548	71	1,548	71		
	AIX-12004.7.1	105	49	0.8349	0.0071	1,449	68	1,449	68		
	AIX-12004.7.2	90	40	0.8257	0.0075	1,539	73	1,539	73	χ^2 test: (df = 3, N = 4) T=5.3 (5% 7.8)	
	AIX-12004.7.3	105	46	0.8209	0.0074	1,585	73	1,585	73	weighted mean: 1484 +/-36	
	AIX-12004.7.4	109	48	0.8426	0.0072	1,376	69	1,376	69		
										χ2 for all replicates: (df = 7, N = 7) T=6.3 (5% 14.1)	
										Weighted mean: 1495 +/-25	
1905	Aix-12023.1.1	102	44	0.0529	0.0019	23,607	283	23,610	280		
	Aix-12023.1.2	94	38	0.0553	0.0020	23,251	293	23,250	290		
	Aix-12023.1.3	87	37	0.0558	0.0020	23,188	283	23,190	280	χ2 test: (df = 3, N = 4) T = 2.9 (5% 7.8)	
	Aix-12023.1.4	245	99	0.0569	0.0014	23,020	192	23,020	190	weighted mean: 23220 +/-130	
	Aix-12023.2.1	101	41	0.0510	0.0017	23,903	264	23,900	260		
	Aix-12023.2.2	93	39	0.0542	0.0019	23,412	279	23,410	280		
	Aix-12023.2.3	99	39	0.0518	0.0020	23,780	304	23,780	300	χ2 test: (df = 3, N = 4) T = 2.3 (5% 7.8)	
	Aix-12023.2.4	97	40	0.0539	0.0018	23,461	275	23,460	270	weighted mean: 23650 +/-140	
										χ2 test for all replicates: (df = 7, N = 8) T = 10.1 (5% 14.1)	
										weighted mean: 23,420 +/-100	
1860	Aix-12022.1.1	91	43	0.0227	0.0015	30,421	518	30,420	520		
	Aix-12022.1.2	101	41	0.0223	0.0014	30,554	509	30,550	510		
	Aix-12022.1.3	90	39	0.0190	0.0015	31,822	625	31,820	630	χ2 test: (df=2, N = 3) T = 1.5 (5% 6.0)	Big discharges inside source during measurement - not included in X2 test
	Aix-12022.1.4	93	38	0.0248	0.0016	29,699	519	29,700	520	weighted mean: 30,250 +/-300	
	Aix-12022.2.1	98	43	0.0240	0.0014	29,972	484	29,970	480		
	Aix-12022.2.2	98	43	0.0243	0.0015	29,865	481	29,860	480		
	Aix-12022.2.3	97	35	0.0255	0.0015	29,473	461	29,470	460	χ2 test: (df = 3, N = 4) T = 0.6 (5% 7.8)	
	Aix-12022.2.4	227	96	0.0245	0.0011	29,800	374	29,800	370	weighted mean: 29780 +/-220	
										χ2 test for all replicates: (df = 6, N = 7) T=3.7 (5% 12.6)	
										weighted mean: 29,950 +/- 180	

Pretreatment and gaseous radiocarbon dating of 40-100 mg archaeological bone

Supplementary Dataset S2 – Radiocarbon dates for all samples in the study dated with graphite targets and the gas ion source

		~500mg extraction, solid graphite target dates							~500mg bone extraction, EA-GIS-AMS dates (Fewlass et al., 2018)					<100mg bone extraction							
R-EVA	Site	R-EVA	Bone wt (mg)	Coll yld (%)	C:N	AMS lab code	^{14}C age	±	R-EVA	AMS lab code	GIS C (µg)	^{14}C age	± (err 2)	Session	R-EVA	Batch	Form	Bone wt (mg)	Coll yld (mg)	Coll yld (%)	C:N
123	Brown Bank, North sea Plains Mammoth, rib	123.53	559.40	11.2	3.2	Aix-12003.1.1	34390	240	123.53	Aix-12003.5.1	89	34260	750	Dec-17	123.81	P	piece	60.7	7.9	13.0	3.2
						Aix-12003.1.2	34320	240	123.53	Aix-12003.5.2	78	34820	770								
						MAMS-26876	34360	300	123.53	Aix-12003.5.3	75	34710	680								
									123.53	Aix-12003.5.4	98	34260	760								
														Jun 17	123.68	A1	piece	75	7.6	10.1	3.3
														Jun 17	123.69	A2	piece	82.4	9.0	10.9	3.2
														Jun 17	123.70	A3	powder	79.9	2.4	3.0	3.2
														Jun 17	123.71	A4	powder	94.5	5.7	6.0	3.2

Pretreatment and gaseous radiocarbon dating of 40-100 mg archaeological bone

Supplementary Dataset S2 – Radiocarbon dates for all samples in the study dated with graphite targets and the gas ion source

R-EVA	<100mg bone extraction, EA-GIS-AMS dates							Adjusted age		Statistical agreement of replicate measurements	Notes
	AMS lab code	Coll wgt (µg)	GIS C (µg)	$F^{14}C$	±	^{14}C age	±	^{14}C age	±	*T is the calculated χ2 value and should be lower than the value given in brackets to be considered contamporaneous at 95% confidence. The degrees of freedom are given by 'df'.*	
123	Aix-12003.10.1	102	45	0.0143	0.0012	34,138	699	34,140	700		χ2 test including the Fewlass et al 2017 gas measurements:
	Aix-12003.10.2	91	38	0.0135	0.0012	34,555	728	34,550	730		(df = 23, N = 24) T = 19.2 (5% 35.2)
	Aix-12003.10.3	105	43	0.0116	0.0012	35,835	829	35,830	+880/-780	χ2 test: (df = 3, N = 4) T = 2.8 (5% 7.8)	weighted mean: 34400 +/- 160
	Aix-12003.10.4	239	98	0.0136	0.0012	34,546	707	34,550	710	weighted mean: 34,730 +/-360	
	Aix-12003.6.6	211	86	0.0151	0.0012	33,694	649	33,690	650		
	Aix-12003.6.7	72	29	0.0147	0.0014	33,919	772	33,920	770		
	Aix-12003.6.8	86	34	0.0157	0.0014	33,347	735	33,350	740	χ2 test: (df = 3, N = 4) T = 1.8 (5% 7.8)	
	Aix-12003.6.9	76	31	0.0133	0.0013	34,725	810	34,720	810	weighted mean: 33,910 +/-360	
	Aix-12003.7.5	205	83	0.0128	0.0012	35,028	765	35,030	760		
	Aix-12003.7.6	72	29	0.0152	0.0014	33,637	742	33,640	740		
	Aix-12003.7.7	78	32	0.0132	0.0014	34,777	835	34,780	+880/-790	χ2 test: (df = 3, N = 4) T = 2.0 (5% 7.8)	
	Aix-12003.7.8	71	26	0.0142	0.0014	34,186	782	34,190	780	weighted mean: 34,430 +/-390	
	Aix-12003.8.5	209	67	0.0131	0.0013	34,842	792	34,840	+830/-760		Large sample size corrected with small size background - Overcorrected
	Aix-12003.8.6	85	25	0.0159	0.0015	33,281	765	33,280	+800/-730		
	Aix-12003.8.7	69	28	0.0157	0.0015	33,347	757	33,350	+800/-720	χ2 test: (df = 3, N = 4) T = 2.7 (5% 7.8)	
	Aix-12003.8.8	79	23	0.0141	0.0014	34,260	824	34,260	+870/-780	weighted mean: 33,970 +/-390	
	Aix-12003.9.5	209	70	0.0113	0.0012	36,013	869	36,010	+920/-830		Large sample size corrected with small size background - Overcorrected
	Aix-12003.9.6	82	25	0.0131	0.0014	34,847	874	34,850	+930/-830		
	Aix-12003.9.7	81	21	0.0153	0.0016	33,589	856	33,590	+900/-810	χ2 test: (df = 3, N = 4) T = 4.5 (5% 7.8)	
	Aix-12003.9.8	79	na	0.0140	0.0015	34,285	837	34,290	+880/-800	weighted mean: 34,820 +/-430	
										χ2 test for all replicates: (df=19, N = 20) T = 18.5 (5% 30.1)	
										weighted mean: 34,380 +/-170	

Pretreatment and gaseous radiocarbon dating of 40-100 mg archaeological bone

Supplementary Dataset S2 – Radiocarbon dates for all samples in the study dated with graphite targets and the gas ion source

		~500mg extraction, solid graphite target dates							~500mg bone extraction, EA-GIS-AMS dates (Fewlass et al., 2018)					<100mg bone extraction							
R-EVA	Site	R-EVA	Bone wt (mg)	Coll yld (%)	C:N	AMS lab code	^{14}C age	±	R-EVA	AMS lab code	GIS C (µg)	^{14}C age	± (err 2)	Session	R-EVA	Batch	Form	Bone wt (mg)	Coll yld (mg)	Coll yld (%)	C:N
570	Teixoneres, Spain Unknown fauna, long bone	570.2	451.9	3.4	3.4	MAMS-34680	34270	190						Dec 17	570.19	U	piece	43.8	2.2	5.0	3.4
														Jun 17	570.3	H	piece	90.1	2.9	4.4	3.3
														Jun 17	570.8	J	piece	69.8	3.5	5.0	3.3
														Jun 17	570.13	A1	piece	87	2.2	2.5	3.3
														Jun 17	570.14	A2	piece	90.1	4.0	4.4	3.3
548	Teixoneres, Spain Unknown fauna, long bone	548.17	597.5	0.8	3.4	MAMS-34677	39390	320						Jun 17	548.3	H	piece	71.2	1.5	2.1	3.3
														Jun 17	548.8	J	piece	84.7	1.5	1.8	3.2
														Jun 17	548.13	A1	piece	78.1	0.6	0.8	3.4
														Jun 17	548.14	A2	piece	86.4	1.1	1.3	3.3

Pretreatment and gaseous radiocarbon dating of 40-100 mg archaeological bone

Supplementary Dataset S2 – Radiocarbon dates for all samples in the study dated with graphite targets and the gas ion source

	<100mg bone extraction, EA-GIS-AMS dates							Adjusted age		Statistical agreement of replicate measurements	Notes
R-EVA	AMS lab code	Coll wgt (µg)	GIS C (µg)	$F^{14}C$	±	^{14}C age	±	^{14}C age	±	*T is the calculated χ2 value and should be lower than the value given in brackets to be considered contamporaneous at 95% confidence. The degrees of freedom are given by 'df'.*	
570	Aix-12015.6.1	95	42	0.0150	0.0013	33,755	689	33,750	690		
	Aix-12015.6.2	104	46	0.0135	0.0013	34,606	748	34,610	750		
	Aix-12015.6.3	98	44	0.0135	0.0012	34,608	724	34,610	720	χ2 test: (df = 3, N = 4) T= 0.9 (5% 7.8)	
	Aix-12015.6.4	223	99	0.0138	0.0010	34,410	600	34,410	600	weighted mean: 34,340 +/-340	
	Aix-12015.5.1	200	82	0.0132	0.0011	34,768	647	34,770	650		
	Aix-12015.5.2	73	na	0.0147	0.0014	33,879	765	33,880	760		
	Aix-12015.5.3	84	32	0.0147	0.0014	33,921	763	33,920	760	χ2 test: (df = 3, N = 4) T = 1.4 (5% 7.8)	
	Aix-12015.5.4	76	31	0.0131	0.0014	34,830	836	34,830	+880/-800	weighted mean: 34,390 +/-380	
	Aix-12015.2.5	199	81	0.0132	0.0013	34,777	790	34,780	790		
	Aix-12015.2.6	78	31	0.0125	0.0013	35,177	862	35,180	+910/-820		
	Aix-12015.2.7	74	31	0.0132	0.0013	34,768	812	34,770	810	χ2 test: (df = 3, N = 4) T = 1.4 (5% 7.8)	
	Aix-12015.2.8	79	32	0.0147	0.0014	33,916	755	33,920	760	weighted mean: 34,670 +/-400	
	Aix-12015.3.5	194	79	0.0145	0.0012	33,988	643	33,990	640		
	Aix-12015.3.6	69	28	0.0159	0.0014	33,274	721	33,270	720		
	Aix-12015.3.7	87	35	0.0132	0.0013	34,772	806	34,770	810	χ2 test: (df = 3, N = 4) T = 2.0 (5% 7.8)	
	Aix-12015.3.8	74	30	0.0146	0.0014	33,971	768	33,970	770	weighted mean: 34,010 +/-370	
	Aix-12015.4.5	209	86	0.0128	0.0012	35,037	772	35,040	770		
	Aix-12015.4.6	86	34	0.0128	0.0013	34,992	835	34,990	840		
	Aix-12015.4.7	77	33	0.0147	0.0014	33,925	779	33,930	780	χ2 test: (df = 3, N = 4) T = 2.0 (5% 7.8)	
	Aix-12015.4.8	69	28	0.0121	0.0013	35,469	863	35,470	+910/-820	weighted mean: 34,870 +/-400	
										χ2 test for all replicates: (df=19, N =20) T=10.7 (5% 30.1)	
										weighted mean: 34,450 +/-170	
548	Aix-12017.2.1	191	71	0.0076	0.0011	39,247	1,145	39,250	+1,240/-1,070		
	Aix-12017.2.2	68	27	0.0069	0.0012	39,986	1,417	39,990	+1,560/-1,310		χ2 test for replicates from R-EVA 570.3 and R-EVA 570.8:
	Aix-12017.2.3	84	31	0.0065	0.0012	40,479	1,521	40,480	+1,690/-1,400	χ2 test: (df = 3, N = 4) T = 0.7 (5% 7.8)	(df = 6, N = 7) T = 3.5 (5% 12.6)
	Aix-12017.2.4	72	26	0.0077	0.0012	39,115	1,272	39,120	+1,380/-1,180	weighted mean: 39,640 +/-660	weighted mean: 39050 +/-460
	Aix-12017.1.2	71	28	0.0077	0.0012	39,129	1,264	39,130	+1,380/-1,170		
	Aix-12017.1.3	70	26	0.0086	0.0013	38,229	1,177	38,230	+1,270/-1,100	χ2 test: (df = 2, N = 3) T = 0.7 (5% 6.0)	
	Aix-12017.1.4	201	81	0.0091	0.0011	37,749	973	37,750	+1,040/-920	weighted mean: 38,300 +/-650	
	Aix-12017.3.1	64	25	0.0316	0.0017	27,747	439	27,750	440	χ2 test: (df = 1, N = 2) T = 0.2 (5% 3.8)	Very low collagen yield
	Aix-12017.3.2	69	29	0.0305	0.0018	28,027	461	28,030	460	weighted mean: 27,880 +/-320	
	Aix-12017.4.1	71	28	0.0168	0.0014	32,833	688	32,830	690		Very low collagen yield
	Aix-12017.4.2	72	28	0.0102	0.0013	36,862	1,040	36,860	+1,110/-980	χ2 test: (df = 2, N = 3) T=12.3 (5% 6.0)	
	Aix-12017.4.3	69	27	0.0122	0.0014	35,378	907	35,380	+960/-860	weighted mean: 34,930 +/-490	
										χ2 test for all replicates: (df = 11, N =12) T = 339.3 (5% 19.7)	

Pretreatment and gaseous radiocarbon dating of 40-100 mg archaeological bone

Supplementary Dataset S2 – Radiocarbon dates for all samples in the study dated with graphite targets and the gas ion source

		~500mg extraction, solid graphite target dates							~500mg bone extraction, EA-GIS-AMS dates (Fewlass et al., 2018)					<100mg bone extraction							
R-EVA	Site	R-EVA	Bone wt (mg)	Coll yld (%)	C:N	AMS lab code	^{14}C age	±	R-EVA	AMS lab code	GIS C (µg)	^{14}C age	± (err 2)	Session	R-EVA	Batch	Form	Bone wt (mg)	Coll yld (mg)	Coll yld (%)	C:N
124	Brown Bank, North sea Plains Woolly Rhino, long bone (Previously labeled as Bison)	124.43	639.5	11.7	3.1	MAMS-26877	50150	+2080/–1650	124.43	Aix-12002.4.1	84		>45430								
						Aix-12002.1.2	49300	+1610/–1340	124.43	Aix-12002.4.2	89		>43770	Jun 17	124.58	A1	piece	70.6	10.2	14.4	3.2
						Aix-12002.1.3	48800	+1530/–1290	124.43	Aix-12002.4.3	80	48610	+4930/-3030								
									124.43	Aix-12002.4.4	74		>43590								
														Jun 17	124.59	A2	piece	90.2	13.3	14.7	3.2
														Jun 17	124.60	A3	powder	88.8	3.5	3.9	3.2
														Jun 17	124.61	A4	powder	83.1	6.1	7.3	3.2

Pretreatment and gaseous radiocarbon dating of 40-100 mg archaeological bone

Supplementary Dataset S2 – Radiocarbon dates for all samples in the study dated with graphite targets and the gas ion source

R-EVA	<100mg bone extraction, EA-GIS-AMS dates							Adjusted age		Statistical agreement of replicate measurements	Notes
	AMS lab code	Coll wgt (µg)	GIS C (µg)	$F^{14}C$	±	^{14}C age	±	^{14}C age	±	*T is the calculated χ2 value and should be lower than the value given in brackets to be considered contamporaneous at 95% confidence. The degrees of freedom are given by 'df'.*	
124	Aix-12002.5.2	213	89	0.0038	0.0011	44,678	2,228	44,680	+2,610/-1,970		χ2 test including the Fewlass et al 2017 gas measurements:
	Aix-12002.5.3	67	27	0.0029	0.0011	46,959	3,156	46,960	+4,010/-2,660	χ2 test: (df = 2, N = 3) T = 1.5 (5% 6.0)	(df=18, N=19) T = 10.1 (5% 28.9)
	Aix-12002.5.4	82	34	0.0019	0.0011	50,193	4,503		>44,150	weighted mean: 47,030 +/-1780	weighted mean: 49210 +/- 930
	Aix-12002.6.1	218	91	0.0025	0.0010	48,114	3,263	48,110	+4,190/-2,740		
	Aix-12002.6.2	74	31	0.0031	0.0011	46,451	2,908	46,450	+3,610/-2,480		
	Aix-12002.6.3	76	32	0.0023	0.0011	48,845	3,745	48,840	+5,040/-3,070	χ2 test: (df = 3, N = 4) T = 0.3 (5% 7.8)	
	Aix-12002.6.4	77	32	0.0024	0.0011	48,528	3,698	48,530	+4950/-3040	weighted mean: 47,900 +/-1680	
	Aix-12002.7.1	201	73	0.0010	0.0010	55,266	8,199		>46,330		Large sample size corrected with small size background - Overcorrected
	Aix-12002.7.2	78	30	0.0019	0.0011	50,253	4,801		>43,940		
	Aix-12002.7.3	67	24	0.0025	0.0011	48,219	3,701	48,220	+4,960/-3,040	χ2 test: (df = 3, N = 4) T = 1.1 (5% 7.8)	
	Aix-12002.7.4	89	33	0.0020	0.0011	49,849	4,479		>43,830	weighted mean: 50,730 +/-2380	
	Aix-12002.8.1	190	75	0.0039	0.0012	44,586	2,446	44,590	+2,920/-2,140		Large sample size corrected with small size background - Overcorrected
	Aix-12002.8.2	81	28	0.0013	0.0011	53,543	7,035		>45,410		
	Aix-12002.8.3	69	33	0.0013	0.0011	53,475	6,813		>45,510	χ2 test: (df = 3, N = 4) T = 3.8 (5% 7.8)	
	Aix-12002.8.4	80	33	0.0012	0.0011	54,116	7,436		>45,700	weighted mean: 50,580 +/-2450	
										χ2 test for all replicates: (df=14, N =15) T = 9.2 (5% 23.7)	
										Weighted mean: 49,030 +/-1010	

Unknown archaeological samples corrected with collagen backgrounds measured in same session according to size (small or large sample size) and type (extracted in solid or powder form)
All powder samples corrected with 30ug powder backgrounds only (no 100 ug C BG)
3.5 ‰ scatter added to all samples
Absolute error of the blank changed to 0.001
For dates >15,000 BP, values have been rounded to 10
*Asymmetrical errors given wherever F14C ≤ 1σ*10*
"Older than" ages have been calculated for samples where F14C < 2σ, according to convention in van der Plicht and Hogg (2006)
"na" shows missing data.

Pretreatment and gaseous radiocarbon dating of 40-100 mg archaeological bone
Supplementary Dataset S3: EA-GIS-AMS data from background bone R-EVA 1753

Session	R-EVA	AMS lab code	Batch	Form	Bone wt (mg)	Collagen yld (%)	Collagen yld (mg)	GIS C mass (ug)	$F^{14}C$	$F^{14}C$ err	^{14}C age (y)	+-(y)
Small aliquots												
Jun-17	1753.29	Aix-12018.1.2	H	Piece	69.2	11.0	83	32	0.0031	0.0005	46,441	1,173
Jun-17	1753.29	Aix-12018.1.3	H	Piece	69.2	11.0	75	29	0.0036	0.0005	45,181	1,166
Jun-17	1753.34	Aix-12018.3.6	J	Piece	99.4	11.0	79	33	0.0026	0.0004	47,829	1,319
Jun-17	1753.39	Aix-12018.4.7	A1	Piece	99.7	12.2	79	32	0.0035	0.0005	45,333	1,143
Jun-17	1753.39	Aix-12018.4.8	A1	Piece	99.7	12.2	76	32	0.0029	0.0005	46,916	1,318
Jun-17	1753.41	Aix-12018.5.2	A2	Piece	97.6	13.1	69	28	0.0042	0.0006	43,951	1,076
Jun-17	1753.41	Aix-12018.5.3	A2	Piece	97.6	13.1	81	33	0.0028	0.0005	47,101	1,311
Jun-17	1753.43	Aix-12018.6.6	A3	Powder	80.9	2.3	76	27	0.0047	0.0006	43,011	1,013
Jun-17	1753.45	Aix-12018.7.2	A4	Powder	87.8	5.8	76	24	0.0054	0.0006	41,989	941
Jun-17	1753.45	Aix-12018.7.3	A4	Powder	87.8	5.8	81	24	0.0047	0.0008	43,127	1,453
Dec-17	1753.48	Aix-12018.9.1	L	Piece	62	13.5	99	50	0.0043	0.0005	43,680	990
Dec-17	1753.48	Aix-12018.9.2	L	Piece	62	13.5	95	36	0.0046	0.0006	43,300	1,010
Dec-17	1753.56	Aix-12018.12.1	P	Piece	68.7	13.0	90	39	0.0044	0.0005	43,600	940
Dec-17	1753.56	Aix-12018.12.2	P	Piece	68.7	13.0	103	45	0.0038	0.0005	44,830	1,000
Dec-17	1753.59	Aix-12018.13.1	R	Piece	79.9	14.6	90	41	0.0039	0.0006	44,470	1,200
Dec-17	1753.59	Aix-12018.13.2	R	Piece	79.9	14.6	105	46	0.0037	0.0004	44,880	930
Dec-17	1753.60	Aix-12018.10.2	S	Piece	69.3	14.7	99	43	0.0038	0.0005	44,720	1,060
Dec-17	1753.62	Aix-12018.14.1	U	Piece	55.9	15.4	93	41	0.0049	0.0005	42,800	880
Dec-17	1753.62	Aix-12018.14.2	U	Piece	55.9	15.4	112	49	0.0038	0.0005	44,710	1,000
Dec-17	1753.64	Aix-12018.15.1	BK	Piece	76.2	11.0	102	53	0.0040	0.0004	44,450	890
Dec-17	1753.64	Aix-12018.15.2	BK	Piece	76.2	11.0	108	41	0.0038	0.0004	44,700	880
Dec-17	1753.64	Aix-12018.15.3	BK	Piece	76.2	11.0	98	34	0.0039	0.0004	44,630	890
								Arithmetic mean:	**0.0039**			
								SD:	**0.00069**			
Large aliquots												
Jun-17	1753.29	Aix-12018.1.1	H	Piece	69.2	11.0	0.207	79	0.0025	0.0004	48,105	1,348
Jun-17	1753.34	Aix-12018.3.5	J	Piece	99.4	11.0	0.198	82	0.0013	0.0003	53,533	1,772
Jun-17	1753.39	Aix-12018.4.6	A1	Piece	99.7	12.2	0.205	88	0.0018	0.0003	50,621	1,417
Jun-17	1753.41	Aix-12018.5.1	A2	Piece	97.6	13.1	0.218	89	0.0027	0.0004	47,386	1,299
Dec-17	1753.56	Aix-12018.12.3	P	Piece	68.7	13.0	226	97	0.0024	0.0004	48,530	1,210
Dec-17	1753.60	Aix-12018.10.3	S	Piece	69.3	14.7	231	96	0.0026	0.0004	47,870	1,260
Dec-17	1753.60	Aix-12018.10.4	S	Piece	69.3	14.7	221	96	0.0029	0.0004	47,000	1,190
Dec-17	1753.62	Aix-12018.14.3	U	Piece	55.9	15.4	224	97	0.0034	0.0004	45,650	870
Dec-17	1753.64	Aix-12018.15.4	BK	Piece	76.2	11.0	252	98	0.0023	0.0003	48,780	1,060
								Arithmetic mean:	0.0024			
								SD:	0.00061			

Pretreatment and gaseous radiocarbon dating of 40-100 mg archaeological bone
Supplementary Dataset S4: EA-GIS-AMS data from system blanks

Session 1: June 2017							
AMS lab code	**Sample**	**GIS C mass (ug)**	**$F^{14}C$**	**$F^{14}C$ err**	**^{14}C age (y)**	**+-(y)**	**Notes**
Aix-10424.2.10	IAEA-C1	103	0.0022	0.0004	48,982	1,337	
Aix-10424.2.11	IAEA-C1	not recorded - large	0.0026	0.0004	47,787	1,177	
Aix-10424.2.12	IAEA-C1	not recorded - large	0.0039	0.0005	44,607	1,068	
Aix-10424.2.24	IAEA-C1	104	0.0024	0.0005	48,487	1,520	
Aix-10424.2.9	IAEA-C1	120	0.0025	0.0004	48,128	1,214	
Aix-10424.2.13	IAEA-C1	not recorded - small	0.0036	0.0005	45,153	1,111	
Aix-10424.2.14	IAEA-C1	39	0.0046	0.0008	43,311	1,330	
Aix-10424.2.16	IAEA-C1	19	0.0089	0.0009	37,896	832	not included due to small size
Aix-10424.2.17	IAEA-C1	14	0.0067	0.0010	40,164	1,158	not included due to small size
Aix-10424.2.21	IAEA-C1	28	0.0032	0.0005	46,039	1,225	

Session 2: December 2017							
AMS lab code	**Sample**	**GIS C mass (ug)**	**$F^{14}C$**	**$F^{14}C$ err**	**^{14}C age (y)**	**+-(y)**	**Notes**
Aix-10109.2.12	Phthalic anhydride	46	0.0039	0.0004	44,648	870	8.00592.0100 from millipore
Aix-10109.2.13	Phthalic anhydride	117	0.0020	0.0004	49,822	1,598	8.00592.0100 from millipore
Aix-10109.2.14	Phthalic anhydride	43	0.0030	0.0004	46,759	1,046	8.00592.0100 from millipore
Aix-10109.2.15	Phthalic anhydride	133	0.0025	0.0004	48,245	1,300	8.00592.0100 from millipore

Chapter Four

Direct radiocarbon dates of mid Upper Palaeolithic human remains from Dolní Věstonice II and Pavlov I, Czech Republic

H. Fewlass, S. Talamo, B. Kromer, E. Bard, T. Tuna, Y. Fagault, M. Sponheimer, C. Ryder, J.-J. Hublin, A. Perri, S. Sázelová, J. Svoboda

Published in the *Journal of Archaeological Sciences: Reports,* volume 27, 102000
DOI: 10.1016/j.jasrep.2019.102000

Journal of Archaeological Science: Reports 27 (2019) 102000

Contents lists available at ScienceDirect

Journal of Archaeological Science: Reports

journal homepage: www.elsevier.com/locate/jasrep

Direct radiocarbon dates of mid Upper Palaeolithic human remains from Dolní Věstonice II and Pavlov I, Czech Republic

Helen Fewlass[a,*], Sahra Talamo[a,b], Bernd Kromer[c,a], Edouard Bard[d], Thibaut Tuna[d], Yoann Fagault[d], Matt Sponheimer[e], Christina Ryder[e], Jean-Jacques Hublin[a], Angela Perri[f], Sandra Sázelová[g,h], Jiří Svoboda[g]

[a] Department of Human Evolution, Max Planck Institute for Evolutionary Anthropology, Deutscher Platz 6, Leipzig D-04103, Germany
[b] Department of Chemistry "G. Ciamician", University of Bologna, Via Selmi, 2, 40126 Bologna, Italy
[c] Institute of Environmental Physics, University of Heidelberg, INF 229, Heidelberg, D-69120, Germany
[d] CEREGE, Aix Marseille Université, CNRS, IRD, INRA, Collège de France, Technopôle de l'Arbois, BP 80, 13545 Aix-en-Provence, France
[e] Department of Anthropology, University of Colorado Boulder, 1350 Pleasant St, 233 UCB, Boulder, CO 80309-0233, USA
[f] Department of Archaeology, Durham University, South Road, Durham, DH1 3LE, UK
[g] Department of Anthropology, Faculty of Science, Masaryk University, Kotlářská 2, 611 37 Brno, Czech Republic
[h] Institute of Archeology, Czech Academy of Sciences, Brno, Čechyňská 363/19, CZ-602 00, Brno, Czech Republic

ARTICLE INFO

Keywords:
Radiocarbon dating
Accelerator mass spectrometry
Human remains
Gravettian
Dolní Věstonice
Pavlov

ABSTRACT

The ritual human burials and scattered fragments of human bones excavated from Dolní Věstonice II and Pavlov I (Czech Republic) in the 20th century provide a large body of evidence on morphology and funerary practices in the Gravettian as well as the population history of European *Homo sapiens* during the Upper Palaeolithic. A series of radiocarbon dates on charcoal and animal bone places the occupation of the sites predominantly between 31,000–29,000 cal BP (Early-Evolved Pavlovian) but direct radiocarbon dating of the human remains has not been previously undertaken. In 2013, human bones from Dolní Věstonice II and Pavlov I were sampled for aDNA analysis, including three skeletons from a triple burial (DV13, DV14, DV15), two skeletons from single burials (Pav1, DV16) and two unarticulated human bones (DV42, DV43). Small amounts of bone material were left over from the aDNA sampling, providing the first opportunity to directly date seven of the human individuals. Non-destructive pre-screening with near-infrared (NIR) spectroscopy indicated that sufficient collagen was preserved in the bone material for radiocarbon dating. We sampled very small amounts (32–202 mg) of bone material for collagen extraction, ultrafiltration and accelerator mass spectrometer (AMS) dating. Each collagen extract was dated multiple times using both graphite targets (ca. 800 μg C) and the gas ion source (< 100 μg C) of the AixMICADAS to obtain accurate and precise radiocarbon ages. The direct dates confirm the Pavlovian origin of the human remains and indicate that several of the radiocarbon dates carried out in the 1980s on associated charcoals were likely affected by low-level contamination of modern carbon. The results add seven individuals to the small collection of reliably dated Upper Palaeolithic humans in Europe.

1. Introduction

Human remains excavated from Gravettian contexts across Eurasia have been the focus of considerable palaeobiological research, including numerous elaborate ritual burials that offer fascinating insights into the biology and behaviour of mid Upper Palaeolithic people (see inventories in Henry-Gambier, 2008; Pettitt, 2011; Trinkaus et al., 2014; Vanhaeren and d'Errico, 2002). The large hunter-gatherer settlements at Dolní Věstonice and Pavlov, located on the northeastern slopes of the Pavlov Hills in Czech Republic (Fig. 1), have yielded extensive evidence of Pavlovian behaviour (a local variant of the Eastern Gravettian culture). The Dolní Věstonice-Pavlov region, which includes the large site clusters of Dolní Věstonice I (DVI), DVII, DVIII, Pavlov I and Pavlov II, is particularly notable for some of the earliest examples of carved mammoth ivory and fired clay objects of human and animal figurines, notably the fired clay Venus of Věstonice from DVI (Absolon, 1933; Vandiver et al., 1989). Over the course of the 20th century, several ritual human burials and numerous disarticulated human bones were excavated from these sites, including the famous triple burial from DVII (Klima, 1987; Sázelová et al., 2018; Sládek et al.,

* Corresponding author.
E-mail address: helen_fewlass@eva.mpg.de (H. Fewlass).

https://doi.org/10.1016/j.jasrep.2019.102000
Received 18 June 2019; Received in revised form 14 August 2019; Accepted 3 September 2019

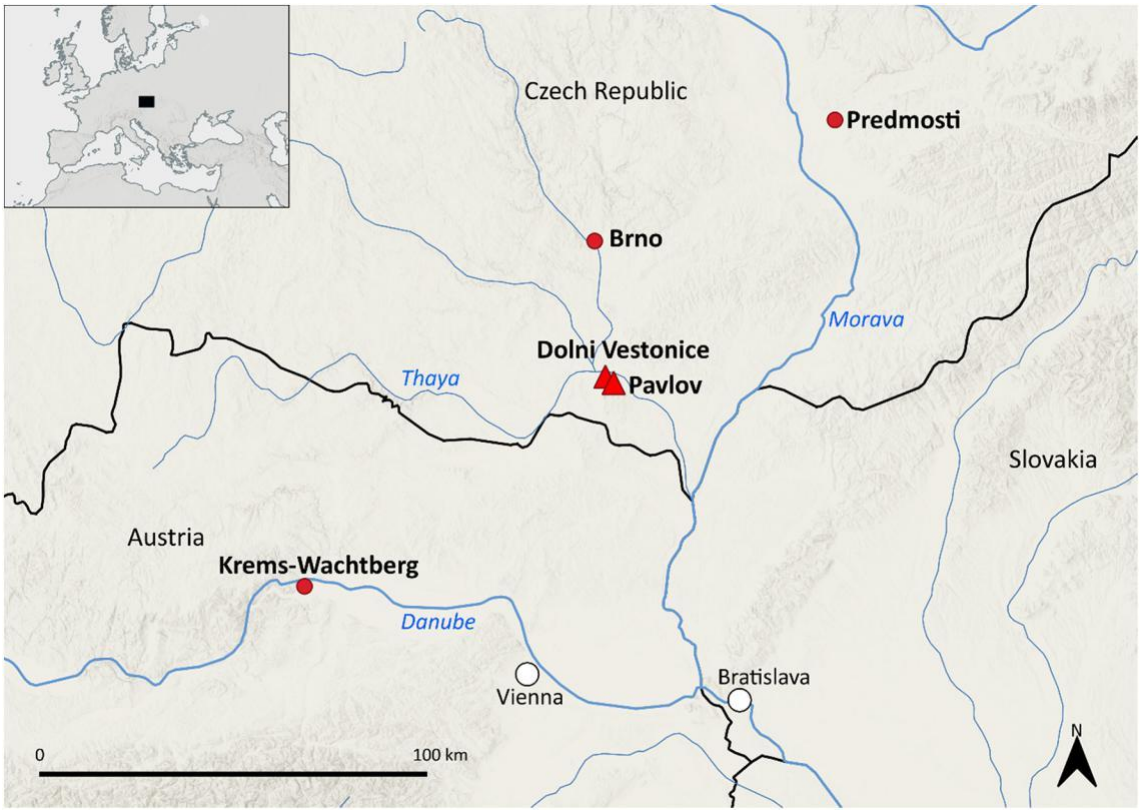

Fig. 1. Map of the Middle Danube region of central Europe showing the locations of Dolní Věstonice, Pavlov, and other nearby sites containing Gravettian burials mentioned in the text.

2000; Svoboda, 1987, 2016; Trinkaus and Svoboda, 2006; Trinkaus et al., 2010; Trinkaus et al., 2017; Vlcek, 1997). A series of radiocarbon dates on charcoal and bone measured at the Oxford and Groningen laboratories place the main occupations of DVII and Pavlov I between ~31,000–29,000 cal BP (Svoboda et al., 2016).

The human skeletal collection from Dolní Věstonice-Pavlov is the largest sample of human remains existing for this time period. Extensive analysis of this collection has greatly contributed to our understanding of the morphological variability, pathology and burial practices of Pavlovian people (Trinkaus and Svoboda, 2006). In 2013, 13 human bones from DVII and Pavlov I were sampled for aDNA analysis (Mittnik and Krause, 2016) and the results constitute a relatively large proportion of the genetic data used to investigate the population history of Upper Palaeolithic Europe (Fu et al., 2016). Given their importance within the assemblage of Upper Palaeolithic human skeletal material, it became increasingly important to directly date the human remains. Here we show the results of a new radiocarbon dating program of seven individuals using small amounts of bone material (< 200 mg) which were left over following aDNA analysis. We used rigorous methods of sample pretreatment established for small and precious Palaeolithic bones and obtained replicate radiocarbon measurements from each bone using two AMS dating methods (Fewlass et al., 2019). The directly dated individuals include the three skeletons from the triple burial (DV13, DV14, DV15), two skeletons from single burials (Pav1, DV16) and two unarticulated human bones (fibula fragment DV42 and femoral fragment DV43). aDNA analysis was also carried out for isolated human bones DV40, DV41, DV45, DV56 and DV57 from DVII but no material remained for dating (Mittnik and Krause, 2016).

2. Archaeological context of the human remains

2.1. Dolní Věstonice II

DVII has been excavated in a series of salvage excavations since the 1980s. The site complex is located 220–240 m above sea level (asl) on a loess elevation above the Dyje River. It is made up of distinct settlement units with central hearths, formed through repeated, short-term occupations. Although the area is large (almost 500 m^2), the occupation of DVII was less intensive than nearby DVI or Pavlov I and lacks the iconic artistic and decorative objects (Svoboda, 2006a). In addition to the ritual burials (DV13, DV14, DV15, DV16) a high number of unarticulated human bone fragments were found scattered throughout the cultural layers (Fig. 2; Sládek et al., 2000; Svoboda, 2006a; Trinkaus et al., 2000). The site is one of the most extensively dated Pavlovian settle-ments (Svoboda et al., 2016). A cluster of dates around 27,000 ^{14}C BP (end of the Early Pavlovian phase) was associated with some un-articulated human remains but the majority of the human burials were associated with dates from the Evolved Pavlovian phase between 27,000–25,000 ^{14}C BP (Table 1; Svoboda et al., 2016; Trinkaus and Svoboda, 2006).

In 1986, a triple human burial (Fig. 3) was discovered during excavation of the upper southern periphery of the site-top area (settle-ment units K7–9; Klima, 1987). The central figure (DV15) was lain on his back and showed evidence of congenital abnormalities (Trinkaus et al., 2016). The left figure (DV13) was also on his back, slightly twisted towards the central figure. The figure on the right (DV14) was lying on his front. The arms of the DV13 and DV14 overlapped the central figure, testifying that DV15 was laid out first. All three have been identified as adolescent-young adults (Trinkaus et al., 2016). Genetic analyses confirmed that the three individuals were male and found that DV14 and DV15 were closely maternally related (Mittnik and Krause, 2016). The burial included a small number of perforated

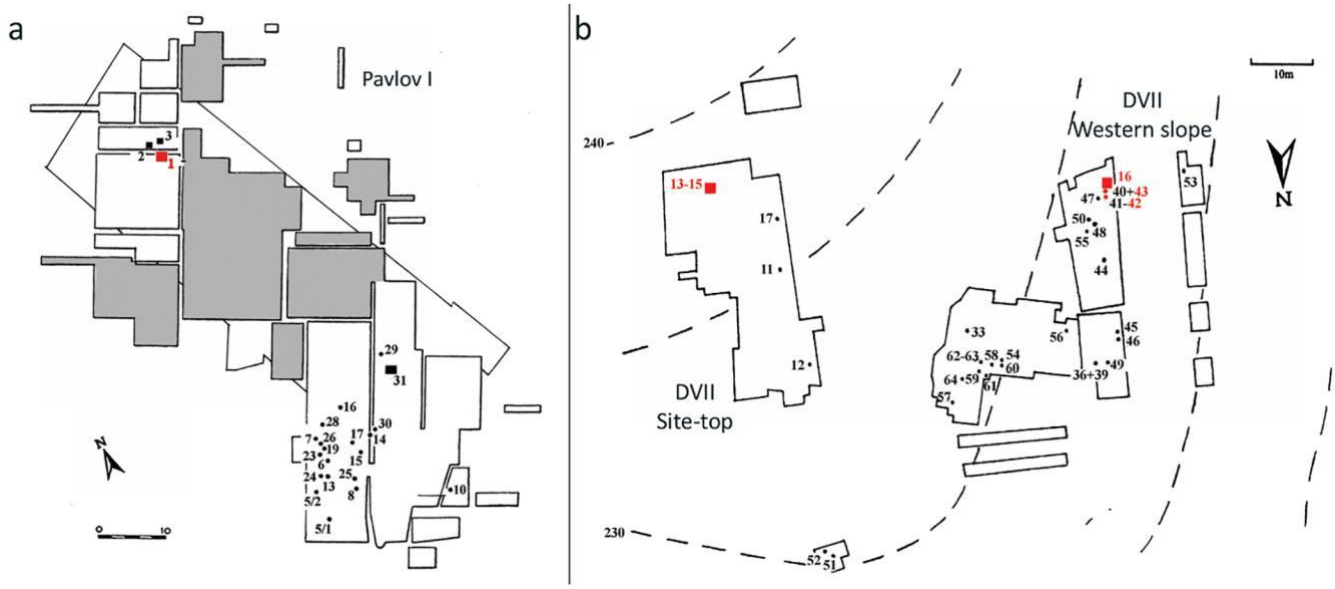

Fig. 2. Plan of (a) Pavlov I and (b) Dolní Věstonice II showing the locations of the human burials (squares) and unarticulated human bones (circles) excavated from the site. The human remains dated in the study are shown in red and those in black are documented elsewhere (Sládek et al., 2000; Trinkaus et al., 2010). In (b) the 230 m and 240 m asl contour lines are shown, with the site sloping down towards the north-northwest. (For interpretation of the references to colour in this figure legend, the reader is referred to the web version of this article.)

canine teeth and ivory pendants and large concentrations of ochre, notably present as thick crusts on the skulls of the three individuals and pelvic area of the central figure. A large amount of charcoal was present in the burial, including the charcoal sample that produced the asso-ciated date (GrN-14831; Table 1).

The burial of DV16, an adult male, was excavated in 1987 (Fig. 3) from settlement unit S1 on the western slope of DVII (Svoboda, 1987, 2006b, 2016). The skeleton was laid on his right side in a flexed position facing the central hearth which was only 20 cm from his knees. The head and pelvic area were covered in a thick layer of ochre, and four perforated carnivore canines were found in association with the skeleton. The dated charcoal sample (GrN-15276) was associated with the burial (Table 1). Extensive root etching on the skeletons of DV13–16, which probably occurred during the Interpleniglacial (MIS3) shortly after deposition, indicates the burials were shallow or the bodies were laid directly on the ancient surface and may have been covered by superstructures for protection (Svoboda, 2006b, 2016; Trinkaus et al., 2010).

DV42 and DV43 were both excavated in 1987 from the lower part of the western slope but were only identified as human during laboratory processing of the archaeozoological material in 1998 (Holliday et al., 2006; Trinkaus et al., 2000). DV42 is a fragment of human fibula, which was located approximately 1 m from the central hearth in settlement unit S2, where the associated charcoal date (GrN-15279) comes from (Table 1; Svoboda et al., 2016). DV43, a fragment of human femur, was excavated from a depression with faunal bones and traces of fire and red ochre located approximately 1 m from the central hearth and 1 m from the DV16 burial in unit S1 (Svoboda et al., 2016). The associated date (GrN-15277) is from charcoal taken from the S1 hearth (Table 1).

2.2. Pavlov I

Pavlov I was systematically excavated between 1952 and 1972 (north-west and south-east sections) by B. Klima and again between 2013 and 2015 (south-east and south-west sections) by J. Svoboda (Svoboda et al., 2016). Based on dates from the Klima excavations it was thought that Pavlov I formed through a high intensity of repeated occupations during the Evolved Pavlovian period (27,000–25,000 ^{14}C BP; Svoboda, 2006a), but the more recent excavations show that the large site complex has a longer deposition of cultural deposits from the Early Pavlovian (Svoboda et al., 2016). The burial of an adult male (Pavlov 1) was excavated from the north-western part of the site in 1957 (Vlcek, 1997). Post-depositional slope movements caused some displacement of the skeleton. No ochre or artefacts were related to the burial but the skeleton was partially covered by mammoth scapulae. A human maxilla and two mandibles (Pavlov 2–4) were excavated from the same area and isolated human teeth and bone fragments were found throughout the cultural layers (Sázelová et al., 2018; Svoboda et al., 2016; Trinkaus et al., 2017). The charcoal date (GrN-20391; Table 1) was the only date from the north-western portion of the site but was not directly associated with the burial (Svoboda, 2006b).

Table 1
Previously published conventional radiocarbon dates and calibrated ranges (cal BP) of charcoals associated with the human remains from DVII and Pavlov I. DVII dates are reported in Svoboda et al. (2016). Pavlov I date is reported in van der Plicht, (1997). Radiocarbon ages were calibrated using the IntCal13 calibration curve (Reimer et al., 2013) in OxCal 4.2 (Bronk Ramsey, 2009). Dates have been rounded to the nearest 10 years.

Sample ID	Context	Material dated	Lab code	^{14}C age (BP)	Error (1σ)	2σ calibrated range (cal BP)
Pav1	Single burial	Charcoal (unrelated to burial)	GrN-20391	26,170	450	31,110–29,420
DV13	Triple burial	Charcoal in burial	GrN-14831	26,640	110	31,070–30,670
DV14						
DV15						
DV16	Single burial	Charcoal in burial	GrN-15276	25,570	280	30,540–29,040
DV42	Unarticulated	Charcoal in S2 hearth	GrN-15279	26,920	250	31,320–30,700
DV43	Unarticulated	Charcoal in S1 hearth	GrN-15277	25,740	210	30,580–29,400

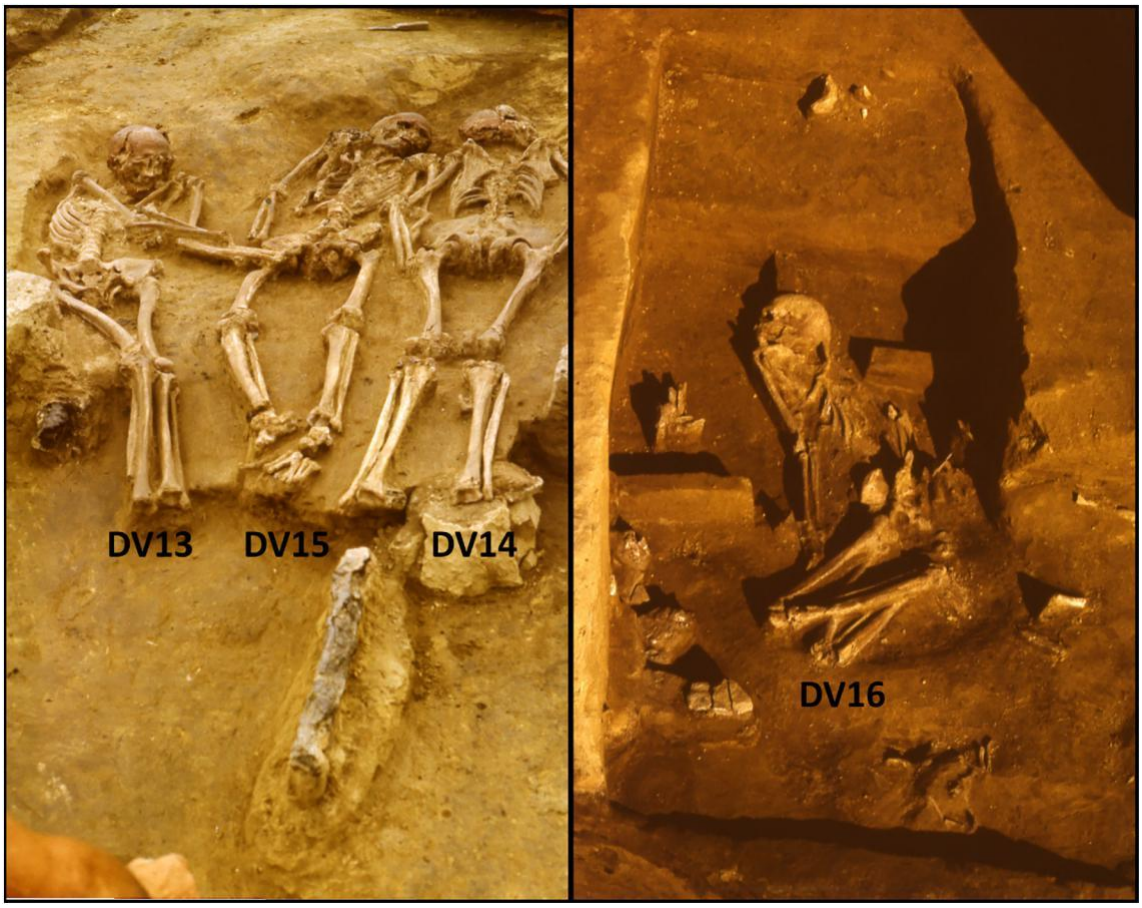

Fig. 3. Photos taken during the excavation of the DVII human burials in the 1980s, showing the DV13, DV14 and DV15 individuals in the triple burial (left) and the single burial of DV16 (right). Photos by J. Svoboda.

3. Materials and methods

The human remains were consolidated immediately following ex-cavation (acrylic resin to the skeletons from the triple burial and PVA to DV16 and the isolated fragments). Various protocols are applied to archaeological bone to remove conservatives prior to collagen extraction as their presence can significantly affect ^{14}C ages through the introduction of non-endogenous carbon (Brock et al., 2017). However, additional pretreatment steps (such as repeated organic solvent washes) increase the likelihood of damage to collagen and the introduction of lab-based contamination. Due to the limited material available from the DVII and Pavlov human remains we decided to apply our standard pretreatment method to very small aliquots of the available bone to reserve some material for further pretreatment if we found evidence of contamination in the first extracts.

During sampling for aDNA analysis, the outer bone surface was removed (Rohland and Hofreiter, 2007). All of the samples were taken from femora, except DV43 which was taken from a fibula. For six samples, a mixture of bone powder and small fragments of whole bone remained after sampling for aDNA. As it has been demonstrated that higher collagen yields are obtained when whole pieces of bone, rather than powdered bone, are pretreated (Fewlass et al., 2019), small whole bone fragments (32.3–70.4 mg material) were selected for pretreat-ment. For DV15, only bone powder was available so a larger sample (203 mg) was taken for collagen extraction.

Recently it has been shown that near-infrared (NIR) spectroscopy is a promising method for effective, fast and non-destructive pre-screening of archaeological bone for the presence of intact collagen (Sponheimer et al., 2019). Using the methods described in Sponheimer et al., (2019), NIR spectroscopy was used to analyse the bone powder of the DVII and Pavlov I burial remains prior to pretreatment to determine if sufficient collagen was preserved for radiocarbon dating. Powdered bone samples were scanned using a fiber-optic reflectance probe attached to a LabSpec 4 NIR spectrometer with a spectral range of 350 nm to 2500 nm. Subsequent data transformations and analyses were undertaken using Unscrambler X software (Camo Analytics, Oslo). A Savitzky-Golay transformation (derivative order = 2; polynomial order = 3; smoothing points = 31) was performed to correct for additive and multiplicative effects in the spectral data. A 1-factor model was used that restricts the spectra to the peaks at 2050 nm and 2180 nm, which have been shown to differ in relation to collagen content (Sponheimer et al., 2019).

Pretreatment was carried out in the Human Evolution department at the Max Planck Institute for Evolutionary Anthropology, Leipzig, following the modified Longin (1971) protocol described in Fewlass et al. (2019). Bone samples were fully demineralized in HCl 0.5 M, treated with a base wash (NaOH 0.1 M) to remove humic acid contamination and reacidified in HCl 0.5 M. The samples were then gelatinized in weakly acidic water (HCl pH 3) at 70 °C for several hours. The resulting gelatin was filtered to remove large particles (>80 μm; Ezee filters, Elkay labs, UK) and ultrafiltered (Sartorius VivaSpin Turbo 15) to concentrate the high molecular weight fraction (>30 kDa; Brown et al., 1988), which was then freeze-dried for 48 h. Ultrafilters were cleaned before use (Brock et al., 2007; Bronk Ramsey et al., 2004). A background bone (dating to >50,000 BP) was pretreated and measured alongside the samples to monitor and account for any contamination introduced in the laboratory.

To assess the quality of the extracts, collagen (ca. 0.5 mg) was packed into tin capsules and measured with a ThermoFinnigan Flash elemental analyser (EA) coupled to a Thermo Delta plus XP isotope

ratio mass spectrometer (IRMS) to determine the elemental (C%, N%, C:N) and stable isotopic values ($\delta^{13}C$, $\delta^{15}N$). Stable carbon isotope ra-tios were expressed relative to Vienna PeeDee Belemnite (VPDB) and stable nitrogen isotope ratios were measured relative to atmospheric N_2 (AIR), using the delta notation (δ) in parts per thousand (‰). Repeated analysis of internal and international standards indicates an analytical error of ± 0.2‰ (1σ). In addition, a small amount (ca. 0.3 mg) of each collagen extract was homogenized in a mortar and pestle, mixed with ~40 mg IR grade KBr powder and pressed into a pellet using a manual hydraulic press (Wasserman). The pellets were analysed with an Agilent Technologies Cary fourier transform infra-red (FTIR) spectrometer with a deuterated triglycine sulfate (DTGS) detector. Sample spectra were recorded in transmission mode at 4 cm^{-1} resolution and averaged for 34 scans between 4000 and 4 cm^{-1} using Resolution Pro software (Agilent Technologies, Santa Clara). The spectra were evaluated and compared to library spectra of well-preserved collagen and bone to look for evidence of incomplete demineralisation, degraded collagen or the presence of any exogenous material in the extracts (D'Elia et al., 2007; DeNiro and Weiner, 1988; Yizhaq et al., 2005).

We made use of the hybrid nature of the ion source of the AixMICADAS (Bard et al., 2015; Wacker et al., 2010c) installed at CEREGE (Centre de Recherche et d'Enseignement de Geosciences de l'Environnement, Aix-en-Provence, France) to date each collagen extract multiple times with both graphite targets (2–3 mg bone collagen) and the gas ion source (Fewlass et al., 2017, 2019). Collagen was weighed into tin cups (ca. 2 mg), graphitized using the AGE 3 (Auto-mated Graphitisation Equipment; Wacker et al., 2010b) and dated using the AixMICADAS. Oxalic acid II standards and background collagen samples were measured in the same session and used in the age calculation of the archaeological samples. An external error of 1‰ was propagated in the error calculation as per standard practice.

Gas measurements were performed using the protocol described in Tuna et al. (2018) and Fewlass et al. (2019). Small aliquots of collagen (< 200 μg collagen) were measured into cleaned silver cups (800 °C, 2 h) and combusted in an Elementar Vario MICRO cube EA (Elementar Analysensysteme GmbH, Germany) which was directly coupled to the gas ion source of the AixMICADAS via the gas interface system (GIS; Ruff et al., 2010; Wacker et al., 2013). The sample CO_2 was mixed with helium (5% CO_2) and fed into the gas ion source at a flow rate of ca. 2 μg C/min. The EA-GIS system was flushed with helium to clean be-tween samples. Precleaned Ti gas targets were presputtered (2 min) in the ion source to remove remaining surface contamination. Oxalic acid NIST standards (from a gas canister) were measured to normalize and correct samples for fractionation. The long-term standard deviation of blanks ($F^{14}C$ = 0.001) was used as the absolute blank error and an external error of 3.5‰ was added (Fewlass et al., 2017; Tuna et al., 2018). The background collagen (^{14}C free) was measured alongside the samples and used in the age calculation of archaeological samples. All data reduction was performed in BATS (Wacker et al., 2010a).

The radiocarbon ages were calibrated in OxCal 4.3 (Bronk Ramsey, 2009) against the IntCal13 dataset (Reimer et al., 2013). To combine the multiple dates we had from each collagen extract we used the R_Combine function in OxCal 4.3 using the $F^{14}C$ and error. As part of this function, a χ^2 test was performed to see if the dates agree statistically (Ward and Wilson, 1978). Following calibration, we used the Combine function to combine the weighted mean of the dates for each individual and the previous charcoal date from within the triple burial.

4. Results

Estimates of collagen preservation in the bone powder from NIR spectroscopy ranged from 7.2 to 9.5% (Table 2). The NIR estimate was identical to the extracted yield for DV14 and DV15 but slightly un-derestimated the collagen yields of Pav1, DV13 and DV16. This discrepancy may relate to the fact that powdered bone was scanned whereas whole bone pieces were extracted for all three individuals. The lower estimates for the powdered aliquots may result from the de-gradation of collagen during the process of transforming whole bone fragments into powder. In all cases, the NIR prescreening correctly determined that the bones had sufficient collagen preserved for ex-traction and analysis.

Following bone pretreatment, the quality of the extracted collagen was assessed based on the yield (as a percentage of the overall weight of the bone where modern bones typically yield ca. 22% weight collagen) and the elemental values determined by EA-IRMS. The collagen yields were excellent (8–14% collagen preserved) for Palaeolithic bone (the generally accepted lower limit for dating is 1%) and the elemental values (C%, N%, C:N) were within the accepted ranges for well-preserved collagen (C%: 30–45%; N%: 11–16%; C:N: 2.9–3.6), indicating that the collagen extracts were suitable for radiocarbon dating (Table 2; van Klinken, 1999). The $\delta^{13}C$ and $\delta^{15}N$ values of the seven individuals fall within the range of stable isotopic values seen for other mid Upper Palaeolithic humans in Eurasia (see Trinkaus et al., 2014). The new direct AMS dates from the seven individuals confirm they belong to the collection of mid Upper Palaeolithic human remains in central Europe. The weighted mean age for each human is shown in Table 2 and the calibrated ranges of the radiocarbon dates are shown in Fig. 4 (all AMS determinations are included in SOM Table S1). The radiocarbon dates determined through both the graphite and direct CO_2 dating methods agree within two standard deviations (2σ; 95.4%) for the six bones from DVII. Although the graphite date from the Pav1 bone collagen is within 2σ of the CO_2 dates from the same collagen extract, it is at the outer limit of this range and the dates just fail the χ^2 test of contemporaneity at the 95% confidence level (χ^2 test: T = 6.6 [5% 6.0], df = 2). The dates from the individuals buried in the triple grave are statistically indistinguishable which is in accordance with the genetic conclusion that DV14 and DV15 were closely maternally related (Mittnik and Krause, 2016) and the archaeological interpretation that the three individuals were interred at the same time (Klima, 1987). When the direct bone dates of the three humans and the previously dated charcoal from the triple burial are combined in OxCal (Fig. 4) the level of agreement is excellent (Acomb = 97.5%, An = 35.5%), giving a narrow calibrated age of 31,010–30,910 cal BP (1σ; 68.2% confidence level).

Although all C%, N% and C:N values of the collagen extracts are all within accepted ranges of well-preserved collagen, the C:N values of DV14, DV42 and Pav1 are at the higher end of this range (Table 2) which can indicate the presence of contaminating carbon (van Klinken, 1999). To assess if there was any evidence of contamination from the conservatives applied in the 1980s, the collagen extracts were analysed with FTIR (D'Elia et al., 2007). All extracts had spectra characteristic of well-preserved collagen with no evidence of exogenous material (Supplementary Online Material [SOM] Fig. S1). The agreement of ^{14}C ages between the collagen extracts from DV14, DV42 and Pav1 and the as-sociated charcoal samples and between DV14 and the other individuals in the triple grave imply that the ^{14}C ages are not significantly affected by carbon contamination from the conservatives applied after excava-tion. The removal of the outer bone surface followed by the acid-base-acid sequence, gelatinisation, ultrafiltration and multiple washes with H_2O during the pretreatment appear to have sufficiently removed any conservatives from the collagen extracts that may have caused erroneous ^{14}C results.

5. Discussion

For Pav1, DV13, DV14, DV15 and DV42, the new dates from the human bone collagen overlap with the associated/proximal charcoal dates at 1σ (68.2% probability) or 2σ (95.4% probability). For the single burial DV16, the dates from the human skeleton (27,220 ± 110 ^{14}C BP) are approximately 1850 ^{14}C years older than the date from charcoal within the grave (25,570 ± 280 ^{14}C BP; GrN-15276) and there is a very low level of agreement when they are combined in OxCal (Acomb = 0.9%, An = 50.0%). The DVII charcoal samples were

Table 2
Pretreatment data and accelerator mass spectrometer (AMS) radiocarbon determinations for the human bones pretreated from DVII and Pavlov I. Weighted mean ages and 1σ errors are given for replicate AMS measurements made from each collagen extract (shown in SOM Table S1). Calibrated ranges (cal BP) were determined in OxCal 4.3 (Bronk Ramsey, 2009), against the IntCal13 dataset (Reimer et al., 2013). All dates have been rounded to the nearest 10 years.

Sample ID	Bone used (mg)	NIR prediction collagen (%)	Collagen yield (mg)	Collagen yield (%)	$\delta^{13}C$ (‰)	$\delta^{15}N$ (‰)	C%	N%	C:N	^{14}C age (BP)	Error (1σ)	1σ calibrated range (cal BP)	2σ calibrated range (cal BP)
Pav 1	50.4	7.2[a]	4.7	9.3	−19.5	13.6	41.2	14.3	3.4	25,490	90	29,720–29,410	29,910–29,260
DV13	42.3	9.3[a]	5.7	13.5	−19.3	12.9	38.5	14.0	3.2	27,040	100	31,170–30,980	31,250–30,880
DV14	37.9	9.4[a]	3.6	9.5	−20.2	13.3	39.0	13.1	3.5	26,760	100	31,040–30,830	31,120–30,730
DV15	201.5	8.0	16.2	8.0	−19.4	12.6	37.1	13.3	3.2	26,680	70	31,020–30,820	31,110–30,720
DV16	32.3	9.5[a]	4.5	13.9	−19.7	12.5	38.5	13.8	3.3	27,220	110	31,250–31,060	31,350–30,970
DV42	53.1		4.8	9.0	−19.8	12.7	39.2	13.5	3.4	26,880	110	31,110–30,900	31,180–30,790
DV43	70.4		7.2	10.2	−19.6	12.6	38.9	13.7	3.3	27,070	110	31,190–30,990	31,270–30,890

[a] Near-infrared spectroscopic estimates were made for powdered bone whereas whole pieces were pretreated for all the individuals except DV15, where only powder was available.

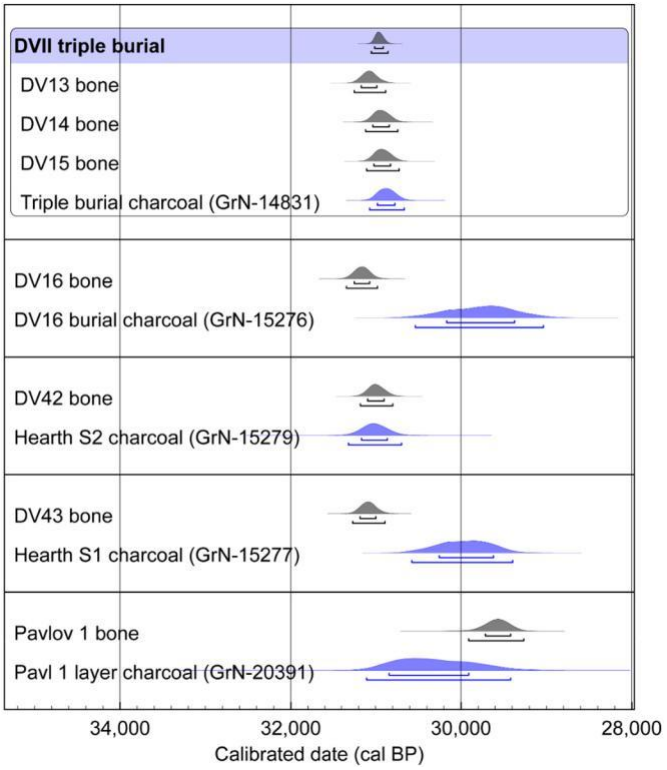

Fig. 4. Calibrated ranges of the new direct dates from the human remains (dark grey) and the associated charcoal dates produced in the 1980s (blue). The range shown for each bone date represents the weighted mean of replicate measurements from one collagen extract. The brackets beneath each distribution show the 1σ (68.2%) and 2σ (95.4%) probability ranges. The dates from the individuals in the triple burial and the associated charcoal date were combined (boxed). Calibrations were performed in OxCal 4.3 (Bronk Ramsey, 2009) using the IntCal13 dataset (Reimer et al., 2013). (For interpretation of the references to colour in this figure legend, the reader is referred to the web version of this article.)

pretreated before rigorous acid-base-wet oxidation (ABOX) pretreat-ment methods had been established to remove contamination from charcoal samples (Bird et al., 1999, 2014). Ultrafiltration of Palaeolithic bone collagen often produces older ages compared to non-ultrafiltered collagen from the same bone, which is attributed to the removal of small molecular weight contaminants from the final sample (Higham et al., 2006; Talamo and Richards, 2011). As any modern carbon con-tamination present in a sample at the time of dating will make an age younger, older dates are generally considered more accurate (Higham et al., 2006; Higham, 2011). It is therefore likely that the discrepancy in age between the DV16 bone and associated charcoal date is due to a small amount of modern carbon contamination not removed from the charcoal sample in the 1980s, which led to an underestimation in age. The new direct dates place the DV16 burial slightly older than the triple burial, falling within the late Early Pavlovian range of dates (around 27,000 ^{14}C BP; 31,000 cal BP) obtained from other charcoals at the site (Svoboda et al., 2016). The bone date for DV43 is also older than the date from the charcoal in the nearby S1 hearth. Either the hearth was made after the human had died, or the charcoal date is also an un-derestimation due to incomplete purification of the sample in the 1980s (more likely this scenario, considering DV16; Fig. 4). The new bone dates indicate that the Pavlov 1 burial dates slightly later than the burials at DVII.

Ritual and isolated human remains are present at a significant number of Upper Palaeolithic sites in addition to DV and Pavlov (see Pettitt, 2011). At several sites, human bones have been found scattered throughout the occupational sequences as well as in ritualistic burials. At Sunghir, Russia, the individuals Sunghir 1, 2 and 3 were interred in spectacularly rich burials (most recently dated between ~30,000–28,000 ^{14}C BP by compound specific radiocarbon dating; Marom et al., 2012; Nalawade-Chavan et al., 2014). Fragmented human bones (Sunghir 4 and 5) were found associated with the burials, potentially with cultural significance, and in the cultural layer (Sunghir 7) (Trinkaus and Buzhilova, 2018). This phenomenon has led to many questions about variable mortuary practices in the mid Upper Palaeolithic. The differential treatment of the dead at DV and Pavlov has been discussed previously in terms of both human behaviour and taphonomic factors (Sázelová et al., 2018; Svoboda, 2008; Trinkaus et al., 2000; Trinkaus et al., 2010; Trinkaus et al., 2019). The contemporaneous dates from the burials and the fragmentary unarticulated bones at DVII (Fig. 4) further demonstrate that postmortem treatment of different individuals varied concurrently, either naturally or though human intervention.

The DVII human burials are contemporary with other burials in the Middle Danube region of Central Europe (Fig. 5; Einwögerer et al., 2006; Svoboda, 2008). A large collection of human burial remains (>20 individuals) was excavated in the 19th and 20th centuries from Predmosti, located close to the Moravian Gate around 100 km north-east of DV/Pavlov (Fig. 1), but lamentably the majority of the collection was destroyed in a fire in 1945 (Svoboda, 2008). The few fragmentary remains have not been directly radiocarbon dated but the layer associated with the burials dates to the Evolved Pavlovian period (27,000–25,000 ^{14}C BP), which would make them roughly contemporaneous or slightly later than the DVII and Pavlov burials. A double burial of new-born infants (Burial 1), sealed with a large mammoth scapula and containing large amounts of ochre and ornaments, was excavated at Krems-Wachtberg, Austria (Fig. 1), along with another single infant burial (Burial 2; Einwögerer et al., 2006). The skeletons have not been directly dated but both burials were associated

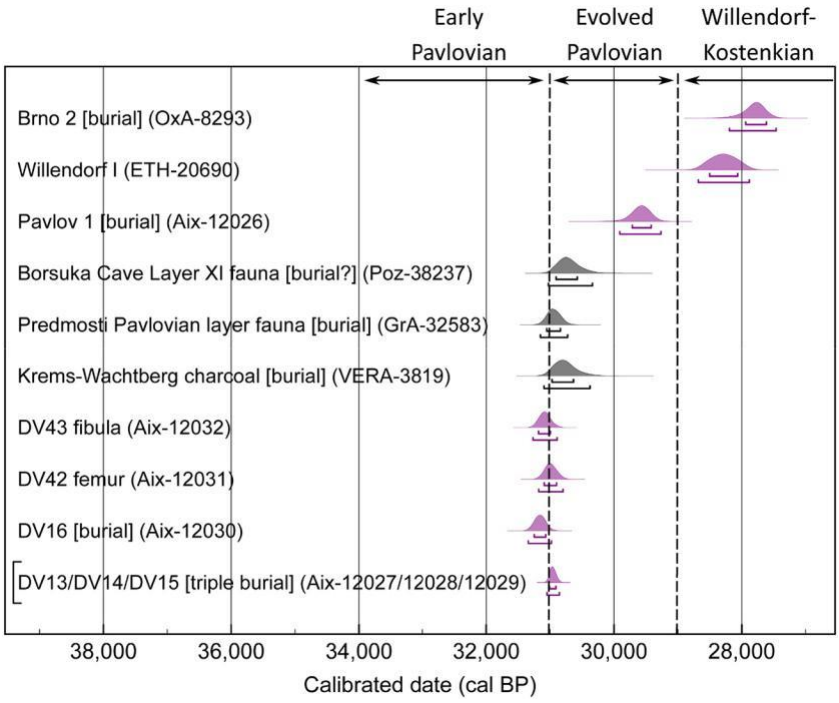

Fig. 5. Calibrated dates of the DVII and Pavlov 1 human remains in comparison to other central European mid Upper Palaeolithic human remains discussed in the text. Direct dates on human remains are shown in purple and associated dates are shown in black. DV35 is not shown as the date is thought to be anomalously young. Figure produced in OxCal 4.3 (Bronk Ramsey, 2009) using the IntCal13 (Reimer et al., 2013) dataset. (For interpretation of the references to colour in this figure legend, the reader is referred to the web version of this article.)

with a well-preserved living floor dated to ca. 27,000 ^{14}C BP and charcoal associated with Burial 1 gave a date of 26,520 + 210/−200 ^{14}C BP (VERA-3819; 68.2%: 30,970–30,630 cal BP), making it contemporaneous with the DVII triple burial (Einwögerer et al., 2009). A collection of six deciduous human teeth and 112 pendants made of large herbivore teeth from Borsuka Cave, Poland (~300 km NE of DV/ Pavlov), has also been interpreted as an infant burial, although the context is highly disturbed (Wilczyński et al., 2016). The human teeth have not been dated directly but two of the pendants were dated to 27,350 ± 450 ^{14}C BP (Poz-32394: 68.2%: 31,640–30,930 cal BP) and 25,150 ± 160 ^{14}C BP (Poz-38236: 68.2%: 29,400–28,980 cal BP) and a reindeer metatarsus from the associated Layer VI was dated to 26,430 ± 180 ^{14}C BP (Poz-38237) (Wilczyński et al., 2012; Wilczyński et al., 2016). Although not contemporaneous to each other, the dates suggest that the infant remains may originate from a similar time range as the remains from DV/Pavlov, and led to the association of the burial with the Pavlovian culture, despite a lack of associated diagnostic ar-tefacts (Wilczyński et al., 2016).

The only other directly dated human remains from the Middle Danube region fall within the later Willendorf-Kostenkian stage of the Gravettian (25,000–21,000 ^{14}C BP; Fig. 5). An isolated femur (Willendorf I) was excavated at Willendorf, a large open-air site complex located on the bank of the Danube River, Austria, in the 1880s. The bone yielded a direct radiocarbon age of 24,250 ± 180 ^{14}C BP (ETH-20690; 68.2%: 28,500–26,070 cal BP; Teschler-Nicola and Trinkaus, 2001), but information on its original context is lacking. The exceptionally rich Brno 2 burial (40 km north of DV and Pavlov; Fig. 1) was directly dated to 23,680 ± 200 ^{14}C BP (OxA-8293; 68.2%: 27,940–27,610 cal BP; Pettitt and Trinkaus et al., 2000). In closer proximity, an unarticulated human femur (DV35) from nearby DVI is the only previously directly dated human bone from the DV/Pavlov area and is dated to 22,840 ± 200 ^{14}C BP (OxA-8292; 68.2%: 27,420–26,980 cal BP; Trinkaus et al., 1999). However, DV35 was only identified as human in the 1990s so its exact context within DVI is uncertain. The much younger age compared to the other Early or Evolved Pavlovian dates from the site indicate that the sample was contaminated (Svoboda et al., 2016; Trinkaus et al., 1999). It is worth noting that Willendorf I, Brno 2 and DV35 were pretreated before the wide spread application of ultrafiltration and it has been suggested that the dates provide little more than confirmation that these human remains belong to the Gravettian (Trinkaus et al., 2014).

6. Conclusion

The results of this study confirm the Pavlovian origin of the seven human bones from DVII and Pavlov I, in two cases (DV16 and DV43) pushing back the age assigned to the human remains from associated charcoal dates. The collagen sample chemistry and the consistency of the ages from the triple burial and with the charcoal dates carried out in the 1980s lend confidence to the reliability of the results. This study further confirms the suitability of NIR spectroscopy as a collagen pre-screening method for radiocarbon dating archaeological bone (Sponheimer et al., 2019). The method is completely non-destructive which makes it ideal for prescreening precious archaeological bone prior to pretreatment to determine if collagen preservation is sufficient. Radiocarbon datasets such as reported here are crucial for refining our understanding of the chronology of Gravettian cultural evolution.

Acknowledgements

This research was funded by the Max Planck Society (Germany) and Czech National Institutional support to the Institute of Archaeology of the Czech Academy of Sciences, Brno (RVO: 68081758) and Masaryk University, Brno (MUNI/A/1528/2018) in the Czech Republic. The AixMICADAS was acquired and operated in the framework of the EQUIPEX project ASTER-CEREGE (P.I.: E. Bard) with additional matching funds from the Collège de France. The authors thank the three reviewers for their helpful comments.

Declaration of competing interest

The authors declare that they have no known competing financial interests or personal relationships that could have appeared to influence the work reported in this paper.

Appendix A. Supplementary data

Supplementary data to this article can be found online at https://

doi.org/10.1016/j.jasrep.2019.102000.

References

Absolon, V., 1933. Les statuettes miolithiques modelées de l'Aurignacien supérieur en Moravie. Anthropologie 11, 273–278.

Bard, E., et al., 2015. AixMICADAS, the accelerator mass spectrometer dedicated to ^{14}C recently installed in Aix-en-Provence, France. Nucl. Instrum. Methods Phys. Res., Sect. B 361, 80–86.

Bird, M.I., et al., 1999. Radiocarbon dating of "old" charcoal using a wet oxidation, stepped-combustion procedure. Radiocarbon 41, 127–140.

Bird, M.I., et al., 2014. The efficiency of charcoal decontamination for radiocarbon dating by three pre-treatments- ABOX, ABA and hypy. Quat. Geochronol. 22, 25–32.

Brock, F., et al., 2007. Quality assurance of ultrafiltered bone dating. Radiocarbon 49, 187–192.

Bronk Ramsey, C., 2009. Bayesian analysis of radiocarbon dates. Radiocarbon 51, 337–360.

Brock, F., Dee, M., Hughes, A., Snoeck, C., Staff, R., Bronk Ramsey, C., 2017. Testing the effectiveness of protocols for removal of common conservation treatments for radiocarbon dating. Radiocarbon 60, 35–50.

Bronk Ramsey, C., et al., 2004. Improvements to the pretreatment of bone at Oxford. Radiocarbon 46, 155–164.

Brown, T.A., et al., 1988. Improved collagen extraction by modified Longin method. Radiocarbon 30, 171–177.

D'Elia, M., et al., 2007. Evaluation of possible contamination sources in the ^{14}C analysis of bone samples by FTIR spectroscopy. Radiocarbon 49, 201–210.

DeNiro, M.J., Weiner, S., 1988. Chemical, enzymatic and spectroscopic characterization of "collagen" and other organic fractions from prehistoric bones. Geochim. Cosmochim. Acta 52, 2197–2206.

Einwögerer, T., et al., 2006. Upper Palaeolithic infant burials. Nature 444, 285. Einwögerer, T., et al., 2009. ^{14}C dating of the Upper Paleolithic site at Krems-Wachtberg, Austria. Radiocarbon 51, 847–855.

Fewlass, H., et al., 2017. Size matters: radiocarbon dates of < 200 μg ancient collagen samples with AixMICADAS and its gas ion source. Radiocarbon 60, 425–439.

Fewlass, H., et al., 2019. Pretreatment and gaseous radiocarbon dating of 40–100 mg archaeological bone. Sci. Rep. 9, 5342.

Fu, Q., et al., 2016. The genetic history of Ice Age Europe. Nature 534, 200–205.

Henry-Gambier, D., 2008. Comportement des populations d'Europe au Gravettien: Pratiques funéraires et interprétations. Paléo 20, 165–204.

Higham, T., 2011. European Middle and Upper Palaeolithic radiocarbon dates are often older than they look: problems with previous dates and some remedies. Antiquity 85, 235–249.

Higham, T., et al., 2006. AMS radiocarbon dating of ancient bone using ultrafiltration. Radiocarbon 48, 179–195.

Holliday, T.W., et al., 2006. The human remains: a summary inventory. In: Trinkaus, E., Svoboda, J. (Eds.), Early Modern Human Evolution in Central Europe: The People of Dolní Věstonice and Pavlov. Oxford University Press, New York, pp. 27–30.

Klima, B., 1987. A triple burial from the Upper Paleolithic of Dolní Věstonice, Czechoslovakia. J. Hum. Evol. 16, 831–835.

Longin, R., 1971. New method of collagen extraction for radiocarbon dating. Nature 231, 241–242.

Marom, A., McCullagh, J.S.O., Higham, T.F.G., Sinitsyn, A.A., Hedges, R.E.M., 2012. Single amino acid radiocarbon dating of Upper Paleolithic modern humans. Proc. Natl. Acad. Sci. U. S. A. 109, 6878–6881.

Mittnik, A., Krause, J., 2016. Genetic analysis of the Dolní Věstonice human remains. In: Svoboda, J. (Ed.), Dolní Věstonice II: Chronostratigraphy, Paleoethnology, Palaeoanthropology. Academy of Sciences of the Czech Republic, Institute of Archaeology, Brno, pp. 377–384.

Nalawade-Chavan, S., McCullagh, J., Hedges, R., 2014. New hydroxyproline radiocarbon dates from Sungir, Russia, confirm early Mid Upper Palaeolithic burials in Eurasia. PLoS ONE 9, e76896.

Pettitt, P., 2011. The Palaeolithic Origins of Human Burial. Routledge, London.

Pettitt, P., Trinkaus, E., 2000. Direct radiocarbon dating of the Brno 2 Gravettian human remains. Anthropologie 38, 149–150.

Reimer, P.J., et al., 2013. IntCal13 and Marine13 radiocarbon age calibration curves 0–50,000 years cal BP. Radiocarbon 55, 1869–1887.

Rohland, N., Hofreiter, M., 2007. Ancient DNA extraction from bones and teeth. Nat. Protoc. 2, 1756–1762.

Ruff, M., et al., 2010. On-line radiocarbon measurements of small samples using elemental analyzer and MICADAS gas ion source. Radiocarbon 52, 1645–1656.

Sázelová, S., Svoboda, J., Wilczyński, J., Wojtal, P., Trinkaus, E., 2018. Puzzling pairs from Pavlov and mortuary diversity in the Mid Upper Paleolithic. Přehled Výzkumů 59, 69–88.

Sládek, V., et al., 2000. The People of the Pavlovian. Skeletal Catalogue and Osteometrics of the Gravettian Fossil Hominids From Dolní Věstonice and Pavlov. Academy of Sciences of the Czech Republic, Institute of Archaeology, Brno.

Sponheimer, M., Ryder, C., Fewlass, H., Smith, E., Pestle, W., Talamo, S., 2019. Saving old bones: a non-destructive method for bone collagen prescreening. Sci. Rep In press.

Svoboda, J., 1987. A new male burial from Dolní Věstonice. J. Hum. Evol. 16, 827–830.

Svoboda, J., 2006a. The archaeological contexts of the human remains. In: Trinkaus, E., Svoboda, J. (Eds.), Early Modern Human Evolution in Central Europe: The People of Dolní Věstonice and Pavlov. Oxford Unversity Press, New York, pp. 9–14.

Svoboda, J., 2006b. The burials: rituals and taphonomy. In: Trinkaus, E., Svoboda, J. (Eds.), Early Modern Human Evolution in Central Europe: The People of Dolní Věstonice and Pavlov. Oxford University Press, New York, pp. 15–26.

Svoboda, J., 2008. The Upper Paleolithic burial area at Předmostí: ritual and taphonomy. J. Hum. Evol. 54, 15–33.

Svoboda, J., 2016. Dolní Věstonice II: Chronostratigraphy, Paleoethnology, Palaeoanthropology. Academy of Sciences of the Czech Republic, Institute of Archaeology, Brno.

Svoboda, J., et al., 2016. Pavlov I: a large Gravettian site in space and time. Quat. Int. 406, 95–105.

Talamo, S., Richards, M., 2011. A comparison of bone pretreatment methods for AMS dating of samples > 30,000 BP. Radiocarbon 53, 443–449.

Teschler-Nicola, M., Trinkaus, E., 2001. Human remains from the Austrian Gravettian: the Willendorf femoral diaphysis and mandibular symphysis. J. Hum. Evol. 40, 451–465.

Trinkaus, E., Buzhilova, A.P., 2018. Diversity and differential disposal of the dead at Sunghir. Antiquity 92, 7–21.

Trinkaus, E., Svoboda, J., 2006. Early Modern Human Evolution in Central Europe: The People of Dolní Věstonice and Pavlov. Oxford University Press, New York.

Trinkaus, E., et al., 1999. Human remains from the Moravian Gravettian: the Dolní Věstonice 35 femoral diaphysis. Anthropologie 37, 167–175.

Trinkaus, E., et al., 2000. Human remains from the Moravian Gravettian: morphology and taphonomy of isolated elements from the DolníVěstonice II site. J. Archaeol. Sci. 27, 1115–1132.

Trinkaus, E., et al., 2010. Human remains from the Moravian Gravettian: morphology and taphonomy of additional elements from Dolní Věstonice II and Pavlov I. Int. J. Osteoarchaeol. 20, 645–669.

Trinkaus, E., et al., 2014. The People of Sunghir: Burials, Bodies and Behavior in the Earlier Upper Paleolithic. Oxford University Press, New York.

Trinkaus, E., et al., 2016. Human burials and biology. In: Svoboda, J. (Ed.), Dolni Vestonice II. Chronostratigraphy, Paleoethnology, Palaeoanthropology. Academy of Sciences of the Czech Republic, Institute of Archaeology, Brno, pp. 328–344.

Trinkaus, E., et al., 2017. Palmar, patellar, and pedal human remains from Pavlov. PaleoAnthropology 2017, 73–101.

Trinkaus, E., et al., 2019. Pieces of people in the Pavlovian: burials, body parts and bones in the earlier upper Palaeolithic. Human Remains and Violence 5, 70–87.

Tuna, T., et al., 2018. Development of small CO_2 gas measurements with AixMICADAS. Nucl. Instrum. Methods Phys. Res., Sect. B 437, 93–97.

van der Plicht, J., 1997. The radiocarbon dating. In: Svoboda, J. (Ed.), Pavlov I - Northwest. The Upper Paleolithic Burial and its Settlement Context. Academy of Sciences of the Czech Republic, Institute of Archaeology, Brno, pp. 427–436.

van Klinken, G.J., 1999. Bone collagen quality indicators for palaeodietary and radio-carbon measurements. J. Archaeol. Sci. 26, 687–695.

Vandiver, P.B., et al., 1989. The origins of ceramic technology at Dolni Věstonice, Czechoslovakia. Science 246, 1002–1008.

Vanhaeren, M., d'Errico, F., 2002. The body ornaments associated with the burial. In: Zilhão, J., Trinkaus, E. (Eds.), Portrait of the Artist as a Child. The Gravettian Human Skeleton From the Abrigo Do Lagar Velho and its Archeological Context. Instituto Português de Arqueologia, Lisbon, pp. 154–186.

Vlcek, E., 1997. Human remains from Pavlov and the biological anthropology of the Gravettian human population of South Moravia. In: Svoboda, J. (Ed.), Pavlov I - Northwest. The Upper Paleolithic Burial and its Settlement Context. Academy of Sciences of the Czech Republic, Institute of Archaeology and Department of Paleolithic and Paleoethnology, Brno, pp. 53–154.

Wacker, L., et al., 2010a. Bats: a new tool for AMS data reduction. Nucl. Instrum. Methods Phys. Res., Sect. B 268, 976–979.

Wacker, L., et al., 2010b. A revolutionary graphitisation system: fully automated, com-pact and simple. Nucl. Instrum. Methods Phys. Res., Sect. B 268, 931–934.

Wacker, L., et al., 2010c. MICADAS: routine and high-precision radiocarbon dating. Radiocarbon 52, 252–262.

Wacker, L., et al., 2013. A versatile gas interface for routine radiocarbon analysis with a gas ion source. Nucl. Instrum. Methods Phys. Res., Sect. B 294, 315–319.

Ward, G.K., Wilson, S.R., 1978. Procedures for comparing and combining radiocarbon age determinations: a critique. Archaeometry 20, 19–31.

Wilczyński, J., et al., 2012. Faunal remains from Borsuka Cave - an example of local climate variability during Late Pleistocene in southern Poland. Acta Zool. Cracov. 55, 131–155.

Wilczyński, J., et al., 2016. A Mid Upper Palaeolithic child burial from Borsuka cave (Southern Poland). Int. J. Osteoarchaeol. 26, 151–162.

Yizhaq, M., et al., 2005. Quality controlled radiocarbon dating of bones and charcoal from the early pre-pottery Neolithic B (PPNB) of Motza (Israel). Radiocarbon 47, 193–206.

Supplementary Online Material (SOM)

Direct radiocarbon dates of mid Upper Palaeolithic human remains from Dolní Věstonice II and Pavlov I, Czech Republic

Helen Fewlass[a,*], Sahra Talamo[a,b], Bernd Kromer[c,a], Edouard Bard[d], Thibaut Tuna[d], Yoann Fagault[d], Matt Sponheimer[e], Christina Ryder[e], Jean-Jacques Hublin[a], Angela Perri[f], Sandra Sázelová[g,h], Jiří Svoboda[g]

[a] *Department of Human Evolution, Max Planck Institute for Evolutionary Anthropology, Deutscher Platz 6, Leipzig, D-04103, Germany*

[b] *Department of Chemistry "G. Ciamician", University of Bologna, Via Selmi, 2, 40126 Bologna, Italy*

[c] *Institute of Environmental Physics, University of Heidelberg, INF 229, Heidelberg, D-69120, Germany*

[d] *CEREGE, Aix Marseille Université, CNRS, IRD, INRA, Collège de France, Technopôle de l'Arbois, BP 80, 13545 Aix-en-Provence, France*

[e] *Department of Anthropology, University of Colorado Boulder, 1350 Pleasant St, 233 UCB, Boulder, CO 80309-0233, USA*

[f] *Department of Archaeology, Durham University, South Road, Durham, DH1 3LE, UK*

[g] *Department of Anthropology, Faculty of Science, Masaryk University, Kotlářská 2, 611 37 Brno, Czech Republic*

[h] *Institute of Archeology, Czech Academy of Sciences, Brno, Čechyňská 363/19, CZ-602 00 Brno, Czech Republic*

*Corresponding author (H. Fewlass)

E-mail address: helen_fewlass@eva.mpg.de

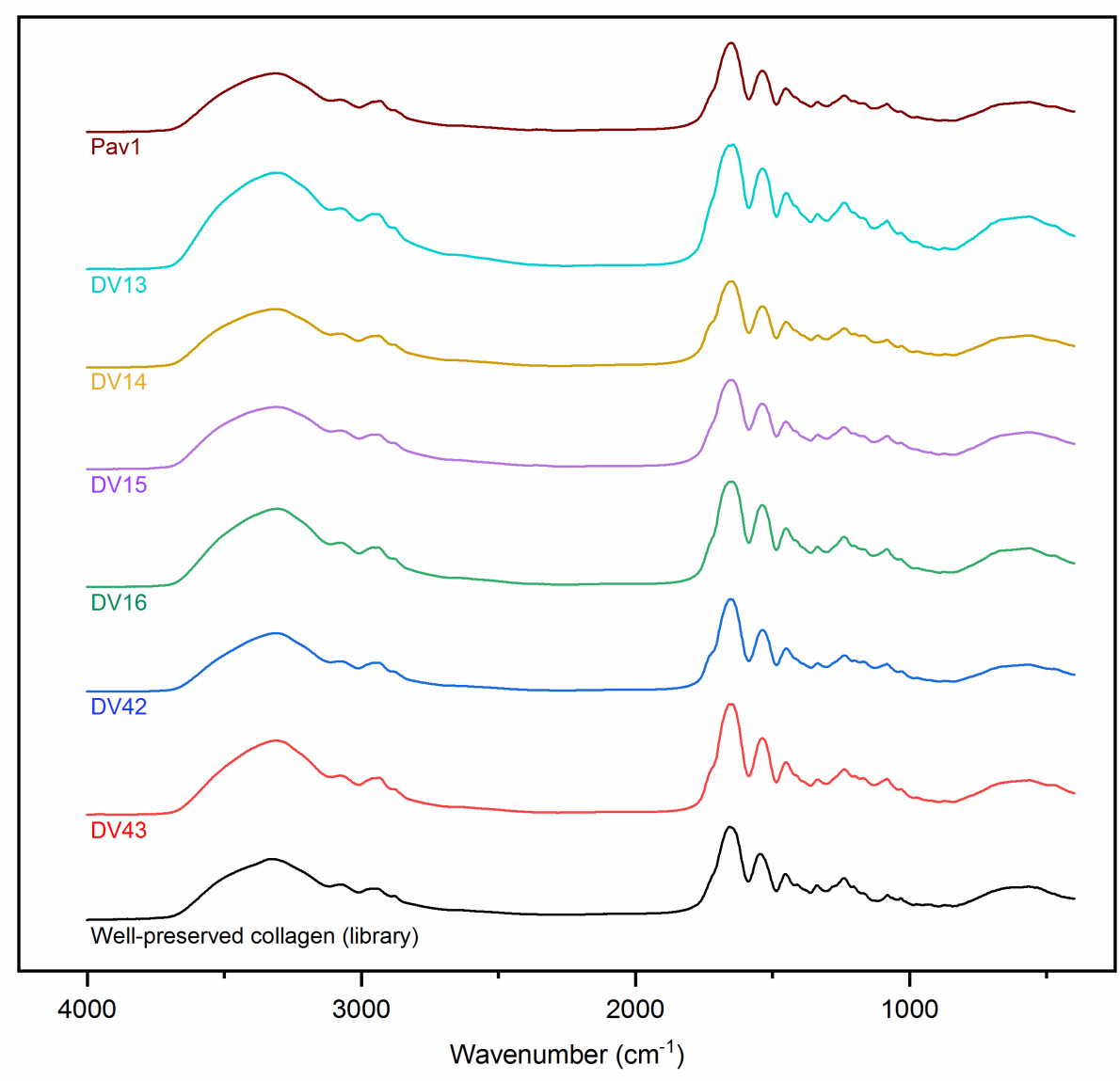

SOM Figure S1. Fourier transform infra-red (FTIR) spectra of the collagen extracts from the seven human bones from Pavlov I and Dolní Věstonice II. The bottom-most library spectra of well-preserved collagen is included for comparison.

SOM Table S1. New accelerator mass spectrometer (AMS) determinations from bone collagen from the Pavlov I and Dolní Věstonice II human remains showing the dating method used (CO_2 gas ion source or graphite target) and amount of carbon (µg C) measured by the elemental analyser (EA) following combustion of the sample. Based on series of measurements of various standards, the precision of AMS $\delta^{13}C$ is ca. 1 ‰ for graphite samples (Bard, et al., 2015) and ca. 2 ‰ for CO_2 gas samples (Tuna, et al., 2018). The $\delta^{13}C$ for gas samples is usually shifted by -2 ‰ with respect to the accurate analyses of graphite samples. Tuna et al. (2018) attributed this shift to isotopic fractionation in the elemental analyser + gas interface system for unknown samples, by contrast to the standard measured directly on a CO_2 bottle of oxalic acid. This small bias in the $\delta^{13}C$ calculation for unknown samples has no influence on their ^{14}C age determination. All dates have been rounded to nearest 10 years.

Sample ID	AMS lab code	Dating method	EA sample size (µg C)	^{14}C age (BP)	Error (1σ)	AMS $\delta^{13}C$ (‰)
Pavlov 1	Aix-12026.1.1	CO_2	85	26,220	370	-23.5
	Aix-12026.1.3	CO_2	97	25,790	250	-23.2
	Aix-12026.2.1	graphite	756	25,390	100	-18.8
DV13	Aix-12027.1.1	CO_2	80	26,950	390	-21.5
	Aix-12027.1.2	CO_2	98	26,990	390	-22.1
	Aix-12027.1.3	CO_2	94	27,510	290	-21.9
	Aix-12027.2.1	graphite	740	26,970	120	-18.4
DV14	Aix-12028.1.1	CO_2	92	26,670	370	-21.0
	Aix-12028.1.2	CO_2	91	26,490	360	-20.8
	Aix-12028.1.3	CO_2	102	27,190	410	-21.4
	Aix-12028.2.1	graphite	742	26,740	120	-18.6
DV15	Aix-12029.1.1	CO_2	93	27,310	400	-19.8
	Aix-12029.1.2	CO_2	84	26,890	390	-22.4
	Aix-12029.1.3	CO_2	93	26,990	380	-20.4
	Aix-12029.2.1	graphite	775	26,630	120	-16.2
DV16	Aix-12030.1.1	CO_2	85	27,960	430	-21.2
	Aix-12030.1.2	CO_2	97	27,380	420	-22.0
	Aix-12030.1.3	CO_2	99	26,950	380	-20.3
	Aix-12030.2.1	graphite	792	27,160	120	-18.1
DV42	Aix-12031.1.1	CO_2	87	27,040	380	-21.4
	Aix-12031.2.1	graphite	789	26,860	120	-21.8
DV43	Aix-12032.1.1	CO_2	88	26,570	360	-21.0
	Aix-12032.2.1	graphite	769	27,110	120	-18.7

References

Bard, E., et al., 2015. AixMICADAS, the accelerator mass spectrometer dedicated to ^{14}C recently installed in Aix-en-Provence, France. Nuclear Instruments and Methods in Physics Research Section B: Beam Interactions with Materials and Atoms 361, 80-86.

Tuna, T., et al., 2018. Development of small CO_2 gas measurements with AixMICADAS. Nuclear Instruments and Methods in Physics Research Section B: Beam Interactions with Materials and Atoms 437, 93-97.

Chapter Five

New ^{14}C chronology for Middle–to–Upper Palaeolithic transition at Bacho Kiro Cave, Bulgaria

H. Fewlass, S. Talamo, L. Wacker, B. Kromer, T. Tuna, Y. Fagault, E. Bard, S. McPherron, V. Aldeias, R. Maria, N.L. Martisius, L. Paskulin, Z. Rezek, V. Sinet-Mathiot, S. Sirakova, G.M. Smith, R. Spasov, F. Welker, T. Tsanova, N. Sirakov, J.-J Hublin

Under review at *Nature Ecology and Evolution*

New ^{14}C chronology for Middle–to–Upper Palaeolithic transition at Bacho Kiro Cave, Bulgaria

Fewlass, H.[1]*, Talamo, S.[1,2], Wacker, L.[3], Kromer, B.[1,4], Tuna, T.[5], Fagault, Y.[5], Bard, E.[5], McPherron, S. P.[1], Aldeias, V.[6,1], Maria, R.[1], Martisius, N. L.[7], Paskulin, L.[8], Rezek, Z.[1, 9], Sinet-Mathiot, V.[1], Sirakova, S.[10], Smith, G.M[1], Spasov, R.[11], Welker, F.[12,1], Tsanova, T.[1], Sirakov, N.[10], Hublin, J.-J.[1]

1) Department of Human Evolution, Max Planck Institute for Evolutionary Anthropology, Leipzig, Germany
2) Department of Chemistry "G. Ciamician", University of Bologna, Bologna, Italy
3) Ion Beam Physics, ETH-Zurich, Zürich, Switzerland
4) Institute of Environmental Physics, University of Heidelberg, Heidelberg, Germany
5) CEREGE, Aix-Marseille University, CNRS, IRD, INRA, Collège de France, Aix-en-Provence, France
6) ICArEHB, University of Algarve, Campus de Gambelas, Faro, Portugal
7) Department of Anthropology, University of California, Davis, USA
8) Department of Archaeology, University of Aberdeen, Aberdeen, Scotland
9) University of Pennsylvania Museum of Archaeology and Anthropology, Philadelphia, PA, USA
10) National Institute of Archaeology and Museum, Bulgarian Academy of Sciences, Sofia, Bulgaria
11) Archaeology Department, New Bulgarian University, Sofia, Bulgaria
12) Evolutionary Genomics Section, Globe Institute, University of Copenhagen, Copenhagen, Denmark.

*__Corresponding author__: helen_fewlass@eva.mpg.de

Abstract

The stratigraphy at Bacho Kiro Cave, Bulgaria, spans the Middle to Upper Palaeolithic transition, including an Initial Upper Palaeolithic (IUP) assemblage argued to represent the earliest arrival of Upper Palaeolithic *Homo sapiens* in Europe. We applied the latest techniques in ^{14}C dating to an extensive dataset of newly excavated animal and human bones to produce a robust, high precision radiocarbon chronology for the site. At the base of the stratigraphy, the Middle Palaeolithic (MP) occupation dates to >51,000 BP. A chronological gap of over 3000 years separates the MP occupation from the occupation of the cave by *Homo sapiens,* which extends to 35,000 cal BP. The extensive IUP assemblage, now securely associated with *Homo sapiens* fossils at this site, dates to 46,930-43,830 cal BP (95% probability), coinciding with global climatic changes spanning Greenland Interstadial 12. The results provide crucial chronological context for the early occupation of Europe by Upper Palaeolithic *Homo sapiens*.

Introduction

Bacho Kiro Cave in north-central Bulgaria (Fig. 1a) has an archaeological sequence spanning the late Middle Palaeolithic (MP) through the early Upper Palaeolithic. First excavated in 1938[1] and again in 1971-1975[2], the cave is particularly notable for its distinctive lithic assemblages from Layers 11 and 11a[2] consisting of elongated Levallois-like blades, retouched points, end-scrapers and splintered pieces, along with pendants made of animal bone and teeth[2-4]. A radiocarbon date of >43,000 ^{14}C BP (GrN-7545) (Table 1) on charcoal from Layer 11 made it perhaps one of the earliest Upper Palaeolithic (UP) assemblages in Europe[2]. The Bachokirian, as it became known, is now recognised as part of the Initial Upper Palaeolithic (IUP)[3,5] and is argued to represent one of the earliest occurrences of Upper Palaeolithic *Homo sapiens* in Europe[4,6].

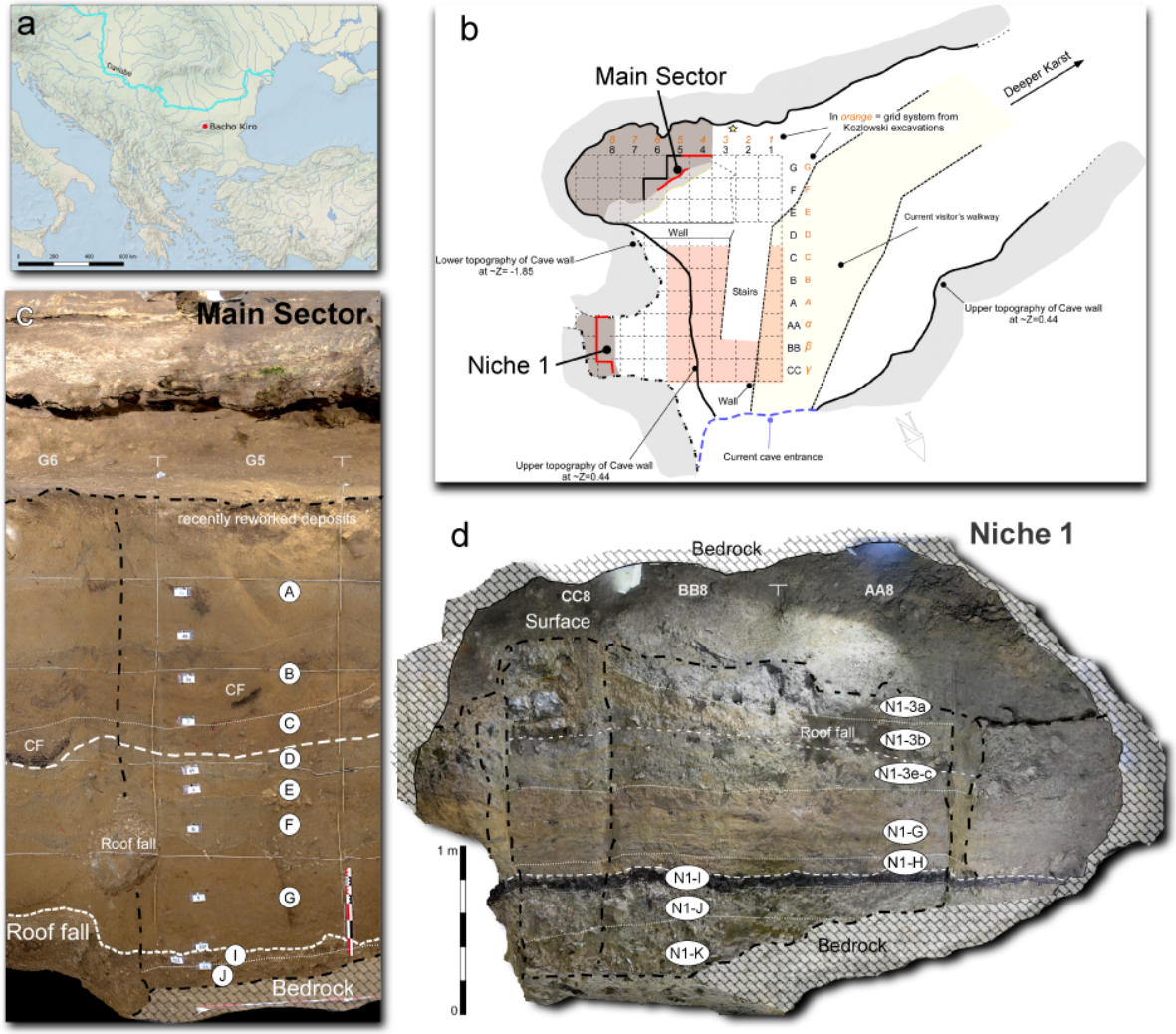

Figure 1. Bacho Kiro Cave: **a)** location of the cave in Bulgaria, Balkan Peninsula, south-eastern Europe (base map from naturalearthdata.com); **b)** site plan showing the location of excavations carried out in 1971-1975 (centre, light orange) and the new excavations, in the Main Sector (top) and in the Niche 1 (left). The locations of the profiles shown in c-d are marked by red lines; **c)** stratigraphic sequence in the Main Sector, along squares G6 and G5 in 2015. Note the presence of Layer J overlying the bedrock at the bottom of the sequence; **d)** Extract from a 3D model of Niche 1, showing the stratigraphic sequence. Layer attributions from this sector have an 'N1-' prefix. Note the distinctive dark colour of Layer N1-I.

In 2015, the National Archaeological Institute with Museum (NAIM-BAS, Sofia) and the Department of Human Evolution at Max Planck Institute for Evolutionary Anthropology (MPI-EVA, Leipzig) re-opened the cave with the primary goals of re-sampling the lithic assemblages of the site and re-dating the IUP Layers 11 and 11a[7]. Two excavation areas adjacent to the area of the 1970s excavations were established (Fig. 1b) and excavated to bedrock. The Main Sector (see Fig. 1b) encompasses the entire sequence as previously described[2]. The other, Niche 1, is a small and low ceilinged lateral chamber located to the east, preserving only the lower portion of the sequence, including the IUP and underlying Middle Palaeolithic. Layer designations were kept separate between these two areas, with the layers from Niche 1 having an "N1-" prefix. The two areas are approximately 4 m apart (see Fig. 1b; Supplementary Fig. 1). Previous excavations removed the deposits connecting these two areas, but field observations of sedimentary characteristics, morphology and archaeological content allow some layers to be correlated (see Fig. 2; Supplementary Text 1). Here we use the new stratigraphic nomenclature (Fig. 2) wherein Layer 11[2] corresponds to Layer I in the Main Sector and Layer N1-I in the Niche 1 and Layer 11a[2] to Layers J and N1-J.

The new excavations confirm the previously reported stratigraphy and archaeological sequence[2] (Fig. 2). In the Main Sector (Fig. 1c), the stratigraphy begins with the upper part of Layer J, which overlies bedrock and continues through to Layer A0 at the current surface of the cave deposit. The Niche 1 stratigraphy (Fig. 1d) starts with Layer N1-K deposited directly on the bedrock, continuing through Layer N1-J and the stratigraphically distinctive Layer N1-I, into deposits ending with Layer N1-3a. Based on archaeological and geological observations, Layers N1-J, N1-I and N1-G in the Niche 1 clearly correspond, respectively, to Layers J, I, and G in the Main sector. The labelling of layers in the upper part of the Niche 1 stratigraphy with numbers (N1-3a-e) reflects the lack of correlation of these layers to lettered layers (A-J) in the Main Sector, although the erosive lower contact of Layers C and N1-3b can be used as a stratigraphic marker in these two areas.

The overall sequence is characterized by an exceptionally high artefact density in Layers I and N1-I (15 finds >2 cm per litre of sediment) and low densities in other layers. During the new excavations, we recovered approximately 14,000 bones and about 2,000 lithics (>2 cm), with over 70% of these coming from Layers I and N1-I. These quantities allow the lithic and bone industry to be correlated with previously excavated material and characterised as IUP[2,3] (Supplementary Table 1). In both the old and new lithic collections, the material from Layers J and N1-J is technologically consistent with the Layer I/N1-I assemblage, but the lower number of finds from this layer (0.6 finds per litre of sediment) adds some uncertainty to this characterization. However, the lower part of Layer N1-J contains some artefacts that are consistent with the Middle Palaeolithic assemblage of the underlying Layer N1-K (Levallois flakes from coarse-grained syenite porphyry). Therefore, we can place the change from Middle Palaeolithic into IUP most parsimoniously into the lower part of Layer N1-J. In addition to changes in typology and technology from flakes to blades, this transition is marked by a shift in raw material use, from coarser syenite porphyry to fine-grained flint[2]. Layers H—D and N1-H—N1-3a contain no lithic artefacts and a very low density of animal bones. Layers C, B, A2 and A1 in the upper part of the stratigraphy contain characteristic Upper Palaeolithic artefacts, including retouched blades, backed bladelets, carinated end-scrapers, burins, bone

tools and pendants. However, their lithic assemblages are poor in diagnostic technological attributes to any particular Upper Palaeolithic industry (Supplementary Table 1).

In the 1980s and 1990s, radiocarbon dating was attempted on material from the 1970s excavation[2,8]. Although several of the samples produced dates of great antiquity, the sequence of dates was inconsistent with the stratigraphy (Table 1). In particular, a wide range (>43,000 – 34,800 ± 1,150 ^{14}C BP) was obtained from Layer 11 and a much younger date (33,750 ± 850 ^{14}C BP) from the underlying Layer 11a. This finding suggested that either the site was affected by post-depositional mixing between layers, or storage and sampling of the material was problematic, and/or that modern carbon contamination had been insufficiently removed from some of the ^{14}C samples prior to dating, leading to an under-estimation of their true ages[8]. Since then the establishment of more stringent methods of sample pretreatment, including acid-base-wet oxidation (ABOX) pretreatment for charcoal samples[9,10], and ultrafiltration of bone collagen[11-13], have greatly improved the reliability of radiocarbon dates on Palaeolithic samples[14].

Table 1. Previously published radiocarbon dates on material excavated from Bacho Kiro Cave from 1971-1975.

Layer	Sample type	AMS lab number	^{14}C age	1σ error (years)	Reference
7	Charcoal	OxA-3181	32,200	780	8
6a/7	Bone	Ly1102	29,150	950	2,15
6b	Charcoal	OxA-3182	33,300	820	8
6b	Bone (no. 972)	GrN-7569	32,700	300	2
11	Charcoal from hearth	GrN-7545	>43,000		2
11	Bone	OxA-3213	38,500	1,700	8
11	Charcoal	OxA-3183	37,650	1,450	8
11	Tooth	OxA-3212	34,800	1,150	8
11a	Bone	OxA-3184	33,750	850	8
13	Bone (nos. 933 and 936)	GrN-7570	>47,000		2

During recent ZooMS (Zooarchaeology by Mass Spectrometry)[16] screening of undiagnostic bone fragments from Bacho Kiro Cave, 4 fragmentary bones from Layer N1-I, 1 from Layer B and 1 from the 1970s collection (Layer B/C) were identified as hominin[4]. DNA analysis confirmed their attribution to *Homo sapiens*[4]. Given the presence of a unique assemblage of human bone fragments and IUP artefacts, we sought to establish the range of the IUP at Bacho Kiro Cave and resolve the previous age anomalies by conducting a large-scale dating program. In this paper, we present an extensive dataset of high-precision accelerator mass spectrometer (AMS) radiocarbon dates, which includes direct dating of the newly discovered hominin remains[4]. We also used the Aix-MICADAS gas ion source[17-19] to date minute aliquots of bone collagen from the two hominin bones from Layer B to cross-check the ages obtained from more commonly used AMS graphite targets.

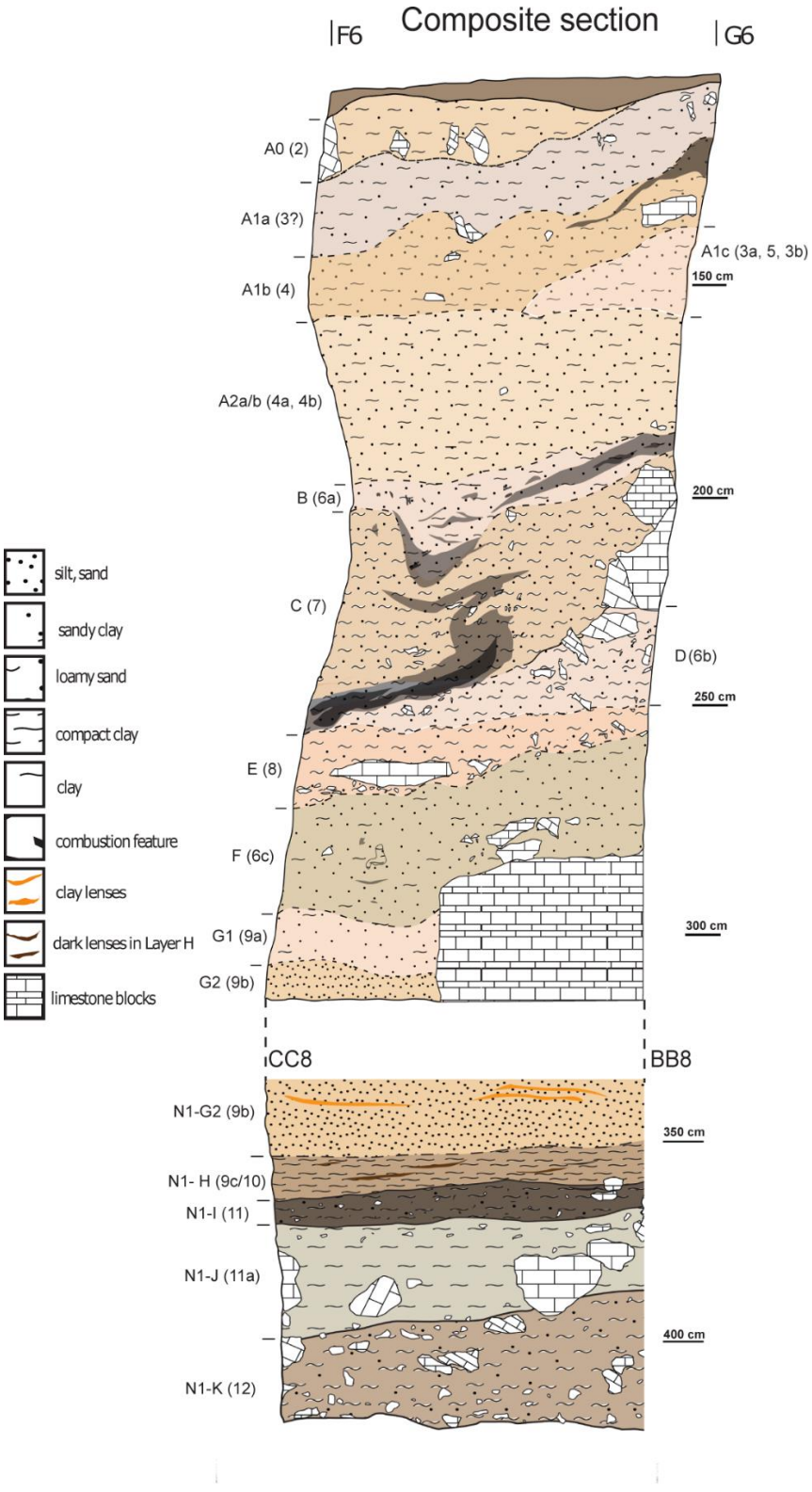

Figure 2. Bacho Kiro Cave: Drawings of composite longitudinal stratigraphic profiles of the Main Sector (top) and the Niche 1 (bottom). Layer attributions in the Niche 1 have an 'N1-' prefix. Numbers in parentheses show the layer attributions from the 1970s excavations. Original drawings by I. Krumov and N. Zahariev.

Materials and Methods

Sample selection for radiocarbon dating

Bones were selected for radiocarbon dating from finds excavated during the 2015-2017 field seasons spanning the stratigraphy in both the Main Sector (Supplementary Figs. 2-3) and the Niche 1 (Supplementary Figs. 4-5). In total, 141 animal bones and 6 hominin bones were selected for collagen extraction. Where possible, animal bones that had signs of anthropogenic modification (cut-marks, impact fractures) on their surfaces were selected (53% of the sample set) (Fig. 3). A particular focus was given to sampling the IUP in Layer N1-I, where the layer was extensively exposed. Due to the exceptionally high density of bone in this layer (Supplementary Fig. 5), we were able to select a high number of bones (77%) with anthropogenic modifications. A small number of samples were also taken from Layer I in the Main Sector to confirm the stratigraphic link between the two areas through radiocarbon dating. During excavation of the contact zone between Layers I and J in the Main Sector, precise attribution of the finds to either Layer I or J was sometimes impossible to make, due to the sediment moistness and the presence of large limestone rubble. These finds are labelled as "I/J" to indicate that they come from the contact zone between these two layers.

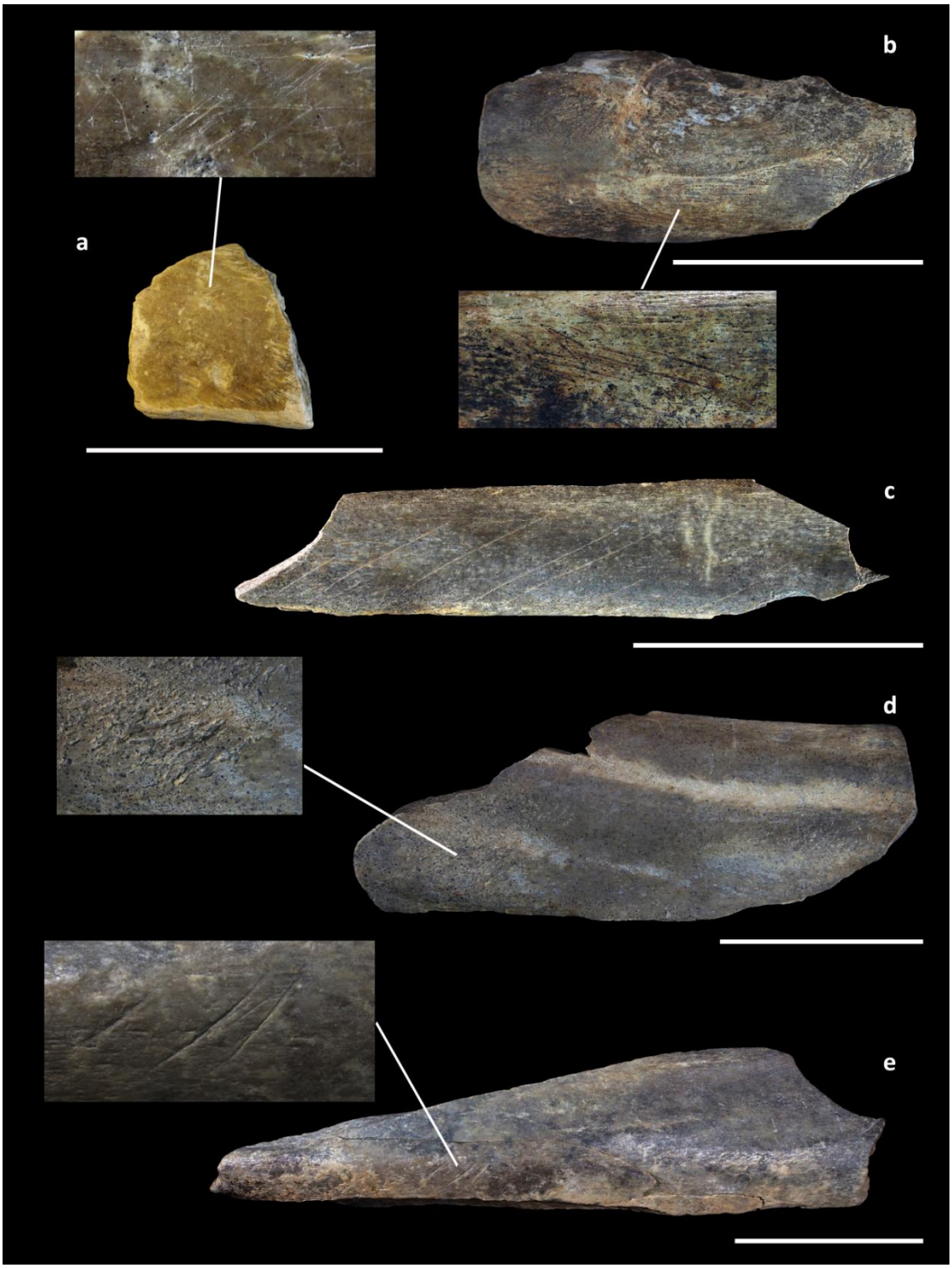

Figure 3. A selection of bone specimens from Bacho Kiro Cave with human bone surface modification that were radiocarbon dated in this study: **a)** *Equidae* bone (R-EVA 2298/CC7-2607) from the lower part of Layer N1-J with cut-marks (ETH-86787: 44,890 ± 450 ^{14}C BP); **b)** *Ursidae* bone (R-EVA 2290/BB8-207) from Layer N1-I with a large impact fracture scar, scrape marks and marks consistent with use as a retoucher (ETH-86783: 40,340 ± 280 ^{14}C BP); **c)** *Bos/Bison* rib (R-EVA 2352/F5-182) from the contact zone between Layers I and J in the Main sector with parallel cut-marks (ETH-86813: 40,160 ± 270 ^{14}C BP); **d)** *Bos/Bison* long bone (R-EVA 2333/F5-107) excavated from Layer I used as a retoucher (ETH-86808: 41,350 ± 310 ^{14}C BP); **e)** *Bos/Bison* long bone (R-EVA 2311/CC7-2750) from layer N1-K with cut-marks (ETH-86793: >51,000 ^{14}C BP). Scale bar is 5 cm.

Bone pretreatment

The bones were pre-treated in the Department of Human Evolution at the MPI-EVA, following the collagen extraction plus ultrafiltration protocol described in Fewlass et al[19] (see Supplementary Text 2 for further details). To preserve as much material as possible for aDNA and palaeoproteomic analysis, small aliquots of the hominin bones were sampled (80-110 mg) for direct ^{14}C dating. The quality of all the collagen extracts was assessed based on collagen yield, elemental (C%, N%, C:N) and stable isotopic values ($\delta^{13}C$, $\delta^{15}N$)[20]. All collagen extracts were analysed with Fourier transformed infra-red (FTIR) spectroscopy prior to dating to look for evidence of incomplete demineralisation, degraded collagen or the presence of any exogenous material in the extracts[21-23].

AMS measurement

Collagen extracts from 6 human bones and 89 animal bones were selected for radiocarbon dating based on stratigraphic position, signs of human modification and the level of collagen preservation. Collagen extracts were graphitised using the AGE III[24] and dated using the latest model of the MICADAS[25] in the Laboratory of Ion Beam Physics at ETH Zurich, Switzerland (lab code: ETH). Oxalic Acid II standards and collagen backgrounds extracted alongside the samples were measured in the same magazine and used in the age calculation. Data reduction was performed using BATS software[26]. An additional 1‰ was added to the error calculation of the samples, as per standard practice.

Several collagen samples were split and dated in a second AMS lab to cross check the measurements. Eleven collagen samples plus collagen extraction backgrounds were weighed into cleaned tin cups and sent to the Klaus-Tschira-AMS facility in Mannheim, Germany (lab code: MAMS), where they were catalytically converted to graphite and dated with the MICADAS-AMS[27]. Here, data reduction was also carried out using BATS software[26], and errors were calculated from the blanks and standards measured in the same magazine. An additional 1‰ was included in the final error calculation, as per the standard practice at MAMS. In addition to graphitisation, small aliquots of collagen (<100 μg C) from hominin bones F6-597 and BK-1653 were measured using the gas ion source of the Aix-MICADAS[17-19].

Data Analysis and modelling

Bayesian chronological analysis and calibration was performed against the IntCal13 dataset[28] using OxCal 4.3[29]. The dates were ordered by ^{14}C age, as the variable thickness of the deposits meant ordering by absolute depth was not appropriate. The R_Combine function in OxCal 4.3[29] was used to combine multiple dates from these same collagen extracts. As part of this function, a chi-squared (χ^2) test is performed to see if the dates are in statistical agreement[30].

ZooMS collagen fingerprinting

All bone specimens (n=147) in the radiocarbon study were also analyzed using MALDI-TOF-MS collagen peptide mass fingerprinting[16,31] in order to provide accurate species identifications for each specimen (see Supplementary Text 3 for details).

Results

We successfully extracted collagen from 139 of the 147 pretreated bones. Supplementary Table 2 includes information on all samples in the study. The average % collagen yield across all layers was 8.3% with several bones in the lowest layers yielding up to 15% collagen (Supplementary Fig. 6), which is much greater than the minimum level of 1% collagen preservation generally accepted for radiocarbon dating[20] and exceptional for a site of this age range. Isotopic and elemental analysis showed that all collagen extracts are within the range of well-preserved collagen, suitable for ^{14}C dating[20]. Although the C:N values of all extracts (range: 3.0 – 3.4) were within the range of well-preserved collagen, 4 extracts had C% and N% values slightly above the normal range (marked in red in Supplementary Table 2), potentially indicating the presence of exogenous material. Only one of these was selected for dating and the age was identical to other bones in close proximity with acceptable C% and N% values. The FTIR spectra of all extracts were characteristic of pure collagen, with no evidence of exogenous material.

It has previously been suggested that the level of deamidation measured in ZooMS analysis could be an efficient pre-screening tool to identify bones with well-preserved collagen for ^{14}C dating[32]. The large dataset in this study allowed us to robustly compare deamidation rates of two collagen peptides (P1106 and P1705) with collagen yields following extraction for ^{14}C dating. No correlation was observed between deamidation rates of peptides P1106 and P1705 and collagen yields, indicating that deamidation rates would be an unsuitable method of pre-screening for ^{14}C sampling (Supplementary Text 4; Supplementary Fig. 7).

In total, we dated 95 bones, including 6 hominin bones (Supplementary Table 2). 63% of the dates obtained from animal bones are from specimens that were anthropogenically modified (Supplementary Text 5 for faunal composition of the dataset). Due to the high ion currents, high rate of transmission, and the low and stable instrument background (53,000 ^{14}C BP) of the latest model of the MICADAS at ETH-Zurich, we were able to reach exceptional levels of precision. Nine of the bones dated beyond the radiocarbon range (>51,000 BP). All of these come from the bottom of the stratigraphic sequence in the Niche 1 area, from Layer N1-K, the Layer N1-J/K contact, and the lower part of Layer N1-J. The finite dates span 48,750 - 34,190 cal BP (modelled range, 95.4% probability; Supplementary Tables 2-4).

Eleven of the faunal collagen samples were dated in a second AMS lab (MAMS). The radiocarbon dates from the two labs are in statistical agreement for 8 of the 11 samples (from Layers C, E, F and N1-I). However, combining dates from the two labs failed for 3 samples (R-EVA 1735, R-EVA 1737 and R-EVA 1739) from layer N1-I, all dating to >40,000 BP. The reasons for this are not understood, and so the dates were excluded from further analysis.

Figure 4 shows a comparison of the dates from graphite targets (*ca.* 2.5 mg collagen) and the gas ion source (<0.3 mg collagen) of the MICADAS system obtained for hominin bones F6-597 and BK-1653. The level of precision achieved was excellent for both methods, despite a ten-fold reduction in sample size using the gas ion source, and the dates from the different methods are in statistical agreement (Supplementary Table 5).

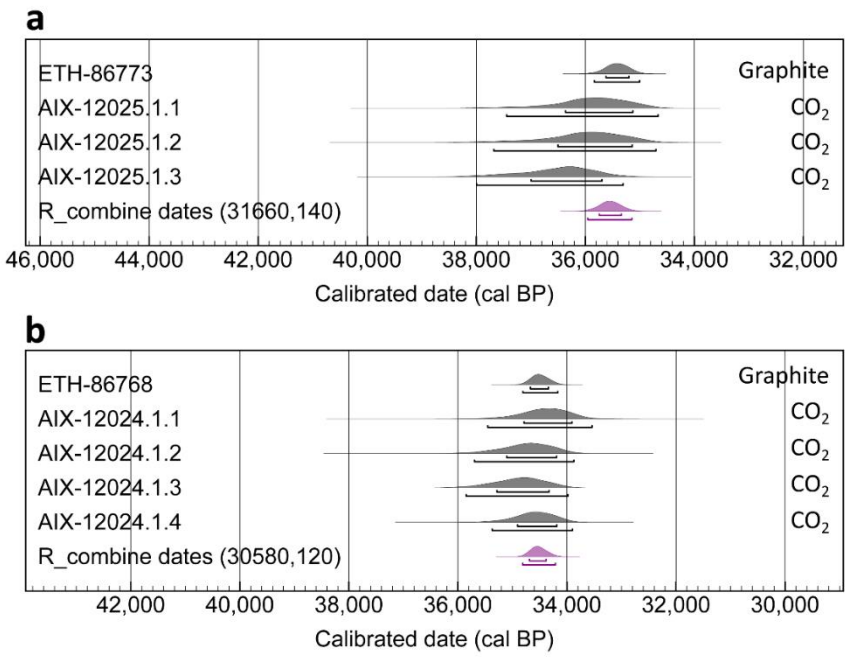

Figure 4. Radiocarbon dates of collagen extracted from two hominin bones identified through ZooMS screening: **a)** F6-597 comes from the new excavations and **b)** BK-1653 comes from the 1970s collection that is stored in the National Museum of Natural History in Sofia. The purple range shows the weighted mean age and error of all the dates measured from graphite targets and directly from CO_2 gas, calculated using the R_Combine function in OxCal 4.3[29].

Some of the dates were excluded from the Bayesian chronological analysis: 9 dating beyond 51,000 BP; 4 from the upper N1-3 layers; 10 from the Layer I/J contact zone; 3 from Layer N1-I which failed the χ^2 test; and 1 (ETH-71326) which was identified post-excavation as originating from next to the 1970s backfill (see Supplementary Table 2). Outlier analysis was performed for the rest of the dataset (n=68) so that outliers could be manually eliminated[33]. Each layer was assigned a phase, and we used a general outlier model with prior probabilities set to 0.05[33] to consider the dates under three scenarios. Dates from the Main Sector (model 1) and Niche 1 (model 2) were first considered separately. As Layers I and J have been archaeologically and geologically correlated between the two areas, the dates were then combined in a third model (model 3). The likelihood of individual dates being outliers was considered based on their depositional histories, outlier posterior probabilities and agreement index (<60% indicates the date could be incompatible with the model) in the three models (Supplementary Table 3). In most cases, the agreement index and outlier analysis identified the same samples as problematic. Based on this information, 14 of 68 dates (shown in red in Supplementary Table 3 and discussed in Supplementary Text 6) were excluded from the models, which were then run again without outlier analysis[33] (Supplementary Table 4).

The agreement index was 83.7 for model 1 (Main Sector dates), 78.9 for model 2 (Niche 1 dates) and 33.2 for model 3 (combined areas) (Supplementary Table 4). The high agreement index for the two separate areas indicates that the dates included are in keeping with their stratigraphic positions. The lower

agreement index of the model combining dates from the two areas can be explained by the different depositional history of Layer J in the two areas and the much larger number of dates from Layer I in the Niche 1 (n=21) compared to the Main Sector (n=4). Although the agreement index is lower, the boundaries given in model 3 (combined model) consider the full range of dates in the two areas and are therefore considered the most accurate representation of the site's chronology. The combined model gives a posterior density estimate of 45,370 – 43,830 cal BP (95.4% probability) for the range of the IUP in Layer I. As the model constrains the age range of the layers based on the prior information, the un-modelled ranges of the peripheral dates from the hominin bones CC7-335 (46,790 - 44,830 cal BP at 95.4% probability) and AA7-738 (44,210 – 42,810 cal BP at 95.4% probability) extend beyond the modelled posterior boundaries of Layer I. The Bayesian model combining dates from across the site is shown in Figure 5 (see Supplementary Text 7 for OxCal code).

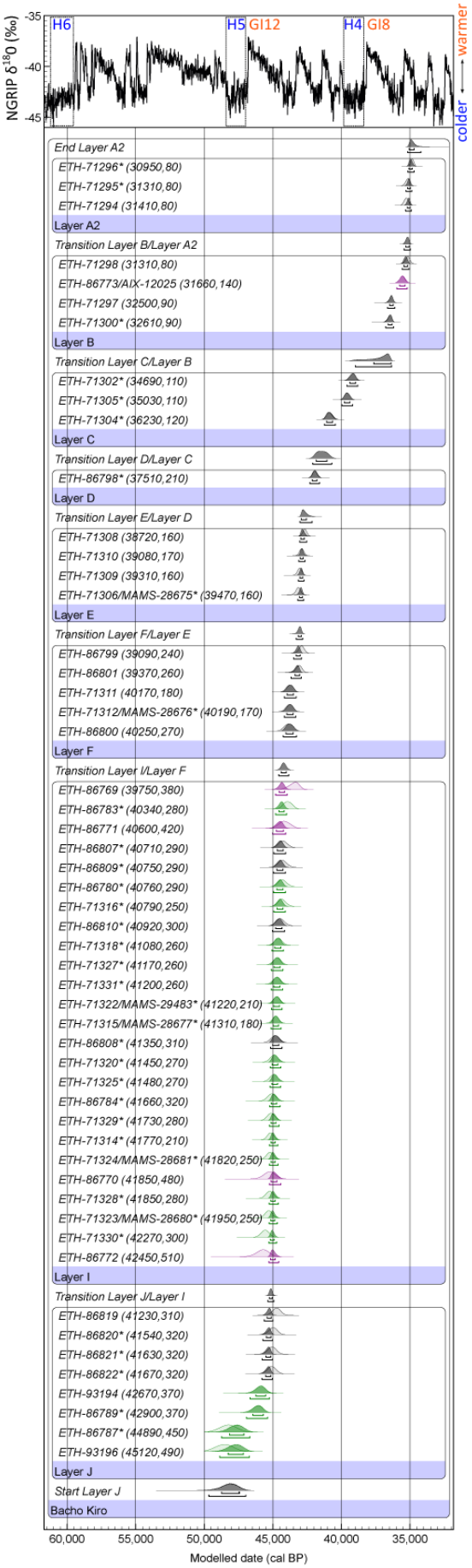

Figure 5. Bayesian chronological model (model 3; Supplementary Table 4) for Bacho Kiro Cave on material excavated during the 2015-2017 field seasons from the Main Sector and Niche 1 compared to the North Greenland Ice Core Project (NGRIP) Greenland Ice Core Chronology 2005 (GICC05) $\delta^{18}O$ palaeo-environmental record[34] with Greenland Interstadials (GI) 12 and 8 and Heinrich Events (H) 6, 5 and 4 indicated. The lab numbers are shown on the left side along with the measured ^{14}C age (BP) and associated 1σ error (years). Where more than one measurement was made from the same collagen extract, dates were combined (R_Combine) in OxCal 4.3. The dates were calibrated against the IntCal13 dataset[28], and the modelling was performed in OxCal 4.3[29]. **The distributions of dates from the Niche 1 are shown in green and from the Main Sector in black. The dates from the hominin bones from Layer N1-I and Layer B are shown in purple.** The radiocarbon likelihoods of calibrated dates (without modelling) are shown in the lighter shade and the posterior distributions (after modelling) are darkly shaded. Brackets show the 68.2% and 95.4% probability ranges of the calibrated dates. Dates marked with an asterisk (*) are from bones bearing signs of anthropogenic modification. Note that 2 dates from the bottom of Layer N1-J date to >51,000 BP (beyond model range). Further information is included in Supplementary Tables 2-4.

Discussion

Over the past two decades, the addition of an ultrafiltration step following collagen extraction has shown to be important for removing carbon contamination from Palaeolithic bones[14]. The new Bacho Kiro Cave results indicate that several of the 1980s and 1990s dates (Table 1) were affected by carbon contamination, making them appear younger than their actual ages. Our dates resolve the issues of the wide age range previously obtained for Layer I and the young age estimation obtained in Layer J (Table 1).

At the base of the sequence, resting on bedrock, Layer N1-K contains a small (n=82) Middle Palaeolithic assemblage. All 5 dates from this layer are from *Cervid/Saiga* or *Bos/Bison* (including one with cut-marks) and are older than 51,000 BP. Overlying Layer N1-K, there are three age clusters represented in Layer N1-J, which accumulated relatively slowly (Supplementary Fig. 5). First, an anthropogenically modified *Ursidae* bone (ETH-86788) and a *Cervid/Saiga* bone (ETH-93195) from the very bottom of Layer N1-J are also older than 51,000 BP. Second, a minimum of 5,000 ^{14}C years separates these 2 dates from the next occupation represented by a cut-marked horse bone (ETH-86787), also excavated from the lower part of Layer N1-J, indicating that hominins were present sometime between 48,730 – 46,670 cal BP (modelled age, 94.5% probability), which coincides with the cold period of Heinrich event 5 (Fig. 5). A small number of lithics were recovered from the lower part of Layer N1-J. Some (n=6) are consistent with the overlying IUP and some (n=8) are consistent with the underlying Middle Palaeolithic, which is in agreement with the findings of the 1970s excavations[2]. From a radiocarbon perspective, it is impossible to know whether the lower part of Layer N1-J relates more to the overlying IUP or more to the underlying Middle Palaeolithic. However, the high resolution of the radiocarbon data presented here suggests temporally distinct occupations in this lower part, which makes an in-situ transition between Middle Palaeolithic and IUP less likely. The last occupation phase —in the upper part of Layer N1-J — spans from 46,930 – 44,990 cal BP (modelled range, 95.4% probability) and is associated with a low density of IUP artefacts which share the techno-typological characteristics of those in the overlying Layer N1-I. The appearance of the IUP in Layer N1-J coincides with the onset of climatic warming in the Northern Hemisphere marked by the beginning of Greenland Interstadial 12 (GI12) at 46,950 ± 1000 BP in the GICC05 NGRIP ice core[34] (Fig. 5) and beginning at ~47,600 BP in the Hulu Cave speleothem δ^{18}O records in China[35]. In closer proximity to Bacho Kiro Cave, the mild climatic conditions of GI12 are reproduced in a speleothem δ^{13}C record from Ascunsa Cave (AC) in the South Carpathians in East-Central Europe (~400 km NW of Bacho Kiro Cave) and various palaeoclimatic records from the Black Sea[36,37] and northern Greece[38]. The age ranges from the upper part of Layer N1-J and from Layer N1-I, together with high artefact densities, imply relatively continuous human use of the cave during this interval. The dates from Layer J in the Main Sector are at the younger end of the Layer N1-J range, which supports the geoarchaeological interpretation that only the upper part of this layer is preserved in the Main Sector (where it overlies bedrock and abuts against it towards the south; Supplementary Text 1).

The evidence for the age range of Layer I/N1-I is extremely robust. Twenty-five dates on hominin remains and anthropogenically modified bones set the modelled age range for the IUP from these correlated layers from 45,370 to 43,830 cal BP (95.4% probability). The radiocarbon dates from the 4 hominin bones span the full range of dates coming from anthropogenically modified bones. We chose to focus more on the dating of Layer N1-I in the Niche 1 where this layer is more extensively exposed and more clearly

delineated in the stratigraphic sequence. Nevertheless, the 4 dates from Layer I in the Main Sector fall entirely within the range of Layer N1-I, supporting the archaeological and geological link made between these two areas. The dates from the contact zone I/J in the Main Sector fall within the range of Layer I and the upper part of Layer J.

Site formation processes and the low number of artefacts in the layers above Layer I make it difficult to determine when the IUP ended at Bacho Kiro Cave. Layers N1-H, N1-G and G are thick water laid deposits with a low density of artefacts at the base (Layers N1-H and G). These were likely re-deposited from Layer N1-I/I by a stream originating from the cave's inner karst system. These layers essentially seal the underlying Layers N1-K, N1-J/J and N1-I/I[4]. Layers F and E are thick with very low densities of bones and no lithic artefacts. The tight age range from these layers overlap with the youngest age range of Layer I and suggest a rapid rate of sedimentation for Layers G through E. Although no lithics were excavated from Layers F-D during the new excavations, the low density of artefacts recovered during the 1970s excavation indicate that the IUP characteristics continue from Layer J to Layer D[4] (Supplementary Table 1). In the new collection, a relative increase in artefact density occurs in Layer C (42,100 – 36,340 cal BP), Layer B (39,000 – 34,970 cal BP) and Layer A2 (35,440 – 34,190 cal BP). The lithic artefacts within these layers are not characteristic of the IUP but rather of various phases of the subsequent Upper Palaeolithic (specifically bladelet production, platforms consistent with the appearance of soft hammer percussion in Layer C, and backed bladelets similar to Gravettian types in Layer A1; Supplementary Table 1). In the Main Sector, the Upper Palaeolithic occupation extends to 34,190 cal BP (modelled range) in Layer A2. In Layer A1, the date of 27,610 – 27,250 cal BP (95%) on a cut-marked *Bos/Bison* bone is consistent with the Gravettian backed bladelets and can be considered the youngest preserved layer. The Dansgaard-Oeschger climatic cycles in the Northern Hemisphere between the end of GI12 and the end of GI8 (~44,000-36,000 BP; Fig. 5) may be a cause of the demographic turnover seen in archaeological and genetic studies during this interval in Europe[39,40], which is indicated at Bacho Kiro Cave by the change in technology seen between the IUP in Layers J and I and the UP forms in Layers C and above.

The Niche 1 has a shorter Upper Palaeolithic sequence than the Main Sector and the same differences in artefact densities. Nevertheless, we attempted to date the layers above Layer N1-I in part to help correlate its stratigraphy to that of the Main Sector. Unlike the rest of the deposits in this area, collagen preservation was very poor in these layers, and only 4 of the 11 bones had sufficient collagen yields. At least 1 of the resulting dates (R-EVA 2271 or R-EVA 2273) is inconsistent with its stratigraphic position (Supplementary Table 2), and it was not possible to make any connections between the upper layers of the Niche 1 and the Main Sector based on the radiocarbon evidence.

The dates from the hominin bone F6-597 (35,960 – 35,150 cal BP, 95.4% probability) from Layer B agree with the range of dates from the fauna in this layer. The hominin bone BK-1653 identified using ZooMS from the 1970s collection was labelled Layer "6a/7", which corresponds to the contact of Layers B and C in the new excavation. This bone was excluded from the Bayesian modelling because of uncertainties of its exact stratigraphic context, but its age (34,810 – 34,210 cal BP, 95.4% probability) fits with the dates on fauna from Layer A2. Both hominin bones from the Upper Palaeolithic levels of the site (BK-1653 and F6-597) were dated using the gas ion source and graphite methods to cross check the obtained ages (Fig. 5). The high level of agreement between the two methods measured in two different laboratories (ETH

and Aix) serves as further evidence of the suitability of the gas ion source of the MICADAS for dating precious and/or small archaeological samples at good levels of precision[18,19].

Conclusion

The chronology presented here for Bacho Kiro Cave constitutes an extensive set of high-quality collagen samples radiocarbon dated at exceptional precision. To the best of our knowledge, this study represents one of the largest ^{14}C datasets from a single Palaeolithic site processed by one team. This large effort was made to resolve the questions left open by the previous dates from this eponym site. The integrity of the stratigraphic sequence is clearly indicated by the dates. The extensive dataset allows us to securely place the IUP from correlated Layers I and N1-I in the interval from 45,370 to 43,830 cal BP (95.4% probability). The start date for the IUP at Bacho Kiro Cave falls during the accumulation of Layer N1-J, likely from 46,930 cal BP (95.4% probability) at the onset of GI12, but perhaps earlier (Fig. 5).

As the precision of AMS measurements increases, the chronological resolution we can achieve is ultimately limited by the imprecision of the calibration curve in this time range. The output of the Bayesian modelling presented here may well change as the resolution of the calibration curve improves[35,41,42]. On-going work in this area is crucial for enhancing our understanding of the timing of major events in hominin adaptations and demographic processes during this time period.

Data Availability

All data is available in the manuscript and supplementary materials.

Code Availability

OxCal script is included in the supplementary information.

References

1 Garrod, D., Howe, B. & Gaul, J. Excavations in the cave of Bacho Kiro, north-east Bulgaria. *Bulletin of the American School of Prehistoric research* **15**, 46-76 (1939).

2 Kozłowski, J. K. *Excavation in the Bacho Kiro Cave (Bulgaria): Final Report*. (Państwowe Wydawnictwo Naukowe, 1982).

3 Tsanova, T. *Les Débuts du Paléolithique Supérieur dans l'Est des Balkans. Réflexion à Partir de l'Étude Taphonomique et Techno-Économique des En-sembles Lithiques de Bacho Kiro (Couche 11), Temnata (Couches VI et 4) et Kozarnika (Niveau VII)* Vol. 1752 (BAR International Series, 2008).

4 Hublin, J.-J. *et al.* Initial Upper Palaeolithic *Homo sapiens* remains from Bacho Kiro Cave (Bulgaria) *Nature* (In review).

5 Kuhn, S. L. & Zwyns, N. Rethinking the Initial Upper Paleolithic. *Quaternary International* **347**, 29-38, doi:10.1016/j.quaint.2014.05.040 (2014).

6 Hublin, J.-J. The modern human colonization of western Eurasia: when and where? *Quaternary Science Reviews* **118**, 194-210, doi:10.1016/j.quascirev.2014.08.011 (2015).

7 Sirakov, N. *et al.* Reopened Bacho Kiro - new data on Middle/Upper Palaeolithic transition and Early-Middle stages of Upper Palaeolithic. (Bulgarian Academy of Sciences, Sofia, 2017).

8 Hedges, R. E. M., Housley, R. A., Bronk Ramsey, C. & van Klinken, G. J. Radiocarbon dates from the Oxford AMS system: Archaeometry datelist 18. *Archaeometry* **36**, 337-374, doi:10.1111/j.1475-4754.1994.tb00975.x (1994).

9 Bird, M. *et al.* Radiocarbon dating of "old" charcoal using a wet oxidation, stepped-combustion procedure. *Radiocarbon* **41**, 127-140 (1999).

10 Wood, R. E. *et al.* Testing the ABOx-SC method: dating known-age charcoals associated with the Campanian Ignimbrite. *Quaternary Geochronology* **9**, 16-26, doi:10.1016/j.quageo.2012.02.003 (2012).

11 Brown, T. A., Nelson, D. E., Vogel, J. S. & Southon, J. R. Improved collagen extraction by modified Longin method. *Radiocarbon* **30**, 171-177 (1988).

12 Bronk Ramsey, C., Higham, T., Bowles, A. & Hedges, R. Improvements to the pretreatment of bone at Oxford. *Radiocarbon* **46**, 155-164 (2004).

13 Talamo, S. & Richards, M. A comparison of bone pretreatment methods for AMS dating of samples >30,000 BP. *Radiocarbon* **53**, 443-449 (2011).

14 Higham, T. European Middle and Upper Palaeolithic radiocarbon dates are often older than they look: problems with previous dates and some remedies. *Antiquity* **85**, 235-249 (2011).

15 Evin, J., Marien, G. & Pachiaudi, C. Lyon natural radiocarbon measurements VII. *Radiocarbon* **20**, 19-57 (1978).

16 Buckley, M., Collins, M., Thomas-Oates, J. & Wilson, J. C. Species identification by analysis of bone collagen using matrix-assisted laser desorption/ionisation time-of-flight mass spectrometry. *Rapid Communications in Mass Spectrometry* **23**, 3843-3854, doi:10.1002/rcm.4316 (2009).

17 Bard, E. *et al.* AixMICADAS, the accelerator mass spectrometer dedicated to ^{14}C recently installed in Aix-en-Provence, France. *Nuclear Instruments and Methods in Physics Research Section B: Beam Interactions with Materials and Atoms* **361**, 80-86, doi:10.1016/j.nimb.2015.01.075 (2015).

18 Fewlass, H. *et al.* Size matters: radiocarbon dates of <200 μg ancient collagen samples with AixMICADAS and its gas ion source. *Radiocarbon* **60**, 425-439, doi:10.1017/rdc.2017.98 (2017).

19 Fewlass, H. *et al.* Pretreatment and gaseous radiocarbon dating of 40–100 mg archaeological bone. *Scientific Reports* **9**, 5342, doi:10.1038/s41598-019-41557-8 (2019).

20 van Klinken, G. J. Bone collagen quality indicators for palaeodietary and radiocarbon measurements. *Journal of Archaeological Science* **26**, 687–695 (1999).

21 DeNiro, M. J. & Weiner, S. Chemical, enzymatic and spectroscopic characterization of “collagen” and other organic fractions from prehistoric bones. *Geochimica et Cosmochimica Acta* **52**, 2197-2206, doi:10.1016/0016-7037(88)90122-6 (1988).
22 Yizhaq, M. *et al.* Quality controlled radiocarbon dating of bones and charcoal from the early pre-pottery Neolithic B (PPNB) of Motza (Israel). *Radiocarbon* **47**, 193-206, doi:10.1017/S003382220001969X (2005).
23 D'Elia, M. *et al.* Evaluation of possible contamination sources in the ^{14}C analysis of bone samples by FTIR spectroscopy. *Radiocarbon* **49**, 201-210 (2007).
24 Wacker, L., Němec, M. & Bourquin, J. A revolutionary graphitisation system: fully automated, compact and simple. *Nuclear Instruments and Methods in Physics Research Section B: Beam Interactions with Materials and Atoms* **268**, 931-934, doi:10.1016/j.nimb.2009.10.067 (2010).
25 Wacker, L. *et al.* MICADAS: routine and high-precision radiocarbon dating. *Radiocarbon* **52**, 252–262 (2010).
26 Wacker, L., Christl, M. & Synal, H.-A. Bats: a new tool for AMS data reduction. *Nuclear Instruments and Methods in Physics Research Section B: Beam Interactions with Materials and Atoms* **268**, 976-979, doi:10.1016/j.nimb.2009.10.078 (2010).
27 Kromer, B., Lindauer, S., Synal, H.-A. & Wacker, L. MAMS - A new AMS facility at the Curt-Engelhorn-Centre for Achaeometry, Mannheim, Germany. *Nuclear Instruments and Methods in Physics Research Section B: Beam Interactions with Materials and Atoms* **294**, 11-13, doi:10.1016/j.nimb.2012.01.015 (2013).
28 Reimer, P. J. *et al.* IntCal13 and Marine13 radiocarbon age calibration curves 0–50,000 years cal BP. *Radiocarbon* **55**, 1869–1887 (2013).
29 Bronk Ramsey, C. Bayesian analysis of radiocarbon dates. *Radiocarbon* **51**, 337-360 (2009).
30 Ward, G. K. & Wilson, S. R. Procedures for comparing and combining radiocarbon age determinations: a critique. *Archaeometry* **20**, 19-31, doi:10.1111/j.1475-4754.1978.tb00208.x (1978).
31 Welker, F. *et al.* Palaeoproteomic evidence identifies archaic hominins associated with the Châtelperronian at the Grotte du Renne. *Proceedings of the National Academy of Sciences* **113**, 11162 (2016).
32 Wilson, J., van Doorn, N. L. & Collins, M. J. Assessing the extent of bone degradation using glutamine deamidation in collagen. *Analytical Chemistry* **84**, 9041-9048, doi:10.1021/ac301333t (2012).
33 Bronk Ramsey, C. Dealing with outliers and offsets in radiocarbon dating. *Radiocarbon* **51**, 1023-1045 (2009).
34 Svensson, A. *et al.* A 60 000 year Greenland stratigraphic ice core chronology. *Climate of the Past* **4**, 47-57 (2008).
35 Cheng, H. *et al.* Atmospheric $^{14}C/^{12}C$ changes during the last glacial period from Hulu Cave. *Science* **362**, 1293-1297, doi:10.1126/science.aau0747 (2018).
36 Nowaczyk, N. R., Arz, H. W., Frank, U., Kind, J. & Plessen, B. Dynamics of the Laschamp geomagnetic excursion from Black Sea sediments. *Earth and Planetary Science Letters* **351-352**, 54-69, doi:10.1016/j.epsl.2012.06.050 (2012).
37 Wegwerth, A. *et al.* Black Sea temperature response to glacial millennial-scale climate variability. *Geophysical Research Letters* **42**, 8147-8154, doi:10.1002/2015gl065499 (2015).
38 Müller, U. C. *et al.* The role of climate in the spread of modern humans into Europe. *Quaternary Science Reviews* **30**, 273-279, doi:10.1016/j.quascirev.2010.11.016 (2011).
39 Fu, Q. *et al.* The genetic history of Ice Age Europe. *Nature* **534**, 200-205, doi:10.1038/nature17993 (2016).

40 Staubwasser, M. *et al.* Impact of climate change on the transition of Neanderthals to modern humans in Europe. *Proceedings of the National Academy of Sciences* **115**, 9116-9121, doi:10.1073/pnas.1808647115 (2018).
41 Talamo, S. *et al.* RESOLUTION: Radiocarbon, tree rings, and solar variability provide the accurate time scale for human evolution, presented at: *7th Annual Meeting of the European Society for the Study of Human Evolution.* Abstract in: PESHE, Vol. 6, 194 (Leiden, The Netherlands, 2017).
42 Reimer, P. J. *et al.* A preview of the IntCal19 radiocarbon calibration curves, presented at: *23rd International Radiocarbon conference* (Trondheim, Norway, 2018).

Acknowledgements

The re-excavation of Bacho Kiro Cave is a joint project between the National Institute of Archaeology and Museum, Bulgarian Academy of Sciences, Sofia and the Human Evolution department of the Max Planck Institute for Evolutionary Anthropology, Leipzig. This work was funded by the Max Planck Society. Graphitisation and AMS dating in Switzerland were funded by ETH Zurich. The AixMICADAS and its operation are funded by the Collège de France and the EQUIPEX ASTER-CEREGE (PI E.B.). The authors acknowledge the vital contribution of all the excavators who have worked at Bacho Kiro Cave since 2015.

Author contributions

The study was devised by J.-J.H, S.T., S.M., Ts.Ts, N.S. and H.F. Archaeological excavation was undertaken by Ts.Ts., N.S., Z.R. and S.M., who all contributed contextual information. The excavation lab and collection was organised by V.S.-M. Lithic analysis was performed by Ts.Ts., N.S., S.S. and S.M. Zooarchaeological analysis was performed by G.S. and R.S. N.M. classified the bone tools in the sample set. Micromorphological analysis was carried out by V.A. ZooMS was carried out by F.W., L.P. and V.S.-M. Sample pretreatment and EA-IRMS analyses were carried out by H.F. FTIR analyses were carried out by H.F. and R.M. Graphitisation and AMS dating at ETH Zurich was carried out by L.W., B.K. and H.F. Dating with the AixMICADAS was carried out by E.B., Y.F. and Th.T. Bayesian modelling was carried out by H.F. and S.T. H.F. wrote the paper with input from all authors.

Competing Interests

The authors declare no competing interests.

Supplementary Information

New ^{14}C chronology for Middle–to–Upper Palaeolithic transition at Bacho Kiro Cave, Bulgaria

Supplementary Text

1. Stratigraphy and site formation
2. Collagen extraction and quality control methods
3. ZooMS collagen fingerprinting methods
4. Comparison of degradation measured through collagen extraction for radiocarbon dating and ZooMS analysis
5. Faunal composition of the ^{14}C dataset
6. Outlier analysis of dates
7. OxCal v4.3 code for Bayesian model of Bacho Kiro Cave chronology (Fig.5)

Supplementary Figures

1. Photo of excavated areas of Bacho Kiro Cave
2. Stratigraphic profile in the Main Sector showing the location of all the bones dated in the study
3. Stratigraphic profile in the Main Sector showing all the finds separated by layer
4. Stratigraphic profile in the Niche 1 showing the location of all the bones dated in the study
5. Stratigraphic profile in the Niche 1 showing all the finds separated by layer
6. Collagen yields of pretreated bones
7. Relationship between collagen preservation (^{14}C data) and glutamine deamidation (ZooMS data)

Supplementary Tables

1. Cultural identification of the stone assemblages from each layer of Bacho Kiro Cave
2. Sample information of all bones from Bacho Kiro Cave (accompanying table)
3. Comparison of outlier analysis and agreement index of models (accompanying table)
4. Comparison of model output for Bacho Kiro Cave chronology (accompanying table)
5. Radiocarbon dates of two Upper Palaeolithic human bone fragments (BK-1653 and F6-597)

Supplementary Information

New ^{14}C chronology for Middle–to–Upper Palaeolithic transition at Bacho Kiro Cave, Bulgaria

Fewlass, H.[1]*, Talamo, S.[1,2], Wacker, L.[3], Kromer, B.[1,4], Tuna, T.[5], Fagault, Y.[5], Bard, E.[5], McPherron, S. P.[1], Aldeias, V.[6,1], Maria, R.[1], Martisius, N. L.[7], Paskulin, L.[8], Rezek, Z.[1, 9], Sinet-Mathiot, V.[1], Sirakova, S.[10], Smith, G.M[1], Spasov, R.[11], Welker, F.[12,1], Tsanova, T.[1], Sirakov, N.[10], Hublin, J.-J.[1]

1) Department of Human Evolution, Max Planck Institute for Evolutionary Anthropology, Leipzig, Germany
2) Department of Chemistry "G. Ciamician", University of Bologna, Bologna, Italy
3) Ion Beam Physics, ETH-Zurich, Zürich, Switzerland
4) Institute of Environmental Physics, University of Heidelberg, Heidelberg, Germany
5) CEREGE, Aix-Marseille University, CNRS, IRD, INRA, Collège de France, Aix-en-Provence, France
6) ICArEHB, University of Algarve, Campus de Gambelas, Faro, Portugal
7) Department of Anthropology, University of California, Davis, USA
8) Department of Archaeology, University of Aberdeen, Aberdeen, Scotland
9) University of Pennsylvania Museum of Archaeology and Anthropology, Philadelphia, PA, USA
10) National Institute of Archaeology and Museum, Bulgarian Academy of Sciences, Sofia, Bulgaria
11) Archaeology Department, New Bulgarian University, Sofia, Bulgaria
12) Evolutionary Genomics Section, Globe Institute, University of Copenhagen, Copenhagen, Denmark.

* **Corresponding author:** helen_fewlass@eva.mpg.de

Supplementary Text

1. Stratigraphy and site formation

Bacho Kiro Cave is formed on Cretaceous sandy limestones and sandstones and is a deep and labyrinthine karst system extending for more than 3 km[1], with evidence of human occupation near the cave's entrance. The current entrance is ~4 m wide and connects in the SW to the inner karst system. The bottom Pleistocene deposits (Layer K, J, and I) consist of sand, silt and clay originating from siliciclastic accumulations present inside the karst system and interstratified with common angular limestone debris (gravel-size and larger) resulting from local spalling of the cave's roof and walls. The cave's floor morphology dips towards the cave's entrance, and hence these lower Pleistocene layers are thicker near the entrance and eventually pinch out towards its interior. Therefore, as one approaches the south part of the cave in the Main Sector, Layer K is absent and Layers J and I eventually disappear, with only the upper (more recent) part of Layer J being present along grid rows F-G and eventually also abutting against bedrock (Fig. 1c). Layers K, J and I are, thus, better represented in the Niche 1 area (Fig. 1d). Here, Layer N1-K rests directly on bedrock and is loamy sands showing some lateral variability in terms of the frequency of limestone clasts (normally in the 3-8 cm range and rarer large clasts up to 15 cm at the top of the layer N1-K), and varies from reddish brown in the SE to lighter brown towards the NW. It contains rare domains (diameter of max 10 cm) of darker sediments with small (<1 cm width) charcoal fragments. These seem to be remnants of poorly preserved combustion features. Towards its top, there is a marked increase in weathered limestones, which may point to some weathering of the surface of N1-K deposits. Layer N1-J is a greenish brown loamy clay, ~20 cm thick and pinching out against the bedrock towards the south. It has frequent limestone clasts, typically around 5 cm in diameter, but also a few larger angular limestone clasts up to 20 cm wide, attesting to local contribution of roof fall, with a relative increase of small limestone clasts and granules towards its top. The contact with the above Layer N1-I is sharp and clear in Niche 1 where Layer N1-I is a particularly distinctive dark brown sticky loamy clay that thins out towards the cave walls (5-8 cm thick in the eastern profile of Niche 1). In the Main Sector, Layer I is thinner and consists of dark brown sandy clays with common limestone rubbles (typically in the 4-10 cm range and occasional dm-sized blocks). In both the field and in thin section, there are abundant charcoals and bones (some burned), including evidence of trampling (in-situ broken bones). These characteristics point to a relative depositional stasis with an increase of anthropogenic inputs, including abundant accumulation of combustion and occupational debris. The frequency of archaeological material and the reduced thickness of this layer show that human occupants were basically living on top of debris from previous occupations, pointing to a slower sedimentation rate. Despite some lateral variability and the fact that we are at the spatial limit of the extension of Layer I in the Main Sector, combined stratigraphic, sedimentary and archaeological content make the correlation between Layers N1-I and I clear.

Layers I/N1-I have a sharp, erosive contact with the overlying Layers G and N1-H/G. In the Main Sector this contact is associated with dm-sized limestone blocks. Layers G and N1-H/G are well-laminated silts and sands that mark a shift in the sedimentation mechanisms at the site, with rapid accumulation from runoff by a low-energy stream originating from inside the karst system. Layer N1-H should be seen as a

subdivision of Layer N1-G present only in the Niche 1 sequence. Under thin section, the alternating and bedded nature of silts and fine sands are evident, including clay-rich lenses, small (few µm in size) rounded carnivore coprolites and clay papules. The very rare archaeological artefacts (bone fragments) are in the lowermost contact and are reworked, ripped up material from the surface of Layer I.

Layers F, E and D in the Main Sector and Layers N1-3e, N1-3d and N1-3c in the Niche 1 are sub-horizontal deposits composed of fine silts and clays with some sand, varying from increased clay content (grey lenses) to silty sands (orange lenses) with rare stones in the Niche 1 and few limestones clasts (typically 7-10 cm) in the Main Sector. Sedimentary sources relate mainly to reworking of fine siliciclastic deposits from inside the cave system and point to relatively rapid deposition rates. The top of these deposits is truncated and associated with partial erosion towards the south (in Niche 1) and southeast (in the Main Sector), indicating the presence of a sedimentary outlet and the continuation of the cave's chamber (albeit probably small-sized opening) into the south-southeast. Layers N1-3b and C are thus stratigraphic markers in both excavation areas, showing a change in sedimentary dynamics with preferential accumulation of coarser rubble from local spalling of the cave roof and walls. The above Layers B and A are preserved in the Main Sector and relate to formation processes like those described for Layers F-D. These are fine sediments, with few stones and varying from darker brown lenses intercalated with orange brown silty clays. As with Layers F-D, stratigraphic contacts are often diffuse and show an undulating morphology pointing to plastic alteration of the deposits occurring post-depositionally. Such folding is particularly visible in the convoluted morphology of the rare, discrete charcoal-rich combustion features present in Layers B and A (see Fig. 1c). The uppermost section of Layer A (A0) corresponds to the current surface of the cave floor cut by previous excavations and incorporating recent materials.

2. Collagen extraction and quality control methods

Bone collagen was extracted in the Department of Human Evolution at the MPI-EVA, Leipzig, following the protocol described in Fewlass et al[2]. Briefly, the outer surface of the bone was removed with a sand blaster and samples were removed with a Dremel drill. Bones were demineralised in HCl 0.5M until soft and CO_2 effervescence had stopped. Samples were treated with NaOH 0.1M to remove humic acid contamination and re-acidified in HCl 0.5M. The samples were gelatinised in weakly acidic water (HCl pH3) based on the method described by Longin[3]. Soluble collagen samples were passed through a pre-cleaned Ezee filter (Elkay labs, UK) and pre-cleaned ultrafilter (Sartorius Vivaspin Turbo 15) to concentrate the large molecular weight fraction (>30 kD) for AMS dating[4-6]. Background-level bones (older than 50,000 BP) kindly supplied by D. Döppes (Mannheim, Germany) were extracted alongside the samples in order to assess contamination introduced in the laboratory.

Approximately 0.5 mg collagen from each extract was weighed into a tin cup and measured on a ThermoFinnigan Flash elemental analyser (EA) coupled to a Thermo Delta plus XP isotope ratio mass spectrometer (IRMS) to determine their stable isotopic ($\delta^{13}C$ and $\delta^{15}N$) and elemental values (C%, N%, C:N). Stable carbon isotope ratios were expressed relative to VPDB (Vienna PeeDee Belemnite) and stable nitrogen isotope ratios were measured relative to AIR (atmospheric N_2) using the delta notation (δ) in

parts per thousand (‰). Repeated analysis of internal and international standards indicates an analytical error of 0.2‰ (1σ) for $\delta^{13}C$ and $\delta^{15}N$.

A small aliquot of each collagen sample (*ca*. 300 µg) was homogenized in an agate mortar and pestle, then mixed with ~40 mg of IR grade KBr powder, pressed into a pellet using a manual hydraulic press (Wasserman) and analysed with an Agilent Technologies Cary 660 Fourier transform infra-red (FTIR) spectrometer (Agilent Technologies, Santa Clara) with a deuterated triglycine sulfate (DTGS) detector. Spectra were recorded in transmission mode at 4 cm^{-1} resolution and averaging of 34 scans between 4000 and 400 cm^{-1} using Resolution Pro software (Agilent Technologies, Santa Clara). The obtained spectra were evaluated and compared to library spectra of well-preserved collagen and bone.

3. ZooMS collagen fingerprinting methods

All 147 bone specimens that were pretreated in the radiocarbon study were also analyzed though MALDI-TOF-MS collagen peptide mass fingerprinting (ZooMS)[7,8]. A small bone sample (<20 mg) was taken from each bone or dentine specimen independent of the radiocarbon sample. An ammonium-bicarbonate buffer extraction was performed, including digestion with trypsin (0.5µg/µL, Promega), pH acidification using TFA (10% TFA) and cleaning on C18 ZipTips (Sigma-Aldrich/Thermo Scientific). Digested peptides were analysed on a MALDI-TOF-MS using previously published protocols[9]. MALDI-TOF-MS spectra were compared to a reference database containing collagen peptide marker masses of all medium to larger sized genera in existence in western Eurasia during the Late Pleistocene[9].

4. Comparison of degradation measured through collagen extraction for radiocarbon dating and ZooMS analysis

For each ZooMS spectrum, the extent of deamidation was assessed for two peptides containing a single glutamine (peptides P1105 and P1706)[10-12]. This allows us to assess the existence of any formal relationship between the different measures of collagen/proteome degradation used in either radiocarbon dating or ZooMS. For radiocarbon dating, we took the frequently reported values of the collagen % and C:N ratio as indicators of collagen preservation. For ZooMS, we took the number of observed peptide markers and P1105 and P1706 deamidation as indicators of collagen preservation.

Independently, measures of preservation show tight clustering in areas that, for each measure, are indicative of well-preserved proteins (Supplementary Fig. 7). For example, most ZooMS spectra contain nine observable peptide markers (out of nine possible). We observe no obvious correlations where higher rates of deamidation are linked to samples with more divergent C:N ratios or lower collagen % (Supplementary Fig. 7c, d, e, f). The only suggestion of such a correlation might be for the number of peptide markers, as ZooMS spectra with less than four observable peptide markers also result in collagen percentage below 5% (Supplementary Fig. 7b). In addition, specimens without any peptide markers present also have extremely low, or no, collagen percentages after extraction for radiocarbon dating. This

does not hold for all specimens, as there are also bone specimens with the majority of peptide markers present but that also have low collagen yields (<0.5%). From the Bacho Kiro Cave dataset, we therefore conclude that ZooMS spectral quality and/or glutamine deamidation measures in ZooMS spectra is a poor predictor for the successful extraction of collagen for radiocarbon dating.

5. Faunal composition of the ^{14}C dataset

ZooMS analysis shows that the faunal sample set includes a large amount of *Ursidae*, *Bos/Bison*, *Equidae*, *Cervid/Saiga* and *Capra sp.* and two bones of *Rhinoceratidae* (Supplementary Table 2), fully in agreement with the zooarchaeological interpretation of the whole faunal collection[8]. Signs of human modification are present (63% of the dated bones across all layers) on bones of all represented species, except the 2 *Rhinoceratidae* bones. Whereas 16.5% of the faunal collection from Layer N1-I/I shows signs of human modification, only 1.8% has traces of carnivore modification (tooth marks, signs of gnawing or digestion), indicating that human agency played a large role in the composition of the faunal assemblage in the IUP layers in the cave[8]. Many of the *Ursidae* remains (Cave bear/Brown bear), both in the overall dataset and in the ^{14}C dataset, bear traces of human modification, including perforated teeth and butchery marks indicative of skinning. The evidence suggests close interactions between the humans occupying the cave and bears, with humans either scavenging dead animals for furs, bone and teeth, or hunting them due to competition for food or shelter[13,14]. Ongoing zooarchaeological analyses will help more clearly define this relationship alongside other human subsistence behaviours at Bacho Kiro Cave.

6. Outlier analysis of dates

Fourteen dates out of the 68 included in the outlier analysis were identified as outliers based on their posterior outlier probabilities, agreement index and depositional histories (shown in red in supplementary Table 2). The 3 dates from the uppermost Layer A1 are wide-ranging. The layer contains the youngest-dated bone in the sequence at 23,130 ± 60 ^{14}C BP (ETH-86796) which is over 7,000 years younger than any other obtained date from the site. No micromorphological factor has so far been identified to be responsible for the wide range of dates in this layer. However, since the reason for such a wide range of dates is currently unknown all 3 dates were excluded from the modelling.

One date from Layer B (ETH-71299) was slightly younger than the other dates from the layer and was identified as an outlier. This date is statistically identical to the date (ETH-86768) of the hominin bone from the 1970s collection which was labelled as layer 6a/7 (B/C). The inclusion of the hominin bone in the model may have affected the posterior outlier probability of ETH-71299, but as the exact stratigraphic context of this hominin bone is unknown it was not included and we excluded ETH-71299 as an outlier.

ETH-71303 (41,720 ± 180 ^{14}C BP) is much older than the other dates within Layer C, but we have no explanation for this outlier. It was excluded from further analysis.

ETH-71307 (36,500 ± 110 ^{14}C BP) is younger than the other dates in Layer E. As this bone was excavated from close to the contact zone of Layers E and D the prior probability was also set to 1.0 in the outlier analysis, and it was also excluded from the modelling.

Micromorphological analysis indicates that Layer G is water deposited sediment and the artefacts within it were re-deposited from the underlying Layer I by water moving through the cave. The radiocarbon dates support this interpretation so the prior probabilities of these dates were set to 1.0 during outlier analysis, and the 5 dates from Layer G and N1-G were excluded from modelling. Two of the youngest dates from Layer I (ETH-86779; ETH-86782) were identified as outliers based on their agreement index and posterior outlier probabilities. One date from the upper part of Layer J (ETH-93193) was inconsistent with its stratigraphic position with a posterior outlier probability of 1.0. These 3 dates were also excluded.

7. OxCal v4.3 code for Bayesian model of Bacho Kiro Cave chronology (Fig.5)

```
Plot()
{
 Sequence("Bacho Kiro")
 {
  Boundary("Start Layer J");
  Phase("Layer J")
  {
   R_Date("ETH-93196", 45120, 490)
   {
    color="green ";
   };
   R_Date("ETH-86787", 44890, 450)
   {
    color="green ";
   };
   R_Date("ETH-86789", 42900, 370)
```

```
 {
  color="green ";
 };
 R_Date("ETH-93194", 42670, 370)
 {
  color="green ";
 };
 R_Date("ETH-86822", 41670, 320)
 {
 };
 R_Date("ETH-86821", 41630, 320)
 {
 };
 R_Date("ETH-86820", 41540, 320)
 {
 };
 R_Date("ETH-86819", 41230, 310)
 {
 };
};
Boundary("Transition Layer J/Layer I");
Phase("Layer I")
{
 R_Date("ETH-86772", 42450, 510)
 {
```

```
 color="purple";
};
R_Date("ETH-71330", 42270, 300)
{
 color="green";
};
R_Date("R_combine R-EVA 1741", 41950, 250)
{
 color="green";
};
R_Date("ETH-71328", 41850, 280)
{
 color="green";
};
R_Date("ETH-86770", 41850, 480)
{
 color="purple";
};
R_Date("R_combine R-EVA 1742", 41820, 250)
{
 color="green";
};
R_Date("ETH-71314", 41770, 210)
{
 color="green";
```

```
};
R_Date("ETH-71329", 41730, 280)
{
 color="green";
};
R_Date("ETH-86784", 41660, 320)
{
 color="green";
};
R_Date("ETH-71325", 41480, 270)
{
 color="green";
};
R_Date("ETH-71320", 41450, 270)
{
 color="green";
};
R_Date("ETH-86808", 41350, 310)
{
};
R_Date("R_combine R-EVA 1733", 41310, 180)
{
 color="green";
};
R_Date("R_combine R-EVA 1740", 41220, 210)
```

```
{
 color="green";
};
R_Date("ETH-71331", 41200, 260)
{
 color="green";
};
R_Date("ETH-71327", 41170, 260)
{
 color="green";
};
R_Date("ETH-71318", 41080, 260)
{
 color="green";
};
R_Date("ETH-86810", 40920, 300)
{
};
R_Date("ETH-71316", 40790, 250)
{
 color="green";
};
R_Date("ETH-86780", 40760, 290)
{
 color="green";
```

```
 };
 R_Date("ETH-86809", 40750, 290)
 {
 };
 R_Date("ETH-86807", 40710, 290)
 {
 };
 R_Date("ETH-86771", 40600, 420)
 {
  color="purple";
 };
 R_Date("ETH-86783", 40340, 280)
 {
  color="green";
 };
 R_Date("ETH-86769", 39750, 380)
 {
  color="purple";
 };
};
Boundary("Transition Layer I/Layer F");
Phase("Layer F")
{
 R_Date("ETH-86800", 40250, 270)
 {
```

```
 };
 R_Date("combine_R-EVA 1730", 40190, 170)
 {
 };
 R_Date("ETH-71311", 40170, 180)
 {
 };
 R_Date("ETH-86801", 39370, 260)
 {
 };
 R_Date("ETH-86799", 39090, 240)
 {
 };
};
Boundary("Transition Layer F/Layer E");
Phase("Layer E")
{
 R_Date("combine_R-EVA 1724", 39470, 160)
 {
 };
 R_Date("ETH-71309", 39310, 160)
 {
 };
 R_Date("ETH-71310", 39080, 170)
 {
```

```
 };
 R_Date("ETH-71308", 38720, 160)
 {
 };
};
Boundary("Transition Layer E/Layer D");
Phase("Layer D")
{
 R_Date("ETH-86798", 37510, 210)
 {
 };
};
Boundary("Transition Layer D/Layer C");
Phase("Layer C")
{
 R_Date("ETH-71304", 36230, 120)
 {
 };
 R_Date("ETH-71305", 35030, 110)
 {
 };
 R_Date("ETH-71302", 34690, 110)
 {
 };
};
```

```
 Boundary("Transition Layer C/Layer B");
 Phase("Layer B")
 {
  R_Date("ETH-71300", 32610, 90)
  {
  };
  R_Date("ETH-71297", 32500, 90)
  {
  };
  R_Date("R_combine R-EVA 2665", 31660, 140)
  {
   color="purple";
  };
  R_Date("ETH-71298", 31310, 80)
  {
  };
 };
 Boundary("Transition Layer B/Layer A2");
 Phase("Layer A2")
 {
  R_Date("ETH-71294", 31410, 80)
  {
  };
  R_Date("ETH-71295", 31310, 80)
  {
```

```
  };
  R_Date("ETH-71296", 30950, 80)
  {
  };
 };
 Boundary("End Layer A2");
};
};
```

Supplementary Figures

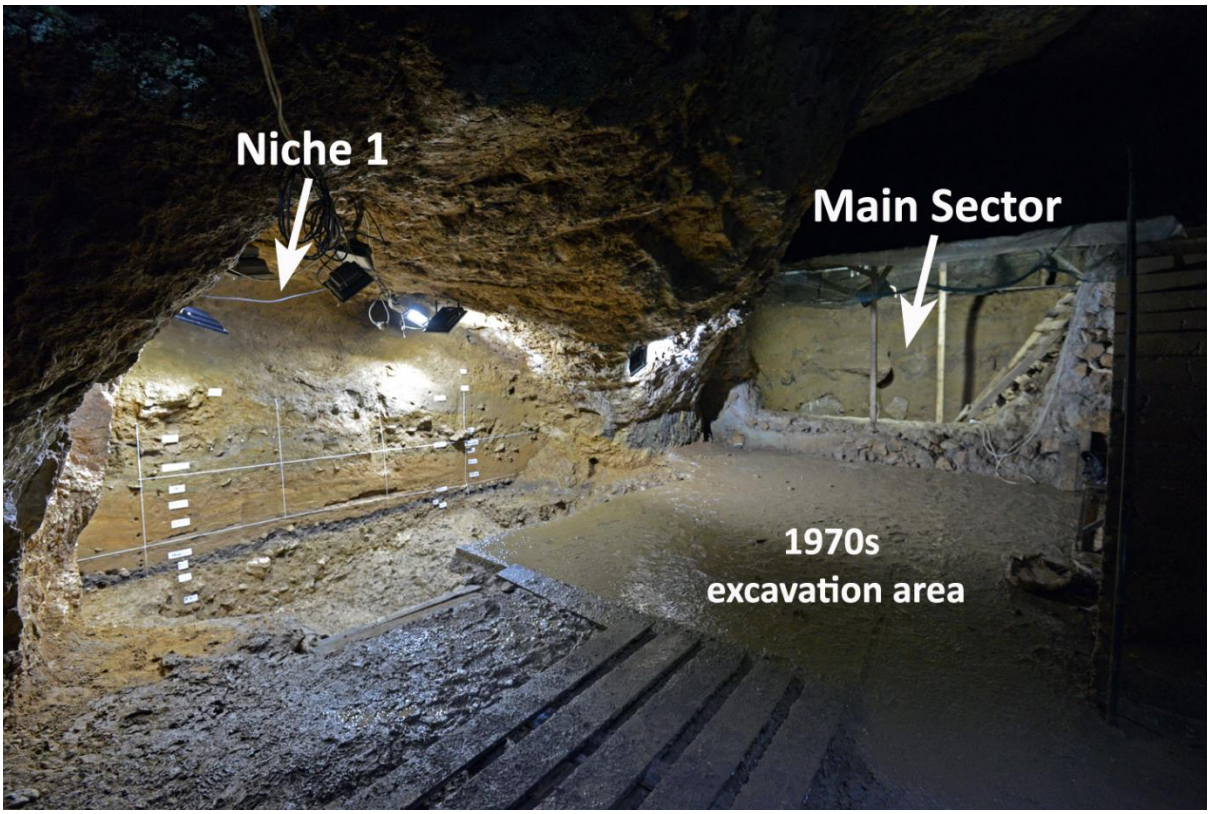

Supplementary Figure 1. View of the Niche 1 *(left)* and Main Section *(right)* during excavations of Bacho Kiro Cave in 2019. The concrete floor in the centre covers the 1970s excavation area. Photo is looking toward the south in the cave.

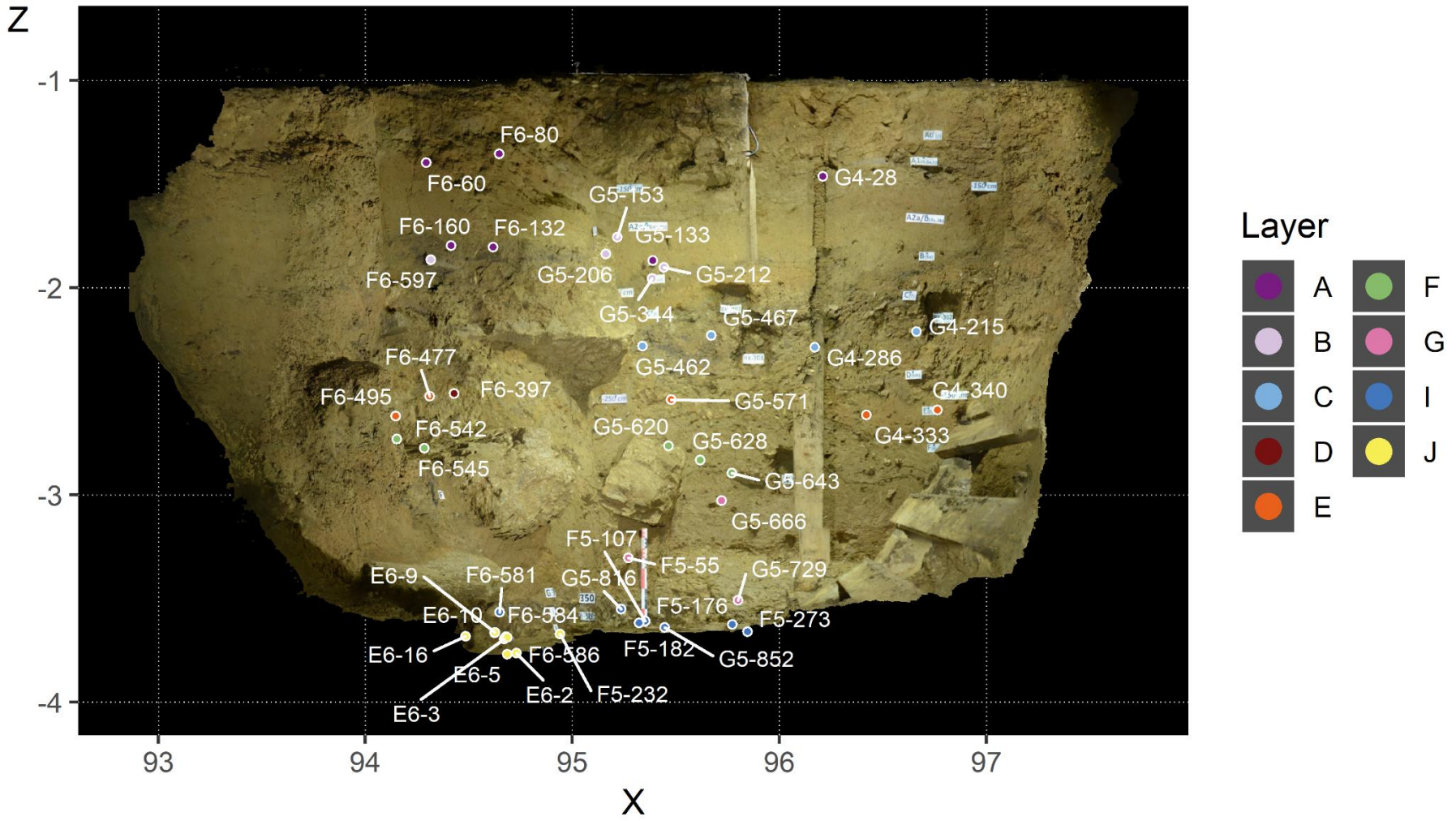

Supplementary Figure 2. Stratigraphic profile (facing north-east) in the Main Sector showing the location of all the bones dated in the study marked with their square ID (corresponding to Supplementary Tables 2-4) according to layer.

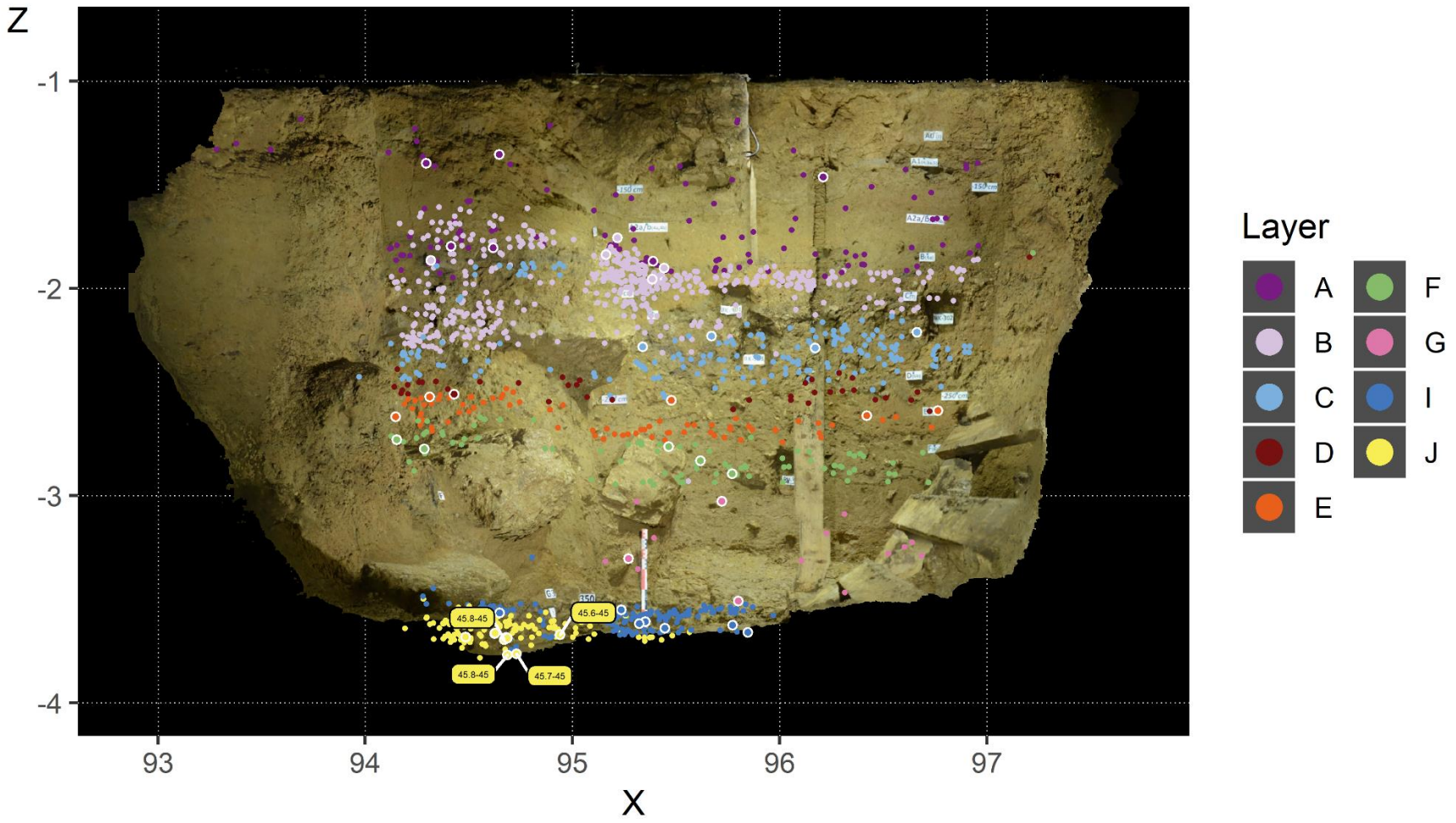

Supplementary Figure 3. Stratigraphic profile (facing north-east) in the Main Sector showing all the finds separated by layer excavated during 2015-2019. The bones dated in the study are marked with a white circle. Select radiocarbon dates are shown (95% calibrated range). Note the variable density of finds between layers.

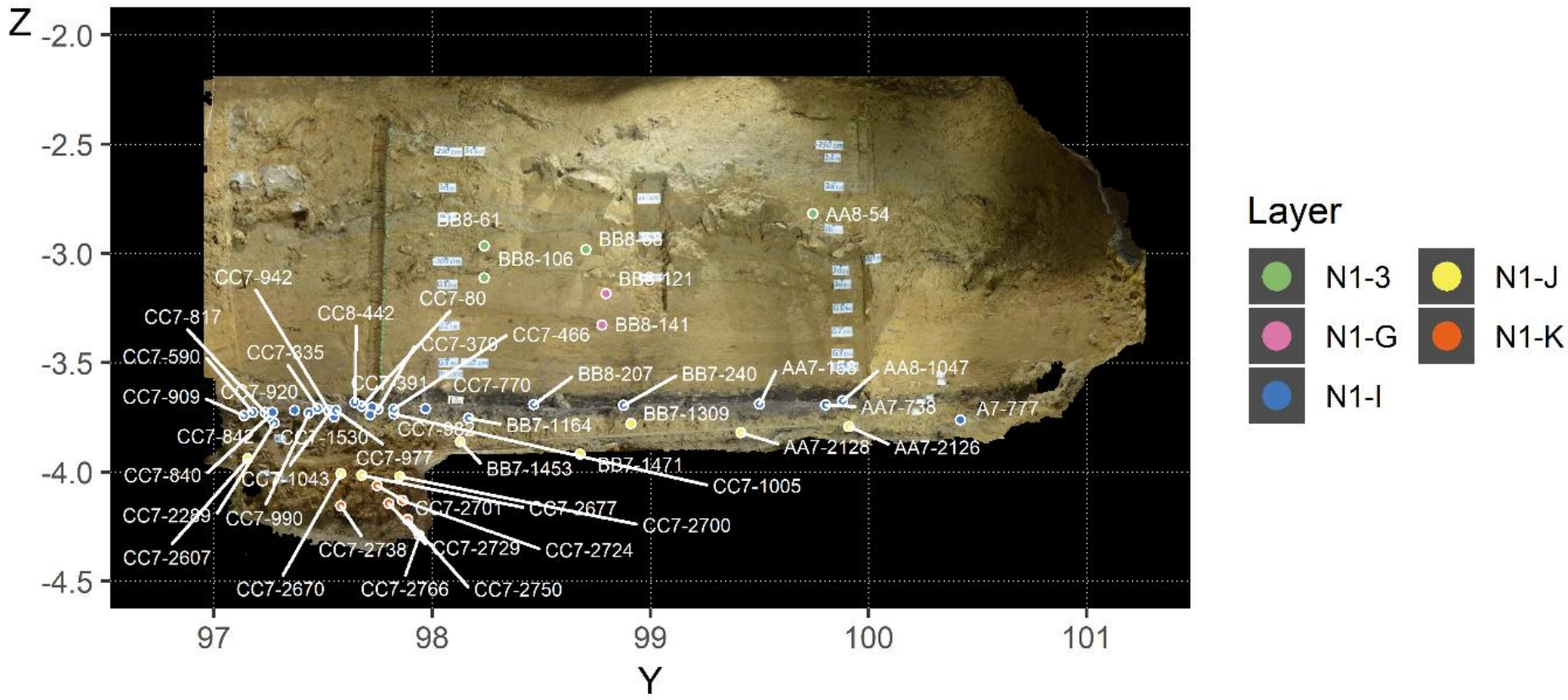

Supplementary Figure 4. Stratigraphic profile (facing north-west) in the Niche 1 showing the location of all the bones dated in the study marked with their square ID (corresponding to Supplementary Tables 2-4) separated according to layer.

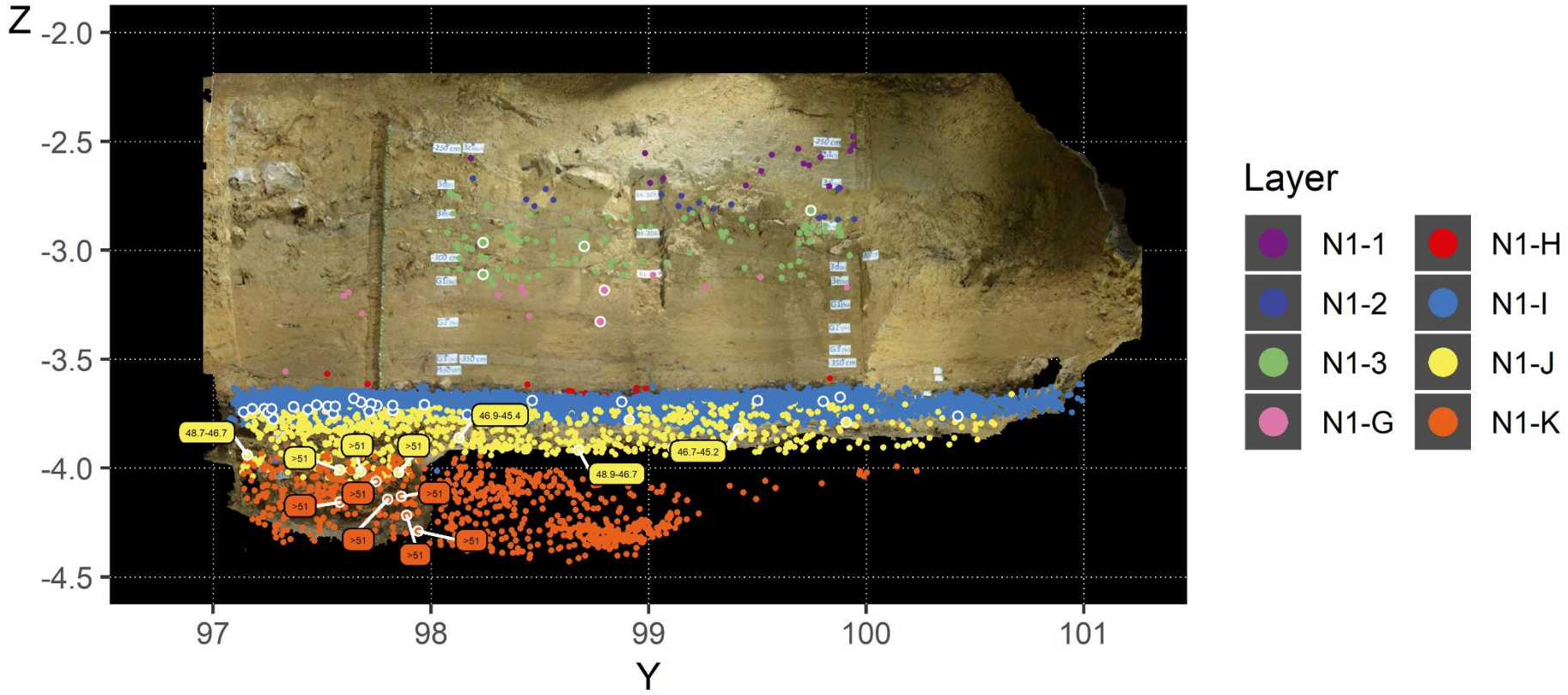

Supplementary Figure 5. Stratigraphic profile (facing north-west) in the Niche 1 showing all the finds separated by layer excavated during 2015-2019. The bones dated in the study are marked with a white circle. Select radiocarbon dates are shown (95% calibrated range). Note the variable density of finds between layers and the exceptionally high density in Layer N1-I.

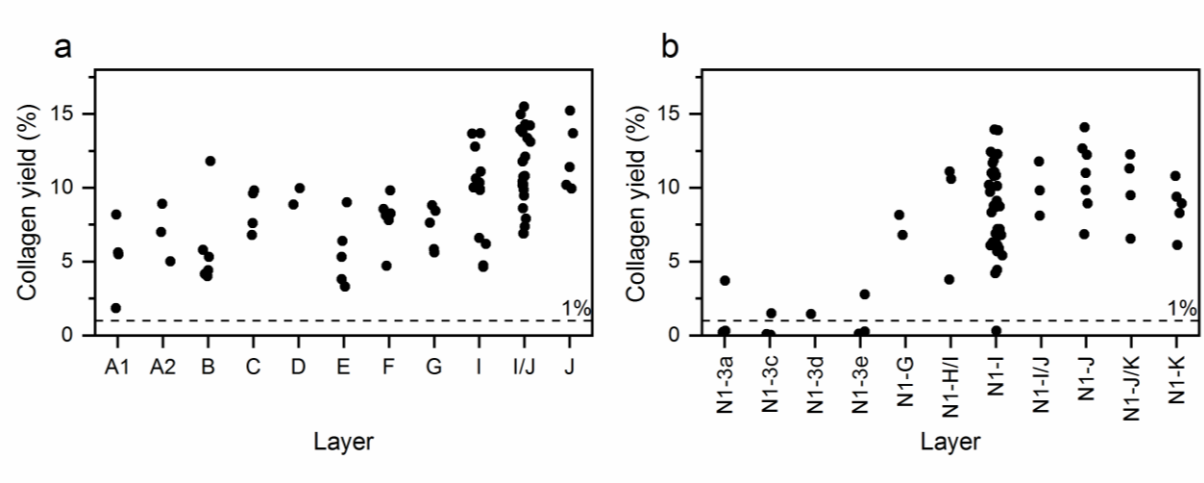

Supplementary Figure 6. Collagen yields of pretreated bones from each layer and layer contact zones (I/J, N1-J/K, N1-I/J, N1-H/I) in the **a)** Main Sector and **b)** Niche 1. The dashed line shows the minimum level of collagen preservation generally considered suitable for ^{14}C dating.

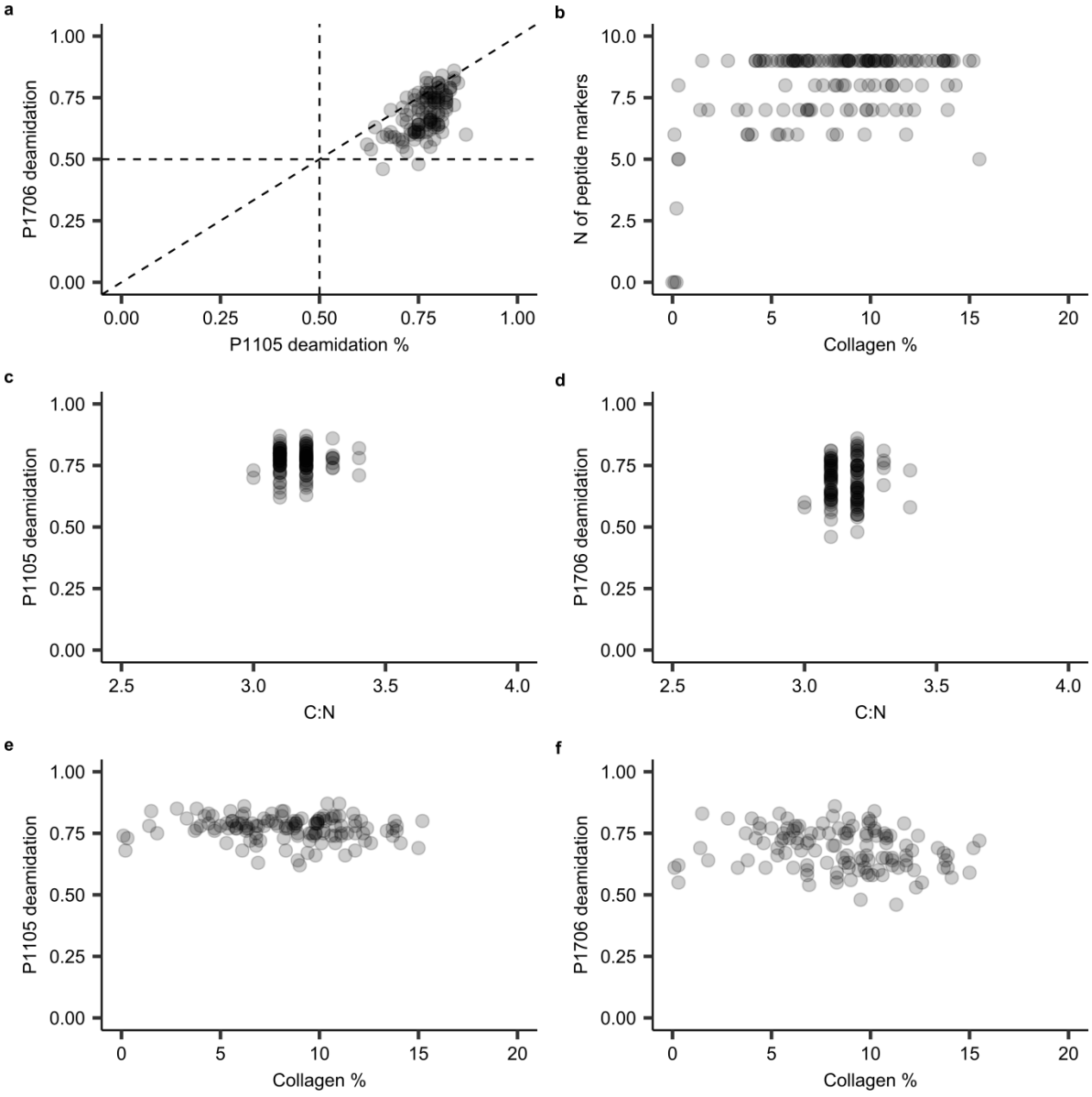

Supplementary Figure 7. Relationship between collagen preservation (^{14}C data) and glutamine deamidation (ZooMS data): **a)** Correlation between collagen peptide P1105 and P1706 deamidation; **b)** Relationship between the collagen % and number of observed peptide markers; **c)** Relationship between the C:N ratio and P1105 deamidation; **d)** Relationship between the C:N ratio and P1706 deamidation; **e)** Relationship between collagen % and P1105 deamidation; **f)** Relationship between collagen % and P1706 deamidation. For deamidation, 1 indicates no deamidation and 0 indicates complete deamidation of the single glutamine in either the P1105 or P1706 peptide.

Supplementary Tables

Supplementary Table 1. Cultural identification of the stone assemblages from each layer of Bacho Kiro Cave, showing the correlation of the layers from the excavation in the 1970s[15] and the new excavation (2015-2018)[8].

Layers Niche 1	**Layers Main Sector**	**Layers 1971-75 excavations**	**Summary of techno-typological assemblages**
N1-1?	A1	4, 3a, 5	• 2015-2018 - Very low density (n=6) of Upper Palaeolithic forms including 2 backed bladelets, characteristic of the Gravettian. • 1970s – Very poor lithic assemblage named 'backed piece tradition' interpreted as Epigravettian.
N1-2?	A2	4a, 4b	• 2015-2018 - Low density of Upper Palaeolithic forms (n=12) without diagnostic attributes. • 1970s - 194 lithics interpreted as 'Aurignacian-like', including many flakes, a few blades and tools such as end-scrapers, burins, denticulate flakes and side-scrapers.
N1-3a?	B	6a	• 2015-2018 - Upper Palaeolithic assemblage (n=87) with Aurignacian elements (bladelet cores with carenoidal end-scrapers, burins, retouched blades and engraved bone). • 1970s – Upper Palaeolithic assemblage (n=521) considered as typical Balkan Aurignacian (carenoidal and nosed end-scrapers, dihedral burins and spalls, retouched blades, thin backed bladelets with fine or step retouch).
N1-3b	C	7	• 2015-2018 - Low-density Upper Palaeolithic assemblage (n=13) of retouched blades, worked bone and platforms consistent with the appearance of soft hammer percussion. No other diagnostic attributes. • 1970s – Also attributed to the Aurignacian (lithics n=521): tools with typical Aurignacian retouch and typology, burins and bladelet cores.
N1-3c	D	6b	• 2015-2018 - No lithics recovered. • 1970s – Low density present only at borders with over- and under-lying layers: many flakes and a few blades, cores and tools (end-scrapers, burins and retouched blades).
N1-3d	E	8	• 2015-2018 - No lithics recovered. • 1970s – 2 lithics and 1 bone point (Mladeč type similar to Moravian Aurignacian, Czech Republic).
N1-3e	F	6c	• 2015-2018 - No lithics recovered. • 1970s – 1 lithic and 5 bone retouchers (and 4 bones with cutmarks).

N1-G	G	9c -9a	• 2015-2018 - Low density (n=3) of lithics reworked from layer N1-I/I (water-laid deposit). • 1970s – Lithics (n=239) fitting with the technology and typology of the underlying Bachokirian assemblage. Aurignacian elements (retouched blades, high end-scrapers, bone points) gradually increase in Layers 9-7.
N1-H	Not present	9c/10	• 2015-2018 - Low density of lithics (n=12) reworked from underlying layer N1-I (water-laid deposit). • 1970s – No lithics in Layer 10.
N1-I	I	11	• 2015-2018 - High-density IUP assemblage (n=1302) consistent with 1970s excavation, made on various imported fine-grained flints, consisting of Levallois-like blades, retouched blade points, end-scrapers and splintered pieces. Assemblage is very fragmented and reworked. Also includes worked bone tools (awls, lissoirs, retouchers) and pendants (bear/ungulate teeth). • 1970s – Assemblage called 'Bachokirian Upper Palaeolithic' made on fine-grained imported flint. Tools types: end-scrapers, retouched blades and flakes splintered pieces and burins.
N1-J	J	11a	• 2015-2018 - Consistent with previous excavations, the upper part of the layer contains low density of IUP as in Layer N1-I/I (above). Lower layer contains low density of lithics: 6 characteristic of IUP as in N1-I; 8 characteristic of MP assemblage in N1-K. • 1970s – Layer 11a upper contains assemblage consistent with Layer 11 above with much lower density. Layer 11a lower contains some MP artefacts consistent with Layer 12. Change from volcanic rock to flint at border of Layers 12/11a.
N1-K	Not present	12	• 2015-2018 - Middle Palaeolithic assemblage (n=5) consistent with 1970s excavation containing Levallois flakes. Raw material is local coarse-grained syenite porphyry. • 1970s – Middle Palaeolithic (Levallois flakes, bone retouchers) on local volcanic rock extends from Layer 14 to bottom of Layer 11a.

Supplementary Table 2. Sample information of all bones from Bacho Kiro Cave extracted in the radiocarbon study (*uploaded as accompanying .xlsx file*).

Supplementary Table 3. Comparison of outlier analysis and agreement index of three models from Bacho Kiro Cave (*uploaded as accompanying .xlsx file*).

Supplementary Table 4. Comparison of model output for Bacho Kiro Cave chronology (outliers excluded) (*uploaded as accompanying .xlsx file*).

Supplementary Table 5. Radiocarbon dates of the two Upper Palaeolithic human bone fragments, BK-1653 and F6-597, using 2.5-3 mg collagen in graphite targets measured with the MICADAS at ETH-Zurich, and using 100-300 µg collagen for the gas ion source of the AixMICADAS. The bottom line shows the weighted mean ^{14}C age and 1σ error of all the dates from each extract, calculated using the R_Combine function in OxCal version 4.3[16]. The output of the X^2 test is included in the bottom line showing that all the dates are statistically indistinguishable for the two bones (for the dates to be in statistical agreement the T value must be less than the X^2 value which is shown in parentheses). All dates have been rounded to the nearest 10 years.

	BK-1653						**F6-597**					
Dating method	**AMS Lab no**	**µg C**	**F^{14}C**	**error**	**^{14}C age (BP)**	**1 σ error**	**AMS Lab no**	**µg C**	**F^{14}C**	**error**	**^{14}C age (BP)**	**1σ error**
Graphite	ETH-86768	996	0.0223	0.0004	30540	140	ETH-86773	940	0.0197	0.0004	31540	150
CO_2	AIX-12024.1.1	48	0.0229	0.0015	30330	530	AIX-12025.1.1	84	0.0189	0.0013	31880	570
CO_2	AIX-12024.1.2	36	0.0218	0.0013	30720	490	AIX-12025.1.2	68	0.0187	0.0014	31960	600
CO_2	AIX-12024.1.3	39	0.0214	0.0013	30870	490	AIX-12025.1.3	90	0.0177	0.0011	32400	490
CO_2	AIX-12024.1.4	93	0.0221	0.0011	30610	400						
R_Combine	df = 4, T= 0.8 (5% 9.5)				30570	120	df = 3, T= 3.5 (5% 7.8)				31660	140

References

1 Briestenský, M. *et al.* Evidence of a plate-wide tectonic pressure pulse provided by extensometric monitoring in the Balkan Mountains (Bulgaria). *Geologica Carpathica* **66**, 427-438 (2015).

2 Fewlass, H. *et al.* Pretreatment and gaseous radiocarbon dating of 40–100 mg archaeological bone. *Scientific Reports* **9**, 5342, doi:10.1038/s41598-019-41557-8 (2019).

3 Longin, R. New method of collagen extraction for radiocarbon dating. *Nature* **231**, 241-242 (1971).

4 Brown, T. A., Nelson, D. E., Vogel, J. S. & Southon, J. R. Improved collagen extraction by modified Longin method. *Radiocarbon* **30**, 171-177 (1988).

5 Bronk Ramsey, C., Higham, T., Bowles, A. & Hedges, R. Improvements to the pretreatment of bone at Oxford. *Radiocarbon* **46**, 155-164 (2004).

6 Brock, F., Bronk Ramsey, C. & Higham, T. Quality assurance of ultrafiltered bone dating. *Radiocarbon* **49**, 187–192 (2007).

7 Buckley, M., Collins, M., Thomas-Oates, J. & Wilson, J. C. Species identification by analysis of bone collagen using matrix-assisted laser desorption/ionisation time-of-flight mass spectrometry. *Rapid Communications in Mass Spectrometry* **23**, 3843-3854, doi:10.1002/rcm.4316 (2009).

8 Hublin, J.-J. *et al.* Initial Upper Palaeolithic *Homo sapiens* remains from Bacho Kiro Cave (Bulgaria). *Nature* (In review).

9 Welker, F. *et al.* Palaeoproteomic evidence identifies archaic hominins associated with the Châtelperronian at the Grotte du Renne. *Proceedings of the National Academy of Sciences* **113**, 11162 (2016).

10 Wilson, J., van Doorn, N. L. & Collins, M. J. Assessing the extent of bone degradation using glutamine deamidation in collagen. *Analytical Chemistry* **84**, 9041-9048, doi:10.1021/ac301333t (2012).

11 Doorn, N. L., Wilson, J., Hollund, H., Soressi, M. & Collins, M. J. Site-specific deamidation of glutamine: a new marker of bone collagen deterioration. *Rapid Communications in Mass Spectrometry* **26**, 2319-2327, doi:10.1002/rcm.6351 (2012).

12 Welker, F. *et al.* Variations in glutamine deamidation for a Châtelperronian bone assemblage as measured by peptide mass fingerprinting of collagen. *STAR: Science & Technology of Archaeological Research* **3**, 15-27, doi:10.1080/20548923.2016.1258825 (2017).

13 Romandini, M. *et al.* Bears and humans, a Neanderthal tale. Reconstructing uncommon behaviors from zooarchaeological evidence in southern Europe. *Journal of Archaeological Science* **90**, 71-91, doi:10.1016/j.jas.2017.12.004 (2018).

14 Terlato, G. *et al.* Chronological and isotopic data support a revision for the timing of cave bear extinction in Mediterranean Europe. *Historical Biology*, 1-11, doi:10.1080/08912963.2018.1448395 (2018).

15 Kozłowski, J. K. *Excavation in the Bacho Kiro cave (Bulgaria): Final Report*. (Państwowe Wydawnictwo Naukowe, 1982).

16 Bronk Ramsey, C. Bayesian analysis of radiocarbon dates. *Radiocarbon* **51**, 337-360 (2009).

New ^{14}C chronology for Middle–to–Upper Palaeolithic transition at Bacho Kiro Cave, Bulgaria

Supplementary Table 2. Sample information of all bones from Bacho Kiro Cave extracted in the radiocarbon study.

R-EVA	Sample Info											Sample Size			Quality checks			
	Excavation year	Pretreatment year	Sample ID	Layer	Material	ZooMS ID	Peptide markers	P1105	P1706	Species (ZooMS)	Anth. Mod.	Bone sampled [mg]	Collagen yld [mg]	Collagen yld (%)	%C	%N	C:N	FTIR
Main Profile																		
1616	2015	2016	F6-60	A1	bone	BK-22	7	0.8	0.73	Ursidae	-	624.5	35	5.6	47.9	17.6	3.2	collagen
2314	2016	2017	G4-47	A1 (A1/c)	long bone	BK-1264	9	0.84	0.72	Ursidae	-	396.0	21.7	5.5	43.1	16.0	3.1	collagen
2315	2015	2017	G4-28	A1	bone (metatarsal)	BK-12	9	0.84	0.86	Bos/Bison	Cut-marks	564.2	46.1	8.2	44.9	16.6	3.2	collagen
2316	2015	2017	F6-80	A1	long bone	BK-5	7	0.75	0.64	Ursidae	Cut-marks	508.4	9.4	1.8	38.9	14.4	3.1	collagen
1711	2016	2016	F6-160	A2	bone	BK-53	9	0.74	0.76	Cervid/Saiga	-	500.0	44.5	8.9	43.8	15.5	3.3	collagen
1712	2016	2016	F6-132	A2	bone	BK-54	7	0.72	0.75	Ursidae	Cut-marks	497.7	34.8	7.0	42.5	15.3	3.2	collagen
1713	2016	2016	G5-133	A2	bone	BK-55	9	0.78	0.77	Capra sp.	Cut-marks	461.2	22.9	5.0	42.9	15.3	3.3	collagen
1714	2016	2016	G5-153	B1	bone	BK-56	6	0.78	0.81	Ursidae	-	547.1	22.0	4.0	40.9	14.6	3.3	collagen
1715	2016	2016	G5-206	B	bone	BK-57	6	0.79	0.69	Ursidae	-	516.6	27.6	5.3	39.5	14.3	3.2	collagen
1716	2016	2016	G5-212	B	bone	BK-58	9	0.83	0.79	Capra sp.	Cut-marks	419.7	18.4	4.4	39.7	14.5	3.2	collagen
1717	2016	2016	G5-344	B	bone	BK-59	6	0.77	0.81	Ursidae	Cut-marks	504.7	29.3	5.8	39.9	14.6	3.2	collagen
2665	2016	2017	F6-597	B(B1)	bone	BK-835	9			Hominin	-	81.9	3.4	4.2	40.2	14.9	3.2	collagen
1751	1970s	2017	BK-1653	6a/7 = B/C	bone	BK-50	6	0.68	0.7	Hominin	-	89.0	10.5	11.8	42.0	15.6	3.2	collagen
1720	2016	2016	G4-215	C	bone	BK-62	9	0.75	0.64	Capra sp.	Cut-marks	539.6	51.8	9.6	41.8	15.3	3.2	collagen
1721	2016	2016	G4-286	C	bone	BK-63	7	0.75	0.66	Ursidae	Cut-marks	549.7	54.1	9.8	44.3	16.2	3.2	collagen
1722	2016	2016	G5-462	C	bone	BK-64	8	0.83		Bos/Bison	Cut-marks	519.4	39.3	7.6	43.5	16.0	3.2	collagen
1723	2016	2016	G5-467	C	bone	BK-65	9	0.75	0.71	Capra sp.	Cut-marks	510.4	34.6	6.8	43.2	16.0	3.1	collagen
2317	2016	2017	F6-397	D	long bone	BK-1266	9	0.79	0.64	Ursidae	Cut-marks	436.2	43.4	9.9	45.9	17.0	3.1	collagen
2318	2016	2017	F6-445	D	long bone	BK-1267	9	0.8	0.81	Bos/Bison	-	585.4	51.9	8.9	46.4	17.2	3.1	collagen

New ^{14}C chronology for Middle–to–Upper Palaeolithic transition at Bacho Kiro Cave, Bulgaria

Supplementary Table 2. Sample information of all bones from Bacho Kiro Cave extracted in the radiocarbon study.

R-EVA	ETH ^{14}C dates					Calibrated range (NO model)				MAMS ^{14}C dates			Notes
	AMS lab number	F^{14}C	error	^{14}C age	1σ error	1σ (68.2%) (cal BP)		2σ (95.4%) (cal BP)		AMS lab number	^{14}C age	1σ error	
					years	from	to	from	to		BP	years	
Main Profile													
1616						35380	35020	35570	34870	MAMS-27346	31340	120	
2314													
2315	ETH-86796	0.0562	0.0004	23130	60	27520	27350	27610	27250				
2316	ETH-86797	0.0140	0.0003	34290	150	38920	38580	39150	38420				
1711	ETH-71294	0.0200	0.0002	31410	80	35430	35110	35580	34970				
1712	ETH-71295	0.0203	0.0002	31310	80	35310	35010	35490	34870				
1713	ETH-71296	0.0212	0.0002	30950	80	34950	34720	35070	34610				
1714	ETH-71297	0.0175	0.0002	32500	90	36490	36240	36670	36120				
1715	ETH-71298	0.0203	0.0002	31310	80	35310	35010	35490	34870				
1716	ETH-71299	0.0223	0.0002	30570	80	34670	34410	34780	34260				
1717	ETH-71300	0.0172	0.0002	32610	90	36610	36330	36810	36210				
2665	ETH-86773	0.0197	0.0004	31540	150	35750	35340	35960	35150				R_combine value 31660 ± 140 used for calibration - see Supplementary Table 5 for CO_2 dates made with the AixMICADAS
1751	ETH-86768	0.0223	0.0004	30540	140	34690	34380	34810	34210				R_combine value 30570 ± 120 used for calibration - see Supplementary Table 5 for CO_2 dates made with the
1720	ETH-71302	0.01333	0.00018	34690	110	39380	38970	39590	38800				
1721	ETH-71303	0.00559	0.00014	41670	200	45350	44910	45570	44690	MAMS-29490	41900	370	R-Combine value 41720 ± 80 used for calibration
1722	ETH-71304	0.0110	0.00017	36230	120	41120	40710	41290	40480				
1723	ETH-71305	0.01277	0.00017	35030	110	39790	39390	39960	39180				
2317	ETH-86798	0.00937	0.00024	37510	210	42100	41760	42270	41570				
2318													

New ^{14}C chronology for Middle–to–Upper Palaeolithic transition at Bacho Kiro Cave, Bulgaria

Supplementary Table 2. Sample information of all bones from Bacho Kiro Cave extracted in the radiocarbon study.

R-EVA	Sample Info											Sample Size			Quality checks			
	Excavation year	Pretreatment year	Sample ID	Layer	Material	ZooMS ID	Peptide markers	P1105	P1706	Species (ZooMS)	Anth. Mod.	Bone sampled [mg]	Collagen yld [mg]	Collagen yld (%)	%C	%N	C:N	FTIR
1725	2016	2016	G4-340	E (contact E/D)	bone	BK-67	7	0.77	0.78	Ursidae	-	516.5	33.4	6.4	43.6	16.3	3.1	collagen
1724	2016	2016	G4-333	E	bone	BK-66	7	0.62	0.56	Ursidae	Cut-marks	521.2	46.9	9.0	41.3	15.5	3.1	collagen
1726	2016	2016	G5-571	E	bone	BK-68	9	0.71	0.66	Cervid/Saiga	-	547.9	28.8	5.3	43.9	16.2	3.2	collagen
1727	2016	2016	F6-477	E	tooth (dentine)	BK-69	7	0.81	0.61	Ursidae	-	485.2	16.0	3.3	39.9	14.8	3.1	collagen
1728	2016	2016	F6-495	E	tooth (dentine)	BK-70	6	0.85		Ursidae	-	537.3	20.2	3.8	41.2	15.6	3.1	collagen
1729	2016	2016	G5-628	F	tooth (dentine)	BK-71	7	0.76		Ursidae	-	550.9	25.9	4.7	43.2	16.2	3.1	collagen
2319	2016	2017	G5-620	F (F1)	bone (skull)	BK-1271	8	0.79	0.65	Ursidae	-	475.3	40.7	8.6	45.3	17.0	3.1	collagen
2320	2016	2017	F6-527	F (F1/F2)	long bone	BK-1270	6	0.82	0.7	Ursidae	-	490.4	39.9	8.1	46.4	17.4	3.1	collagen
1730	2016	2016	F6-545	F2	bone	BK-72	7	0.75	0.7	Ursidae	Cut-marks	550.2	54.1	9.8	43.9	16.6	3.1	collagen
2321	2016	2017	F6-542	F (F2)	bone (rib)	BK-1269	6	0.77	0.57	Rhinocerotid	-	622.9	51.4	8.3	45.9	17.2	3.1	collagen
2322	2016	2017	G5-643	F (F3)	long bone	BK-1268	7	0.79	0.63	Rhinocerotid	-	485.0	37.8	7.8	45.7	17.2	3.1	collagen
2323	2016	2017	G5-666	G1	long bone	BK-1273	9	0.79	0.73	Bos/Bison	-	467.7	41.2	8.8	46.5	17.3	3.1	collagen
2324	2016	2017	G5-706	G2	bone	BK-1274	9	0.77	0.77	Bos/Bison	-	378.8	31.9	8.4	46.3	17.3	3.1	collagen
2325	2017	2017	G5-729	G3	long bone	BK-1276	9	0.77	0.77	Bos/Bison	-	541.4	31.6	5.8	46.1	17.2	3.1	collagen
2326	2016	2017	G4-397	G1	long bone	BK-1272	9	0.8	0.75	Bos/Bison	-	466.1	26.2	5.6	45.4	16.9	3.1	collagen
2327	2016	2017	F5-55	G (G2)	long bone	BK-1275	9	0.8	0.79	Bos/Bison	Cut-marks	552.2	42.1	7.6	46.7	17.5	3.1	collagen
2328	2017	2017	G5-812	I	bone	BK-1278	9	0.75	0.64	Ursidae	-	508.4	56.4	11.1	45.7	17.1	3.1	collagen
2329	2017	2017	G5-815	I	long bone	BK-1280	9	0.77	0.61	Cervid/Saiga	-	464.2	22	4.7	44.0	16.4	3.1	collagen
2330	2017	2017	G5-806	I	long bone	BK-1279	9	0.82	0.71	Bos/Bison	-	419.3	19.4	4.6	41.8	15.8	3.1	collagen
2331	2017	2017	G5-816	I	bone	BK-1277	9	0.81	0.65	Ursidae	Cut-marks	442.3	46.9	10.6	44.8	16.8	3.1	collagen
2332	2017	2017	F5-97	I	long bone	BK-1287	9	0.8	0.74	Bos/Bison	-	454.7	47	10.3	46.9	17.5	3.1	collagen
2333	2017	2017	F5-107	I	long bone	BK-1288	9	0.79	0.74	Bos/Bison	Retoucher	472.5	46.5	9.8	46.6	17.4	3.1	collagen
2334	2017	2017	F5-106	I	long bone	BK-1285	9	0.83	0.78	Bos/Bison	-	412.3	25.5	6.2	43.6	16.5	3.1	collagen

New ^{14}C chronology for Middle–to–Upper Palaeolithic transition at Bacho Kiro Cave, Bulgaria

Supplementary Table 2. Sample information of all bones from Bacho Kiro Cave extracted in the radiocarbon study.

R-EVA	ETH ^{14}C dates					Calibrated range (NO model)				MAMS ^{14}C dates			Notes
	AMS lab number	F^{14}C	error	^{14}C age	1σ error	1σ (68.2%) (cal BP)		2σ (95.4%) (cal BP)		AMS lab number	^{14}C age	1σ error	
					years	from	to	from	to		BP	years	
1725	ETH-71307	0.01061	0.00017	36520	130	41360	41010	41500	40800	MAMS-29489	36440	200	R_combine value 36500 ± 110 used for calibration
1724	ETH-71306	0.00735	0.00015	39470	170	43320	42980	43510	42820	MAMS-28675	39470	410	R_combine value 39470 ± 160 used for calibration
1726	ETH-71308	0.00806	0.00016	38720	160	42820	42530	42970	42380				
1727	ETH-71309	0.0075	0.00015	39310	160	43200	42880	43370	42730				
1728	ETH-71310	0.00771	0.00016	39080	170	43050	42740	43210	42590				
1729	ETH-71311	0.00673	0.00015	40170	180	44000	43500	44250	43300				
2319	ETH-86799	0.00771	0.00023	39090	240	43100	42710	43310	42530				
2320													
1730	ETH-71312	0.00672	0.00015	40180	180	44020	43530	44260	43330	MAMS-28676	40260	430	R_combine value 40190 ± 170 used for calibration
2321	ETH-86800	0.00667	0.00023	40250	270	44150	43520	44430	43270				
2322	ETH-86801	0.00744	0.00024	39370	260	43310	42870	43590	42670				
2323	ETH-86802	0.00649	0.00023	40470	280	44360	43730	44640	43420				
2324													
2325	ETH-86806	0.00604	0.00022	41040	300	44880	44270	45190	43940				
2326													
2327	ETH-86804	0.00623	0.00022	40800	290	44670	44050	44970	43700				
2328													
2329													
2330													
2331	ETH-86807	0.0063	0.00023	40710	290	44590	43960	44880	43610				
2332													
2333	ETH-86808	0.00581	0.00022	41350	310	45130	44520	45450	44240				
2334													

New ^{14}C chronology for Middle–to–Upper Palaeolithic transition at Bacho Kiro Cave, Bulgaria

Supplementary Table 2. Sample information of all bones from Bacho Kiro Cave extracted in the radiocarbon study.

R-EVA	Sample Info											Sample Size			Quality checks			
	Excavation year	Pretreatment year	Sample ID	Layer	Material	ZooMS ID	Peptide markers	P1105	P1706	Species (ZooMS)	Anth. Mod.	Bone sampled [mg]	Collagen yld [mg]	Collagen yld (%)	%C	%N	C:N	FTIR
2335	2017	2017	F5-273	I	bone (rib)	BK-1286	9	0.8	0.81	Capra sp.	Cut-marks	343.3	34	9.9	44.2	16.8	3.1	collagen
2336	2017	2017	F6-570	I	bone	BK-1281	9	0.77	0.67	Ursidae	-	453.2	61.9	13.7	46.2	17.1	3.2	collagen
2337	2017	2017	F6-571	I	long bone	BK-1283	9	0.81	0.8	Bos/Bison	-	458.0	45.9	10.0	46.4	16.8	3.2	collagen
2338	2017	2017	F6-579	I	bone	BK-964	9			Bos/Bison	-	474.3	60.6	12.8	45.8	17.0	3.2	collagen
2339	2017	2017	F6-580	I	long bone	BK-1282	9	0.74	0.61	Ursidae	-	358.9	49.1	13.7	46.1	17.0	3.2	collagen
2340	2017	2017	F6-581	I	long bone	BK-1284	9	0.79		Bos/Bison	Cut-marks + marrow break	461.8	30.5	6.6	45.6	16.8	3.2	collagen
2341	2017	2017	G5-877	I/J	long bone	BK-1300	7	0.63	0.54	Ursidae	-	400.3	27.6	6.9	46.4	16.9	3.2	collagen
2342	2017	2017	G5-852	I/J	long bone	BK-1301	9	0.87	0.6	Equidae	Cut-marks	500.7	52.2	10.4	44.3	16.5	3.1	collagen
2343	2017	2017	G5-853	I/J	bone (vertebra)	BK-1299	8	0.8	0.64	Equidae	-	338.0	39.9	11.8	44.4	16.6	3.1	collagen
2344	2017	2017	G5-862	I/J	bone (skull)	BK-1298	8	0.75	0.48	Ursidae	Cut-marks	511.2	48.4	9.5	43.3	15.8	3.2	collagen
2345	2017	2017	F5-132	I/J	long bone	BK-1295	9	0.8	0.64	Ursidae	Cut-marks	474.5	65.3	13.8	47.4	17.3	3.2	collagen
2346	2017	2017	F5-155	I/J	long bone	BK-1294	9	0.78	0.75	Capra sp.	-	509.0	40.2	7.9	45.3	16.8	3.1	collagen
2347	2017	2017	F5-143	I/J	bone (ulna)	BK-1293	9	0.82	0.75	Capra sp.	-	556.0	59.7	10.7	46.2	17.0	3.2	collagen
2348	2017	2017	F5-168	I/J	long bone	BK-1292	9	0.8	0.75	Bos/Bison	Cut-marks	519.0	38.2	7.4	45.8	16.6	3.2	collagen
2349	2017	2017	F5-172	I/J	bone (rib)	BK-1291	9	0.78	0.65	Ursidae	Cut-marks	436.0	47	10.8	46.2	16.9	3.2	collagen
2350	2017	2017	F5-176	I/J	bone (mandible)	BK-1296	9	0.78	0.72	Cervid/Saiga	Cut-marks	460.6	31.7	6.9	43.2	15.8	3.2	collagen
2351	2017	2017	F5-177	I/J	bone (phalanx)	BK-1290	9	0.8	0.68	Ursidae	-	432.3	52.3	12.1	45.6	17.0	3.1	collagen
2352	2017	2017	F5-182	I/J	bone (rib)	BK-1289	9	0.82	0.76	Bos/Bison	Cut-marks	473.5	48.1	10.2	45.4	16.9	3.1	collagen
2353	2017	2017	F5-195	I/J	long bone	BK-1297	9	0.75	0.77	Bos/Bison	Cut-marks	508.4	51.9	10.2	45.8	17.0	3.1	collagen
2354	2017	2017	E6-11	I/J	bone (skull)	BK-1302	9	0.76	0.69	Ursidae	-	440.0	58.8	13.4	51.8	19.2	3.1	collagen
2355	2017	2017	E6-10	I/J	long bone	BK-940	9			Bos/Bison	-	611.3	52.6	8.6	46.6	17.0	3.2	collagen
2356	2017	2017	E6-16	I/J	long bone	BK-1305	9	0.69	0.59	Ursidae	Cut-marks	387.8	58	15.0	47.6	17.4	3.2	collagen
2357	2017	2017	E6-21	I/J	long bone	BK-932	8			Ursidae	Cut-marks	426.9	61	14.3	49.0	17.9	3.2	collagen
2358	2017	2017	E6-12	I/J	bone (rib)	BK-1304	8	0.79	0.58	Ursidae	-	369.2	36.4	9.9	44.9	16.6	3.2	collagen
2359	2017	2017	E6-9	I/J	bone (rib)	BK-1303	9	0.78	0.66	Ursidae	Cut-marks	529.8	62.4	11.8	45.1	16.6	3.2	collagen

New ^{14}C chronology for Middle–to–Upper Palaeolithic transition at Bacho Kiro Cave, Bulgaria

Supplementary Table 2. Sample information of all bones from Bacho Kiro Cave extracted in the radiocarbon study.

R-EVA	ETH ^{14}C dates					Calibrated range (NO model)				MAMS ^{14}C dates			Notes
	AMS lab number	F^{14}C	error	^{14}C age	1σ error	1σ (68.2%) (cal BP)		2σ (95.4%) (cal BP)		AMS lab number	^{14}C age	1σ error	
					years	from	to	from	to		BP	years	
2335	ETH-86809	0.00626	0.00023	40750	290	44630	44000	44920	43650				
2336													
2337													
2338													
2339													
2340	ETH-86810	0.00614	0.00023	40920	300	44780	44160	45090	43810				
2341													
2342	ETH-86811	0.00656	0.00023	40380	280	44280	43640	44560	43350				not modelled - contact zone
2343													
2344													
2345													
2346													
2347													
2348													
2349													
2350	ETH-86812	0.00727	0.00023	39560	260	43460	42980	43800	42790				not modelled - contact zone
2351													
2352	ETH-86813	0.00675	0.00023	40160	270	44060	43440	44360	43210				not modelled - contact zone
2353													
2354													
2355	ETH-86814	0.0060	0.0002	41040	300	44880	44270	45190	43940				not modelled - contact zone
2356	ETH-86815	0.0059	0.0002	41210	300	45010	44420	45320	44120				not modelled - contact zone
2357													
2358													
2359	ETH-86816	0.0058	0.0002	41380	310	45150	44550	45470	44270				not modelled - contact zone

New ^{14}C chronology for Middle–to–Upper Palaeolithic transition at Bacho Kiro Cave, Bulgaria

Supplementary Table 2. Sample information of all bones from Bacho Kiro Cave extracted in the radiocarbon study.

R-EVA	Sample Info											Sample Size			Quality checks			
	Excavation year	Pretreatment year	Sample ID	Layer	Material	ZooMS ID	Peptide markers	P1105	P1706	Species (ZooMS)	Anth. Mod.	Bone sampled [mg]	Collagen yld [mg]	Collagen yld (%)	%C	%N	C:N	FTIR
2360	2017	2017	F6-584	I/J	bone	BK-933	9			Ursidae	-	360.8	50.3	13.9	45.3	16.8	3.1	collagen
2361	2017	2017	F6-586	I/J	bone	BK-586	5		0.72	Ursidae	-	599.6	92.9	15.5	46.4	17.1	3.2	collagen
2362	2017	2017	F6-587	I/J	bone (rib)	BK-938	9			Ursidae	-	449.1	58.9	13.1	54.6	20.1	3.2	collagen
2363	2017	2017	F6-587	I/J	bone (femur head)	BK-938	9			Ursidae	-	472.3	67.1	14.2	46.1	16.8	3.2	collagen
2364	2017	2017	F5-200	J	long bone	BK-1306	9	0.8	0.79	Capra sp.	-	351.4	34.9	9.9	46.4	17.1	3.2	collagen
2365	2017	2017	F5-232	J	bone	BK-970	9			Bos/Bison	-	329.5	45.1	13.7	46.3	17.0	3.2	collagen
2366	2017	2017	E6-2	J	bone (cranial)	BK-1309	9	0.81	0.84	Capra sp.	Cut-marks	520.8	53	10.2	45.5	16.8	3.2	collagen
2367	2017	2017	E6-5	J	long bone	BK-1308	9	0.8	0.69	Ursidae	Cut-marks	438.5	66.7	15.2	46.8	17.4	3.1	collagen
2368	2017	2017	E6-3	J	bone (rib)	BK-1307	9	0.75	0.61	Ursidae	Cut-marks	393.0	44.8	11.4	49.2	18.0	3.2	collagen
Niche																		
2275	2016	2017	AA8-59	N1-3a	bone (cranial?)	BK-1217	0			*Indet*	Cut-marks	553.6	1.1	0.2	-	-	-	-
2276	2016	2017	AA8-190	N1-3a	bone	BK-1218	3	0.68		Carnivora/Bovic	-	444.5	1	0.2	-	-	-	-
1718	2016	2016	AA8-54	N1-3a	bone	BK-60	7	0.76	0.75	Bos/Bison	-	509.9	18.9	3.7	42.5	15.3	3.2	collagen
1719	2016	2016	AA8-65	N1-3a	bone	BK-61	5		0.55	*Indet*	-	505.7	1.3	0.3	21.1	7.8	3.2	collagen
2272	2016	2017	BB8-47	N1-3c	bone (cranial?)	BK-1221	0			*Indet*	-	443.1	0.1	0.0	-	-	-	-
2273	2016	2017	BB8-61	N1-3c	bone	BK-1220	9	0.84	0.83	Bos/Bison	-	347.1	5.2	1.5	42.0	15.5	3.2	collagen
2274	2016	2017	AA8-73	N1-3c	bone	BK-1219	0			*Indet*	-	564.9	0.5	0.1	-	-	-	-
2271	2016	2017	BB8-68	N1-3d	long bone	BK-1222	7	0.78	0.69	Ursidae	-	368.0	5.3	1.4	39.6	14.8	3.1	collagen
2268	2016	2017	BB8-96	N1-3e	long bone	BK-1225	8	0.73	0.62	Ursidae	-	526.6	1.4	0.3	-	-	-	-
2269	2016	2017	BB8-83	N1-3e	long bone	BK-1224	6	0.74	0.61	Ursidae	-	495.5	0.5	0.1	-	-	-	-
2270	2016	2017	BB8-106	N1-3e	long bone	BK-1223	9	0.85	0.81	Bos/Bison	-	464.7	12.9	2.8	43.1	15.9	3.2	collagen
1731	2016	2016	BB8-141	N1-G	bone	BK-73	7	0.73	0.6	Ursidae	Cut-marks	521.2	35.5	6.8	41.4	16.1	3.0	collagen
2277	2016	2017	BB8-121	N1-G1	long bone	BK-1226	8	0.73	0.7	Bos/Bison	Possible marrow fracture?	221.8	18.1	8.2	44.8	16.7	3.1	collagen

New ^{14}C chronology for Middle–to–Upper Palaeolithic transition at Bacho Kiro Cave, Bulgaria

Supplementary Table 2. Sample information of all bones from Bacho Kiro Cave extracted in the radiocarbon study.

R-EVA	ETH ^{14}C dates					Calibrated range (NO model)				MAMS ^{14}C dates			Notes
	AMS lab number	F^{14}C	error	^{14}C age	1σ error	1σ (68.2%) (cal BP)		2σ (95.4%) (cal BP)		AMS lab number	^{14}C age	1σ error	
					years	from	to	from	to		BP	years	
2360	ETH-86817	0.0058	0.0002	41350	310	45130	44520	45450	44240				not modelled - contact zone
2361	ETH-86818	0.0054	0.0002	42010	330	45670	45050	46000	44740				not modelled - contact zone
2362													
2363													
2364													
2365	ETH-86819	0.0059	0.0002	41230	310	45030	44430	45350	44120				
2366	ETH-86820	0.0057	0.0002	41540	320	45290	44670	45600	44380				
2367	ETH-86821	0.0056	0.0002	41630	320	45360	44750	45670	44450				
2368	ETH-86822	0.0056	0.0002	41670	320	45390	44780	45700	44480				
Niche													
2275													
2276													
1718	ETH-71301	0.01282	0.00018	35000	110	39760	39350	39940	39140				Not modelled - archaeology unclear
1719													
2272													
2273	ETH-86776	0.00839	0.00024	38410	230	42670	42300	42850	42130				Not modelled - archaeology unclear
2274													
2271	ETH-86775	0.01153	0.00025	35850	180	40740	40220	41010	39990				Not modelled - archaeology unclear
2268													
2269													
2270	ETH-86774	0.00725	0.00023	39580	260	43480	42990	43820	42790				Not modelled - archaeology unclear
1731	ETH-71313	0.00617	0.00015	40870	190	44660	44200	44900	43930				
2277	ETH-86777	0.00665	0.00023	40270	280	44170	43540	44460	43270				

New ^{14}C chronology for Middle–to–Upper Palaeolithic transition at Bacho Kiro Cave, Bulgaria

Supplementary Table 2. Sample information of all bones from Bacho Kiro Cave extracted in the radiocarbon study.

R-EVA	Sample Info											Sample Size			Quality checks			
	Excavation year	Pretreatment year	Sample ID	Layer	Material	ZooMS ID	Peptide markers	P1105	P1706	Species (ZooMS)	Anth. Mod.	Bone sampled [mg]	Collagen yld [mg]	Collagen yld (%)	%C	%N	C:N	FTIR
2278	2017	2017	A7-196	N1-H/I	bone	BK-1228	6	0.77	0.64	Ursidae	Cut-marks	489.4	18.5	3.8	44.2	16.3	3.2	collagen
2279	2017	2017	A7-275	N1-H/I	long bone	BK-1227	8	0.74	0.62	Ursidae	Cut-marks	623.6	69.1	11.1	44.7	16.5	3.2	collagen
2280	2017	2017	BB8-292	N1-H/I	long bone	BK-1229	7	0.74	0.58	Equidae	-	352.0	37.3	10.6	45.8	16.8	3.2	collagen
1732	2016	2016	CC7-80	N1-I	bone	BK-74	7	0.7	0.58	Cervidae/Bovid	Cut-marks	512.2	35.0	6.8	42.0	16.2	3.0	collagen
1733	2016	2016	CC7-379	N1-I	bone	BK-75	9	0.82	0.73	Bos/Bison	Cut-marks	502.3	21.2	4.2	44.6	15.3	3.4	collagen
1734	2016	2016	CC7-391	N1-I	bone	BK-76	9	0.78		Bos/Bison	Cut-marks	515.5	37.3	7.2	44.1	15.2	3.4	collagen
1735	2016	2016	CC7-466	N1-I	bone	BK-77	7	0.71	0.58	Ursidae	Cut-marks	504.2	51.0	10.1	45.5	15.8	3.4	collagen
1736	2016	2016	CC7-590	N1-I	bone	BK-78	9	0.86		Capra sp.	Cut-marks	490.4	30.2	6.2	43.3	15.2	3.3	collagen
1737	2016	2016	CC7-770	N1-I	bone	BK-79	9	0.74	0.74	Bos/Bison	Cut-marks	529.1	56.9	10.8	46.7	16.5	3.3	collagen
1738	2016	2016	CC7-817	N1-I	bone	BK-80	8	0.78	0.67	Bos/Bison	Cut-marks	496.4	28.2	5.7	43.3	15.5	3.3	collagen
1739	2016	2016	CC7-840	N1-I	bone	BK-81	9			Equidae	Cut-marks	520.8	36.1	6.9	44.1	15.8	3.3	collagen
1740	2016	2016	CC7-842	N1-I	bone	BK-82	6	0.74	0.61	Ursidae	Cut-marks	534.1	51.9	9.7	43.9	15.9	3.2	collagen
1741	2016	2016	CC7-909	N1-I	bone	BK-83	8	0.76		Equidae	Cut-marks	503.8	51.6	10.2	41.9	14.9	3.3	collagen
1742	2016	2016	CC7-920	N1-I	bone	BK-84	9	0.87		Bos/Bison	Cut-marks	482.9	53.2	11.0	38.9	14.0	3.2	collagen
1743	2016	2016	CC7-942	N1-I	bone	BK-85	9	0.79	0.73	Bos/Bison	Cut-marks	407.7	24.2	5.9	40.4	14.5	3.2	collagen
1744	2016	2016	CC7-977	N1-I	bone	BK-86	9	0.79		Capra sp.	Cut-marks	541.6	33.3	6.1	42.8	15.4	3.3	collagen
1745	2016	2016	CC7-982	N1-I	bone	BK-87	6	0.77	0.83	Ursidae	Cut-marks	461.4	24.7	5.4	42.4	15.4	3.2	collagen
1746	2016	2016	CC7-990	N1-I	bone	BK-88	8	0.81	0.68	Equidae	Cut-marks	542.4	38.9	7.2	42.1	15.6	3.2	collagen
1747	2016	2016	CC7-1005	N1-I	bone	BK-89	6	0.78	0.77	Ursidae	Cut-marks	573.5	36.2	6.3	42.0	15.7	3.1	collagen
1748	2016	2016	CC7-1043	N1-I	bone	BK-90	9	0.81	0.78	Capra sp.	Cut-marks	580.9	53.1	9.1	41.2	15.4	3.1	collagen
1749	2016	2016	CC7-1530	N1-I	bone	BK-91	9	0.82	0.76	Bos/Bison	Cut-marks	564.6	34.7	6.1	41.8	15.6	3.1	collagen
1750	2016	2016	CC7-2130	N1-I	bone	BK-92	5			*Indet*	Cut-marks	553.9	1.8	0.3	-	-	-	no collagen

New ^{14}C chronology for Middle–to–Upper Palaeolithic transition at Bacho Kiro Cave, Bulgaria

Supplementary Table 2. Sample information of all bones from Bacho Kiro Cave extracted in the radiocarbon study.

R-EVA	ETH ^{14}C dates					Calibrated range (NO model)				MAMS ^{14}C dates			Notes
	AMS lab number	F^{14}C	error	^{14}C age	1σ error	1σ (68.2%) (cal BP)		2σ (95.4%) (cal BP)		AMS lab number	^{14}C age	1σ error	
					years	from	to	from	to		BP	years	
2278													Carnivore tooth mark as well as cutmarks
2279													
2280													
1732	ETH-71314	0.0055	0.0001	41770	210	45400	44930	45640	44700				
1733	ETH-71315	0.0058	0.0001	41410	200	45010	44570	45230	44360	MAMS-28677	40720	460	R_combine value 41310 ± 180 used for calibration
1734	ETH-71316	0.0062	0.0002	40790	250	44630	44070	44900	43750				
1735	ETH-71317	0.0061	0.0002	40930	260	44760	44190	45050	43880	MAMS-28678	43,110	597	Not modelled - Failed X^2 - also other dates: (MAMS-29487) 42440 ± 380 and (MAMS-29488) 42240 ± 380
1736	ETH-71318	0.0060	0.0002	41080	260	44880	44340	45170	44060				
1737	ETH-71319	0.0062	0.0002	40820	250	44660	44100	44930	43780	MAMS-28679	42,358	544	Not modelled - Failed X^2 - also other dates: (MAMS-29485) 41850 ± 350 and (MAMS-29486) 42170 ± 370
1738	ETH-71320	0.0057	0.0002	41450	270	45180	44630	45460	44370				
1739	ETH-71321	0.0069	0.0002	40000	230	43870	43320	44170	43120	MAMS-29484	42020	380	Not modelled - Failed X^2
1740	ETH-71322	0.0061	0.0002	41020	260	44950	44480	45200	44260	MAMS-29483	41540	350	R_combine value 41220 ± 210 used for calibration
1741	ETH-71323	0.0055	0.0002	41860	280	45570	45050	45830	44800	MAMS-28680	42270	550	R_combine value 41950 ± 250 used for calibration
1742	ETH-71324	0.0056	0.0002	41720	280	45460	44950	45730	44690	MAMS-28681	42140	540	R_combine value 41820 ± 250 used for calibration
1743	ETH-71325	0.0057	0.0002	41480	270	45200	44660	45480	44400				
1744	ETH-71326	0.0059	0.0002	41220	260	44990	44450	45270	44190				Not modelled - near backfill - context uncertain
1745	ETH-71327	0.0059	0.0002	41170	260	44950	44410	45230	44140				
1746	*	0.0055	0.0002	41850	280	45510	44950	45790	44680				
1747	ETH-71329	0.0055	0.0002	41730	280	45410	44860	45700	44580				
1748	ETH-71330	0.0052	0.0002	42270	300	45850	45270	46170	44990				
1749	ETH-71331	0.0059	0.0002	41200	260	44970	44440	45260	44170				
1750													

New ^{14}C chronology for Middle–to–Upper Palaeolithic transition at Bacho Kiro Cave, Bulgaria

Supplementary Table 2. Sample information of all bones from Bacho Kiro Cave extracted in the radiocarbon study.

R-EVA	Sample Info											Sample Size			Quality checks			
	Excavation year	Pretreatment year	Sample ID	Layer	Material	ZooMS ID	Peptide markers	P1105	P1706	Species (ZooMS)	Anth. Mod.	Bone sampled [mg]	Collagen yld [mg]	Collagen yld (%)	%C	%N	C:N	FTIR
2663	2016	2017	CC7-2289	N1-I	bone	BK-505	9			Hominin	-	89.6	3.8	4.2	42.7	15.9	3.1	collagen
2664	2016	2017	CC7-335	N1-I	bone	BK-602	9	0.87	0.66	Hominin	-	109.7	13	11.9	42.7	16.0	3.1	collagen
2281	2017	2017	A7-528	N1-I	long bone	BK-1230	7	0.78	0.66	Ursidae	Cut-marks	500.8	44.2	8.8	44.2	16.3	3.2	collagen
2282	2017	2017	A7-531	N1-I	long bone	BK-1231	8	0.78	0.65	Ursidae	Cut-marks	431.4	47.8	11.1	46.1	16.9	3.2	collagen
2283	2017	2017	AA7-1488	N1-I	long bone	BK-1232	9	0.77	0.71	Bos/Bison	Cut-marks	501.8	31.6	6.3	44.3	16.4	3.1	collagen
2284	2016	2017	AA7-1186	N1-I	long bone	BK-1241	7	0.78	0.66	Ursidae	Cut-marks	517.0	72.1	13.9	46.4	17.1	3.2	collagen
2285	2016	2017	AA7-158	N1-I	long bone	BK-1233	9	0.76	0.73	Bos/Bison	Chisel + retoucher	410.4	25.9	6.3	44.5	16.5	3.1	collagen
2661	2016	2017	AA7-738	N1-I	bone	BK-459	9	0.83	0.71	Hominin	-	81.4	10	12.3	44.0	16.4	3.1	collagen
2662	2016	2017	BB7-240	N1-I	bone	BK-473	8	0.77	0.6	Hominin	-	80.2	7.2	9.0	44.4	16.5	3.1	collagen
2286	2017	2017	BB7-1164	N1-I	bone	BK-1242	9	0.77	0.74	Bos/Bison	Cut-marks	477.1	59.3	12.4	47.2	17.4	3.2	collagen
2287	2016	2017	BB7-962	N1-I	long bone	BK-1234	9	0.79	0.75	Bos/Bison	Cut-marks + impact fracture	514.0	45.1	8.8	46.1	17.0	3.2	collagen
2288	2017	2017	AA8-628	N1-I	flat bone	BK-1236	9	0.79	0.77	Bos/Bison	Cut-marks	520.0	23	4.4	48.6	17.9	3.2	collagen
2289	2017	2017	AA8-1047	N1-I	long bone	BK-1235	8	0.82	0.73	Bos/Bison	Cut-marks	537.5	58.3	10.8	46.2	17.1	3.2	collagen
2290	2017	2017	BB8-207	N1-I	long bone	BK-1237	8	0.8	0.63	Ursidae	Retoucher + cut-marks + large impact fracture	466.2	40.5	8.7	46.2	17.2	3.1	collagen
2291	2017	2017	BB8-674	N1-I	long bone	BK-1238	8	0.76	0.61	Ursidae	Cut-marks	196.8	27.3	13.9	46.0	17.0	3.2	collagen
2292	2017	2017	CC8-401	N1-I	long bone	BK-1240	9	0.83	0.79	Bos/Bison	-	610.5	71.3	11.7	46.9	17.3	3.2	collagen
2293	2017	2017	CC8-777	N1-I	long bone	BK-1239	8	0.78	0.55	Equidae	Cut-marks	403.0	33.6	8.3	47.4	17.4	3.2	collagen
2294	2017	2017	CC8-442	N1-I	long bone	BK-1243	9	0.77	0.75	Bos/Bison	Cut-marks	551.5	48.1	8.7	48.5	17.8	3.2	collagen
2295	2017	2017	A7-777	N1-I/J	long bone	BK-1244	9	0.84	0.82	Bos/Bison	Cut-marks	491.5	39.8	8.1	45.9	16.9	3.2	collagen
2296	2017	2017	BB7-1309	N1-I/J	bone (scapula)	BK-1245	9	0.79	0.75	Capra sp.	Cut-marks	545.2	53.5	9.8	45.6	16.9	3.1	collagen
2297	2017	2017	AA7-1419	N1-I/J	long bone	BK-1246	7	0.75	0.62	Equidae	-	575.6	67.8	11.8	46.5	17.1	3.2	collagen

New ^{14}C chronology for Middle–to–Upper Palaeolithic transition at Bacho Kiro Cave, Bulgaria

Supplementary Table 2. Sample information of all bones from Bacho Kiro Cave extracted in the radiocarbon study.

R-EVA	ETH ^{14}C dates					Calibrated range (NO model)				MAMS ^{14}C dates			Notes
	AMS lab number	F^{14}C	error	^{14}C age	1σ error	1σ (68.2%) (cal BP)		2σ (95.4%) (cal BP)		AMS lab number	^{14}C age	1σ error	
					years	from	to	from	to		BP	years	
2663	ETH-86771	0.0064	0.0003	40600	420	44580	43720	44980	43340				
2664	ETH-86772	0.0051	0.0003	42450	510	46190	45250	46790	44830				
2281													
2282													
2283													
2284													
2285	ETH-86779	0.0078	0.0002	38940	240	43000	42620	43200	42440				
2661	ETH-86769	0.0071	0.0003	39750	380	43760	43050	44210	42810				
2662	ETH-86770	0.0055	0.0003	41850	480	45660	44800	46130	44400				
2286	ETH-86780	0.0063	0.0002	40760	290	44640	44010	44930	43660				
2287													
2288													
2289	ETH-86782	0.0071	0.0002	39710	260	43600	43080	43950	42890				
2290	ETH-86783	0.0066	0.0002	40340	280	44240	43600	44520	43320				
2291													
2292													
2293													
2294	ETH-86784	0.0056	0.0002	41660	320	45380	44770	45690	44480				
2295	ETH-86785	0.0073	0.0002	39570	260	43470	42990	43810	42790				not modelled - contact zone
2296	ETH-86786	0.0055	0.0002	41740	320	45450	44840	45760	44540				not modelled - contact zone
2297													

New ^{14}C chronology for Middle–to–Upper Palaeolithic transition at Bacho Kiro Cave, Bulgaria

Supplementary Table 2. Sample information of all bones from Bacho Kiro Cave extracted in the radiocarbon study.

R-EVA	Sample Info											Sample Size			Quality checks			
	Excavation year	Pretreatment year	Sample ID	Layer	Material	ZooMS ID	Peptide markers	P1105	P1706	Species (ZooMS)	Anth. Mod.	Bone sampled [mg]	Collagen yld [mg]	Collagen yld (%)	%C	%N	C:N	FTIR
2303	2017	2017	AA7-2126	N1-J upper	bone	BK-1251	9	0.78	0.62	Ursidae	-	623.0	42.6	6.8	45.3	17.0	3.1	collagen
2304	2017	2017	AA7-2128	N1-J upper	bone	BK-1253	9	0.82	0.74	Cervid/Saiga	-	520.6	57.2	11.0	44.9	16.9	3.1	collagen
2302	2017	2017	BB7-1453	N1-J mid	long bone	BK-1252	9	0.75	0.61	Ursidae	Cut-marks	440.9	39.4	8.9	45.6	16.9	3.1	collagen
2298	2017	2017	CC7-2607	N1-J lower	bone	BK-1247	7	0.75	0.6	Equidae	Cut-marks	446.7	54.6	12.2	46.6	17.1	3.2	collagen
2301	2017	2017	BB7-1471	N1-J lower	long bone	BK-1250	9	0.71	0.57	Ursidae	-	494.9	69.7	14.1	46.4	17.1	3.2	collagen
2299	2017	2017	CC7-2670	N1-J lower	long bone	BK-1248	8	0.71	0.55	Ursidae	Cut-marks + impact fracture	498.3	63	12.6	45.8	16.7	3.2	collagen
2300	2017	2017	CC7-2677	N1-J lower	long bone	BK-1249	9	0.66	0.59	Cervid/Saiga	-	457.1	45	9.8	48.0	17.5	3.2	collagen
2305	2017	2017	CC7-2699	N1-J/K contact	long bone	BK-1256	7	0.66	0.46	Ursidae	-	611.4	69.1	11.3	44.8	16.8	3.1	collagen
2306	2017	2017	CC7-2697	N1-J/K contact	bone	BK-1254	9	0.72	0.65	Capra sp.	-	497.2	47.1	9.5	45.4	17.0	3.1	collagen
2307	2017	2017	CC7-2700	N1-J/K contact	bone (rib)	BK-1257	9	0.72	0.68	Capra sp.	-	592.5	38.8	6.5	44.0	16.5	3.1	collagen
2308	2017	2017	CC7-2701	N1-J/K contact	long bone	BK-1255	9	0.72	0.53	Ursidae	-	571.9	70.1	12.3	45.3	16.9	3.1	collagen
2309	2017	2017	CC7-2724	N1-K	long bone	BK-1262	9	0.67	0.6	Cervid/Saiga	-	536.9	50.4	9.4	46.2	17.1	3.2	collagen
2310	2017	2017	CC7-2729	N1-K	long bone	BK-1260	9	0.68	0.59	Cervid/Saiga	-	431.0	35.7	8.3	46.0	17.3	3.1	collagen
2311	2017	2017	CC7-2750	N1-K	long bone	BK-1261	9	0.68	0.61	Bos/Bison	Cut-marks	474.2	29	6.1	44.8	16.8	3.1	collagen
2312	2017	2017	CC7-2738	N1-K	bone	BK-1258	9	0.64	0.63	Bos/Bison	-	541.2	48.4	8.9	44.4	16.7	3.1	collagen
2313	2017	2017	CC7-2766	N1-K	bone	BK-1259	9	0.71	0.71	Bos/Bison	-	500.6	54	10.8	45.9	17.2	3.1	collagen

New ^{14}C chronology for Middle–to–Upper Palaeolithic transition at Bacho Kiro Cave, Bulgaria

Supplementary Table 2. Sample information of all bones from Bacho Kiro Cave extracted in the radiocarbon study.

R-EVA	ETH ^{14}C dates					Calibrated range (NO model)				MAMS ^{14}C dates			Notes
	AMS lab number	F^{14}C	error	^{14}C age	1σ error	1σ (68.2%) (cal BP)		2σ (95.4%) (cal BP)		AMS lab number	^{14}C age	1σ error	
					years	from	to	from	to		BP	years	
2303	ETH-93193	0.0070	0.0002	39890	280	43800	43210	44150	43000				
2304	ETH-93194	0.0049	0.0002	42670	370	46250	45530	46690	45200				
2302	ETH-86789	0.0048	0.0002	42900	370	46460	45700	46940	45380				
2298	ETH-86787	0.0037	0.0002	44890	450	48870	47630	49500	47080				
2301	ETH-93196	0.0036	0.0002	45120	490	49190	47900	49790	47330				
2299	ETH-86788	0.0011	0.0002	>51,000									Near backfill - context uncertain. Not modelled - beyond range
2300	ETH-93195	0.0008	0.0002	>51,000									Not modelled - beyond range
2305													
2306													
2307	ETH-93197	0.0009	0.0002	>51,000									Not modelled - beyond range
2308	ETH-86790	0.00114	0.0002	>51,000									Not modelled - beyond range
2309	ETH-86791	0.00034	0.0002	>51,000									Not modelled - beyond range
2310	ETH-86792	0.00086	0.0002	>51,000									Not modelled - beyond range
2311	ETH-86793	0.00063	0.0002	>51,000									Not modelled - beyond range
2312	ETH-86794	0.00057	0.0002	>51,000									Not modelled - beyond range
2313	ETH-86795	0.00041	0.0002	>51,000									Not modelled - beyond range

indet = indeterminable

All radiocarbon dates are rounded to the nearest 10 years.

New ^{14}C chronology for Middle–to–Upper Palaeolithic transition at Bacho Kiro Cave, Bulgaria

Supplementary Table 3. Comparison of outlier analysis and agreement index of three models from Bacho Kiro Cave

Name (^{14}C date, error)		Calibrated ranges: NO MODEL (cal BP)				Model 1 - Main Profile (cal BP)						Model 2 - Niche 1 (cal BP)						Model 3 - combined areas (cal BP)					
		68.2%		95.4%		68.2%		95.4%				68.2%		95.4%				68.2%		95.4%			
	O	from	to	from	to	from	to	from	to	O	A	from	to	from	to	O	A	from	to	from	to	O	A
End Layer A1						**35180**	**26180**	**35240**	**22540**									**35170**	**26580**	**35250**	**22990**		
Layer A1																							
ETH-86796 (23130,60)	0.05	27520	27340	27610	27250	35100	27300	35300	27140	60	45							35110	27320	35260	27190	63	42
MAMS-27346 (31340,120)	0.05	35380	35010	35570	34860	35110	34800	35310	31960	21	51.7							35100	34830	35290	33680	14	58
ETH-86797 (34290,150)	0.05	38930	38570	39150	38420	35180	34080	35270	31220	100	5.6							35180	34460	35310	31710	100	5.5
Transition Layer A2/Layer A1						**35140**	**34900**	**35290**	**34600**									**35140**	**34910**	**35280**	**34720**		
Layer A2																							
ETH-71296 (30950,80)	0.05	34960	34710	35070	34600	35160	34940	35290	34790	8	43.8							35170	34950	35290	34820	8	39
ETH-71295 (31310,80)	0.05	35320	35000	35490	34870	35200	35000	35310	34910	1	119							35200	35010	35310	34920	1	121
ETH-71294 (31410,80)	0.05	35430	35110	35590	34970	35210	35010	35330	34930	2	88							35210	35010	35330	34930	1	89
Transition Layer B/Layer A2						**35280**	**35050**	**35430**	**34970**									**35280**	**35050**	**35440**	**34970**		
Layer B																							
ETH-71299 (30570,80)	0.05	34680	34400	34790	34250	36260	35160	37280	35050	100	5.6							36230	35190	37150	35040	100	5.5
ETH-71298 (31310,80)	0.05	35320	35000	35490	34870	35440	35160	35720	35000	6	84.1							35430	35160	35800	35000	7	84
ETH-86773/AIX-12025 (31660,140) (hominin)	0.05	35750	35340	35970	35140	35760	35360	35990	35190	3	106							35760	35360	35980	35190	2	106
ETH-71297 (32500,90)	0.05	36500	36230	36670	36110	36490	36230	36680	36080	3	104							36490	36230	36680	36080	3	104
ETH-71300 (32610,90)	0.05	36620	36320	36810	36210	36590	36300	36820	36170	3	104							36590	36300	36810	36170	3	105
Transition Layer C/Layer B						**37630**	**36370**	**39000**	**36330**									**37570**	**36370**	**38980**	**36330**		
Layer C																							
ETH-71302 (34690,110)	0.05	39380	38960	39590	38800	39400	38960	39660	38750	4	101							39390	38970	39650	38760	3	101
ETH-71305 (35030,110)	0.05	39790	39390	39970	39180	39790	39370	40020	39130	4	102							39800	39380	40010	39130	3	102
ETH-71304 (36230,120)	0.05	41120	40700	41290	40470	41100	40650	41320	40370	4	99.8							41100	40650	41330	40360	4	100
ETH-71303/MAMS-29490 (41720,180)	0.05	45350	44900	45570	44690	41760	39880	42050	38120	100	5.5							41730	39810	42020	37820	100	5.5
Transition Layer D/Layer C						**41970**	**41170**	**42200**	**40730**									**41960**	**41150**	**42200**	**40710**		
Layer D																							
ETH-86798 (37510,210)	0.05	42100	41750	42270	41560	42150	41790	42340	41590	3	102							42150	41780	42340	41590	2	102
Transition Layer E/Layer D						**42930**	**42450**	**43010**	**42010**									**42930**	**42460**	**43020**	**42030**		
Layer E																							
ETH-71307/MAMS-29489 (36500,110)	1.00	41360	41010	41510	40790	43070	42680	43230	42260	100	5.6							43070	42690	43240	42290	100	5.6
ETH-71308 (38720,160)	0.05	42820	42520	42980	42380	42960	42660	43060	42490	2	87.4							42960	42670	43060	42490	2	87
ETH-71310 (39080,170)	0.05	43060	42730	43220	42580	43020	42780	43130	42640	1	118							43020	42780	43130	42640	1	118

New ^{14}C chronology for Middle–to–Upper Palaeolithic transition at Bacho Kiro Cave, Bulgaria

Supplementary Table 3. Comparison of outlier analysis and agreement index of three models from Bacho Kiro Cave

Name (^{14}C date, error)		Calibrated ranges: NO MODEL (cal BP)				Model 1 - Main Profile (cal BP)						Model 2 - Niche 1 (cal BP)						Model 3 - combined areas (cal BP)					
		68.2%		95.4%		68.2%		95.4%				68.2%		95.4%				68.2%		95.4%			
	O	from	to	from	to	from	to	from	to	O	A	from	to	from	to	O	A	from	to	from	to	O	A
ETH-71309 (39310,160)	0.05	43200	42880	43370	42720	43060	42830	43200	42710	1	106							43060	42830	43200	42710	1	107
ETH-71306/MAMS-28675 (39470,160)	0.05	43320	42980	43510	42810	43090	42850	43250	42740	3	83.3							43100	42850	43250	42740	2	84
Transition Layer F/Layer E						**43210**	**42920**	**43410**	**42820**									**43210**	**42920**	**43410**	**42820**		
Layer F																							
ETH-86799 (39090,240)	0.05	43100	42710	43310	42530	43350	43020	43630	42900	8	53.1							43350	43020	43630	42890	8	53
ETH-86801 (39370,260)	0.05	43310	42860	43590	42660	43440	43070	43680	42950	2	91.6							43440	43070	43680	42950	2	92
ETH-71311 (40170,180)	0.05	44000	43490	44250	43290	43800	43400	44030	43240	2	104							43800	43400	44010	43240	2	104
ETH-71312/MAMS-28676 (40190,170)	0.05	44020	43520	44260	43320	43810	43410	44030	43260	2	102							43810	43410	44030	43260	2	102
ETH-86800 (40250,270)	0.05	44150	43520	44440	43260	43820	43370	44070	43210	2	101							43820	43370	44060	43210	2	101
Transition Layer G/Layer F						**44120**	**43640**	**44350**	**43430**			**44090**	**42380**	**44310**	**41190**			**44100**	**43630**	**44340**	**43430**		
Layer G																							
ETH-86777 (40270,280)	1.00	44180	43530	44470	43270							44230	43140	44540	42220	100	101	44310	43830	44550	43610	100	101
ETH-86802 (40470,280)	1.00	44370	43720	44640	43410	44340	43870	44530	43640	100	102							44310	43830	44550	43610	100	101
ETH-86804 (40800,290)	1.00	44680	44040	44970	43690	44350	43880	44540	43640	100	102							44310	43830	44560	43620	100	101
ETH-71313 (40870,190)	1.00	44660	44190	44900	43930							44250	43170	44550	42280	100	100	44310	43830	44550	43620	100	100
ETH-86806 (41040,300)	1.00	44880	44270	45190	43930	44350	43880	44540	43640	100	101							44310	43840	44550	43620	100	101
Transition Layer I/Layer G						**44540**	**44120**	**44700**	**43860**			**44400**	**43670**	**44690**	**43010**			**44510**	**44030**	**44770**	**43830**		
Layer I																							
ETH-86779 (38940,240)	0.05	43000	42620	43200	42440							45130	44070	45520	42990	94	8	44980	44370	45210	44080	100	5.5
ETH-86782 (39710,260)	0.05	43610	43080	43950	42880							44850	43680	45340	43340	44	23	44920	44190	45160	43930	72	6
ETH-86769 (39750,380) (hominin)	0.05	43760	43050	44210	42810							44590	43790	45210	43380	20	35	44770	44160	45070	43950	33	12
ETH-86783 (40340,280)	0.05	44240	43600	44520	43320							44550	43940	44940	43600	7	79	44680	44180	44940	43990	10	49
ETH-86771 (40600,420) (hominin)	0.05	44580	43720	44980	43340							44770	44080	45130	43730	3	100	44840	44310	45050	44060	3	90
ETH-86807 (40710,290)	0.05	44600	43950	44890	43600	44660	44310	44820	44100	2	109							44780	44300	44980	44080	3	94
ETH-86809 (40750,290)	0.05	44630	43990	44930	43640	44670	44320	44830	44110	2	115							44790	44320	44990	44090	2	98
ETH-86780 (40760,290)	0.05	44640	44000	44940	43650							44730	44160	45030	43870	2	104	44800	44330	44990	44090	2	99
ETH-71316 (40790,250)	0.05	44640	44070	44910	43750							44710	44190	44990	43910	2	104	44770	44320	44970	44110	2	100
ETH-86810 (40920,300)	0.05	44790	44150	45100	43810	44690	44340	44850	44150	1	129							44860	44390	45060	44150	2	111
ETH-71318 (41080,260)	0.05	44880	44330	45170	44050							44900	44380	45170	44120	2	106	44890	44450	45090	44240	1	114
ETH-71327 (41170,260)	0.05	44950	44410	45240	44140							44960	44440	45230	44200	2	106	44930	44500	45120	44290	1	115

New ^{14}C chronology for Middle–to–Upper Palaeolithic transition at Bacho Kiro Cave, Bulgaria

Supplementary Table 3. Comparison of outlier analysis and agreement index of three models from Bacho Kiro Cave

Name (^{14}C date, error)		Calibrated ranges: NO MODEL (cal BP)				Model 1 - Main Profile (cal BP)						Model 2 - Niche 1 (cal BP)						Model 3 - combined areas (cal BP)					
		68.2%		95.4%		68.2%		95.4%				68.2%		95.4%				68.2%		95.4%			
	O	from	to	from	to	from	to	from	to	O	A	from	to	from	to	O	A	from	to	from	to	O	A
ETH-71331 (41200,260)	0.05	44980	44430	45260	44170							44980	44460	45240	44220	2	106	44940	44510	45130	44300	1	116
ETH-71322/MAMS-29483 (41220,210)	0.05	44960	44480	45210	44260							44960	44500	45200	44280	2	105	44940	44530	45120	44340	1	113
ETH-71315/MAMS-28677 (41310,180)	0.05	45010	44570	45230	44360							45010	44580	45230	44370	2	105	44970	44590	45140	44410	1	113
ETH-86808 (41350,310)	0.05	45130	44520	45450	44230	44730	44400	44910	44230	2	96.6							45020	44580	45200	44350	1	119
ETH-71320 (41450,270)	0.05	45180	44630	45460	44370							45160	44640	45390	44390	2	108	45050	44640	45220	44420	1	116
ETH-71325 (41480,270)	0.05	45210	44650	45490	44390							45180	44670	45400	44410	2	108	45060	44650	45230	44430	1	116
ETH-86784 (41660,320)	0.05	45390	44770	45700	44470							45290	44770	45500	44480	2	111	45110	44700	45270	44480	2	108
ETH-71329 (41730,280)	0.05	45420	44850	45700	44580							45320	44840	45520	44570	2	110	45130	44740	45290	44540	2	101
ETH-71314 (41770,210)	0.05	45400	44920	45640	44700							45320	44900	45510	44670	2	109	45140	44790	45290	44620	2	94
ETH-71324/MAMS-28681 (41820,250)	0.05	45470	44940	45730	44690							45350	44910	45550	44660	2	109	45150	44790	45310	44600	3	89
ETH-86770 (41850,480) (hominin)	0.05	45660	44800	46130	44400							45370	44780	45590	44420	2	113	45130	44680	45290	44420	3	99
ETH-71328 (41850,280)	0.05	45510	44950	45790	44670							45370	44910	45560	44640	2	109	45150	44780	45310	44580	3	87
ETH-71323/MAMS-28680 (41950,250)	0.05	45570	45040	45830	44800							45390	44980	45590	44730	3	106	45170	44820	45330	44630	4	71
ETH-71330 (42270,300)	0.05	45860	45260	46180	44980							45470	45050	45700	44780	5	82	45210	44850	45380	44590	13	33
ETH-86772 (42450,510) (hominin)	0.05	46190	45250	46790	44830							45480	44970	45700	44610	5	76	45180	44780	45350	44520	9	37
Transition Layer J/Layer I						**44890**	**44530**	**45060**	**44370**			**45630**	**45260**	**45850**	**45090**			**45320**	**45010**	**45440**	**44830**		
Layer J																							
ETH-93193 (39890,280)	0.05	43800	43200	44160	43000							46760	45360	48280	45190	100	5.3	45770	45090	47290	44890	100	5.3
ETH-86819 (41230,310)	0.05	45040	44420	45360	44120	45060	44700	45260	44540	2	114							45460	45100	45900	44820	12	34
ETH-86820 (41540,320)	0.05	45290	44670	45600	44380	45110	44730	45340	44580	1	124							45490	45130	45760	44930	4	78
ETH-86821 (41630,320)	0.05	45360	44740	45670	44450	45130	44740	45370	44590	2	119							45500	45150	45770	44950	4	91
ETH-86822 (41670,320)	0.05	45400	44770	45710	44480	45130	44750	45380	44590	2	116							45510	45150	45780	44960	3	96
ETH-93194 (42670,370)	0.05	46250	45520	46700	45190							46260	45610	46760	45380	3	107	45930	45240	46500	45110	3	89
ETH-86789 (42900,370)	0.05	46460	45700	46950	45370							46460	45730	46990	45460	3	105	46080	45240	46710	45130	5	75
ETH-86787 (44890,450)	0.05	48880	47630	49500	47080							48530	47330	49240	46670	6	96	48040	45120	48670	45030	57	41
ETH-93196 (45120,490)	0.05	49190	47890	49790	47330							48680	47400	49500	46700	7	89	48130	45120	48790	45030	59	34
Start Layer J						**45390**	**44850**	**45890**	**44660**			**49530**	**47790**	**51360**	**47030**			**48600**	**45210**	**49360**	**45140**		

O - Posterior outlier probability

A - Individual Agreement indices

New ^{14}C chronology for Middle–to–Upper Palaeolithic transition at Bacho Kiro Cave, Bulgaria

Supplementary Table 4. Comparison of model output for Bacho Kiro Cave chronology (outliers excluded)

Name	Unmodelled (BP)				Model 1 - Main profile					Model 2 - Niche-1					Model 3 - combined				
	Modelled (BP)								A_{model}	Modelled (BP)				A_{model}	Modelled (BP)				A_{model}
	68.2		95.4		68.2		95.4		83.7	68.2		95.4		78.9	68.2		95.4		33.2
	from	to	from	to	from	to	from	to	A	from	to	from	to	A	from	to	from	to	A
End Layer A2					**35070**	**34730**	**35190**	**34340**							**35070**	**34690**	**35170**	**34190**	
Layer A2																			
ETH-71296 (30950,80)	34960	34710	35070	34600	35090	34850	35180	34710	74.5						35080	34830	35170	34700	78.6
ETH-71295 (31310,80)	35320	35000	35490	34870	35180	34970	35290	34870	105.9						35180	34970	35290	34870	105.2
ETH-71294 (31410,80)	35430	35110	35590	34970	35200	34990	35320	34900	78.1						35210	34990	35330	34890	78.4
Transition Layer B/Layer A2					**35300**	**35060**	**35430**	**34960**							**35310**	**35060**	**35440**	**34970**	
Layer B																			
ETH-71298 (31310,80)	35320	35000	35490	34870	35440	35180	35570	35070	81.9						35450	35180	35570	35080	80.7
ETH-86773/AIX-12025 (31660,140) (hominin)	35750	35340	35970	35140	35750	35360	35960	35210	104.1						35750	35370	35960	35210	104.2
ETH-71297 (32500,90)	36500	36230	36670	36110	36490	36230	36650	36110	101.6						36490	36230	36650	36110	101.7
ETH-71300 (32610,90)	36620	36320	36810	36210	36590	36310	36770	36200	102.2						36590	36310	36770	36200	102.2
Transition Layer C/Layer B					**37650**	**36380**	**38990**	**36340**							**37650**	**36380**	**39000**	**36340**	
Layer C																			
ETH-71302 (34690,110)	39380	38960	39590	38800	39390	38970	39600	38800	99.8						39390	38970	39600	38800	99.8
ETH-71305 (35030,110)	39790	39390	39970	39180	39790	39380	39970	39180	100						39790	39380	39970	39180	100
ETH-71304 (36230,120)	41120	40700	41290	40470	41080	40650	41250	40430	98.3						41080	40650	41250	40430	98.3
Transition Layer D/Layer C					**41840**	**41040**	**42100**	**40710**							**41840**	**41040**	**42100**	**40700**	
Layer D																			
ETH-86798 (37510,210)	42100	41750	42270	41560	42130	41780	42300	41600	100.1						42130	41780	42300	41600	100
Transition Layer E/Layer D					**42940**	**42540**	**43030**	**42120**							**42940**	**42550**	**43020**	**42130**	
Layer E																			
ETH-71308 (38720,160)	42820	42520	42980	42380	42970	42700	43050	42520	80.4						42970	42700	43050	42530	79.9
ETH-71310 (39080,170)	43060	42730	43220	42580	43010	42790	43120	42660	115.9						43010	42790	43110	42660	116.6
ETH-71309 (39310,160)	43200	42880	43370	42720	43050	42830	43170	42720	102						43040	42830	43160	42720	101.1
ETH-71306/MAMS-28675 (39470,160)	43320	42980	43510	42810	43070	42850	43200	42750	76						43060	42840	43180	42750	73.8
Transition Layer F/Layer E					**43170**	**42920**	**43330**	**42820**							**43150**	**42910**	**43300**	**42820**	
Layer F																			
ETH-86799 (39090,240)	43100	42710	43310	42530	43310	43010	43510	42900	59						43290	43010	43490	42900	61.5
ETH-86801 (39370,260)	43310	42860	43590	42660	43410	43050	43670	42930	93.5						43400	43040	43670	42930	94.9
ETH-71311 (40170,180)	44000	43490	44250	43290	43900	43450	44120	43280	104.2						43960	43490	44170	43300	104.2
ETH-71312/MAMS-28676 (40190,170)	44020	43520	44260	43320	43910	43470	44130	43300	103.6						43980	43520	44170	43330	104.2
ETH-86800 (40250,270)	44150	43520	44440	43260	43950	43440	44200	43250	104.4						44050	43510	44240	43270	106.9

New ^{14}C chronology for Middle–to–Upper Palaeolithic transition at Bacho Kiro Cave, Bulgaria

Supplementary Table 4. Comparison of model output for Bacho Kiro Cave chronology (outliers excluded)

Name	Unmodelled (BP)				Model 1 - Main profile					Model 2 - Niche-1					Model 3 - combined				
					Modelled (BP)				A_{model}	Modelled (BP)				A_{model}	Modelled (BP)				A_{model}
	68.2		95.4		68.2		95.4		83.7	68.2		95.4		78.9	68.2		95.4		33.2
	from	to	from	to	from	to	from	to	A	from	to	from	to	A	from	to	from	to	A
Transition Layer I/Layer F					**44350**	**43850**	**44560**	**43600**		**44390**	**43940**	**44580**	**43650**		**44390**	**44030**	**44570**	**43830**	
Layer I																			
ETH-86769 (39750,380) (hominin)	43760	43050	44210	42810						44540	44070	44800	43800	19.6	44540	44130	44800	43950	13.8
ETH-86783 (40340,280)	44240	43600	44520	43320						44560	44110	44790	43860	66.5	44560	44170	44800	43990	57.8
ETH-86771 (40600,420) (hominin)	44580	43720	44980	43340						44750	44170	45100	43930	96.2	44750	44240	45030	44050	94.9
ETH-86807 (40710,290)	44600	43950	44890	43600	44600	44180	44780	43950	114.1						44690	44240	44940	44060	101.1
ETH-86809 (40750,290)	44630	43990	44930	43640	44610	44200	44790	43960	116.3						44710	44260	44960	44080	103.8
ETH-86780 (40760,290)	44640	44000	44940	43650						44710	44220	44990	43990	104.2	44710	44260	44960	44080	104.4
ETH-71316 (40790,250)	44640	44070	44910	43750						44690	44240	44950	44020	104.7	44700	44270	44930	44090	105
ETH-86810 (40920,300)	44790	44150	45100	43810	44650	44250	44830	44020	120						44800	44320	45040	44140	110.5
ETH-71318 (41080,260)	44880	44330	45170	44050						44880	44390	45150	44180	105.1	44870	44410	45080	44220	109.4
ETH-71327 (41170,260)	44950	44410	45240	44140						44940	44440	45210	44230	104.2	44920	44460	45110	44270	109.5
ETH-71331 (41200,260)	44980	44430	45260	44170						44970	44460	45220	44250	104	44940	44480	45120	44280	109.6
ETH-71322/MAMS-29483 (41220,210)	44960	44480	45210	44260						44950	44490	45180	44300	102.5	44930	44510	45110	44320	107.1
ETH-71315/MAMS-28677 (41310,180)	45010	44570	45230	44360						45010	44570	45210	44380	101.6	44980	44590	45130	44400	106.7
ETH-86808 (41350,310)	45130	44520	45450	44230	44740	44360	44920	44170	88.5						45020	44560	45180	44330	112.8
ETH-71320 (41450,270)	45180	44630	45460	44370						45160	44640	45380	44400	104.3	45060	44640	45200	44410	111
ETH-71325 (41480,270)	45210	44650	45490	44390						45170	44660	45390	44420	104.5	45070	44660	45200	44430	110.8
ETH-86784 (41660,320)	45390	44770	45700	44470						45300	44780	45490	44490	107.6	45120	44720	45240	44470	104.8
ETH-71329 (41730,280)	45420	44850	45700	44580						45320	44850	45510	44580	107	45130	44770	45250	44550	98.8
ETH-71314 (41770,210)	45400	44920	45640	44700						45330	44920	45500	44690	106	45140	44830	45260	44640	93
ETH-71324/MAMS-28681 (41820,250)	45470	44940	45730	44690						45350	44920	45530	44680	106.6	45150	44820	45260	44620	88.2
ETH-86770 (41850,480) (hominin)	45660	44800	46130	44400						45380	44790	45570	44440	110.2	45130	44700	45250	44410	94.7
ETH-71328 (41850,280)	45510	44950	45790	44670						45360	44920	45550	44660	106.8	45150	44820	45270	44600	85.8
ETH-71323/MAMS-28680 (41950,250)	45570	45040	45830	44800						45390	44990	45570	44760	104.2	45160	44860	45280	44670	70.3
ETH-71330 (42270,300)	45860	45260	46180	44980						45460	45070	45650	44860	82.3	45180	44900	45290	44720	31.2
ETH-86772 (42450,510) (hominin)	46190	45250	46790	44830						45470	45000	45670	44680	76	45180	44830	45300	44580	35.9
Transition Layer J/Layer I					**44920**	**44560**	**45090**	**44380**		**45620**	**45280**	**45830**	**45130**		**45260**	**45040**	**45370**	**44920**	
Layer J																			
ETH-86819 (41230,310)	45040	44420	45360	44120	45060	44710	45240	44550	111						45420	45120	45630	44990	32.5
ETH-86820 (41540,320)	45290	44670	45600	44380	45090	44730	45300	44570	120.8						45490	45140	45740	45010	73.6
ETH-86821 (41630,320)	45360	44740	45670	44450	45100	44740	45320	44580	115.1						45510	45140	45780	45020	84.8
ETH-86822 (41670,320)	45400	44770	45710	44480	45110	44740	45330	44580	111.5						45520	45150	45800	45020	89.3
ETH-93194 (42670,370)	46250	45520	46700	45190						46250	45610	46690	45390	105.3	46250	45530	46660	45240	101.4
ETH-86789 (42900,370)	46460	45700	46950	45370						46450	45730	46930	45480	103.1	46450	45690	46930	45390	100.5
ETH-86787 (44890,450)	48880	47630	49500	47080						48610	47450	49200	46930	100	48170	47100	48730	46670	81.3
ETH-93196 (45120,490)	49190	47890	49790	47330						48780	47560	49410	47020	95.1	48230	47130	48870	46690	67.6
Start Layer J					**45300**	**44840**	**45690**	**44660**		**49980**	**47930**	**52280**	**47280**		**48750**	**47410**	**49620**	**46940**	

Chapter six
Conclusion

Project 1

Testing the suitability of the MICADAS gas ion source for dating Palaeolithic collagen

We established a collaboration with Professor Edouard Bard and his team at CEREGE, Aix-Marseilles University, to test the accuracy, reproducibility and precision of the gas ion source of the AixMICADAS (Bard et al., 2015) to ^{14}C date small archaeological bone collagen samples. The pilot study in Chapter 2 represented the first use of a MICADAS gas ion source for dating archaeological bone collagen and for dating samples of Pleistocene age (Fewlass et al., 2017). The preliminary study was carried out on large collagen samples split into multiple aliquots. This was done to rule out any variation arising through pretreatment so we could focus the test on the instrumental accuracy, precision and reproducibility. We used three techniques of producing CO_2 from bone collagen to see what effect these had on the measurements. We determined that the optimal method of CO_2 production was the EA and zeolite trap directly coupled to the gas ion source (Wacker et al., 2013). The method is fast and automated, and the results indicated that the zeolite trap did not contribute to the instrumental background at the sample size measured. Measurements of ^{14}C from the gas ion source were statistically indistinguishable from measurements made with graphite targets. The first results demonstrated that the gas ion source system could produce accurate, reproducible results for sample sizes <100 µg C back to 35,000 ^{14}C BP (Fewlass et al., 2017).

Building on the successful preliminary tests of the gas ion source, further measurements were carried out on small collagen aliquots (<100 µg C) extracted from small pieces (40 – 80 mg) of bone at varying levels of collagen preservation (Chapter 3; Fewlass et al., 2019b). This was to test the gas ion source for a wider range of samples (age, collagen preservation), explore the effect of sample size reduction in the gas interface system and determine if the extraction of small bone aliquots produced accurate and consistent results.

In the expanded study, we reduced the C sample size to determine the effect on the background level of the EA-GIS-AMS system. We compared measurements of 30 µg C to 90 µg C measured over the duration of multiple titanium targets. At both 30 µg C and 90 µg C, the bone collagen

background ^{14}C measurements were equivalent to the instrument background level of equal size demonstrating that no significant carbon contamination resulted from the pretreatment. As expected, we saw a systematic effect on the background level with reduction in sample size, likely arising from the carbon contribution of the silver cups used to introduce the collagen into the EA. This can be accounted for by measuring background collagen samples of equal size to the unknown samples and using these measurements in the age correction. We observed a significant improvement in the instrumental background level of the EA-GIS-AMS system in the second study (0.4 pMC) compared to the pilot study (0.65 pMC) (see Table 6 in Chapter 2 compared to Supplementary Dataset S3 in Chapter 3). Following the pilot study, a leaking capillary in the gas interface system was identified and fixed, which improved the instrumental background level. The results reported in chapter 3 demonstrate that the limit of the gas ion source for dating samples is approximately 45,000 BP with any measurements older than this being infinite.

Although the precision achieved with the gas ion source is lower than graphite targets due to the lower ion currents, the level of precision now achievable with the MICADAS gas ion source is nevertheless useful for addressing archaeological questions, particularly for the Palaeolithic. For example, for mammoth collagen extract R-EVA 123.53, compare graphite date Aix-12003.1.1: 34390 ± 240 ^{14}C BP (988 µg C) with CO_2 date Aix-12003.10.4: 34550 ± 710 ^{14}C BP (98 µg C), measured from ten times less carbon (Fewlass et al., 2017; Fewlass et al., 2019b). In fact, the error ranges achieved with the gas ion source in these studies is similar to error ranges that have been quoted for graphite dates in the same time range over the past two decades (e.g. Trinkaus et al., 2003; Higham et al., 2011; Pleurdeau et al., 2016), although we are now moving towards unprecedented levels of precision from graphitised samples (see Chapter 4; Fewlass et al., in review).

The research described in chapters 2 and 3 clearly demonstrates the high level of accuracy and reproducibility of ^{14}C measurements with the gas ion source and the moderate level of precision which can be achieved. The results demonstrate the suitability of the gas ion source of the Aix-MICADAS for dating archaeological collagen in situations where sample material is limited (e.g. collagen yield of 1-3 mg).

Project 2

Pretreatment of <100 mg bone samples

The work detailed in Chapter 3 was undertaken in the labs at the MPI-EVA to optimize our standard collagen extraction protocol for <100 mg bone material (Fewlass et al., 2019b). Consistent yields of high quality collagen were obtained with the reduction of bone material from 500 mg to 100 mg to <50 mg. We confirmed previous observations that pretreatment of whole pieces of bone results in higher yields of collagen compared to pretreatment of powdered bone. This may imply that collagen is damaged by heat during the drilling of bone powder and/or is increasingly solubilised or lost during the various steps of pretreatment. The most significant alteration to our standard protocol for ~500 mg bone is a reduced duration of the gelatinisation step. Regular monitoring and removal of <100 mg samples from the heater block as soon as gelatinsation occurred resulted in higher collagen yields compared to leaving samples for 20 hours as per standard practice. This modification is more labour-intensive than the standard protocol, necessitating smaller numbers of samples to be prepared in tandem. However, the reduction in sample size and modifications to the pretreatment protocol means that collagen extraction and filtration of <100 mg bone can be completed in ~1 week compared to the ~2-4 weeks generally required for well preserved samples of ~500 mg bone.

Notably, the ^{14}C measurements of collagen extracts from 40-100 mg 'background' bone samples (>50,000 BP) indicate that no significant C contamination was introduced in the lab during pretreatment. This implies that the cleaning steps we routinely use for the ultrafilters sufficiently removed the humectant coating on the filter and no exogenous carbon was introduced to the >30 kDa gelatin fractions. Due to the high sensitivity of small samples to contamination, we pretreat three aliquots of the background bone (>50,000 BP) of varying sizes <100 mg alongside <100 mg samples (in order to achieve approximately the same amount of collagen as the samples) and measure them in the same batch to monitor lab based contamination.

The dates obtained from the small bone extracts were accurate and reproducible across the range of the ^{14}C timescale at various levels of collagen preservation. The dating results demonstrate that <100 mg bone samples can be successfully and consistently pretreated without introducing additional modern carbon contamination during lab work and handling, which is a key concern in the reduction of sample size.

Project 3

Pretreatment and dating of human remains from Dolní Věstonice II and Pavlov I, Czech Republic

The methods established during projects 1 and 2 were applied to small fragments of human bone from Dolní Věstonice II and Pavlov I, Czech Republic (Fewlass et al., 2019a). Extensive analysis of the human skeletal material from these sites has yielded fascinating insights into the morphology and behaviour of Gravettian populations. Human bones representing both ritual human burials and disarticulated remains were sampled for aDNA analysis in 2013, contributing a large amount of genetic information to the study of ancient European *Homo sapiens* populations (Fu et al., 2016).

Following their excavation in the 1950s and 1980s, the human remains were not directly dated in order to preserve the material from destructive analysis. However, small amounts of bone material were left over from seven individuals following the aDNA analysis in 2013. Very small aliquots of bone (37-203 mg) were sampled and pretreated using the methods described in chapter 3. Elemental and stable isotopic analysis indicated that samples were well preserved and analysis with FTIR did not show any sign of external contaminants, indicating that the extracts were suitable for ^{14}C dating. The collagen yields were sufficiently high for the ages to be cross-checked with both the gas ion source of the AixMICADAS and with solid graphite targets. The results confirm the Gravettian origin of the human bones and are in keeping with their archaeological context and previous ages obtained from the site. The replicate measurements are in agreement with each other and in some cases with dates on associated charcoals, lending confidence to their reliability. It appears that some charcoal samples from the site radiocarbon dated in the 1980s were affected by contamination, leading to underestimation of their ages. The study serves as further evidence of the suitability of the gas ion source for producing accurate results from small amounts of bone. The direct dates from the human remains will allow a more nuanced discussion of the occupation of these sites and, within a wider context, the chronology of occupation of the Middle Danube region during the Gravettian.

Project 4

Pretreatment and dating of small bone fragments from Bacho Kiro Cave, Bulgaria

A comprehensive program of radiocarbon dating was undertaken to establish a new, reliable site chronology for Bacho Kiro Cave, Bulgaria (Fewlass et al., in review). The latest methods and instrumentation in ^{14}C dating were applied to a large, high quality dataset of newly excavated material to produce a robust, reliable site chronology at exceptional levels of accuracy and precision. Ninety-five new AMS dates set the range of occupation at the site from >51,000 BP to ~35,000 cal BP, spanning the Middle to Upper Palaeolithic transition. The Initial Upper Palaeolithic (IUP) assemblage is now securely dated from 46,930-43,830 cal BP (95% probability).

The pretreatment methods established during the course of this research (chapter 3) were applied to six fragments of human bone excavated from Bacho Kiro Cave in 2016, four from the IUP layers and two from the Upper Palaeolithic layers. The bone fragments, identified through ZooMS screening, were characteristically small, leaving limited material available for direct radiocarbon dating and further molecular analysis (aDNA, palaeoproteomics). Small aliquots of the human bones (80-110 mg) were pretreated and the resulting high quality collagen extracts were dated, along with the fauna from the site, at exceptionally high precision with graphite targets at ETH Zurich in collaboration with Dr Lukas Wacker. The two human collagen extracts from the Upper Palaeolithic layers were dated with the gas ion source of the AixMICADAS to corroborate the graphite dates and further confirm the reliability of the CO_2 method, producing ages of 35,960 - 35,150 cal BP at 95% probability (F6-597; 31,660 ± 140 ^{14}C BP) and 34,810 - 34,210 cal BP at 95% probability (BK-1653; 30,570 ± 120 ^{14}C BP) (Fig. 4; Chapter 5).

The direct radiocarbon dates demonstrate that the four bone fragments from the IUP layer are the earliest remains of Upper Palaeolithic *Homo sapiens* known in Europe, dating between 46,790 - 42,810 cal BP (95% probability) in full agreement with the other dates from the IUP assemblage. Their secure association with a high density of IUP artefacts and the new robust site chronology make Bacho Kiro Cave crucial in the discussion of the early occupation of Europe by *Homo sapiens* in the Upper Palaeolithic (Hublin et al., in review).

NIR spectroscopy: a non-destructive pre-screening method for collagen preservation

We recently collaborated with Professor Matt Sponheimer (University of Colorado, Boulder) on a pilot study establishing a non-destructive method of assessing collagen preservation in bone using near infra-red (NIR) spectroscopy (Sponheimer et al., In press). This technique enables entirely non-destructive and fast pre-screening of bone to ascertain if sufficient collagen is preserved for radiocarbon dating. The proof-of-concept study demonstrates a high level of agreement between predicted and actual collagen yields following extraction with an error of prediction of ± 2%, which likely reflects the inter-lab reproducibility of replicate collagen extractions from a single bone (~1.7%). The NIR instrument is ruggedized and small enough to take as hand luggage during travel so the analysis can take place onsite at excavations or museums, circumnavigating the complex issue of exporting precious material or removing them from the safety of museums. This method was successfully utilized for the human burial remains from Dolní Věstonice II and Pavlov I, described in chapter 4. In future, this innovation will allow us to selectively sample bone where chances of successful collagen extraction are high and has profound implications for minimising destruction to precious bone artefacts.

Archaeological implications

We can successfully and reproducibly pretreat <100 mg Palaeolithic bone material for radiocarbon dating. When collagen extraction produces suitably high yields (>3mg), ^{14}C dates at very high precision can be achieved with graphite targets using the MICADAS AMS. When the extraction of extremely small amounts of bone material or low levels of preservation yield 1-3 mg collagen, the gas ion source of the MICADAS offers an accurate and reproducible method of ^{14}C measurement, but the quality of each sample should be carefully assessed before measurement on a case by case basis.

Using much smaller amounts of bone for radiocarbon dating (Fig. 1) greatly increases the possibilities for directly dating precious artefacts. The research described in this thesis contributes 13 more directly dated individuals to the collection of reliably dated Upper Palaeolithic *Homo sapiens*, including the earliest remains yet identified, in Europe (Fig. 2). By minimising sample destruction, these methodologies have great potential for further applications to small or precious bone artefacts with a high patrimonial value to address significant archaeological questions.

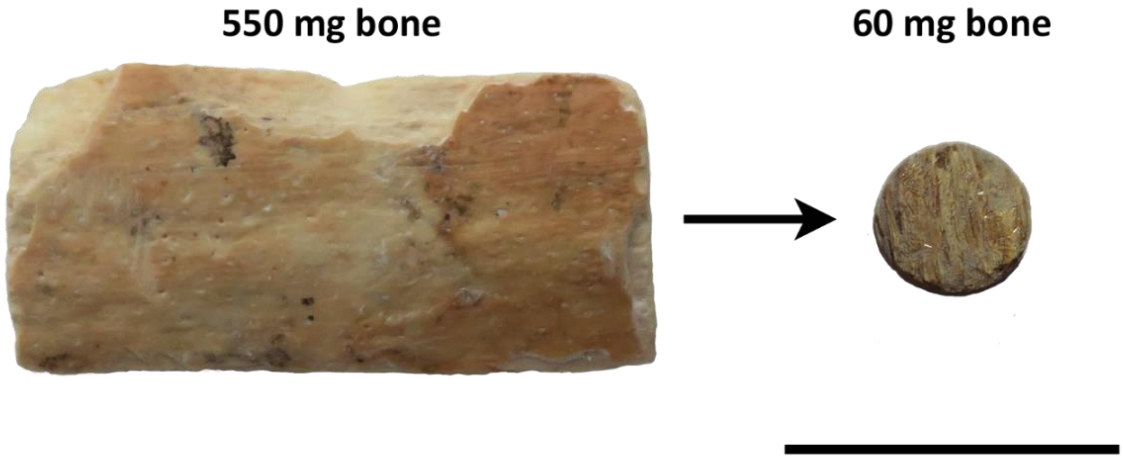

Figure 1. *Comparison of the amount of Palaeolithic bone material pretreated with our standard protocol (left) and with the method detailed in Chapter 3 that can be used to radiocarbon date small or precious bone samples (right). Scale bar is 1 cm.*

The Middle to Upper Palaeolithic Transition

The makers of the so-called 'Transitional' industries present in sites straddling the Middle-to-Upper Palaeolithic transition across Eurasia is a topic of much discussion (D'Errico et al., 1998; Churchill and Smith, 2000; Mellars, 2005; e.g. Hublin, 2013; Hublin, 2015). These industries are stratigraphically sandwiched between underlying Middle Palaeolithic assemblages, produced by Neanderthals, and overlying Upper Palaeolithic assemblages, made by *Homo sapiens*. One such industry, the Châtelperronian, known in western and south-western France and north-eastern Spain, consists of blades, pigments, bone tools and personal ornaments. Whilst the Châtelperronian has an Upper Palaeolithic character, it shows similarities with the Mousterian of Acheuleun Tradition type B (see Soressi and Roussel, 2014) and is associated with Neanderthal remains at several sites (Lévêque and Vandermeersch, 1980; Hublin et al., 1996; Bailey and Hublin, 2006; Welker et al., 2016).

The Châtelperronian layers at Grotte-du-Renne at Arcy sure Cure are notable for the presence of numerous Neanderthal teeth and other fragmented bones alongside a significant number of decorated bone tools, personal body ornaments and large amounts of pigment. However, it has been suggested that the association is the result of vertical mixing between layers. Bar-Yosef and Bordes (2010) suggested that the association is the result of re-working of Neanderthal fossils from the underlying Mousterian layers, whereas Higham et al. (2010) interpreted an inconsistent series of radiocarbon dates from the site as evidence of Upper Palaeolithic artefacts moving downwards through the stratigraphy. This was subsequently challenged based on the stratigraphic integrity of the lithic assemblages at the site and the inconsistent ^{14}C results were attributed to poor collagen preservation and incomplete sample decontamination (Caron et al., 2011). A more recent series of dates on un-consolidated samples selected for good collagen preservation produced stratigraphically consistent results, supporting the association of the Neanderthal fossils and Châtelperronian assemblages at Grotte du Renne (Hublin et al., 2012). A palaeoproteomic study in 2016 identified 28 additional Neanderthal bone fragments from the Châtelperronian layers at Grotte du Renne, and direct ^{14}C dating of one such specimen (Fig. 2) firmly placed it within the Chatelperronian age range (Welker et al., 2016). Direct dates from small amounts of material from the Châtelperronian ornaments could resolve the question of the contemporaneity of the personal ornaments with the Neanderthal remains.

A fragmented maxilla and three teeth (re-fitted post-excavation) were excavated from Kent's Cavern, UK, in 1927 and since their discovery have been identified as Upper Palaeolithic *Homo sapiens* (Keith, 1927). In the 1980s, the maxilla (KC4) was directly AMS radiocarbon dated to 30,900 ± 900 ^{14}C BP (OxA-1621; 37,430-33,410 cal BP at 2σ), which supported its Upper Palaeolithic assignment and, at the time, made it the oldest hominin to have been directly dated by ^{14}C methods (Hedges et al., 1989). It has since been argued that the direct date of KC4 was an

under-estimate of its true age due to incomplete removal of conservatives during sample pretreatment (Jacobi et al., 2006; Higham et al., 2011). In 2011, a second attempt to obtain a direct date using ultrafiltration failed when a small sample of tooth root yielded very little collagen (89 mg dentine powder resulted in 0.38 mg collagen [0.4% weight]) (Higham et al., 2011). As a second direct date was not possible, Higham et al. (2011) used Bayesian techniques to estimate an age for KC4 of 44,180-41,530 cal BP (2σ) based on dates from ultrafiltered collagen from fauna located above and below the maxilla. The validity of this strategy has been strongly questioned based on the lack of reliable contextual information from the 1920s excavation and it has been suggested that the original direct date is more in keeping with the archaeological evidence (White and Pettitt, 2012; Zilhão, 2013). White and Pettitt (2012) stated that "*Radiocarbon dating of unmodified fauna from sites with questionable stratigraphies should not be used to suggest the apparent age of human taxa. […] Without a new direct ultrafiltration date, […] the age of KC4 will […] never be conclusively resolved.*" The authors have defended their techniques and, after incorporating further AMS dates of associated fauna into their model, have provided an even more precise estimate for the age of KC4 from 42,350-40,760 cal BP, although they acknowledgement that the new AMS dates indicate some post-depositional mixing between layers likely occurred (Proctor et al., 2017). They conclude that estimate can only be tested by direct dating of the maxilla, which *"…will not be possible until further technical developments for dating very small samples are more routinely available*" (Proctor et al., 2017).

As KC4 is the only *Homo sapiens* fossil from north-western Europe ≥ 35,000 cal BP its age is crucial in determining the duration and range of overlap between *Homo sapiens* and Neanderthals in this region. The original date for KC4 demonstrates that some collagen is preserved in the maxilla, although details on the chemistry are not provided in the 1989 datelist (Hedges et al., 1989). The results described in Chapter 3 (Fewlass et al., 2019b) demonstrate that in general much lower yields of collagen result from the pretreatment of small amounts of powdered bone compared to whole bone, which likely contributed to the failure of pretreatment outlined in Higham et al (2011). A re-dating program for KC4 could employ NIR pre-screening to assess the level of collagen preservation across the maxilla. The sampling of a tooth root, as attempted by Higham et al. 2011, may somewhat circumnavigate the issue of conservatives and would be less visually invasive. As the fragmented maxilla was found separately from the three teeth, the direct dating of the KC4 bone or tooth should be conducted on the same sample where any possible future DNA sampling would occur. An ultrafiltered collagen extract from <100 mg bone/dentine could provide an accurate radiocarbon date, either through AMS dating with a graphite target or with the gas ion source of the MICADAS. A reliable direct date would resolve the on-going controversy over the early presence of *Homo sapiens* in north-western Europe.

Prior to the discovery of *Homo sapiens* remains in the IUP layers at Bacho Kiro Cave (Fewlass et al., in review; Hublin et al., in review), the oldest known remains of our species in Europe was the

Pestera cu Oase 1 mandible recovered from a cave in Romania in 2002. Morphological analysis identified the mandible as *Homo sapiens* with some archaic features indicative of admixture with Neanderthals (Trinkaus et al., 2003). aDNA analysis later showed that 6-9% of the Oase 1 nuclear genome was derived from Neanderthals, indicating a *Homo sapiens*-Neanderthal admixture event occurred 4-6 generations (<200 years) before Oase 1 lived (Fu et al., 2015).

No archaeology accompanied the human remains so direct radiocarbon dating was necessary to establish the age of the fossil. The first attempt at Oxford (350 mg bone) using ultrafiltration produced a very low yield of collagen (1.5 mg/0.4%) with an acceptable C:N value (C:N=3.3) which produced a minimum age of >35,200 ^{14}C BP (OxA-11711). A second attempt to date the mandible at Groningen (706 mg bone) without ultrafiltration resulted in a higher collagen yield (28.5 mg/4%) but with a C:N value outside the range generally considered suitable for reliable ^{14}C dating (C:N=2.6). The collagen extract was dated to 34,290 +970, -870 ^{14}C BP (GrA-22810). The two dates were combined (34,950 +990, -890 ^{14}C BP), giving a wide calibrated range of 41,760-37,310 cal BP (Trinkaus et al., 2003; Trinkaus, 2013).

The face and fragmented cranium of another *Homo sapiens* individual (Oase 2) was also found in the cave. The first two attempts to directly date the cranium failed due to very poor collagen preservation and a third attempt yielded a minimum age of 28,980 +180, -170 ^{14}C BP (GrA-24398), although the authors suggest that Oase 2 is roughly contemporary with Oase 1 (Rougier et al., 2007; Trinkaus, 2013).

As the current dates confirm the early Upper Palaeolithic origin of the Oase fossils, further sampling is considered unnecessarily destructive (Trinkaus, 2013). In light of the early direct dates of *Homo sapiens* remains from south-eastern Europe at Bacho Kiro Cave and forth-coming improvements in resolution of the calibration curve in this time range (Talamo et al., 2017; Cheng et al., 2018; Reimer et al., 2018), a high precision direct date from <100 mg bone from Oase 1 would play an important role in determining the duration of overlap between *Homo sapiens* and Neanderthals in central Europe (Fig. 2).

Whilst the Aurignacian technocomplex is widely accepted as a proxy for the presence of Upper Palaeolithic *Homo sapiens* in Europe, very few human remains have been found in secure association with diagnostic assemblages (Churchill and Smith, 2000; Mellars, 2006a). The rare (and relatively large) assemblage of human fossils from Mladeĉ (Czech Republic) has been directly dated (without ultrafiltration) to ~31,000 ^{14}C BP (Wild et al., 2005), but the majority of human remains associated with Aurignacian contexts are isolated teeth or fragmentary bones and few have been directly dated (see Ahern et al., 2013).

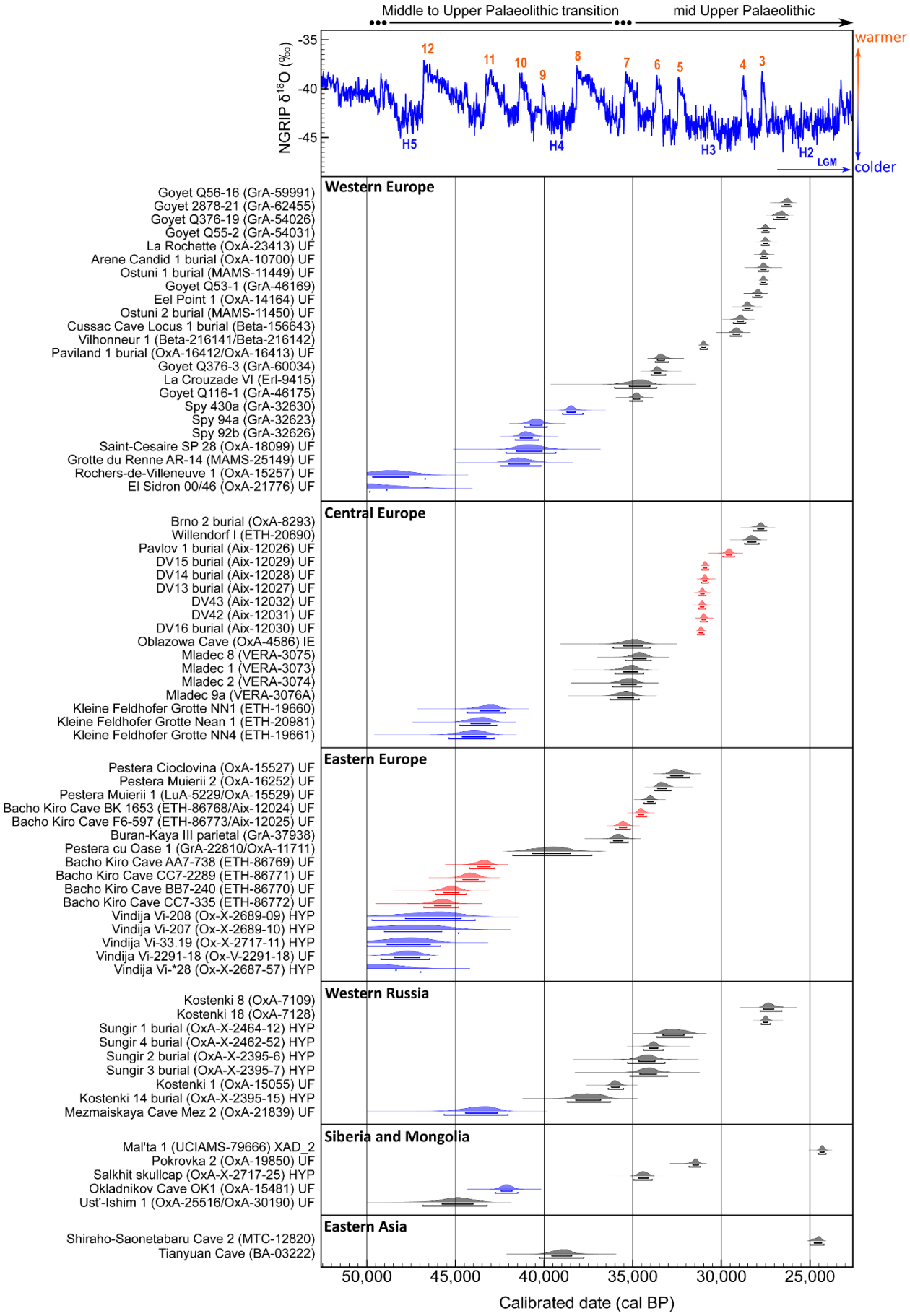
Middle to Upper Palaeolithic transition
mid Upper Palaeolithic
NGRIP δ18O (‰)
-35
-40
-45
12
11
10
9
8
7
6
5
4
3
H5
H4
H3
H2
LGM
warmer
colder
Western Europe
Goyet Q56-16 (GrA-59991)
Goyet 2878-21 (GrA-62455)
Goyet Q376-19 (GrA-54026)
Goyet Q55-2 (GrA-54031)
La Rochette (OxA-23413) UF
Arene Candid 1 burial (OxA-10700) UF
Ostuni 1 burial (MAMS-11449) UF
Goyet Q53-1 (GrA-46169)
Eel Point 1 (OxA-14164) UF
Ostuni 2 burial (MAMS-11450) UF
Cussac Cave Locus 1 burial (Beta-156643)
Vilhonneur 1 (Beta-216141/Beta-216142)
Paviland 1 burial (OxA-16412/OxA-16413) UF
Goyet Q376-3 (GrA-60034)
La Crouzade VI (Erl-9415)
Goyet Q116-1 (GrA-46175)
Spy 430a (GrA-32630)
Spy 94a (GrA-32623)
Spy 92b (GrA-32626)
Saint-Cesaire SP 28 (OxA-18099) UF
Grotte du Renne AR-14 (MAMS-25149) UF
Rochers-de-Villeneuve 1 (OxA-15257) UF
El Sidron 00/46 (OxA-21776) UF
Central Europe
Brno 2 burial (OxA-8293)
Willendorf I (ETH-20690)
Pavlov 1 burial (Aix-12026) UF
DV15 burial (Aix-12029) UF
DV14 burial (Aix-12028) UF
DV13 burial (Aix-12027) UF
DV43 (Aix-12032) UF
DV42 (Aix-12031) UF
DV16 burial (Aix-12030) UF
Oblazowa Cave (OxA-4586) IE
Mladec 8 (VERA-3075)
Mladec 1 (VERA-3073)
Mladec 2 (VERA-3074)
Mladec 9a (VERA-3076A)
Kleine Feldhofer Grotte NN1 (ETH-19660)
Kleine Feldhofer Grotte Nean 1 (ETH-20981)
Kleine Feldhofer Grotte NN4 (ETH-19661)
Eastern Europe
Pestera Cioclovina (OxA-15527) UF
Pestera Muierii 2 (OxA-16252) UF
Pestera Muierii 1 (LuA-5229/OxA-15529) UF
Bacho Kiro Cave BK 1653 (ETH-86768/Aix-12024) UF
Bacho Kiro Cave F6-597 (ETH-86773/Aix-12025) UF
Buran-Kaya III parietal (GrA-37938)
Pestera cu Oase 1 (GrA-22810/OxA-11711)
Bacho Kiro Cave AA7-738 (ETH-86769) UF
Bacho Kiro Cave CC7-2289 (ETH-86771) UF
Bacho Kiro Cave BB7-240 (ETH-86770) UF
Bacho Kiro Cave CC7-335 (ETH-86772) UF
Vindija Vi-208 (Ox-X-2689-09) HYP
Vindija Vi-207 (Ox-X-2689-10) HYP
Vindija Vi-33.19 (Ox-X-2717-11) HYP
Vindija Vi-2291-18 (Ox-V-2291-18) UF
Vindija Vi-*28 (Ox-X-2687-57) HYP
Western Russia
Kostenki 8 (OxA-7109)
Kostenki 18 (OxA-7128)
Sungir 1 burial (OxA-X-2464-12) HYP
Sungir 4 burial (OxA-X-2462-52) HYP
Sungir 2 burial (OxA-X-2395-6) HYP
Sungir 3 burial (OxA-X-2395-7) HYP
Kostenki 1 (OxA-15055) UF
Kostenki 14 burial (OxA-X-2395-15) HYP
Mezmaiskaya Cave Mez 2 (OxA-21839) UF
Siberia and Mongolia
Mal'ta 1 (UCIAMS-79666) XAD_2
Pokrovka 2 (OxA-19850) UF
Salkhit skullcap (OxA-X-2717-25) HYP
Okladnikov Cave OK1 (OxA-15481) UF
Ust'-Ishim 1 (OxA-25516/OxA-30190) UF
Eastern Asia
Shiraho-Saonetabaru Cave 2 (MTC-12820)
Tianyuan Cave (BA-03222)
50,000
45,000
40,000
35,000
30,000
25,000
Calibrated date (cal BP)

Figure 2. *Calibrated ranges of direct ^{14}C AMS dates of human remains in Eurasia dating between 50,000-25,000 cal BP on bulk collagen, filtered collagen (UF/XAD_2/IE) or isolated amino acids (HYP) (where specified in source publication).* Homo sapiens *are shown in black (existing dates) and red (this thesis) and Neanderthals are shown in blue. Sample ID and AMS lab number shown on the left. Dates were calibrated using the IntCal13 dataset (Reimer et al., 2013) in OxCal 4.3 (Bronk Ramsey, 2009). Where two statistically indistinguishable dates are available from one bone the dates have been combined (R_Combine) in OxCal. Dates are shown in comparison to the NGRIP (GICC05) δ^{18}O record (Svensson et al., 2008) which is a proxy for Northern Hemisphere palaeoenvironmental conditions (Greenland Interstadial numbers, Heinrich events (H5, H4, H3, H2) and Last Glacial Maximum (LGM) are indicated). References and pretreatment information are included in Appendix 1.*

Mid Upper Palaeolithic

In comparison to the preceding early Upper Palaeolithic, mid Upper Palaeolithic human remains are relatively abundant. The discovery of both ritualistic and isolated human remains from Gravettian contexts across Eurasia have provided a wealth of morphological, behavioural and genetic insights into Gravettian life and have in particular sparked much discussion about variation in funerary practises (Pettitt, 2011; Trinkaus and Buzhilova, 2018). However, the wider interpretation of these remains is hindered by a lack of accurate, precise direct radiocarbon dates.

The Gravettian technocomplex is wide-spread across Europe and similarities in burial practises (grave goods, ochre, multiple internments) have been observed across large areas (Pettitt, 2011). A trend of increasing richness in burial goods over time was observed by Svoboda (2008), in particular reference to the exceptionally rich single burials at Brno in Moravia (Oliva, 1999; Pettitt and Trinkaus, 2000) and Arene Candide, Italy (Pettitt et al., 2003) and the spectacular burials discovered at Sunghir, Russia, all of which were originally dated to the later Gravettian period (Trinkaus et al., 2014). Over the past two decades, nearly 20 radiocarbon dates ranging from ~30,000-20,000 ^{14}C BP have been made from the four Sunghir burials using various collagen extraction methods (Pettitt and Bader, 2000). The most recent dates suggest the burials date to the early-mid Gravettian (Marom et al., 2012; Kuzmin et al., 2014; Nalawade-Chavan et al., 2014), which conflicts with the theory of a temporal trend in increasing burial richness. Direct dating has demonstrated that several human burials originally assumed to be Gravettian are in fact Holocene intrusions (Trinkaus and Pettitt, 2000; Svoboda et al., 2002; Tillier et al., 2009).

Recent excavations at Borsuka Cave, Poland, uncovered six deciduous human teeth and 112 pendants made of herbivore teeth spread across 4x3 m^2 (Wilczyński et al., 2016). The assemblage was interpreted as a disturbed infant burial. Two of the pendants were radiocarbon dated to 27,350 ± 450 ^{14}C BP (Poz-32394: 68.2%: 31,640-30,930 cal BP) and 25,150 ± 160 ^{14}C BP (Poz-38236: 68.2%: 29,400-28,980 cal BP) and a reindeer metatarsus from the same layer was dated to 26,430 ± 180 ^{14}C BP (Poz-38237) (Wilczyński et al., 2012; Wilczyński et al., 2016). Although the layer lacked diagnostic lithics, the burial was associated with the Pavlovian culture based on the

contemporaneity of the dates with the burial contexts at Dolní Věstonice, Pavlov and Predmosti (see Chapter 5). The lack of agreement between the ^{14}C dates from the two pendants (outside 2σ) raises the question of the association of the pendants to each other, and further, the human teeth with the pendants which forms the basis of the interpretation of a burial. Considering the lack of diagnostic lithics, direct dating of small samples of dentine from the human teeth and pendants could not only confirm whether the human remains fall within the Gravettian time period but also resolve the question of the contemporaneity of the human remains with the pendants, providing a more robust foundation for the inclusion of this burial in the wider discussion of Gravettian funerary practices.

Radiocarbon dating: an evolving field

The absolute nature of radiocarbon enables us to explore broad patterns of human behaviour across time and space (e.g. Mellars, 2006b; Hublin, 2015; Bae et al., 2017). Yet bearing in mind the problems associated with dating in the Palaeolithic period, large-scale statistical models built on existing dates of varying reliability have limited use. In order to circumnavigate these problems, large-scale dating and re-dating programs have been undertaken to generate new AMS radiocarbon dates using rigourous pretreatment methods and robust quality criteria (Higham et al., 2014). The integration of radiocarbon data with other dating techniques and chronometric markers are further approaches undertaken to improve the robusticity of large-scale analyses (Lowe et al., 2012; Davies et al., 2015). Recently, Staubwasser et al. (2018) inferred patterns of depopulation and re-population based on climatic cycles by linking cold, arid periods recorded in stable isotopes in speleothems from the Carpathians with archaeologically sterile layers in Eurasian Middle to Upper Palaeolithic sites. Improved accuracy and higher precision in archaeological chronologies (Fewlass et al., in review) will facilitate closer links between human presence and specific climatic events at increasingly high resolution.

Whilst the extension of the calibration curve back to 50,000 BP (Reimer et al., 2009) represents a huge achievement for researchers working on the chronology of the late Middle and Upper Palaeolithic, the low precision of the curve beyond the dendrochronological record has been the ultimate limit to the chronological resolution possible from high precision measurements. The improvements to the forthcoming calibration curve IntCal19 (Cheng et al., 2018; Reimer et al., 2018) and future work to extend the dendrochronological portion of curve beyond 14,000 BP should greatly increase the accuracy and precision of calibration in this period. This adds greater significance to the need to obtain accurate and precise radiocarbon measurements directly from important Palaeolithic human remains and artefacts. Accuracy and precision at both the ^{14}C measurement and calibration stage are essential for refining the chronology of the arrival and

spread of *Homo sapiens* across Eurasia during the Upper Palaeolithic (Hublin, 2012; 2015; Bae et al., 2017).

As demonstrated over the past 70 years, radiocarbon dating is a continually evolving field, driven forwards by developments in both technology and understanding. The MICADAS represents a huge advance in accuracy and precision for radiocarbon dating in archaeology. An increasing number of AMS facilities across the globe now house a MICADAS, thanks to its compact size and relatively low maintenance costs, meaning that the methods explored in this dissertation have the potential for wide spread application. The field will continue to benefit from improvements in instrumentation and pretreatment methods and will likely see further advances in accuracy and precision from decreasing sample sizes. The results of this project are intended to contribute to a more robust chronological framework for the Upper Palaeolithic period whilst preserving precious archaeological material for future generations.

References

Ahern J.C.M., Janković I., Voisin J.-L., Smith F.H. 2013. Modern human origins in Central Europe. In: Smith FH, Ahern JCM, editors. The Origins of Modern Humans: Biology Reconsidered. 2 ed. Hoboken, NJ: John Wiley & Sons, Inc. p 151-221.

Bae C.J., Douka K., Petraglia M.D. 2017. On the origin of modern humans: Asian perspectives. Science 358(6368).

Bailey S.E., Hublin J.-J. 2006. Dental remains from the Grotte du Renne at Arcy-sur-Cure (Yonne). Journal of Human Evolution 50(5):485-508.

Bar-Yosef O., Bordes J.G. 2010. Who were the makers of the Châtelperronian culture? Journal of Human Evolution 59(5):586-593.

Bard E., Tuna T., Fagault Y., Bonvalot L., Wacker L., Fahrni S., Synal H.-A. 2015. AixMICADAS, the accelerator mass spectrometer dedicated to ^{14}C recently installed in Aix-en-Provence, France. Nuclear Instruments and Methods in Physics Research Section B: Beam Interactions with Materials and Atoms 361:80-86.

Bronk Ramsey C. 2009. Bayesian analysis of radiocarbon dates. Radiocarbon 51(1):337-360.

Caron F., d'Errico F., Del Moral P., Santos F., Zilhão J. 2011. The reality of Neandertal symbolic behavior at the Grotte du Renne, Arcy-sur-Cure, France. PLoS ONE 6(6):e21545.

Cheng H., Edwards R.L., Southon J., Matsumoto K., Feinberg J.M., Sinha A., Zhou W., Li H., Li X., Xu Y., Chen S., Tan M., Wang Q., Wang Y., Ning Y. 2018. Atmospheric $^{14}C/^{12}C$ changes during the last glacial period from Hulu Cave. Science 362(6420):1293-1297.

Churchill S.E., Smith F.H. 2000. Makers of the early Aurignacian of Europe. Yearbook of Physical Anthropology 113(S31):61-115.

D'Errico F., Zilhão J., Julien M., Baffier D., Pelegrin J. 1998. Neanderthal Acculturation in Western Europe? A Critical Review of the Evidence and Its Interpretation. Current Anthropology 39(S1):S1-S44.

Davies W., White D., Lewis M., Stringer C. 2015. Evaluating the transitional mosaic: frameworks of change from Neanderthals to *Homo sapiens* in eastern Europe. Quaternary Science Reviews 118:211-242.

Fewlass H., Talamo S., Tuna T., Fagault Y., Kromer B., Hoffmann H., Pangrazzi C., Hublin J.-J., Bard E. 2017. Size matters: radiocarbon dates of <200 µg ancient collagen samples with AixMICADAS and its gas ion source. Radiocarbon 60(02):425-439.

Fewlass H., Talamo S., Kromer B., Bard E., Tuna T., Fagault Y., Sponheimer M., Ryder C., Hublin J.-J., Perri A., Sázelová S., Svoboda J. 2019a. Direct radiocarbon dates of mid Upper Palaeolithic human remains from Dolní Věstonice II and Pavlov I, Czech Republic. Journal of Archaeological Science: Reports 27.

Fewlass H., Tuna T., Fagault Y., Hublin J.-J., Kromer B., Bard E., Talamo S. 2019b. Pretreatment and gaseous radiocarbon dating of 40–100 mg archaeological bone. Scientific Reports 9(1):5342.

Fewlass H., Talamo S., Wacker L., Kromer B., Tuna T., Fagault Y., Bard E., McPherron S., Aldeias V., Maria R., Martisius N.L., Paskulin L., Rezek Z., Sinet-Mathiot V., Sirakova S., Smith G.M., Spasov R., Welker F., Tsanova T., Sirakov N., Hublin J.-J. in review. New ^{14}C chronology for Middle–to–Upper Palaeolithic transition at Bacho Kiro Cave, Bulgaria. Nature Ecology & Evolution.

Fu Q., Hajdinjak M., Moldovan O.T., Constantin S., Mallick S., Skoglund P., Patterson N., Rohland N., Lazaridis I., Nickel B., Viola B., Prufer K., Meyer M., Kelso J., Reich D., Pääbo S. 2015. An early modern human from Romania with a recent Neanderthal ancestor. Nature 524(7564):216-219.

Fu Q., Posth C., Hajdinjak M., Petr M., Mallick S., Fernandes D., Furtwängler A., Haak W., Meyer M., Mittnik A., Nickel B., Peltzer A., Rohland N., Slon V., Talamo S., Lazaridis I., Lipson M., Mathieson I., Schiffels S., Skoglund P., Derevianko A.P., Drozdov N., Slavinsky V., Tsybankov A., Cremonesi R.G., Mallegni F., Gély B., Vacca E., Morales M.R.G., Straus L.G., Neugebauer-Maresch C., Teschler-Nicola M., Constantin S., Moldovan O.T., Benazzi S., Peresani M., Coppola D., Lari M., Ricci S., Ronchitelli A., Valentin F., Thevenet C., Wehrberger K., Grigorescu D., Rougier H., Crevecoeur I., Flas D., Semal P., Mannino M.A., Cupillard C., Bocherens H., Conard N.J., Harvati K., Moiseyev V., Drucker D.G., Svoboda J., Richards M.P., Caramelli D., Pinhasi R., Kelso J., Patterson N., Krause J., Pääbo S., Reich D. 2016. The genetic history of Ice Age Europe. Nature 534(7606):200-205.

Hedges R.E.M., Housley R.A., Law I.A., Bronk Ramsey C. 1989. Radiocarbon dates from the Oxford AMS system: Archaeometry datelist 9. Archaeometry 31(2):207-234.

Higham T., Jacobi R., Julien M., David F., Basell L., Wood R., Davies W., Bronk Ramsey C. 2010. Chronology of the Grotte du Renne (France) and implications for the context of ornaments and human remains within the Châtelperronian. Proceedings of the National Academy of Sciences 107(47):20234-20239.

Higham T., Compton T., Stringer C., Jacobi R., Shapiro B., Trinkaus E., Chandler B., Groening F., Collins C., Hillson S., O'Higgins P., FitzGerald C., Fagan M. 2011. The earliest evidence for anatomically modern humans in northwestern Europe. Nature 479(7374):521-524.

Higham T., Douka K., Wood R., Bronk Ramsey C., Brock F., Basell L., Camps M., Arrizabalaga A., Baena J., Barroso-Ruiz C., Bergman C., Boitard C., Boscato P., Caparros M., Conard N.J., Draily C., Froment A., Galvan B., Gambassini P., Garcia-Moreno A., Grimaldi S., Haesaerts P., Holt B., Iriarte-Chiapusso M.-J., Jelinek A., Jorda Pardo J.F., Maillo-Fernandez J.-M., Marom A., Maroto J., Menendez M., Metz L., Morin E., Moroni A., Negrino F., Panagopoulou E., Peresani M., Pirson S., de la Rasilla M., Riel-Salvatore J., Ronchitelli A., Santamaria D., Semal P., Slimak L., Soler J., Soler N., Villaluenga A., Pinhasi R., Jacobi R. 2014. The timing and spatiotemporal patterning of Neanderthal disappearance. Nature 512(7514):306-309.

Hublin J.-J., Spoor F., Braun M., Zonneveld F., Condemi S. 1996. A Late Neanderthal associated with Upper Palaeolithic artefacts. Nature 381(6579):224-226.

Hublin J.-J. 2012. The earliest modern human colonization of Europe. Proceedings of the National Academy of Sciences 109(34):13471-13472.

Hublin J.-J., Talamo S., Julien M., David F., Connet N., Bodu P., Vandermeersch B., Richards M.P. 2012. Radiocarbon dates from the Grotte du Renne and Saint-Césaire support a Neandertal origin for the Châtelperronian. Proceedings of the National Academy of Sciences 109(46):18743-18748.

Hublin J.-J. 2013. The Makers of the Early Upper Paleolithic in Western Eurasia. In: Smith FH, Ahern JC, editors. The Origins of Modern Humans: Biology Reconsidered. 2 ed. Hoboken, NJ: John Wiley & Sons, Inc. p 223-252.

Hublin J.-J. 2015. The modern human colonization of western Eurasia: when and where? Quaternary Science Reviews 118:194-210.

Hublin J.-J., Sirakov N., Aldeias V., Bailey S., Bard E., Delvigne V., Fagault Y., Fewlass H., Hajdinjak M., Kromer B., Krumov I., Marreiros J., Martisius N., Paskulin L., Sinet-Mathiot V., Meyer M., Popov V., Pääbo S., Popov V., Režek Z., Sirakova S., Skinner M.M., Smith G.M., Spasov R., Talamo S., Tuna T., Wacker L., Welker F., Wilcke A., Zahariev N., McPherron S.P., Tsanova T. in review. Initial Upper Palaeolithic *Homo sapiens* remains from Bacho Kiro Cave (Bulgaria) Nature.

Jacobi R.M., Higham T., Bronk Ramsey C. 2006. AMS radiocarbon dating of Middle and Upper Palaeolithic bone in the British Isles: improved reliability using ultrafiltration. Journal of Quaternary Science 21(5):557-573.

Keith A. 1927. Report on a fragment of a human jaw. Transactions and Proceedings: Torquay Natural History Society(5):1-2.
Kuzmin Y.V., van der Plicht J., Sulerzhitsky L.D. 2014. Puzzling radiocarbon dates for the Upper Paleolithic site of Sungir (Central Russian Plain). Radiocarbon:451-459.
Lévêque F., Vandermeersch B. 1980. Découverte de restes humains dans un niveau castelperronien à Saint-Césaire (Charente-Maritime). Comptes rendus de l'Académie des Sciences de Paris 291(Sér. II):187-189.
Lowe J., Barton N., Blockley S., Bronk Ramsey C., Cullen V.L., Davies W., Gamble C., Grant K., Hardiman M., Housley R., Lane C.S., Lee S., Lewis M., MacLeod A., Menzies M., Muller W., Pollard M., Price C., Roberts A.P., Rohling E.J., Satow C., Smith V.C., Stringer C.B., Tomlinson E.L., White D., Albert P., Arienzo I., Barker G., Boric S., Carandente A., Civetta L., Ferrier C., Guadelli J.L., Karkanas P., Koumouzelis M., Muller U.C., Orsi G., Pross J., Rosi M., Shalamanov-Korobar L., Sirakov N., Tzedakis P.C. 2012. Volcanic ash layers illuminate the resilience of Neanderthals and early modern humans to natural hazards. Proceedings of the National Academy of Sciences 109(34):13532-13537.
Marom A., McCullagh J.S.O., Higham T.F.G., Sinitsyn A.A., Hedges R.E.M. 2012. Single amino acid radiocarbon dating of Upper Paleolithic modern humans. Proceedings of the National Academy of Sciences 109(18):6878-6881.
Mellars P. 2005. The impossible coincidence. A single-species model for the origins of modern human behavior in Europe. Evolutionary Anthropology 14(1):12-27.
Mellars P. 2006a. Archeology and the dispersal of modern humans in Europe: Deconstructing the “Aurignacian”. Evolutionary Anthropology 15(5):167-182.
Mellars P. 2006b. A new radiocarbon revolution and the dispersal of modern humans in Eurasia. Nature 439(7079):931-935.
Nalawade-Chavan S., McCullagh J., Hedges R. 2014. New hydroxyproline radiocarbon dates from Sungir, Russia, confirm early Mid Upper Palaeolithic burials in Eurasia. PLoS ONE 9(1):e76896.
Oliva M. 1999. The Brno II Upper Palaeolithic burial. In: Roebroeks W, Mussi M, Svoboda J, Fennema K, editors. Hunters of the Golden Age. Leiden: Faculty of Archaeology, University of Leiden. p 143-153.
Pettitt P., Trinkaus E. 2000. Direct radiocarbon dating of the Brno 2 Gravettian human remains. Anthropologie 38(2):149-150.
Pettitt P. 2011. The Palaeolithic Origins of Human Burial. London: Routledge.
Pettitt P.B., Bader N.O. 2000. Direct AMS radiocarbon dates for the Sungir mid Upper Palaeolithic burials. Antiquity 74(284):269-270.
Pettitt P.B., Richards M., Maggi R., Formicola V. 2003. The Gravettian burial known as the Prince (“Il Principe”): new evidence for his age and diet. Antiquity 77(295):15-19.
Pleurdeau D., Moncel M.-H., Pinhasi R., Yeshurun R., Higham T., Agapishvili T., Bokeria M., Muskhelishvili A., Le Bourdonnec F.-X., Nomade S., Poupeau G., Bocherens H., Frouin M., Genty D., Pierre M., Pons-Branchu E., Lordkipanidze D., Tushabramishvili N. 2016. Bondi Cave and the Middle-Upper Palaeolithic transition in western Georgia (south Caucasus). Quaternary Science Reviews 146(Supplement C):77-98.
Proctor C., Douka K., Proctor J.W., Higham T. 2017. The Age and Context of the KC4 Maxilla, Kent's Cavern, UK. European Journal of Archaeology 20(1):74-97.
Reimer P.J., Baillie M.G.L., Bard E., Bayliss A., Beck J.W., Blackwell P.G., Bronk Ramsey C., Buck C.E., Burr G.S., Edwards R.L., Friedrich M., Grootes P.M., Guilderson T.P., Hajdas I., Heaton T.J., Hogg A.G., Hughen K.A., Kaiser K.F., Kromer B., McCormac F.G., Manning S.W., Reimer R.W., Richards D.A., Southon J.R., Talamo S., Turney C.S.M., van der Plicht J., Weyhenmeyer C.E. 2009. IntCal09 and

Marine09 radiocarbon age calibration curves, 0-50,000 years cal BP. Radiocarbon 51(4):1111-1150.

Reimer P.J., Bard E., Bayliss A., Beck J.W., Blackwell P.G., Bronk Ramsey C., Buck C.E., Cheng H., Edwards R.L., Friedrich M., Grootes P.M., Guilderson T.P., Haflidason H., Hajdas I., Hatté C., Heaton T.J., Hoffmann D.L., Hogg A.G., Hughen K.A., Kaiser K.F., Kromer B., Manning S.W., Niu M., Reimer R.W., Richards D.A., Scott E.M., Southon J.R., Staff R.A., Turney C.S.M., van der Plicht J. 2013. IntCal13 and Marine13 radiocarbon age calibration curves 0–50,000 years cal BP. Radiocarbon 55(4):1869–1887.

Reimer P.J., Austin W.E.N., Bard E., Bayliss A., Bronk Ramsey C., Cheng H., Edwards L., Friedrich M., Grootes P.M., Guilderson T.P., Hajdas I., Heaton T.J., Hogg A.G., Hughen K.A., Kromer B., Manning S.W., Muscheler R., Palmer J.G., Pearson C.L., Reimer R.W., Richards D.A., Scott M., Southon J.R., Turney C.S.M., van der Plicht J., Wacker L. 2018. A preview of the IntCal19 radiocarbon calibration curves. 23rd International Radiocarbon conference. Trondheim, Norway.

Rougier H., Milota Ş., Rodrigo R., Gherase M., Sarcină L., Moldovan O., Zilhão J., Constantin S., Franciscus R.G., Zollikofer C.P.E., Ponce de León M., Trinkaus E. 2007. Peştera cu Oase 2 and the cranial morphology of early modern Europeans. Proceedings of the National Academy of Sciences 104(4):1165-1170.

Soressi M., Roussel M. 2014. European Middle to Upper Paleolithic transitional industries: Châtelperronian. In: Smith C, editor. Encyclopedia of Global Archaeology. New York: Springer New York. p 2679-2693.

Sponheimer M., Ryder C., Fewlass H., Smith E., Pestle W., Talamo S. In press. Saving Old Bones: a non-destructive method for bone collagen prescreening. Scientific Reports.

Staubwasser M., Drăgușin V., Onac B.P., Assonov S., Ersek V., Hoffmann D.L., Veres D. 2018. Impact of climate change on the transition of Neanderthals to modern humans in Europe. Proceedings of the National Academy of Sciences 115(37):9116-9121.

Svensson A., Andersen K.K., Bigler M., Clausen H.B., Dahl-Jensen D., Davies S.M., Johnsen S.J., Muscheler R., Parrenin F., Rasmussen S.O., Röthlisberger R., Seierstad I., Steffensen J.P., Vinther B.M. 2008. A 60 000 year Greenland stratigraphic ice core chronology. Climate of the Past 4(1):47-57.

Svoboda J., van der Plicht J., Kuželka V. 2002. Upper Palaeolithic and Mesolithic human fossils from Moravia and Bohemia (Czech Republic): some new ^{14}C dates. Antiquity 76(294):957-962.

Svoboda J. 2008. The Upper Paleolithic burial area at Předmostí: ritual and taphonomy. Journal of Human Evolution 54(1):15-33.

Talamo S., Friedrich M., Adolphi F., Kromer B., Muscheler R., Wacker L. 2017. RESOLUTION: Radiocarbon, tree rings, and solar variability provide the accurate time scale for human evolution. 7th Annual Meeting of the European Society for the Study of Human Evolution. Leiden, The Netherlands. p 194.

Tillier A.M., Mester Z., Bocherens H., Henry-Gambier D., Pap I. 2009. Direct dating of the "Gravettian" Balla child's skeleton from Bukk Mountains (Hungary): unexpected results. Journal of Human Evolution 56(2):209-212.

Trinkaus E., Pettitt P. 2000. The Krems-Hundssteig "Gravettian" human remains are Holocene. HOMO 51(2):258-260.

Trinkaus E., Moldovan O., Milota ş., Bîlgăr A., Sarcina L., Athreya S., Bailey S.E., Rodrigo R., Mircea G., Higham T., Bronk Ramsey C., van der Plicht J. 2003. An early modern human from the Peştera cu Oase, Romania. Proceedings of the National Academy of Sciences 100(20):11231-11236.

Trinkaus E. 2013. Radiocarbon Dating of the Pestera cu Oase Human Remains. In: Trinkaus E, Constantin S, Zilhão J, editors. Life and Death at Pestera cu Oase. A Setting for Modern Human Emergence in Europe. New York: Oxford University Press. p 229-233.

Trinkaus E., Buzhilova A.P., Mednikova M.B., Dobrovolskaya M.V. 2014. The people of Sunghir: burials, bodies, and behavior in the earlier Upper Paleolithic. New York: Oxford University Press.
Trinkaus E., Buzhilova A.P. 2018. Diversity and differential disposal of the dead at Sunghir. Antiquity 92(361):7-21.
Wacker L., Fahrni S.M., Hajdas I., Molnar M., Synal H.-A., Szidat S., Zhang Y.L. 2013. A versatile gas interface for routine radiocarbon analysis with a gas ion source. Nuclear Instruments and Methods in Physics Research Section B: Beam Interactions with Materials and Atoms 294:315-319.
Welker F., Hajdinjak M., Talamo S., Jaouen K., Dannemann M., David F., Julien M., Meyer M., Kelso J., Barnes I., Brace S., Kamminga P., Fischer R., Kessler B.M., Stewart J.R., Pääbo S., Collins M.J., Hublin J.-J. 2016. Palaeoproteomic evidence identifies archaic hominins associated with the Châtelperronian at the Grotte du Renne. Proceedings of the National Academy of Sciences 113(40):11162–11167.
White M., Pettitt P. 2012. Ancient Digs and Modern Myths: The Age and Context of the Kent's Cavern 4 Maxilla and the Earliest *Homo sapiens* Specimens in Europe. European Journal of Archaeology 15(3):392-420.
Wilczyński J., Miękina B., Lipecki G., Lõugas L., Marciszak A., Rzebik-Kowalska B., Stworzewicz E., Szyndlar Z., Wertz K. 2012. Faunal remains from Borsuka Cave - an example of local climate variability during Late Pleistocene in southern Poland. Acta Zoologica Cracoviensia 55(2):131-155.
Wilczyński J., Szczepanek A., Wojtal P., Diakowski M., Wojenka M., Sobieraj D. 2016. A Mid Upper Palaeolithic Child Burial from Borsuka Cave (Southern Poland). International Journal of Osteoarchaeology 26(1):151-162.
Wild E.M., Teschler-Nicola M., Kutschera W., Steier P., Trinkaus E., Wanek W. 2005. Direct dating of Early Upper Palaeolithic human remains from Mladeč. Nature 435:332.
Zilhão J. 2013. Neandertal-Modern Human Contact in Western Eurasia: Issues of Dating, Taxonomy, and Cultural Associations. In: Akazawa T, Nishiaki Y, Aoki K, editors. Dynamics of Learning in Neanderthals and Modern Humans Volume 1: Cultural Perspectives. Tokyo: Springer. p 21-57.

Appendix 1

Pretreatment information, direct AMS radiocarbon dates and references for Fig. 2, Chapter 6. Dates have been rounded to nearest 10 years and calibrated in OxCal 4.3 [1] using the IntCal13 dataset [2]. Multiple dates from the same bone/collagen extract were combined using the R_Combine feature in OxCal [1] when the results were statistically indistinguishable. Under Pretreatment: 'Bulk' denotes unfiltered collagen/gelatin extracts (generally pretreated with protocols based on Longin [3]); 'UF' indicates ultrafiltered [4] gelatinised collagen extracts; 'HYP' indicates individual hydroxyproline amino acids were isolated for compound specific dating[5]; other methods of collagen purification (XAD-2 resin/glass microfiber filter/ion-exchange) are also marked. In general, 1% collagen yield is regarded as the minimum level of preservation suitable for ^{14}C dating. Well-preserved collagen extracts are expected to have C:N ratios In the range of 2.9-3.6 [6] whereas the theoretical C:N ratio of HYP is 5.0 [5]. '-' data not available in source publication.

Sample ID	Species	Country	AMS lab no	Pretreat-ment	Coll yield (%)	C:N	^{14}C age ± 1SD (BP)	1σ calibrated range (cal BP)	2σ calibrated range (cal BP)	Ref
Western Europe										
Goyet Q56-16	*Homo sapiens*	Belgium	GrA-59991	-	-	-	22100 ± 100	26440-26140	26610-26040	[7]
Goyet 2878-21	*Homo sapiens*	Belgium	GrA-62455	-	-	-	22360 ± 110	26860-26420	27060-26270	[7]
Goyet Q376-19	*Homo sapiens*	Belgium	GrA-54026	-	-	-	23260 ± 110	27620-27410	27720-27310	[7]
Goyet Q55-2	*Homo sapiens*	Belgium	GrA-54031	-	-	-	23270 ± 120	27630-27410	27740-27310	[7]
La Rochette	*Homo sapiens*	France	OxA-23413	UF	3.4%	3.1	23400 ± 110	27700-27500	27790-27400	[8]
Arene Candid 1 burial	*Homo sapiens*	Italy	OxA-10700	UF	-	3.2	23440 ± 190	27760-27480	27900-27330	[9]
Ostuni 1 burial	*Homo sapiens*	Italy	MAMS-11449	UF	-	-	23450 ± 110	27730-27530	27820-27430	[10]
Goyet Q53-1	*Homo sapiens*	Belgium	GrA-46169	-	-	-	23920 ± 100	28060-27810	28240-27710	[7]
Eel Point 1	*Homo sapiens*	UK	OxA-14164	UF	7.2%	3.2	24470 ± 110	28680-28390	28790-28220	[11]
Ostuni 2 burial	*Homo sapiens*	Italy	MAMS-11450	UF	-	-	24910 ± 130	29100-28750	29330-28630	[10]
Cussac Cave Locus 1	*Homo sapiens*	France	Beta-156643	-	-	-	25120 ± 120	29340-28980	29500-28830	[12]
Vilhonneur 1	*Homo sapiens*	France	Beta-216141 Beta-216142	Bulk	-	-	26890 ± 140	31110-30890	31210-30780	[13]
Paviland 1 burial	*Homo sapiens*	UK	OxA-16412 OxA-16413	UF	3.4% 2.6%	3.2 3.2	29150 ± 140	33610-33210	33730-32970	[14]
Goyet Q376-3	*Homo sapiens*	Belgium	GrA-60034	-	-	-	29370 ± 180	33800-33430	33950-33150	[7]
La Crouzade VI	*Homo sapiens*	France	Erl-9415	-	-	3.2	30640 ± 640	35200-34020	36020-33650	[15]
Goyet Q116-1	*Homo sapiens*	Belgium	GrA-46175	-	-	-	30880 ± 170	34960-34610	35170-34430	[7]
Spy 430a	Neanderthal	Belgium	GrA-32630	Bulk	7.4%	3.5	33940 ± 220	38720-38240	38950-37810	[16]
Spy 94a	Neanderthal	Belgium	GrA-32623	Bulk	7.8%	3.4	35810 ± 260	40780-40120	41110-39820	[16]
Spy 92b	Neanderthal	Belgium	GrA-32626	Bulk	9%	3.3	36350 ± 310	41360-40670	41620-40300	[16]
Saint-Cesaire SP 28	Neanderthal	France	OxA-18099	UF	0.8%	3.3	36200 ± 750	41550-40110	42150-39340	[17]
Grotte du Renne AR-14	Neanderthal	France	MAMS-25149	UF	3.9%	3.2	36840 ± 660	41980-40840	42430-40180	[18]
Rochers-de-Villeneuve 1	Neanderthal	France	OxA-15257	UF	3.6%	3.3	45200 ± 1100	49670-47640	Out of range	[19]
El Sidron 00/46	Neanderthal	Spain	OxA-21776	UF	3.3%	3.3	48400 ± 3200	Out of range	Out of range	[20]
Central Europe										
Brno 2 burial	*Homo sapiens*	Czech Republic	OxA-8293	Bulk	11%	-	23680 ± 200	27940-27610	28200-27460	[21]
Willendorf I	*Homo sapiens*	Austria	ETH-20690	Bulk	-	-	24250 ± 180	28510-28060	28690-27880	[22]

Pavlov 1	*Homo sapiens*	Czech Republic	Aix-12026	UF	9.3%	3.4	25490 ± 90	29720-29410	29910-29260	[23]
Dolní Věstonice II DV15 burial	*Homo sapiens*	Czech Republic	Aix-12029	UF	8.%	3.2	26730 ± 100	31020-30820	31110-30720	[23]
Dolní Věstonice II DV14 burial	*Homo sapiens*	Czech Republic	Aix-12028	UF	9.5%	3.5	26760 ± 100	31040-30830	31120-30730	[23]
Dolní Věstonice II DV13 burial	*Homo sapiens*	Czech Republic	Aix-12027	UF	13.5%	3.2	27040 ± 100	31170-30980	31250-30880	[23]
Dolní Věstonice II DV43	*Homo sapiens*	Czech Republic	Aix-12032	UF	10.2%	3.3	27070 ± 110	31190-30990	31270-30890	[23]
Dolní Věstonice II DV42	*Homo sapiens*	Czech Republic	Aix-12031	UF	9%	3.4	26880 ± 110	31100-30900	31180-30790	[23]
Dolní Věstonice II DV16 burial	*Homo sapiens*	Czech Republic	Aix-12030	UF	13.9%	3.3	27220 ± 110	31250-31060	31350-30970	[23]
Oblazowa Cave OBC6 P.5546	*Homo sapiens*	Poland	OxA-4586	Ion exchange	3.8%	-	31000 ± 550	35510-34430	36110-34010	[24]
Mladeč 8	*Homo sapiens*	Czech Republic	VERA-3075	Bulk	8.3%	2.7	30680 +380/-360	34960-34250	35410-33960	[25]
Mladeč 1	*Homo sapiens*	Czech Republic	VERA-3073	Bulk	-	-	31190 +400/-390	35510-34710	36010-34380	[25]
Mladeč 2	*Homo sapiens*	Czech Republic	VERA-3074	Bulk	-	-	31320 +410/-390	35640-34810	36130-34510	[25]
Mladeč 9a	*Homo sapiens*	Czech Republic	VERA-3076A	Bulk	-	-	31500 +420/-400	35820-34950	36280-34640	[25]
Kleine Feldhofer Grotte NN1	Neanderthal	Germany	ETH-19660	Bulk	-	-	39240 ± 670	43610-42540	44350-42190	[26]
Kleine Feldhofer Grotte Nean 1	Neanderthal	Germany	ETH-20981	Bulk	-	-	39900 ± 620	44130-43040	44750-42660	[26]
Kleine Feldhofer Grotte NN4	Neanderthal	Germany	ETH-19661	Bulk	-	-	40360 ± 760	44620-43280	45370-42810	[26]
Eastern Europe										
Peştera Cioclovina 1	*Homo sapiens*	Romania	OxA-15527	UF	5.9%	3.4	28510 ± 170	32860-32170	33090-31780	[27]
Peştera Muierii 2	*Homo sapiens*	Romania	OxA-16252	UF	11.2%	3.3	29110 ± 190	33590-33100	33760-32840	[28]
Peştera Muierii 1	*Homo sapiens*	Romania	LuA-5229 OxA-15529	- UF	- 13.3%	- 3.4	29940 ± 170	34170-33850	34370-33710	[28]
Bacho Kiro Cave BK 1653	*Homo sapiens*	Bulgaria	ETH-86768 AIX-12024	UF	11.8%	3.2	30570 ± 120	34690-34380	34820-34210	[29]
Bacho Kiro Cave F6-597	*Homo sapiens*	Bulgaria	ETH-86773 AIX-12025	UF	4.2%	3.2	31660 ± 140	35750-35340	35970-35140	[29]
Buran-Kaya III parietal	*Homo sapiens*	Ukraine	GrA-37938	Bulk	-	3.3	31900 ± 230	36090-35550	36300-35260	[30]
Peştera cu Oase 1	*Homo sapiens*	Romania	GrA-22810 OxA-11711	Bulk UF	4% 0.4%	2.6 3.3	34950 + 990/-890	40040-37610	41070-36470	[31]
Bacho Kiro Cave AA7-738	*Homo sapiens*	Bulgaria	ETH-86769	UF	12.3%	3.1	39750 ± 380	43760-43050	44210-42810	[29]
Bacho Kiro Cave CC7-2289	*Homo sapiens*	Bulgaria	ETH-86771	UF	4.2%	3.1	40600 ± 420	44580-43720	44980-43340	[29]
Bacho Kiro Cave BB7-240	*Homo sapiens*	Bulgaria	ETH-86770	UF	9%	3.1	41850 ± 480	45660-44800	46130-44400	[29]
Bacho Kiro Cave CC7-335	*Homo sapiens*	Bulgaria	ETH-86772	UF	11.9%	3.1	42450 ± 510	46190-45250	46790-44830	[29]
Vindija Vi-208	Neanderthal	Croatia	Ox-X-2689-09	HYP	5.6%	5.6	42700 ± 1600	47830-44690	49690-43890	[32]
Vindija Vi-207	Neanderthal	Croatia	Ox-X-2689-10	HYP	6%	5.6	43900 ± 2000	49010-45770	Out of range	[32]
Vindija Vi-33.19	Neanderthal	Croatia	Ox-X-2717-11	HYP	-	4.9	44300 ± 1200	48860-46430	49950-45850	[32]
Vindija Vi-2291-18	Neanderthal	Croatia	Ox-V-2291-18	UF	-	3.3	44450 ± 550	48430-47010	49210-46450	[33]
Vindija Vi-*28	Neanderthal	Croatia	Ox-X-2687-57	HYP	5.4%	5.0	46200 ± 1500	Out of range	Out of range	[32]
Western Russia										
Kostenki 8	*Homo sapiens*	Russia	OxA-7109	-	-	-	23020 ± 320	27630-27050	27800-26580	[34]

Kostenki 18 burial	*Homo sapiens*	Russia	OxA-X-2666-53	HYP	-	5.4	23230 ± 150	27630-27370	27740-27240	[35]
Sungir 1 burial	*Homo sapiens*	Russia	OxA-X-2464-12	HYP	-	5.0	28650 ± 400	33300-32110	33640-31600	[36]
Sungir 4 burial	*Homo sapiens*	Russia	OxA-X-2462-52	HYP	-	5.1	29670 ± 290	34070-33590	34390-33270	[36]
Sungir 2 burial	*Homo sapiens*	Russia	OxA-X-2395-6	HYP	-	5.0	30100 ± 550	34660-33740	35290-33180	[5]
Sungir 3 burial	*Homo sapiens*	Russia	OxA-X-2395-7	HYP	-	5.0	30000 ± 550	34600-33660	35160-33030	[5]
Kostenki 1	*Homo sapiens*	Russia	OxA-15055	UF	9.6%	3.2	32070 ± 190	36200-35760	36380-35520	[37]
Kostenki 14	*Homo sapiens*	Russia	OxA-X-2395-15	HYP	-	5.1	33250 ± 500	38220-36810	38690-36260	[5]
Mezmaiskaya Cave Mez 2	Neanderthal	Russia	OxA-21839	UF	14.6%	3.2	39700 ± 1100	44430-42640	45630-42030	[38]
Siberia and Mongolia										
Mal'ta MA-1	*Homo sapiens*	Russia (Siberia)	UCIAMS-79666	XAD_2 resin	18.7%	-	20240 ± 60	24430-24200	24520-24090	[39]
Pokrovka 2	*Homo sapiens*	Russia (Siberia)	OxA-19850	UF	6.7%	3.3	27740 ± 150	31600-31300	31830-31180	[40]
Salkhit skullcap	*Homo sapiens*	Mongolia	OxA-X-2717-25	HYP	-	5.0	30430 ± 300	34680-34140	34940-33900	[41]
Okladnikov Cave OK1	Neanderthal	Russia (Siberia)	OxA-15481	UF	5%	3.3	37800 ± 450	42430-41800	42750-41480	[42]
Ust'-Ishim 1	*Homo sapiens*	Russia (Siberia)	OxA-25516 OxA-30190	UF	7.7% 10%	3.2 3.3	41400 ± 950	45750-44010	46840-43210	[43]
Eastern Asia										
Shiraho-Saonetabaru Cave (No. 2)	*Homo sapiens*	Japan	MTC-12820	Glass microfiber filter	0.9%	3.1	20420 ± 110	24760-24340	25000-24210	[44]
Tianyuan Cave (1)	*Homo sapiens*	China	BA-03222	-	-	-	34430 ± 510	39560-38450	40260-37760	[45]

References

1. Bronk Ramsey, C., *Bayesian analysis of radiocarbon dates.* Radiocarbon, 2009. **51**(1): p. 337-360.
2. Reimer, P.J., et al., *IntCal13 and Marine13 radiocarbon age calibration curves 0–50,000 years cal BP.* Radiocarbon, 2013. **55**(4): p. 1869–1887.
3. Longin, R., *New method of collagen extraction for radiocarbon dating.* Nature, 1971. **231**: p. 241-242.
4. Brown, T.A., et al., *Improved collagen extraction by modified Longin method.* Radiocarbon, 1988. **30**(2): p. 171-177.
5. Marom, A., et al., *Single amino acid radiocarbon dating of Upper Paleolithic modern humans.* Proceedings of the National Academy of Sciences, 2012. **109**(18): p. 6878-6881.
6. van Klinken, G.J., *Bone collagen quality indicators for palaeodietary and radiocarbon measurements.* Journal of Archaeological Science, 1999. **26**: p. 687–695.
7. Posth, C., et al., *Pleistocene mitochondrial genomes suggest a single major dispersal of non-Africans and a Late Glacial population turnover in Europe.* Current Biology, 2016. **26**(6): p. 827-833.
8. Benazzi, S., et al., *Early dispersal of modern humans in Europe and implications for Neanderthal behaviour.* Nature, 2011. **479**(7374): p. 525-528.
9. Pettitt, P.B., et al., *The Gravettian burial known as the Prince ("Il Principe"): new evidence for his age and diet.* Antiquity, 2003. **77**(295): p. 15-19.
10. Fu, Q., et al., *The genetic history of Ice Age Europe.* Nature, 2016. **534**(7606): p. 200-205.
11. Schulting, R.J., et al., *A Mid-Upper Palaeolithic human humerus from Eel Point, South Wales, UK.* Journal of Human Evolution, 2005. **48**(5): p. 493-505.
12. Aujoulat, N., et al., *La grotte ornée de Cussac (Dordogne). Observations liminaires.* Paleo, 2001(13): p. 9-18.
13. Henry-Gambier, D., et al., *New hominid remains associated with gravettian parietal art (Les Garennes, Vilhonneur, France).* Journal of Human Evolution, 2007. **53**(6): p. 747-750.
14. Jacobi, R.M. and T. Higham, *The "Red Lady" ages gracefully: new ultrafiltration AMS determinations from Paviland.* Journal of Human Evolution, 2008. **55**(5): p. 898-907.
15. Henry-Gambier, D. and D. Sacchi, *La Crouzade V-VI (Aude, France): un des plus anciens fossiles d'anatomie moderne en Europe occidentale.* Bulletins et Mémoires de la Société d'anthropologie de Paris, 2008. **20**(1-2): p. 79-104.
16. Semal, P., et al., *New data on the late Neandertals: direct dating of the Belgian Spy fossils.* American Journal of Physical Anthropology, 2009. **138**(4): p. 421-8.
17. Hublin, J.-J., et al., *Radiocarbon dates from the Grotte du Renne and Saint-Césaire support a Neandertal origin for the Châtelperronian.* Proceedings of the National Academy of Sciences, 2012. **109**(46): p. 18743-18748.
18. Welker, F., et al., *Palaeoproteomic evidence identifies archaic hominins associated with the Châtelperronian at the Grotte du Renne.* Proceedings of the National Academy of Sciences, 2016. **113**(40): p. 11162–11167.
19. Beauval, C., et al., *Direct radiocarbon dating and stable isotopes of the neandertal femur from Les Rochers-de-Villeneuve (Lussac-les-Châteaux, Vienne).* Bulletins et mémoires de la Société d'Anthropologie de Paris, 2006. **18**(1-2): p. 35-42.
20. Wood, R.E., et al., *A new date for the Neanderthals from El Sidrón Cave (Asturias, Northern Spain).* Archaeometry, 2013. **55**(1): p. 148-158.

21. Pettitt, P. and E. Trinkaus, *Direct radiocarbon dating of the Brno 2 Gravettian human remains.* Anthropologie, 2000. **38**(2): p. 149-150.
22. Teschler-Nicola, M. and E. Trinkaus, *Human remains from the Austrian Gravettian: the Willendorf femoral diaphysis and mandibular symphysis.* Journal of Human Evolution, 2001. **40**(6): p. 451-465.
23. Fewlass, H., et al., *Direct radiocarbon dates of mid Upper Palaeolithic human remains from Dolní Věstonice II and Pavlov I, Czech Republic.* Journal of Archaeological Science: Reports, In press.
24. Housley, R.A., *Radiocarbon dating*, in *Oblazowa Cave: Human Activity, Stratigraphy and Palaeoenvironment*, P. Valde-Nowak, A. Nadachowski, and T. Madeyska, Editors. 2003, Institute of Archaeology and Ethnology Polish Academy of Sciences: Krakow. p. 81-85.
25. Wild, E.M., et al., *Direct dating of Early Upper Palaeolithic human remains from Mladeč.* Nature, 2005. **435**: p. 332.
26. Schmitz, R.W., et al., *The Neandertal type site revisited: Interdisciplinary investigations of skeletal remains from the Neander Valley, Germany.* Proceedings of the National Academy of Sciences, 2002. **99**(20): p. 13342-13347.
27. Soficaru, A., et al., *The human cranium from the Peştera Cioclovina Uscată, Romania: context, age, taphonomy, morphology, and paleopathology.* Current Anthropology, 2007. **48**(4): p. 611-619.
28. Soficaru, A., A. Doboş, and E. Trinkaus, *Early modern humans from the Peştera Muierii, Baia de Fier, Romania.* Proceedings of the National Academy of Sciences, 2006. **103**(46): p. 17196-17201.
29. Fewlass, H., et al., *New ^{14}C chronology for Middle–to–Upper Palaeolithic transition at Bacho Kiro Cave, Bulgaria.* Nature Ecology & Evolution, in review.
30. Prat, S., et al., *The oldest anatomically modern humans from far Southeast Europe: direct dating, culture and behavior.* PLoS ONE, 2011. **6**(6): p. e20834.
31. Trinkaus, E., et al., *An early modern human from the Peştera cu Oase, Romania.* Proceedings of the National Academy of Sciences, 2003. **100**(20): p. 11231-11236.
32. Devièse, T., et al., *Direct dating of Neanderthal remains from the site of Vindija Cave and implications for the Middle to Upper Paleolithic transition.* Proceedings of the National Academy of Sciences, 2017. **114**(40): p. 10606-10611.
33. Green, R.E., et al., *A draft sequence of the Neandertal genome.* Science, 2010. **328**(5979): p. 710-722.
34. Sinitsyn, A. *Les sépultures de Kostenki: chronologie, attribution culturelle, rite funéraire*. in *La spiritualité. Etudes et Recherches Archeologiques de l'Universite de Liege*. 2004. Liege: ERAUL.
35. Reynolds, N., et al., *The Kostënki 18 child burial and the cultural and funerary landscape of Mid Upper Palaeolithic European Russia.* Antiquity, 2017. **91**(360): p. 1435-1450.
36. Nalawade-Chavan, S., J. McCullagh, and R. Hedges, *New hydroxyproline radiocarbon dates from Sungir, Russia, confirm early Mid Upper Palaeolithic burials in Eurasia.* PLoS ONE, 2014. **9**(1): p. e76896.
37. Higham, T., R.M. Jacobi, and C. Bronk Ramsey, *AMS radiocarbon dating of ancient bone using ultrafiltration.* Radiocarbon, 2006. **48**(2): p. 179-195.
38. Pinhasi, R., et al., *Revised age of late Neanderthal occupation and the end of the Middle Paleolithic in the northern Caucasus.* Proceedings of the National Academy of Sciences, 2011. **108**(21): p. 8611-8616.
39. Raghavan, M., et al., *Upper Palaeolithic Siberian genome reveals dual ancestry of Native Americans.* Nature, 2013. **505**: p. 87-91.
40. Akimova, E., et al., *A new direct radiocarbon AMS date for an Upper Palaeolithic human bone from Siberia.* Archaeometry, 2010. **52**(6): p. 1122-1130.

41. Devièse, T., et al., *Compound-specific radiocarbon dating and mitochondrial DNA analysis of the Pleistocene hominin from Salkhit Mongolia.* Nature Communications, 2019. **10**(1): p. 274.
42. Krause, J., et al., *Neanderthals in central Asia and Siberia.* Nature, 2007. **449**(7164): p. 902-904.
43. Fu, Q., et al., *Genome sequence of a 45,000-year-old modern human from western Siberia.* Nature, 2014. **514**(7523): p. 445-9.
44. Nakagawa, R., et al., *Pleistocene human remains from Shiraho-Saonetabaru Cave on Ishigaki Island, Okinawa, Japan, and their radiocarbon dating.* Anthropological Science, 2010. **118**(3): p. 173–183.
45. Shang, H., et al., *An early modern human from Tianyuan Cave, Zhoukoudian, China.* Proceedings of the National Academy of Sciences, 2007. **104**(16): p. 6573-6578.

Summary

Direct radiocarbon dating of human remains is crucial for the accurate interpretation of prehistory. Yet given the scarcity of prehistoric human remains, direct dating is often deemed too destructive for many important fossils. The reduction of sample size necessary for dating bone is therefore of great interest to archaeologists, but the confounding factors of molecular preservation and contamination present great challenges to the radiocarbon dating community.

This dissertation explores the reduction of sample size for radiocarbon dating Palaeolithic bone at the pretreatment and ^{14}C measurement stages. Methodological tests were carried out on a selection of archaeological bones spanning the breadth of the radiocarbon method at varying levels of preservation. Our standard pretreatment protocol for ~500 mg bone was refined for <100 mg bone. Collagen extracted from solid pieces of bone (rather than powdered bone) and a reduced duration of the gelatinisation stage improved collagen yields for small samples. The quality of the extracted collagen was evaluated based on the yield, elemental and stable isotopic values and the obtained ^{14}C measurements.

Following extraction, collagen of suitable quality can be dated by accelerator mass spectrometry (AMS) in two ways. When sufficient material is available, collagen (~one-third carbon) is combusted to CO_2, converted to graphite and measured in an AMS in the form of a solid target, typically containing 0.5-1 mg carbon. The gas ion source of the **Mi**ni **Ca**rbon **Da**ting **S**ystem (MICADAS) AMS, developed at ETH ZURICH, permits the measurement of ^{14}C directly from CO_2 containing <100 µg carbon, but the lower ion currents achieved with the direct measurement of small CO_2 samples result in lower levels of precision compared to larger solid samples. The instrument has been utilised in environmental applications but had not been employed for archaeological samples requiring high accuracy and precision. This dissertation documents extensive testing of the accuracy and precision of the recently improved gas ion source of the AixMICADAS for dating small archaeological collagen samples. The results demonstrate that the gas ion source provides accurate and reproducible results, reaching a level of precision useful for addressing archaeological questions. This indicates the technique is suitable for dating Palaeolithic collagen where the amount of material available for dating is limited.

The human remains from Dolní Věstonice II and Pavlov I, Czech Republic, are one of the most intensively studied skeletal collections from the European mid Upper Palaeolithic and have yielded fascinating insights into the biology and behaviour of Gravettian people. Since their excavation in the 20th century, the human remains have only been dated indirectly from

associated charcoals. Following aDNA analysis of the human remains in 2013, very small amounts of bone material were left over from seven bones from both burial and isolated contexts. Very small bone aliquots (32-203 mg) were pretreated and proved to be exceptionally well preserved. The high level of preservation allowed the collagen extracts to be dated with both graphite targets and the gas ion source, enabling further comparison of the two techniques. The results from the two methods were statistically indistinguishable. The study confirms the Gravettian origin of the individuals and provides a high chronological resolution for these important human remains.

The Bacho Kiro Cave, Bulgaria, contains an extensive Initial Upper Palaeolithic (IUP) assemblage, generally attributed to the first appearance of Upper Palaeolithic *Homo sapiens* in Europe. Recent excavations at the site have been undertaken to gain new material for analysis and establish a robust site chronology. This dissertation includes the results of a radiocarbon dating program and Bayesian model of the entire Middle to Upper Palaeolithic stratigraphy, with a focus on the IUP layers. The extensive dataset includes a predominance of anthropogenically modified fauna with exceptional levels of collagen preservation. The high-precision AMS chronology spans from >51,000 BP in the Middle Palaeolithic layers at the base of the stratigraphy to ~35,000 cal BP at the top of the stratigraphy. During identification of the unidentifiable bone assemblage with collagen peptide fingerprinting (ZooMS), six small human bone fragments were identified from the IUP (n = 4) and Upper Palaeolithic (n = 2) layers. Small aliquots of the human bones (80-110 mg) were pretreated for ^{14}C dating. The high level of collagen preservation permitted all human extracts to be dated at high precision with graphite targets. The two human bones from the upper layers were also dated with gas ion source of the AixMICADAS to cross-check the results. The ^{14}C dates confirm the association of the four human bones with the IUP assemblage. The study provides a robust, high precision site chronology based on human and animal bone for one of the most crucial sites in the investigation of the arrival of Upper Palaeolithic *Homo sapiens* in Europe.

This dissertation focused on the reduction of sample size for radiocarbon dating Palaeolithic bone. The research contributes 13 human individuals to the small collection of directly dated Upper Palaeolithic humans in Europe. Minimising sample destruction should allow a wider range of precious fossils and artefacts to be directly radiocarbon dated. This will provide an increasingly robust chronological framework for high-resolution investigation of the Upper Palaeolithic in Europe.

Samenvatting

Directe koolstofdateringen van menselijke resten zijn crucial voor een correcte interpretatie van de prehistorie. Echter, gezien de schaarste aan prehistorische menselijke resten wordt directe datering voor veel belangrijke fossielen vaak als te destructief beschouwd. De vermindering van de monstergrootte die nodig is voor het dateren van bot is daarom van groot belang voor archeologen, maar de verstorende factoren van moleculaire preservatie en contaminatie vormen grote uitdagingen voor de koolstofdateringsgemeenschap.

Dit proefschrift onderzoekt de vermindering van de monstergrootte in de voorbehandelings- en koolstofmetingstadia voor het koolstofdateren van paleolitisch bot. Methodologische tests werden uitgevoerd op een selectie archeologische botten die de reikwijdte van de koolstofdateringsmethode omvatten op verschillende niveaus van preservatie. Ons standaardprotocol voor ~500 mg bot werd verfijnd tot <100 mg bot. Collageen geëxtraheerd van vaste botfragmenten (in plaats van verpoederd bot) en een gereduceerde lengte van het gelatinisatie-stadium verbeterden collageenopbrengensten voor kleine monsters. De kwaliteit van het geëxtraheerde collageen werd geevalueerd aan de hand van de collageenopbrengst, elementaire en stabiele isotopenwaardes en de verkregen koolstafdateringen.

Na de extractie kan collagen van geschikte kwaliteit gedateerd worden door middel van accelerator massaspectrometrie (AMS) op twee manieren. Als er genoeg materiaal is wordt collageen (~één-derde koolstof) verbrandt tot CO_2, omgezet in grafiet en gemeten in een AMS als vast doelwit, dat normaal gesproken 0.5-1 mg koolstof bevat. De gasionenbron van de **M**ini **C**arbon **D**ating **S**ystem (MICADAS) AMS, ontwikkeld bij ETH ZURICH, maakt het mogelijk ^{14}C uit CO_2 rechtstreeks te meten, voor minder dan 100 µg koolstof, maar de lagere ionenstromen die worden bereikt met de directe meting van kleine CO_2-monsters resulteren in lagere nauwkeurigheidsniveaus in vergelijking met grotere, vaste doelwitten. Het instrument is gebruikt in milieutoepassingen maar niet voor archeologische monsters die een hoge nauwkeurigheid en precisie vereisen. Dit proefschrift documenteert uitgebreide testen van de nauwkeurigheid en precisie van de recent verbeterde gasionenbron van de AixMICADAS voor het dateren van kleine archeologische collageenmonsters. De resultaten tonen aan dat de gasionenbron nauwkeurige en reproduceerbare resultaten oplevert en een nauwkeurigheidsniveau bereikt, dat bruikbaar is voor het beantwoorden van archeologische vragen. Dit geeft aan dat de techniek geschikt is voor het dateren van paleolithisch collageen waarbij de hoeveelheid beschikbaar materiaal voor datering beperkt is.

De menselijke resten van Dolní Věstonice II en Pavlov I, Tjechie, zijn enkele van de meest intensief bestudeerde skeletresten van het Europese laat-paleolithicum en hebben fascinerende inzichten opgeleverd in de biologie en het gedrag van Gravettien-mensen. Sinds hun opgraving in de 20ste eeuw zijn de menselijke resten alleen indirect gedateerd op basis van geassocieerde houtskool. Na oud-DNA onderzoek aan de menselijke skelteresten in 2013 waren alleen zeer kleine hoeveelheden botmateriaal over van zeven botten afkomstig uit zowel graf- als geïsoleerde contexten. Zeer kleine botmonsters (32-203 mg) werden voorbehandeld, en de eerste resultaten gaven aan dat ze exceptioneel goed bewaard waren. Het hoge preservatieniveau stond datering toe van het geëxtraheerde collageen met zowel grafietdoelwitten als de gasionenbron, wat het verder vergelijken van beide methoden mogelijk maakte. De resultaten gaven aan dat de twee methoden statistisch gezien niet te onderscheiden zijn. Het onderzoek bevestigt dat de menselijke resten stammen uit het Gravettien en levert een hoge-resolutie chronologie op van deze belangrijke menselijke skeletresten.

De Bacho Kiro grot in Bulgarije omvat een omvangrijk Initial Upper Palaeolithic (IUP) assemblage, dat normaal gesproken toegewezen wordt aan de eerste verschijning van laat-paleolitische *Homo sapiens* in Europa. Recente opgravingen op de vindplaats hadden als doel nieuw onderzoeksmateriaal te verkrijgen en de opzet van een robuuste chronologie. Dit proefschrift bevat de resultaten van een koolstafdateringsonderzoek en Bayesian model van de gehele midden- tot laat-paleolithische stratigrafie, met een focus op de IUP lagen. De grote dataset omvat voornamelijk menselijk bewerkte faunaresten met uitzonderlijke preservatieniveaus. De hoge-precisie AMS chronologie gaat van >51,000 BP in de midden-paleolititsche lagen onderin de stratigrafie tot ~35,000 BP bovenin de stratigrafie. Tijdens het identificeren van de onidentificeerbare botten door middel van collageen peptide fingerprinting (ZooMS) werden zes kleine menselijke botfragmenten ontdekt in de IUP (n = 4) and laat-paleolithische (n = 2) lagen. Kleine monsters (80-110 mg) van de menselijke botresten werden voorbehandled voor koolstofdatering. Het hoge preservatieniveau van het collageen stond de datering toe van alle menselijke resten door middel van grafietdoelwitten. De twee menselijke botten van de jongste laag werden ook gedateerd door middel van de gasionenbron van de AixMICADAS om de resultaten te verifiëren. De koolstofdateringen bevestigen de associatie van de vier menselijke resten met het IUP assemblage. Het onderzoek levert een robuuste, hoge-precisie chronologie gebaseerd op menselijke en dierlijke skeletresten voor één van de meest cruciale vindplaatsen met betrekkening tot eerste verschijning van *Homo sapiens* in Europa.

Dit proefschrift is gericht op de verkleining van de monstergrootte voor het koolstofdateren van paleolitisch botmateriaal. Het onderzoek draagt 13 menselijke individuen bij aan het kleine aantal direct gedateerde menselijke skeletresten van het laat-paleolithicum in Europa. Het verkleinen van de monstergrootte zou het mogelijk moeten maken een groter aantal unieke menselijke

resten en artefacten direct te dateren door middel van koolstofdatering. Dit maakt het mogelijk om een steeds meer verfijnde chronologie op te stellen van het laat-paleolithicum in Europa.

Acknowledgements

Countless thanks are given to all the people who have provided help during the course of this project. This dissertation would not have been possible without the support of my three supervisors: Sahra Talamo, Bernd Kromer and Jean-Jacques Hublin. To Sahra, thank you so much for all your guidance, encouragement and enthusiasm over the last four years. To Bernd, thank you for all your fascinating insights and willingness to share your never-ending knowledge about radiocarbon. Unending thanks to both of you for always answering every question, email and draft in double quick timing! To Jean-Jacques, thank you for your support throughout the project and the opportunities to work on such incredible projects.

I would like to thank all of my collaborators for providing scientific insights and access to samples. To Edouard Bard, Thibaut Tuna, Yoann Fagault and Lukas Wacker – I thank you all for the care and attention you put into dating so many old bones and for sharing your time and expertise in AMS. To Helene Hoffmann, thank you for taking the time to teach me the ins and outs of a manual vacuum line. To Tsenka Tsanova and Nikolay Sirakov, thank you for the opportunities to visit Bacho Kiro Cave and work on samples from such an incredible site, and for your hospitality during my trips to Dryanovo. To Jiří Svoboda and Sandra Sázelová, thank you for allowing me to work with such amazingly precious human remains.

To all the members of the Dept of Human Evolution at the MPI-EVA over the past four years, thank you for providing a stimulating and welcoming environment. I am particularly proud of and inspired by the many strong female academic role-models in the department who have set wonderful examples. Specific thanks are extended to Shannon McPherron, Tsenka Tsanova, Zeljko Rezek, Geoff Smith, Susann Heinrich, Adeline Le Cabec and Mateja Hajdinjak for always being willing to offer invaluable help and advice.

I am hugely grateful to all the technicians – Lysann Klausnitzer, Manuel Trost, Annabel Reiner, Steffi Hesse and Sven Steinbrenner – who have provided invaluable training and assistance along the way and for running the labs so smoothly, and to all the administrative staff – particularly, Silke Streiber, Candy Felber, Conny Schicke – who provided amazing support.

To my fellow PhD students and pals, past and present, thanks for making the MPI such a great place to be. To Alexa Benson, Steffi Stelzer, Zewdi Tsegai, Frido Welker, Shira Gur-Arieh, Mateja Hajdinjak, Tom Davies, Nic Bourgon, Sarah Pederzani, Julia van Beesel, Micha Hein, Virginie Sinet-Mathiot and Quentin and Arthur – thanks for all the adventures within and beyond the MPI! Most importantly, Senator Sanders – we salute you, long may your reign continue.

To Mikaela Lui, Alexandra Schuh and Elena Zavala, I would not have gotten through these four years without your love and support. I am so happy we got to share the ride! Mikaela and Lukas Schamberger, thanks for all the Lasagne!

To my family - Mum, Dad, Rosie, Nick and Xavier - thank you so much for all your support and encouragement during all these long years of study! Dad, thank you for giving me the book which sparked my interest in anthropology and human evolution and thank you for the 8+ years of proof-reading essays, articles and theses which followed! Mum, thank you for always, always, always supporting me. You have been my rock through all the ups and downs that life has thrown and I would not be who or where I am without you.

To Adam van Casteren, thank you for your unwavering support from near and far and all the happiness you have given me over the last three years.

In addition to the intellectual stimulation offered during the past four years at the MPI, my time in Leipzig has been so fulfilling in all other walks of life. Not only is the city an incredible place to live but I have met so many good friends, travelled far and wide, learnt *a bit* of Deutsch. I am so thankful to have had such an amazing experience.

Curriculum Vitae

The author of this dissertation, Helen Kimberley Fewlass, was born in London, UK, on the 7th of April 1991. After completing her A-levels at St Albans Girls School in 2010, she pursued her interest in biological anthropology by collecting primate behavioural data in the rainforest in Cross River State, Nigeria, whilst volunteering for a primate and rainforest conservation charity. In 2011, she undertook a four-year integrated undergraduate and master's degree program in Archaeological and Anthropological Sciences (Msci) which spanned the departments of Earth Sciences, Archaeology and Anthropology and Chemistry at the University of Bristol, UK. She graduated with a First-Class degree with Honours in 2015. After graduating from Bristol, she started her doctoral research under the supervision of Prof. dr. Sahra Talamo, Dr. Bernd Kromer and Prof. dr. Jean-Jacques Hublin in the Department of Human Evolution at the Max Planck Institute for Evolutionary Anthropology in Leipzig, Germany. After publishing her research in international peer-reviewed journals and presenting her work at conferences in Europe and North America, she submitted her doctoral dissertation to the University of Leiden in the Netherlands in 2019.